Water Technology and Sciences

Included in Thomson Reuters Science Citation Index® (ISI) • Expanded Thomson Reuters Research Alert® (ISI) • EBSCO • ProQuest • Elsevier • Redalyc

Vol. V, No. 4, July-August, 2014

Water Technology and Sciences

Edit Board

Editor in Chief
Dr. Nahún Hamed García Villanueva
Instituto Mexicano de Tecnología del Agua

Editor, Water and Energy
Dr. Humberto Marengo Mogollón
Comisión Federal de Electricidad

Editor, Water Quality
Dra. Blanca Elena Jiménez Cisneros
Organización de las Naciones Unidas para la Educación, la Ciencia y la Cultura

Editor, Hydro-Agricultural Sciences
Dr. Enrique Palacios Vélez
Colegio de Postgraduados, México

Editor, Political and Social Sciences
Dra. Jacinta Palerm Viqueira
Colegio de Postgraduados, México

Editor, Water Management
Dr. Carlos Fernández-Jáuregui
Water Assessment and Advisory-Global Network (WASA-GN)

Editor, Hydraulics
Dr. Felipe I. Arreguín Cortés
Comisión Nacional del Agua

Editor, Hydrology
Dr. Fco. Javier Aparicio Mijares
Consultor

Editor, Scientific and Technological Innovation
Dr. Polioptro F. Martínez Austria
Universidad de las Américas, Puebla

Technical Secretary
M.C. Jorge Arturo Hidalgo Toledo
Instituto Mexicano de Tecnología del Agua

Editorial coordination and careful editing: Helena Rivas-López • **Editorial assistance and editorial layout:** Luisa Guadalupe Ramírez-Martínez • **Figures design:** Luisa Guadalupe Ramírez-Martínez and Rosario Castro-Rivera • **Coordination arbitration:** Elizabeth Peña and Bibiana Bahena • **Proofreading English:** Ellen Weiss • **Logo design and cover:** Oscar Alonso-Barrón • **Design format:** Gema Alín Martínez-Ocampo • **Marketing:** Marco Antonio Bonilla-Rincón.

Editorial Committee

• **Dr. Adrián Pedrozo Acuña,** Universidad Nacional Autónoma de México • **Dr. Alcides Juan León Méndez,** Centro de Investigaciones Hidráulicas, Cuba • **Dr. Aldo Iván Ramírez Orozco,** Centro del Agua para América Latina y el Caribe, México • **Dr. Alejandro López Alvarado,** Pontificia Universidad Católica de Valparaíso, Chile • **Dr. Álvaro A. Aldama Rodríguez,** consultor independiente • **Dr. Andrei S. Jouravlev,** Comisión Económica para América Latina y el Caribe, Chile • **Dr. Andrés Rodríguez,** Universidad Nacional de Córdoba, Argentina • **Dra. Anne Margrethe Hansen Hansen,** Instituto Mexicano de Tecnología del Agua • **Dr. Ariosto Aguilar Chávez,** Instituto Mexicano de Tecnología del Agua • **Dr. Arturo Marcano,** Asociación Internacional de Ingeniería e Investigaciones Hidráulicas, Venezuela • **Dr. Carlos Díaz Delgado,** Universidad Autónoma del Estado de México • **Dr. Carlos Puente,** Universidad de California en Davis, Estados Unidos • **Dr. Cleverson Vitório Andreoli,** Andreoli Engenheiros Associados, Brasil • **Dr. Daene McKinney,** Universidad de Texas en Austin, Estados Unidos • **Dr. Daniel Murillo Licea,** Centro de Investigaciones y Estudios Superiores en Antropología Social • **Dr. Eduardo Varas Castellón,** Pontificia Universidad Católica de Chile • **Dr. Enrique Cabrera Marcet,** Universidad Politécnica de Valencia, España • **Dr. Enrique Playán Jubillar,** Consejo Superior de Investigaciones Científicas, España • **Dr. Ernesto José González Rivas,** Universidad Central de Venezuela • **Dr. Federico Estrada,** Centro de Estudios y Experimentación de Obras Públicas, España • **Dr. Fedro Zazueta,** Universidad de Florida, Estados Unidos • **Dra. Gabriela Eleonora Moeller Chávez,** Instituto Mexicano de Tecnología del Agua • **Dr. Gerardo Buelna,** Dirección de Medio Ambiente y Centro de Investigación Industrial de Quebec, Canadá • **Dr. Gueorguiev Tzatchkov Velitchko,** Instituto Mexicano de Tecnología del Agua • **Ing. Héctor Garduño Velasco,** consultor internacional • **Dr. Ismael Mariño Tapia,** Centro de Investigación y de Estudios Avanzados del Instituto Politécnico Nacional, México • **Dr. Ismael Piedra Cueva,** Instituto de Mecánica de Fluidos e Ingeniería Ambiental, Uruguay • **Dr. Jaime Collado,** Comité Nacional Mexicano para la Comisión Internacional de Irrigación y Drenaje • **Dr. Jaime Iván Ordóñez,** Universidad Nacional, Bogotá, Colombia • **Dr. Joaquín Rodríguez Chaparro,** Ministerio de Medio Ambiente, y Medio Rural y Marino, España • **Dr. José Ángel Raynal Villaseñor,** Universidad de Las Américas, Puebla, México • **Dr. José D. Salas,** Universidad de Colorado, Estados Unidos • **Dr. José Joel Carrillo Rivera,** Universidad Nacional Autónoma de México • **Dr. Juan Pedro Martín Vide,** Universidad Politécnica de Cataluña, España • **Dr. Julio Kuroiwa,** Laboratorio Nacional de Hidráulica, Perú • **Dr. Karim Acuña Askar,** Universidad Autónoma de Nuevo León, México • **Dra. Luciana Coutinho,** Universidade Do Minho, Portugal • **Dr. Luis F. León,** Waterloo University, Canadá • **Dr. Luis Texeira,** Instituto de Mecánica de Fluidos e Ingeniería Ambiental, Uruguay • **Dra. Luisa Paré Ouellet,** Universidad Nacional Autónoma de México • **Ing. Manuel Contijoch Escontria,** Banco Mundial • **Dr. Marcos Von Sperling,** Universidad Federal de Minas Gerais, Brasil • **Dra. María Claudia Campos Pinilla,** Universidad Javeriana, Colombia • **Dra. María Luisa Torregrosa,** Facultad Latinoamericana de Ciencias Sociales , México • **Dra. María Rafaela de Saldanha Matos,** Laboratorio Nacional de Ingeniería Civil, Portugal • **Dra. María Victoria Vélez Otálvaro,** Universidad Nacional de Colombia • **Dr. Michel Rosengaus Moshinsky,** Comisión Nacional del Agua, México • **Dr. Moisés Berezowsky Verduzco,** Universidad Nacional Autónoma de México • **Dra. Natalia Uribe Pando,** Centro UNESCO del País Vasco • **Dr. Óscar F. Ibáñez Hernández,** Comisión Nacional del Agua, México • **Dr. Paulo Salles Alfonso de Almeida,** Universidad Nacional Autónoma de México • **Dr. Rafael Pardo Gómez,** Centro de Investigaciones Hidráulicas, Cuba • **Dr. Rafael Val Segura,** Universidad Nacional Autónoma de México • **Dr. Ramón Domínguez Mora,** Universidad Nacional Autónoma de México • **Dr. Ramón Fuentes Aguilar,** Instituto de Innovación en Minería y Metalurgia, Chile • **Dr. Ramón Ma. Gutiérrez Serret,** Centro de Estudios y Experimentación de Obras Públicas, España • **Ing. Raquel Duque,** Asociación Internacional de Ingeniería e Investigaciones Hidráulicas, Colombia • **Dr. Raúl Antonio Lopardo,** Instituto Nacional del Agua de Argentina • **Dr. Rodolfo Silva Casarín,** Universidad Nacional Autónoma de México • **Dr. Serge Léonard Tamari Wagner,** Instituto Mexicano de Tecnología del Agua • **Dr. Simón González,** Universidad Nacional Autónoma de México • **Dr. Víctor Hugo Alcocer Yamanaka,** Instituto Mexicano de Tecnología del Agua • **Dra. Ximena Vargas Mesa,** Universidad de Chile •

©***Water Technology and Sciences.*** Vol. V, No. 4, July-August, 2014, is a bimonthly publication edited by the Instituto Mexicano de Tecnología del Agua, Paseo Cuauhnáhuac 8532, Colonia Progreso, Jiutepec, Morelos, C.P. 62550, telephone +52 (777) 3 29 36 00, extension 474, www.imta.gob.mx/tyca, fsalinas@tlaloc.imta.mx. Responsible editor, Nahún Hamed García Villanueva; Copyright No. 04-2013-121014514100-203, granted by the Instituto Nacional de Derechos de Autor. ISSN pending. Responsible for the latest update of this issue: Sub-Department of Dissemination and Circulation, Francisco José Salinas Estrada, Paseo Cuauhnáhuac 8532, Colonia Progreso, Jiutepec, Morelos, C.P. 62550.

The contents of the articles are the exclusive responsibility of the authors and do not necessarily reflect the position of the editor of the publication.

The total or partial reproduction of the contents and images of the publication without prior authorization from the Instituto Mexicano de Tecnología del Agua are strictly prohibited.

Water Technology and Sciences is the traslation of *Tecnología y Ciencias del Agua*, which is the continuation of the following journals: *Irrigación en México* (1930-1946); *Ingeniería hidráulica en México* (1947-1971); *Recursos hidráulicos* (1972-1978), and *Ingeniería hidráulica en México*, second period (1985-2009).

For subscriptions, click here

Water Technology and Sciences

Vol. V, No. 4, July-August, 2014

Coordination for editorial comments, click here give

Cover: Sampling for biological indicators in the Balsas river, Mexico.

In the article "Supply Well Protection: Groundwater Quality Indicators" (pp. 5-22) by Paris, M., Tujchneider, O., Pérez, M. and D´Elia, M., the indicators defined for the monitoring of groundwater quality are presented. Groundwater is the only water supply for the city of Esperanza, Santa Fe, Argentina. As described by the article, an indicator is a qualitative or quantitative attribute which describes and evaluates a specific aspect of a system. It must be simple, buildable with accessible data and easy to interpret.

Photo: Rubén I. Huerto.

Montebello Lagoon Chiapas, Mexico.

Photo: Rafael Espinoza Méndez.

Contents

Technical articles

Technical notes

Contenido

Artículos técnicos

Notas técnicas

Supply Well Protection: Groundwater Quality Indicators

• Marta Paris* • Ofelia Tujchneider • Marcela Pérez • Mónica D´Elia •
Universidad Nacional del Litoral, Argentina
*Corresponding Author

Abstract

Paris, M., Tujchneider, O., Pérez, M., & D´Elia, M. (July-August, 2014). Supply Well Protection: Groundwater Quality Indicators. Water Technology and Sciences (in Spanish), 5(4), 5-21.

An indicator is a quantitative or qualitative attribute used to describe and evaluate a specific aspect of a system. It must be simple, buildable with available data and easily represented. Different organizations and programs have developed a compilation of indicators that provide synthetic information of the state and evolution of water systems. Nevertheless, these indicators may need to be adapted in order to reflect the particularities of each environment. This paper presents the indicators defined to monitor groundwater quality for the aquifer underlying the city of Esperanza (Santa Fe, Argentina), the only source of supply for the region. The disruption of the hydraulic equilibrium of the multilayer aquifer system that is being exploited has produced significant chemical changes in the water supply. The results show that, although the electrical conductivity (EC) values (usually used as a quality indicator) of the water have changed, this parameter is not a sufficient indicative of the deterioration of water quality in the exploited aquifer system. Cluster (hierarchical and K-means) and principal methods have made it possible to verify this process, to determine the affectation level and its temporal occurrence for each exploitation well. Other attributes show evidence of the rise in the overlying salt water and of downward flows from the overlying unconfined aquifer, resulting in values for EC threshold and alert levels, total dissolved solid, chlorides, sulfates, nitrates and calcium.

Keywords: Cluster analysis, groundwater quality indicators, well head protection.

Resumen

Paris, M., Tujchneider, O., Pérez, M., & D´Elia, M. (julio-agosto, 2014). Protección de pozos de abastecimiento. Indicadores de la calidad del agua subterránea. Tecnología y Ciencias del Agua, 5(4), 5-21.

Un indicador es un atributo cualitativo o cuantitativo que permite describir y evaluar un aspecto específico de un sistema. Debe ser sencillo, construible con datos accesibles y de fácil interpretación. Diferentes organismos y programas internacionales han logrado una compilación de indicadores que aportan información sintética del estado y evolución de los sistemas hídricos. Sin embargo, es posible que sea necesario recurrir a una adaptación de los mismos, a fin de poder reflejar las particularidades de cada ambiente. En este trabajo se presentan los indicadores definidos para monitorear la calidad del agua subterránea, única fuente de provisión de la ciudad de Esperanza (Santa Fe, Argentina). La ruptura del equilibrio hidráulico del sistema acuífero multicapa explotado para abastecimiento ha producido variaciones químicas significativas en el agua de suministro. La aplicación de los métodos de agrupamiento (jerárquico y por K-medias) y componentes principales ha permitido verificar la presencia de este proceso, determinar cuál es el grado de afectación y ocurrencia temporal en cada uno de los pozos. Los resultados muestran que, si bien existen modificaciones en los valores de conductividad eléctrica del agua (CE) —normalmente utilizado como indicador de calidad—, este parámetro no es lo suficientemente indicativo del deterioro de la calidad del agua del sistema acuífero que se explota. Otros atributos dan indicios del ascenso de agua salada subyacente y de flujos descendentes desde el acuífero libre suprayacente, respectivamente, por lo que se establecen valores umbrales y niveles de alerta para la CE, el residuo seco, cloruros, sulfatos, nitratos y calcio.

Palabras clave: *indicadores de calidad del agua subterránea, protección de pozos, análisis de agrupamiento.*

Introduction and Objectives

Groundwater is an important source of supply in urban as well as rural areas. Nevertheless, the lack of an appropriate diagnostic and/or management guidelines as part of a water

resources management plan result in more than one opportunity for the deterioration of this resource.

The need for safe water (in terms of quantity and quality) demonstrates the importance of developing policies and actions that guarantee the protection of groundwater. For the environmentally reliable administration of groundwater, the best practice is to protect the resources from contamination. Some countries ted to choose to create programs to protect groundwater from contamination based on the establishment of well protection perimeters (WPP) and/or the cartography of the vulnerability of aquifers (Hirata & Rebouças, 1999). In both cases, effective protection of supply wells requires taking into account the hydrogeological complexity of the study area, especially due to the hydraulic relationships and hydrodynamic and hydrochemical characteristics of the aquifers. The correct conceptualization of the aquifer will provide solid foundations to:

- Establish different levels of restrictions and controls over past, present and future land uses, with an acceptable degree of uncertainty
- Develop the legal and economic tools and the administrative and institutional changes needed to limit and control land uses.
- Correctly define exploitation schemes, including location and design of collection works, flows and extraction timetables. The protection areas depend on the exploitation volumes, especially in unconfined aquifers. Pumping which is not correctly planned can disrupt the hydrodynamic balance, resulting in the water influx with a different quality.
- Design a monitoring scheme for the exploitation system my systematic measurements of indicator variables that reflect possible variations in the quality and quantity of the resource. This would provide an early warning which would make it possible to take corrective and/or palliative measures against deterioration.

In the case of the city of Esperanza, the growing demand for water, the danger of contamination from drilling in the urban area and the deterioration in the quality of groundwater from increasing salt water were important reasons to relocate the city's supply wells to a new pumping field in the rural area. This was designed according to a management model developed in 1999 based on prior investigations by this work team (Filí, Tujchneider, Paris, Pérez, & D´Elia, 1999). Although the operation of the wells began in the year 2004, a protection scheme has not been formally designed and carried out, especially to address several factors, including: the intense farming, livestock and industrial activities in the region; the possible ascending and/or descending flows from the discontinuous aquitard stratum overlying the semi-confined aquifer being exploited; the disruption of the hydraulic balance of the lower aquifer with high salinity produced by uncontrolled pumping; as well as the possible effect of the importation of surface water which would complement the water supply in the future. Therefore, the overall objective of this investigation was to define indicators that contribute to monitoring and controlling groundwater quality in the study area based on the hypothesis that the measurement of the electrical conductivity of the water is not sufficient for the early indication of deterioration of the water resources.

Different organizations, associations and international programs have succeeded in compiling and classifying different indicators (Aureli & Taniguchi, 2008; Berger & Iams, 1996; Foster & Loucks, 2006; Vrba & Lipponen, 2007; Webb, Hirata, Kruse, & Vrba, 2006) In Argentina, Blarasin, Cabrera, Matteoda, Damilano and Giuliano-Albo (2008) presented an application to evaluate environmental changes in aquifers, and Bocanegra, Massone, Irutig, Cionchi and Panizos (2009) presented one about exploitation schemes. Nevertheless, it may be necessary to

use an adaptation of these in order to account for the particularities of each environment. With respect to the quality of groundwater, it is especially important to take into account that its quality is the result of the interaction of recharge, reactions with sediments and contact or residence time in the system (Doménico, 1972). Groundwater is a geological agent with a general character. This is due to the water-geology interaction which involves a series of chemical, physical and kinetic processes resulting from a natural evolution which tends to reach a state of equilibrium or minimum energy. The lines of current also have a hierarchical and systematized characteristic which defines the groundwater flow as a transport and distribution mechanism for the phenomena produced (Tóth, 2001). According to Vrba and Lipponen (2007), an indicator of groundwater is an attribute that makes it possible to evaluate and describe a specific aspect of the hydric system. It must enable simple and rapid follow-up on the state of groundwater or the changes produced (Pernia-Llera, Lambán-Jiménez, & Molinero-García, 2005). They can be quantitative or qualitative, but fundamentally simple since it should not only be easy to construct based on measurable or observable data but also interpretable. They support the sustainable management of water resources, provide synthetic information about the actual state and evolution of the groundwater system, contribute to the analysis of natural processes and impacts by anthropic activity in time and space, and facilitate communication and public participation in the planning process and definition of policies.

Principal Characteristics of the Study Area

The city of Esperanza (Department of Las Colonias) is located in the west central portion of the province of Santa Fe (Argentina), at 31° 27′ south latitude and 60° 55′ west longitude, with an average altitude above sea level of 26 m and a population of 35 000 inhabitants. The primary exploited aquifer has good efficiency and quality. A 50 km aqueduct which began functioning in the late 1970s complements the supply of water to a neighboring locality, Rafeal, in the Castellanos district (Figure 1). Over 250 000 persons are supplied with groundwater through the housing network or private extractions in these two provincial departments. This results in an exploitation volume calculated to be over 51 million liters per day, of which 26 million are consumed in the localities of Esperanza and Rafaela alone. The main economic sector supporting the social system of the region is agriculture, livestock and a variety of industrial activities which continuously operate above the aquifer system, modifying its qualitative and quantitative characteristics (Paris, Tujchneider, Pérez, D´Elia, & Fili, 1998). Currently, there is no record of irrigators to enable calculating the volume of groundwater used for irrigating crops. Farming exploitations use groundwater for human consumption, livestock and irrigating crops (D´Elia, Tujchneider, Paris, Pérez, & Pusineri, 2012). Nevertheless, with data from the 2002 National Farming Census (performed by the National Statistics and Census Institute), it has been possible to identify that 13 wells are exploited to irrigate with groundwater in Las Colonias. The 10 establishments that perform this cultural practice mainly produce corn, soybean and vegetables. Although more current information is not available, based on agricultural production and water deficit periods registered, the number of irrigators, to-date, is estimated to be higher and, therefore, the percentage of utilization greater.

Potable water service in the city of Esperanza has been available since 1930 when National Sanitary Works (Obras Sanitarias de la Nación; OSN Spanish acronym) built a distribution network fed by three wells that produced roughly 180 m^3/h (4 320 m^3/day). Later, two more wells were incorporated in 1940, one more in 1969, two in 1974 and nine in 1988. In 1999, there were 18 wells in the urban area, of

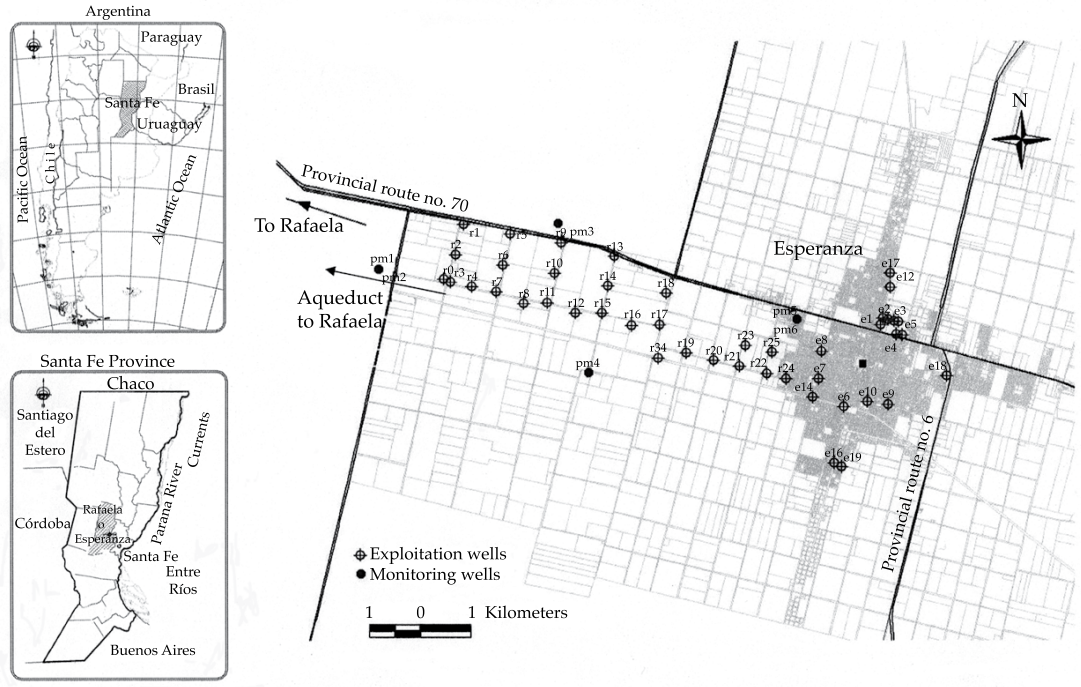

Figure 1. Location of the study area. Lcoation of water supply wells.

which only 8 were functioning due to problems related to the deterioration of the quality of the water (increase in chloride, salinity and/or nitrates) (Paris, Tujchneider, D´Elia, Pérez, & Fili, 1999; Paris, 2005).

In late 1994, a private company (Aguas Provinciales de Santa Fe Sociedad Anónima, APSF) was in charge of the sanitary and sewer water services in the cities of Esperanza and Rafaela (as in other localities in the province). Until roughly 1997 the private company continued with the exploitation described earlier. But the growing demand, dangerous contamination associated with the economic activity in the area (particularly in the urban area) and the lack of sanitation works led to the continuous deterioration of the supply source (Tujchneider, Paris, Fili, D´Elia, & Pérez, 1998; Paris *et al.*, 1998). Since 2006, the sanitary service (potable water and sewers) has been provided by a private company (Aguas Santafesinas Sociedad Anónima, ASSA) in which the state is the majority owner.

Given the importance of groundwater to supply potable water to these two large urban centers, its characterization is crucial to the adequate management of this resource in a region. Therefore, the investigations have focused on the analysis of the functioning of this system and the behavior of the quality of groundwater in the areas with the greatest historical exploitation of the aquifer —the urban area of the city of Esperanza and the pumping field in the rural area. Figure 1 shows the location of the wells that currently make up the supply system for both localities (some are currently out-of-service), the study wells and monitoring wells. This new unified pumping field is located in its entirety in the rural area of Esperanza.

Based on previous conceptualizations (Filí *et al.*, 1999; Tujchneider *et al.*, 1998; Tujchneider, Pérez, Paris, & D´Elia, 2005) and the interpretation of lithological profiles and available studies, Paris (2010) developed a conceptual model for the functioning of the

hydrogeological system in the study area, presented in Figure 2. The upper stratum, with a thicken ranging between 15 and 25 m, corresponds to the Pampa Group (plain sediments) (Pleistocene lacustrine-palustrine-eolian) defined by Tujchneider (2000). This is made up of silt, clays and loess which are light maroon, dark, reddish or gray depending on the deposit environment, with the presence of tufa in some levels. A free aquifer is located here with low production and variable quality. The deepest portion, where the sediments have more clay (2 to 3 m thick on average), it behaves as a discontinuous aquitard (Filí *et al*., 1999; Tujchneider *et al*., 1998; Dalla-Costa, Díaz, & Aceñolaza, 2007). The Ituzaingo Formation ("Puelches" sands) is located underneath (fluvial Ploicene) composed of fine, yellow, medium and thick sands with limonitic cover. Thickness: 25-35 m: T = 600 m^2/day. It contains a semi-confined aquifer with good production and quality. The Paraná Formation is underneath (marine Miocene), with a cusp portion, gray sands, sandy clay and green clays, water with high salinity and a depth between 45 and 53 m. Tujchneider *et al*. (2005) reported the behavior of this system to be multi-layer, with the possibility of ascending and/or descending flow through the aquitard depending on the relationships with the prevailing hydraulic load. The extraction of water from the semi-confined aquifer can not only induce flow from the free aquifer above but can also increase the lateral influx of water in the aquifer itself and increase salinity. As a consequence of uncontrolled pumping, the piezometric level decreased considerably in the eastern region in the year 1994 (Tujchneider *et al*., 1998; Paris *et al*., 1999). Two years later, in 1996, these lines varied considerably in their design, translating into an average decrease of roughly 2 m and a dividing line in the equipotential line of 29 m.

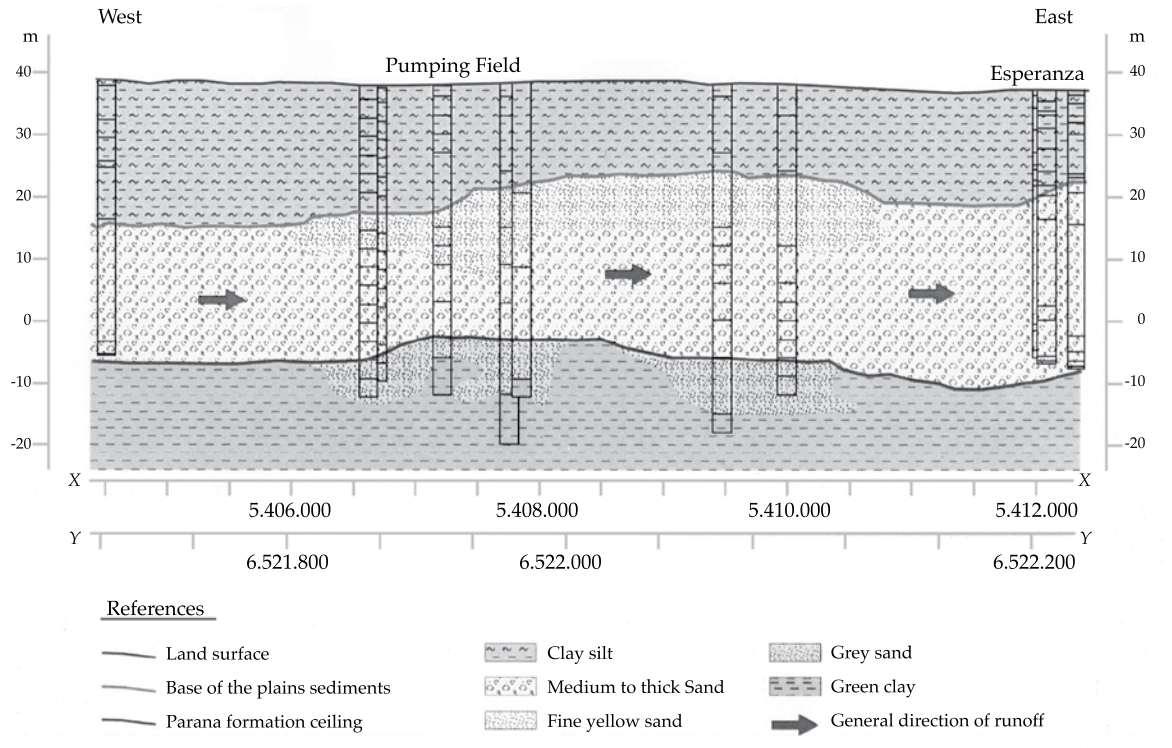

Figure 2. Conceptual model of the functioning of the hydrogeological system in the study area.

By 1999, the levels slowly recovered as a result of changes in the exploitation scheme.

The overall direction of the groundwater flow it west to east. The local recharge in the first level of the aquifer is on the order of 63 mm/year and approximately 18 mm in the second level, through the aquitard. The analysis of INSERTAR Símbolo and INSERTAR Símbolo in groundwater in the groundwater in realtion to the meteoric line shows that the recharge resulting from local precipitation in the summer and autumn months and does not reflect significant evaporation processes. In addition, the tritium values detected indicate that the residence time of the water in the semi-confined aquifer is over 50 years and in the free aquifer represents the mix of sub-modern and recent recharge. In particular, the tritium contents detected in one of the monitoring wells of the semi-confined aquifer suggest the mixing of two aquifer levels. The presence of nitrate would corroborate this situation, which is also favored by the discontinuity of the aquitard (D´Elia, Tujchneider, Paris, & Pérez, 2007; D´Elia, Tujchneider, Paris, Pérez, & Gervasio, 2008). According to previous investigations, the water is sodium bicarbonate (Filí *et al*., 1999; Tujchneider *et al*., 1998; Tujchneider *et al*., 2005). Nevertheless, since the mid 1990s, the water has been observed to have changed to chloride-sodium water in some of the wells in the urban area. And in particular, in the city of Esperanza during the period 1994-1996, the effect of more extraction on the decline in levels and salinity of the water has been demonstrated (expressed in terms of electrical conductivity). Figure 3 shows the changes occurring in water quality in one well that underwent intense extraction. The arrows indicate the substantial change in anion contents resulting from the change in the water type according to the classification by Piper-Hill. Figure 4 presents the increased salinity registered at this observation point over time. The decrease in salinity observed in late 2003 was the result of a change in exploitation according to a new management model (Paris, 2010).

Methodology

The database used consisted of 437 complete records for 8 physio-chemical variables (electrical conductivity EC, total alkalinity TAK, chloride Cl^-, sulfate SO_4^{2-}, nitrate NO_3^-, calcium CA^{2+}, magnesium Mg^{2+}, sodium+potassium Na^++K^+). These records correspond to analytical determinations resulting from samples of water extracted between February 1990 and December 2007 from three sets of wells: a) exploitation wells in the city of Esperanza and the aqueduct of the city of Rafaela (1990 to 2004), b) monitoring wells in the Esperanza district (since 2002), and c) exploitation wells in the new unified pumping field (as of 2004). This database included information from different sources —provincial organizations, companies providing the services, university, among others.

The permissible error in the ionic balance was 10%. This limit was defined based on the salinity values of the water samples.

Multivariate statistical methods (MSM) were used to identify or verify processes that characterize the quality of the water (according to the variables that quantitatively express them) (Furi, Razack, Abiye, Kebede, & Legesse, 2012; Izady *et al*., 2012; Daughney, Moreau-Forunier, Morgenstern, & Raaij, 2012) to determine the degree to which these processes are affected in each of the wells and the periods of occurrence (or temporal variation) (Paris, 2010). To this end, the concentrations are expressed in meq/l, standardized by type according to the Normal Law and normalized using a natural logarithm calculation (Paris, 2005). The volumetric set of data includes:

- The *wells* —refers to the water samples obtained at georeferenced spatial points (observation objects or units);
- *Physical-chemical variables*;
- *Time* —refers to the dates on which the samples were collected.

Figure 5a shows a diagram of the volumetric database and its algebraic representation. It

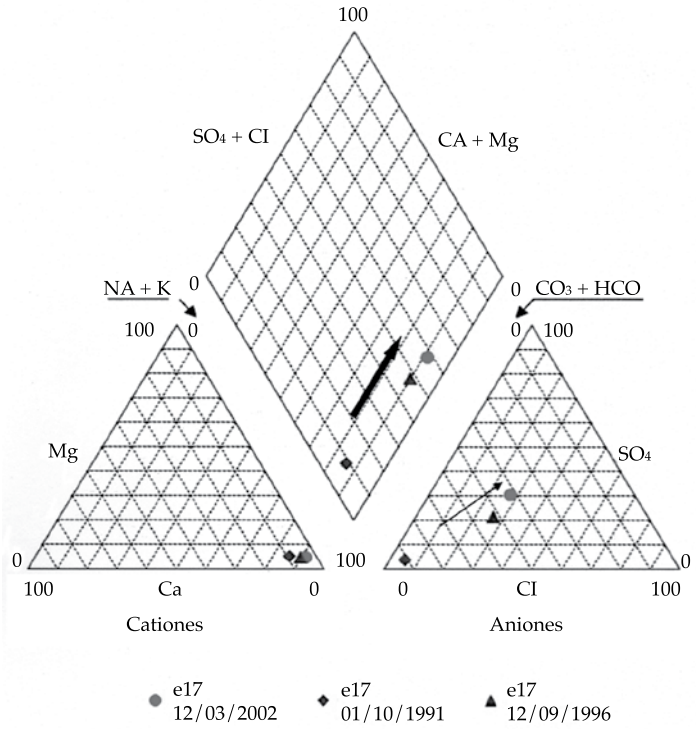

Figure 3. Modifications of water types according to the Piper-Hill classification in well e17.

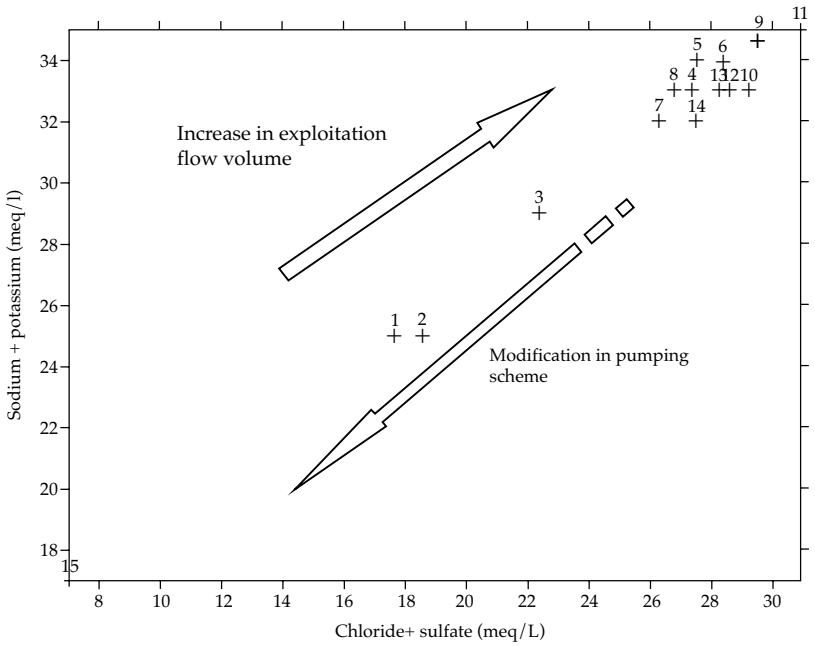

Point	1	2	3	4	5	6	7	8	9	10	11	12	13	14	15
Date	9/1/90	12/1/91	1/1/92	10/1/93	2/1/94	8/1/94	1/1/95	7/1/95	3/7/96	16/5/96	9/12/96	11/7/96	4/1/97	7/2/97	4/12/03

Figure 4. Variations in concentrations of chloride + sulfate *versus* soidum + potassium for well e12.

is notable that the time periods are irregular and the amount of data is not the same. This is because not all of the wells were sampled simultaneously or they were not yet operating and some had been taken out of service. Therefore, the data cube was not "solid" but rather presented "cavities", which can be considerably important depending on the processing method selected.

The processing was performed applying a previous transformation to algebraically define the volumetric base described before in a "data plane" which intrinsically maintains the original dimensions (and, logically, all of the information) (Figure 5b).

This transformation, or "flattening" makes it possible to identify or verify processes that characterize the quality of the water (as a function of the variables that quantitatively express them), the degree to which these processes are affected in each of the wells (thereby determining the areas of occurrence given the wells are spatially georeferenced objects) and establish the periods of occurrence (or temporal variation). It is worth mentioning that, in fact, a complete analysis of the data cubes should include the successive parameterization of each of the dimensions (Paris, 2010), which could result in a tedious implementation and limited interpretation. ON the other hand, the final dimension of the resulting blocks is not adequate in terms of physical and/or algebraic significance, as occurs when few wells or sampled in a time period or when the samples

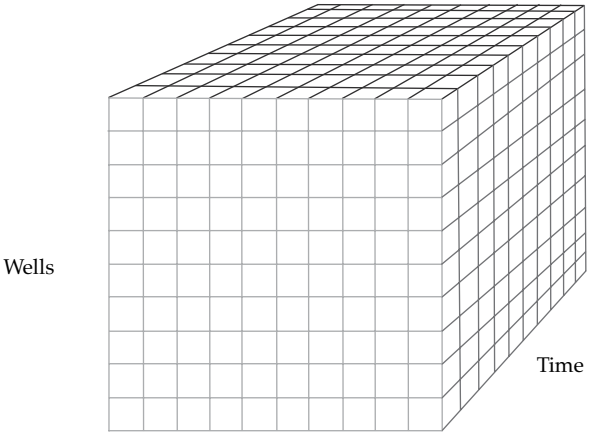

A (*i*, *j*, *k*) $i = 1...N$ $j = 1...M$ $k = 1...P$

a) Outline and algebraic representation of the volumetric data base.

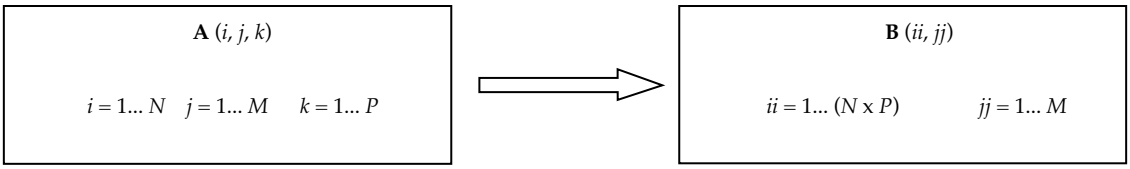

b) Outline and algebraic representation of the conversion to a flat set.

Figure 5. Database, volumetric data and transformation by flattening.

are not collected during the same periods. In addition, the selection of the variable, object or time period poses a significant problem. For example, it is possible to think that if a deterioration in the water quality due to increased salinity is registered, the EC could be the most indicative variables of these changes. Nevertheless, this selection could mask other results or disregard other significant variables.

A hierarchical clustering analysis (CA) was used in R and Q Mode. The measurement of the similarities in the set experimental data is indicated in the R Mode. The similarity matrix was quantified by the correlation coefficient and, in Q mode, by the Euclidean distance coefficient. In both cases, the associations were defined according to hierarchical cluster, by the average of non-weighted pairs as a relationship criterion. The results were validated using the non-hierarchical *K*-Means CA and principal components analysis (PCA) in R and Q Modes. Processing methods with different statistical and mathematical bases were used to decrease the uncertainty in the results caused by mistakes in the definition of the structure of these models (Paris, 2005). The PCA R Mode was also based on the consideration of the correlation matrix. In Q mode, the similarities were quantified with the cosine of theta coeficiente or the proportional similarity index defined by Imbrie and Purdy (1962) (in Jöreskog, Klovan, & Reyment, 1976). The components were retained according to the following criteria: total variance represented (over the threshold of 70%); magnitude and representation of theself-values (value over 1 and/or individual variance over 10%), common value or reconstruction percentage (over 60%); and the self value versus order relation, reflected by the breakpoint in the *scree* diagram. In the non-hierarchical CA, the associations were defined according to the results of the hierarchical CA and the PCA. Finally, graphs of Na^+K^+ vs $Cl^+ + SO_4^{2-}$ were developed with some of the records categorized by group and/or components to complement the interpretation of the results obtained. Three groups reflecting the consequences of the exploitation schemes applied to groundwater quality were defined based on the results of this stage. The statistics were calculated and the fitting to the normal distribution law was evaluated for each of the chemical series. Based on the analysis of this synthetic information, the indicators, their threshold values and warning levels for significant changes in quality were selected.

Results and Discussion

The Mode R cluster analysis demonstrates the strong relationship between CE and Cl^- values, even though the water samples were predominantly bicarbonate (Figure 6). A close relationship is also shown between salinity (expressed by EC) and SO_4^{2-} and $NA^+ + K^+$, which is associated with the sodic nature of the water. This association expresses known increases in Cl^- and SO_4^{2-} ions when the water has higher salinity due to the Kps (product of solubility) of the salts from these anions, especially sodium chloride, whose solubility is independent of the temperature. This group is completed by the Ca^{2+}-Mg^{2+} nucleus (related to the hardness of the water) which with NO_3^- makes up a subgroup. Although pH values are not available related to the acid-alkaline conditions of the medium, nitrification would lead to a decrease in pH, which would favor the dissolution of calcium carbonates and magnesium, with the resulting increase in hardness (Martínez, Bocanegra, & Costa, 1997). TAK is shown to be the only element in the principal remaining group. The CA in Q Mode shows three different principal associations for a cutoff level of 3.5. Due to scale, Figure 6 shows the number of elements (n_i) that make up each level of association (G_i) The groups defined by this statistical hierarchical clustering methodology are compared with those obtained with pCA in R Mode. The associations using this procedure greatly coincide. Three principal components were defined according to the retention criteria for the components mentioned previously.

Figure 7 shows the self values and their variance, represented individually and

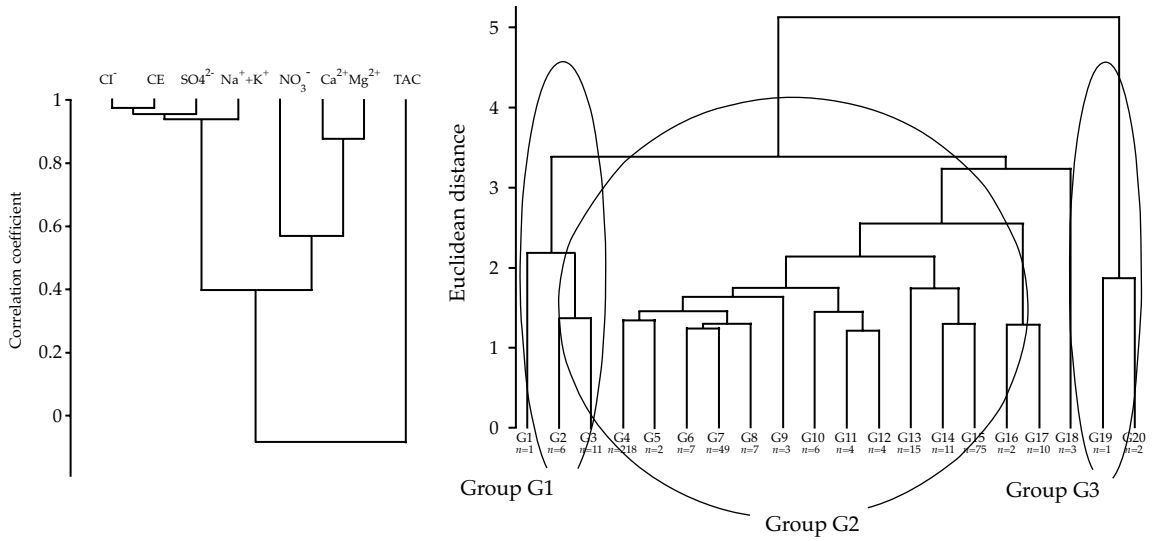

(a) Mode R Dendogram

(b) Mode Q Dendogram

Figure 6. Dendograms.

Self-values and represented variance - PCA Mode R

Order	Self-value	Variance	Total Var
1	4.04	50.55	50.55
2	2.22	27.87	78.42
3	0.89	11.21	89.62
4	0.33	4.16	93.78
5	0.23	2.84	96.62
6	0.14	1.78	98.40
7	0.07	0.92	99.32
8	0.05	0.68	100.00

Principal components load - Mode R

	Comp 1	Comp 2	Comp 3
EC	0.47	-0.12	-0.13
TAK	0.05	-0.43	0.75
Cl^-	0.48	-0.09	-0.13
SO_4^{2-}	0.43	-0.22	-0.29
NO_3^-	0.27	0.35	0.56
CA^{2+}	0.23	0.53	0.05
Mg^{2+}	0.28	0.47	0.07
Na^++K^+	0.40	-0.34	0.07

Graph of *scores* - PCA Mode Q

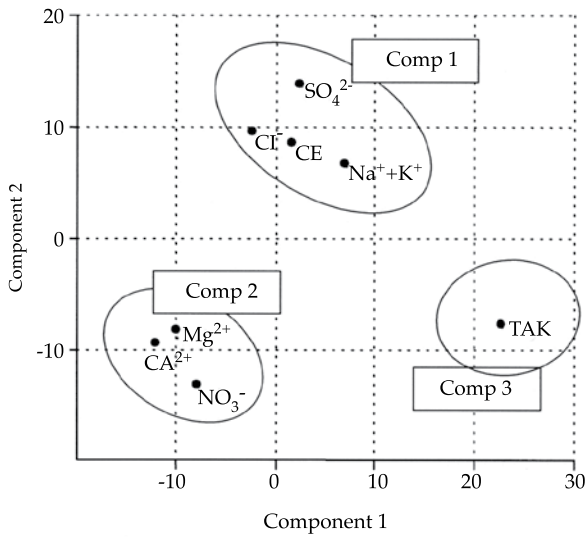

Figure 7. PCA results.

accumulated, as well as the charges that characterize each of the components (Comp) with regard to the chemical variables considered. The values with the largest weight have been shaded in gray. This configuration can also be verified in the graph of the *scores* resulting from the PCA in Q mode for components 1 and 2, shown in the same figure. As can be seen, the conformation of components shows the same association of variables defined by the Mode R CA.

In terms of the association of the records from the wells, Figure 8 represents the records for each one of the three components compared to the associations determined by hierarchical and non-hierarchical clusters (*K*-means). In the case of the PCA, the wells showing evidence of a component being affected have been identified according to the *scores* calculated in Mode R. These affected areas are establish by taking into account the marks above the standard deviation value for each series of *scores* (Lawrence & Upchurch, 1976). This type of graphic representation of the results of the principal components analysis in R Mode is not common, since the *scores* are usually represented by maps in which it is possible to distinguish the areas where the components have the greatest effect as those with values greater than 1 (in some cases all of the positive values are considered).

Given the reasoning related to the "flattening" of the data cubes, a set of maps should be generated (one for each observation period), which would be very difficult to interpret. As was mentioned previously, it is important to take into account that not all of the wells have samples for all the periods, and therefore the density of the information in each map would be very variable and its evaluation very limited. In addition, a comparison with the results from the clusters presented earlier would not be feasible.

Figure 8 indicates that some of the records from the wells are not representative of any of the three components. This is due to the characteristics of the principal components analysis itself, in which the components are selected to ensure the variance threshold represented. This is substantially different than the cluster methodologies which conditioning the association of elements at the selected cutoff level (hierarchical method) or the number of predetermined groups (*K*-Means). Nevertheless, the results are consistent since the records from the most representative wells in each one of the groups coincide.

After performing this crossed validation of the results from the different multivariate statistical methods, Table 1 presents the mean values and central trends for the variables considered, according to the principal groups defined. Group G1 includes the water samples corresponding to the wells with exploitation schedules resulting from high salinity values. For this set, the temporal variation of Cl^{+} $+SO_4^{2-}$ is equivalent to that of $Na^{+}+K^{+}$. The G2 group is composed of the exploitation wells and monitoring wells for periods during which a gradual increase in salinity was observed, although not notable in the EC expression. In this case, the saline contents are modified over time in terms of SO_4^{2-} and $Na^{+}+K^{+}$, while maintaining a Cl^{-} threshold. An increase is also observed in the concentrations of Ca^{2+}. One possible cause for the increase in the ions mentioned may be the increase in chloride-sodium water found in the marine sediments corresponding to the Paraná Formation and the supply of calcium sulfate from the gypsum crystals and calcareous sandy clays from this formation (Iriondo, 2007; Tujchneider, 2000), in the search for equilibrium given the changes in concentrations (an possible pressures) experienced by the system (Principio de Le Châtelier) (Appelo & Postma, 1993). In the G2 group, the concentrations of NO_3^{-} and Mg^{2+} are higher than in group G3, but less than G1. This may indicate the supply of water housed in the overlying free aquifer, especially in the areas where the aquitard could be discontinuous. As previously indicated, the nitrification would produce a decrease in the pH and that would favor the dissolving of calcium carbonates

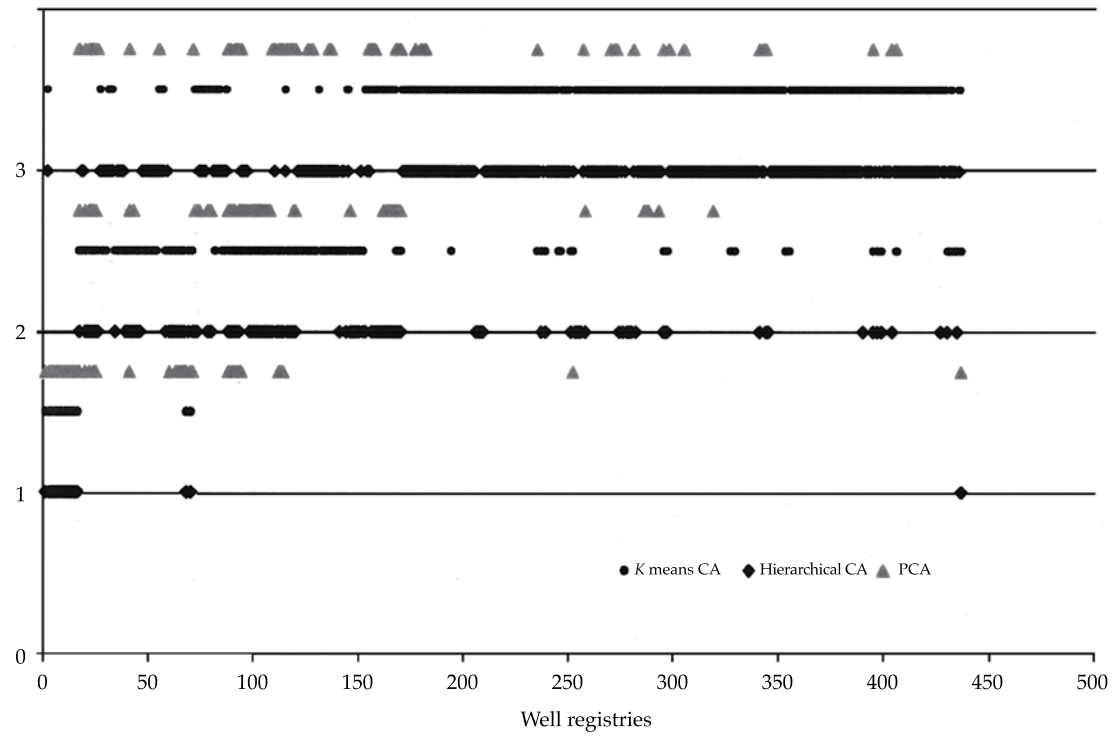

Figure 8. Clusters resulting from hierarchical and non-hierarchical methods (K means) and principal components analysis (Mode R).

and magnesium, with the resulting increase in hardness (Martínez *et al.*, 1997). Group G3 reflects the set of samples of water not yet affected by the salinization process (increase in chloride and sulfate salts). The EC values do not show significant increases with respect to the records from when the wells began to operate, and the temporal changes in the ionic contents are not significant. That is, these groups are different not only because of the increase in the EC (G1 versus G2 and G3) but also because of the increase in the Cl^-, SO_4^{2-}, NO_3^-, CA^{2+} and Mg^{2+} contents. In addition, the three groups identified by the multivariate statistical processing of the chemical series reflect the consequences of the exploitation schemes to which the aquifer was subjected. For example, as a result of the volume of pumping, the same well can have records pertaining to the different groups, as illustrated by well e17 in Figure 9. According to this graph, the temporal states would include the periods 1991-1995, 1995-1999 and 1999-2006. While flow volume records are not available for this period, this chemical behavior is notably consistent with the variations in the piezometric levels described earlier. Therefore, the application of the multivariate statistical methods to identify and verify the rising of the salt water has determined the degree of affectation in each one of the wells and the temporal occurrence.

Accordingly, Groups G1, G2 and G3 include water samples corresponding to the wells, where : a) exploitation schemes that increase salinity have been applied (salinated) (Group G1); b) a gradual increase in salinity has been observed (intermediate state) (Group G2); and c) wells not yet affected by the salinization process (baseline) (Group G3).

The definition of indicators that enable demonstrating early changes in the quality of the water described previously will not

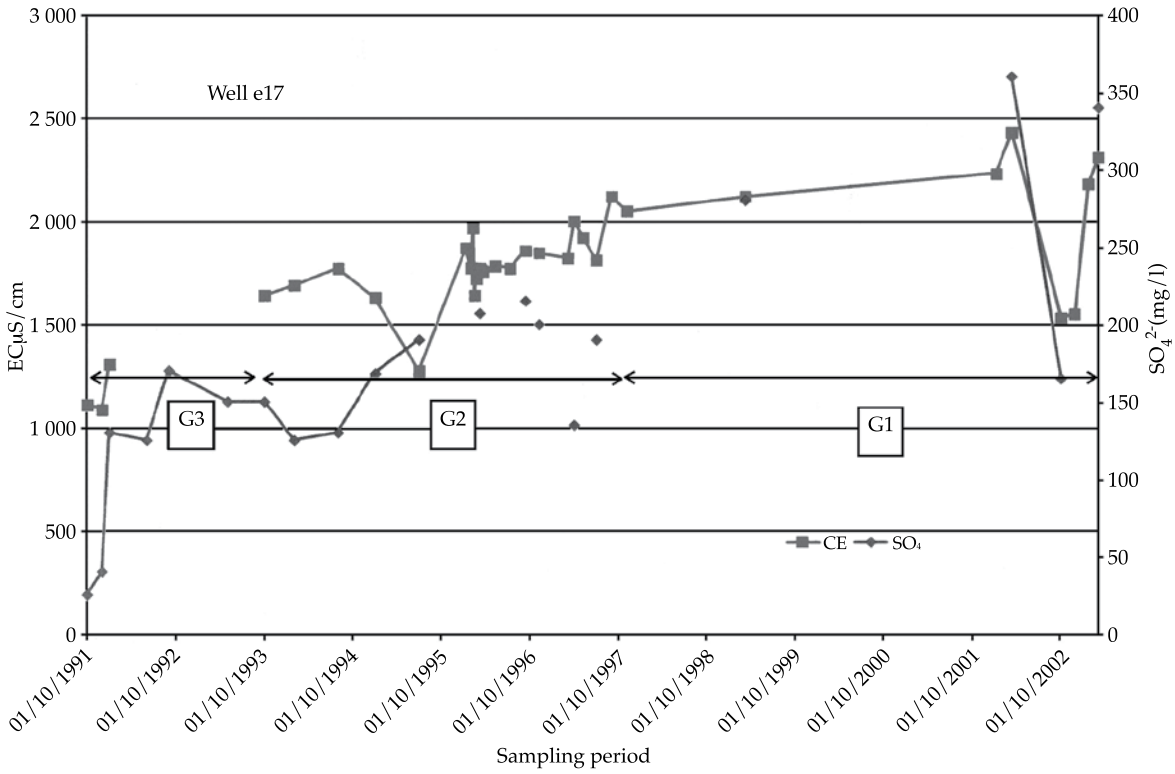

Figure 9. Evolution of EC and $SO_4^=$ in well e17 and its relation with the determined associations.

be proposed. The definition of the indicator should consider the natural base, that is, the values characteristic of the natural composition of the water, based on which the state of the system will be demonstrated —the pressures to which it is submitted and its response. Manzano, Custodio and Nieto (2003) define this natural base of the quality of groundwater as the range of concentrations of a given element, species, or substance in the dissolved phase and derived from natural geological, biological or atmospheric sources. The same authors also mention that the BaSeLiNe (Natural BaSeLiNe Quality in European Aquifers) project decided to operationally adopt the median as the parameter most illustrative of the value that is characteristic of the natural base of groundwater and the percentiles 2.3% and 97.7% to illustrate the range of variation. This ensure that 95.4% of the population studied is within the range. Nevertheless, the same authors indicate that if the statistical distribution is normal or lognormal, the mean or median could be considered characteristic values, though this often does not occur because the quality of the water is the result of more than one process. Investigations performed by Blarasin, Damilano, Cabrera and Matteoda (2006) indicate that the f1 distribution presents a better fit to the empirical distribution and determined an estimator m^* for the natural base, which results from a linear combination of the mean and the median. Nevertheless, they report that the distributions that correspond to the different components need to be studied in more depth if the objective is to determine the natural base using the parametric estimate of the typical concentrations (localization parameters) of each component and its distribution related to these values. The

analysis performed in this aquifer based on the results presented enables defining the indicators of the quality of the water supply, as shown in Table 1b. For this case study, the TAK values are considerably uniform (with a slight increase as the salinity decreases). Therefore, this parameter is not useful to perform a discrimination in the set. While the EC is seen as a variable which is indicative of the rise of water with greater salinity from the Paraná Formation (which is also easy to determine *in situ* and in real-time), the interpretation of the break in the hydrodynamic equilibrium is more eloquently shown when evaluating the relation $Cl^-+SO_4^{2-}$ *versus* NA^++K^+. This is clearly shown in the wells where changes in the salinity of the water begin to be shown (group G2), where SO_4^{2-} and NA^++K^+ are modified but the Cl^- values are maintained. As for the associations among CA^{2+}, Mg^{2+} and NO_3 (the latter also related to TAK), is observed with both the CA as well as the PCA (Mode R), and may indicate supply from the upper (free) aquifer level and pollutant loads from the leaching of livestock wastes and fertilizers in the rural area where the pumping field is located. This situation is more eloquently shown by the higher value of NO_3^- in group G3, primarily made up of samples extract from exploitation and monitoring wells located in the rural area. The threshold value is defined based on the median of group G3 and the warning level for significant changes with the third quartile of group G2. Group G3 describes the baseline conditions of the quality of the groundwater, considering the available information. With respect to EC, its practicality for field and laboratory measurements is evident, and it can actually offer indications of salinization. Nevertheless, as seen in Table 1a, the three quartiles considered do not show differences between groups G3 and G2. Therefore, it is not a parameter for the early warning of the process or for supply from the free aquifer. Values for dry residual (DR) are shown, indicating the regulations for supply of potable water in the Province of Santa Fe (Provincial Law 11220). Table 1c shows the limits established by this norm.

Final considerations

In order to avoid disruptions in the hydraulic equilibrium of a multi-layer aquifer system that supplies to large localities in the province of Santa Fe (Argentina), follow-up should be conducted on the indicators presented in Table 1b. This involves routine chemical determinations which are easily performed and enable demonstrating the relationships among the aquifer located in the "Puelches sands" (semi-confined, where water is extracted for human consumption), the free aquifer located in the plain sediments and the marine salt water in the Paraná Formation.

This investigations has corroborated that, for the case study, the measurement of the electrical conductivity of the water is not sufficient for the early detection of the deterioration in the water resources. The indicators defined acquire solidity and representativeness from the use of different multivariate statistical methods to for the cross validation of the results and, particularly from the support provided by other concrete evidence of the geometry and functioning of the hydrogeological system. The results serve as a basis for different lines of investigation to complement the knowledge about hydraulic relationships among aquifers. Since the vertical descending flow, shown by variations in Ca^{2+}, Mg^{2+} and NO_3^-, can transport pollutants from land uses, through field work and laboratory research, next stages will evaluate the volume of water, per unit area, stored in this layer and which can be released. This will take into account the lithological characteristics of the aquifer, the thickness of the aquitard layer, its presence or absence, and the hydraulic parameters (hydraulic conductivity, transmissivity, storage coefficient, drop factor, etc.). With respect to the transport of pollutants underground, surface runoff characteristics in the rural area near the wells are also considered as well as irrigation practices and the particularities of the natural drainage of the soil. In addition, given the variations detected in

Table 1. Construction of water supply quality indicators.

a) Mean and measured dispersion values for the chemical series, according to group

		EC S/cm	TAK mg/l CO_3Ca	Cl^- mg/l	SO_4^{2-} mg/l	NO_3^- mg/l	Ca^{2+} mg/l	Mg^{2+} mg/l	Na^++K^+ mg/l
Group 1	Mean	3 172.22	515.67	427.56	549.83	19.67	41.61	24.50	682.76
	Deviation	615.29	30.07	127.77	149.02	5.41	14.89	7.37	117.31
	1st quartile	2 535.00	497.50	347.50	406.25	17.25	29.00	17.75	578.03
	Median	3 390.00	515.00	490.00	605.00	21.00	45.00	27.00	747.13
	3rd quartile	3 632.50	528.75	527.50	660.00	22.00	54.00	31.00	758.62
Group 2	Mean	1 388.63	542.79	84.96	94.98	33.26	24.76	13.15	297.93
	Deviation	280.77	48.63	50.26	52.75	32.27	12.37	6.28	70.87
	1st quartile	1 225.00	515.00	38.50	50.00	8.75	17.50	10.00	268.75
	Median	1 399.00	541.00	90.50	100.00	23.50	24.00	13.00	299.50
	3rd quartile	1 540.50	570.00	108.88	135.00	42.00	30.25	16.00	341.96
Group 3	Mean	1 363.25	549.81	69.93	103.99	10.47	13.08	7.82	311.16
	Deviation	161.23	39.71	24.82	34.81	8.69	4.92	2.69	38.88
	1st quartile	1 252.00	520.00	56.00	81.00	6.00	10.00	6.00	288.00
	Median	1 368.00	545.00	68.00	100.00	8.00	12.00	7.00	317.00
	3rd quartile	1 465.00	570.00	80.00	128.05	12.00	16.00	9.00	340.50

b) Indicators of quality of supply water

	CE S/cm	DR(*) mg/l	Cl^- mg/l	SO_4^{2-} mg/l	NO_3^- mg/l	Ca^{2+} mg/l
Threshold	1 368	2 062	68	100	8	12
Warning	1 541	2 335	109	135	42	30

(*) The DR values were estimated as a function of the linear regression function among available data (DR = 1.5853*EC-106.97.

c) Limits established by reference norms for potable water supply

Law 11.220	EC(#) S/cm	DR mg/l	Cl^- mg/l	SO_4^{2-} mg/l	NO_3^- mg/l	Ca^{2+} mg/l
Recommended limit		1 000	250	100	25	100
Mandatory limit		1 500	400	200	45	250

(#) The provincial law does not set limits for EC.

the quality of the water due to the rising of the water from the lower and highly saline aquifer (produced by uncontrolled pumping) and the resulting disruption in hydraulic equilibrium, evaluations will also include pumping tests, water samples, geophysical studies and other field work as well as laboratory analysis of extraction flow volumes. In addition, complementing the chemical and isotopic determinations is considered in order to identify the origin of nitrate supplies in both aquifer bodies.

Acknowledgements

The authors of this work wish to thank the company Aguas Santafesinas, S.A for

providing key information for these investigations.

Received: 17/04/2013
Accepted: 09/11/2013

References

Appelo, C., & Postma, D. (1993). *Geochemistry, Groundwater and Pollution* (536 pp.). Rotterdam: Balkema.

Aureli. A., & Taniguchi, M (contact) (2008). *Groundwater Resources Assessment under the Pressures of Humanity and Climate Changes (GRAPHIC)* (31 pp.). París: UNESCO-IHP.

Blarasin, M., Damilano, G., Cabrera, A., & Matteoda, E. (septiembre, 2006). Hidrogeoquímica del acuífero freático en un agroecosistema y consideraciones sobre el cálculo de la línea de base de la calidad del agua (25 pp.). *Actas* del *VIII Congreso Latinoamericano de Hidrología Subterránea*, Asunción, Paraguay.

Blarasin, M., Cabrera, A., Matteoda, E., Damilano, G., & Giuliano-Albo, J. (2008). Indicadores para evaluar cambios ambientales en acuíferos. Consideraciones sobre el fondo natural de la calidad de agua. En M. Cantú, A. Becker, & J. Bedano (Eds.). *Evaluación de la sustentabilidad ambiental en sistemas agropecuarios* (pp. 69-80). Río Cuarto, Argentina: Editorial UNRC, Río Cuarto.

Berger, A. R., & Iams, W. J. (Eds). (1996). *Geoindicators: Assessing Rapid Environmental Change in Earth Systems* (466 pp.). Rotterdam: A. A. Balkema.

Bocanegra, E., Massone, H., Irutig, M., Cionchi, J., & Panizos, M. (2009). *Indicadores de gestión de los recursos hídricos subterráneos en Mar del Plata, Argentina y su comparación con otras ciudades latinoamericanas* (pp. 113-132). VI Congreso Argentino de Hidrogeología. Taller sobre Planificación y Gestión de las aguas subterráneas, Santa Rosa, La Pampa.

Dalla-Costa, O., Díaz, E., & Aceñolaza, B. (2007). *El aporte de las testificaciones geofísicas en sondeos en el esquema hidrogeológico del campo de bombeo de Esperanza. Provincia de Santa Fe* (pp. 35-42). D. Sosa & J. Ainchill (Comp.). Taller de Geofísica aplicada a la Hidrogeología. V Congreso Argentino de Hidrogeología, Paraná, Entre Ríos, Argentina, del 16 al 19 de octubre.

Daughney, C., Moreau-Forunier, M., Morgenstern, U., & Raaij, R. (2012). Use of Hierarchical Cluster Analysis to Assess the Representativeness of a Baseline Groundwater Qualitu Monitoring Network: Comparison of New Zealand´s National And Regional Groundwater Monitoring. *Hydrogeology Journal, 20*, 185-200.

D´Elia, M., Tujchneider, O., Paris, M., & Pérez, M. (2007). *Evaluación de la recarga a los acuíferos en un sector del centro de la Provincia de Santa Fe* (pp. 479-488). R. Díaz, J. Tomás, M. Santi, M. D´Elia, & O. Dalla-Costa (Comp.) Libro del V Congreso Argentino de Hidrogeología, Paraná, Entre Ríos.

D´Elia, M., Tujchneider, O., Paris, M., Pérez, M., & Gervasio, S. (noviembre, 2008). Groundwater Recharge Assessment Using Environmental Tracing Methods. En *Libro de resúmenes y CD Rom*. V International Conference on Tracers and Tracing Methods-Tracer 5, Minas Gerais, Brasil.

D´Elia, M., Tujchneider, O., Paris, M., Pérez, M., & Pusineri, G. (2012). Acuífero de la cuenca baja del río Salado (Argentina). Metodologías de análisis y aplicación de tecnologías para el manejo sostenible de acuíferos en zonas rurales (58 pp.). En L. Ribeiro, T. Betancour, & M. D´Elia (Eds.). Lisboa: CYTED-Programa Iberoamericano de Ciencia y Tecnología para el Desarrollo.

Doménico, P. (1972). *Concepts and models in Groundwater Hydrology* (405 pp.). Minnesota: McGraw-Hill.

Filí, M., Tujchneider, O., Paris, M., Pérez, M., & D´Elia, M. (1999). *Estudio del sistema de aguas subterráneas en el área de Esperanza-Humboltd y zona de influencia. Servicio Especializado de Asistencia Técnica*. Informe Final 163. Convenio Aguas Provinciales de Santa Fe y la Universidad Nacional del Litoral. Inédito. Santa Fe de la Vera Cruz, Argentina.

Foster, S., & Loucks, D. (Eds.). (2006). *Non-Renewable Groundwater Resources: A Guidebook on Socially-Sustainable Management for Water-Policy Makers* (97 pp). IHP-VI, Series on Groundwater, 10. París: UNESCO.

Furi, W., Razack, M., Abiye, T., Kebede, S., & Legesse, D. (2012). Hydrochemical Characterization of Complex Volcanic Aquifers in a Continental Rifted Zone: The Middel Awash Basin, Ethiopia. *Hydrogeology Journal, 20*, 385-400.

Hirata, R., & Rebouças, A. (1999). La protección de los recursos hídricos subterráneos: una visión integrada, basada en perímetros de protección de pozos y vulnerabilidad de acuíferos. *Boletín Geologico Minero de España, 110*(4), 423-436.

Iriondo, M. (2007). El chaco santafesino. Neógeno y geomorfología. *Comunicación del Museo Provincial de Ciencias Naturales Florentino Ameghino, Santa Fe, Argentina, 13*(1), 39.

Izady, A., Davary, K., Alizadeh, A., Ghahraman, B., Sadeghi, M., & Moghaddamnia, A. (2012). Application of "Panel-Data" Modeling to Predict Groundwater Levels in the Neishaboor Plain, Iran. *Hydrogeology Journal, 20*, 435-447.

Jöreskog, K., Klovan, J., & Reyment, R. (1976). *Geologycal Factor Analysis*. Amsterdam: Elsevier Scientific Publishing Company.

Lawrence, F., & Upchurch, S. (1976). Identification of Geochemical Patterns in Groundwater by Numerical Analysis. *Advances in Groundwater Hydrology* (pp 199-214.). Minneapolis: American Water Resources Association.

Manzano, M., Custodio, E., & Nieto, P. (2003). El fondo natural de la calidad del agua subterránea (pp. 607-620). En: *Memorias I Seminario Hispano-Latinoamericano sobre Temas Actuales de la Hidrología Subterránea* 2, Rosario, Argentina.

Martínez, D., Bocanegra, E., & Costa, J. (1997). Significado de la correlación $pH/NO_3^-/Ca^{2+}/Mg^{2+}$ en aguas subterráneas de loa provincia de Buenos Aires (pp. 193-210). En: *Actas I Congreso Nacional de Hidrogeología*, Bahía Blanca, Argentina.

Paris, M., Tujchneider, O., Pérez, M., D´Elia, M., & Fili, M. (julio, 1998). El conocimiento del sistema hidrogeológico y desarrollo sustentable de una región. Área de caso: Ciudad de Esperanza (Provincia de Santa Fe-República Argentina (pp. 197-199). En: *Actas I Simposio sobre Planificación, Gestión y Economía de los Recursos Hídricos El Agua en el 2000*, Santa Rosa, La Pampa.

Paris, M., Tujchneider, O., D´Elia, M., Pérez, M., & Fili, M. (agosto, 1999). Estudio de la interacción entre el sistema hídrico subterráneo y las actividades industriales de la ciudad de Esperanza (Provincia de Santa Fe, Argentina). Primera fase (pp. 80-89). En: *Anales XVII Congreso Nacional del Agua y II Simposio de Recursos Hídricos del Cono Sur*. Tomo III, Santa Fe, Argentina.

Paris, M. (2005). *Análisis Estadístico Multivariado*: *Métodos y Aplicaciones en Hidrología Subterránea* (251 pp.). Tesis de Maestría en Ingeniería de los Recursos Hídricos. Santa Fe de la Vera Cruz, Argentina: Facultad de Ingeniería y Ciencias Hídricas, Universidad Nacional del Litoral.

Paris, M. (2010). *Métodos estadísticos multivariados aplicados en Hidrología Subterránea* (173 pp). Tesis de doctorado en Ciencias Geológicas. Facultad de Ciencias Exactas, Físico-Químicas y Naturales, Universidad Nacional de Río Cuarto. Río Cuarto, Córdoba, Argentina.

Pernia-Llera, J., Lambán-Jiménez, L., & Molinero-García, A. (2005). *Indicadores e índices sobre el estado cuantitativo de las aguas subterráneas en función del nivel piezométrico. Aplicación al acuífero de la Sierra de Estepa* (pp. 843-853). En J. López-Geta, J. Rubio, & M. Martín-Machuca (Eds.). VI Simposio del Agua en Andalucía, IGME.

Tóth, J. (2001). Las aguas subterráneas como agente geológico: causas, procesos y manifestaciones. *Boletín Geológico y Minero*, *111*(4), 9-26.

Tujchneider, O., Paris, M., Fili, M., D´Elia, M., & Pérez, M. (noviembre, 1998). Protección de aguas subterráneas. Caso de estudio: ciudad de Esperanza (República Argentina). Primera fase: diagnóstico del sistema (pp. 805-821). En *Memorias IV Congreso Latinoamericano de Hidrología Subterránea*. Volumen 2. Montevideo, Uruguay.

Tujchneider, O. (2000). *Sistemas hidrogeológicos en áreas de llanura: cuenca inferior de los Saladillos, Provincia de Santa Fe*. Tesis doctoral. San Miguel de Tucumán, Argentina: Universidad Nacional de Tucumán, Facultad de Ciencias Naturales e Instituto Miguel Lillio.

Tujchneider, O., Pérez, M., Paris, M., y D´Elia, M. (octubre, 2005). Deterioro de fuentes de agua subterránea por ascenso de agua salada (pp. 217-226). En: *Actas IV Congreso Argentino de Hidrogeología*, Río Cuarto, Córdoba, Argentina.

Vrba, J., & Lipponen, A. (Eds.). (2007). Groundwater Resources Sustainability Indicators. Groundwater Indicators Working Group UNESCO, IAEA, IAH. IHP-VI. UNESCO. *Series on Groundwater*, *14*, 123.

Webb, B., Hirata, R., Kruse, E., & Vrba, J. (2006). *Sustainability of Groundwater Resources and Its Indicators* (205 pp). París/ Wallingford, UK: IAHS Press, Institute of Hydrology.

Institutional Address of the Authors

Dra. Marta Paris
Dra. Ofelia Tujchneider
Dra. Marcela Pérez
Dra. Mónica D´Elia

Facultad de Ingeniería y Ciencias Hídricas
Universidad Nacional del Litoral
Ciudad Universitaria
Ruta Nacional 168, km 472
43000 Santa Fe, Argentina
Teléfono: +54 (575) 2333 945, extensiones 150 y 164
parismarta@gmail.com
pichy@fich.unl.edu.ar
maperez@fich.unl.edu.ar
mdelia@fich.unl.edu.ar

Click here to write the autor

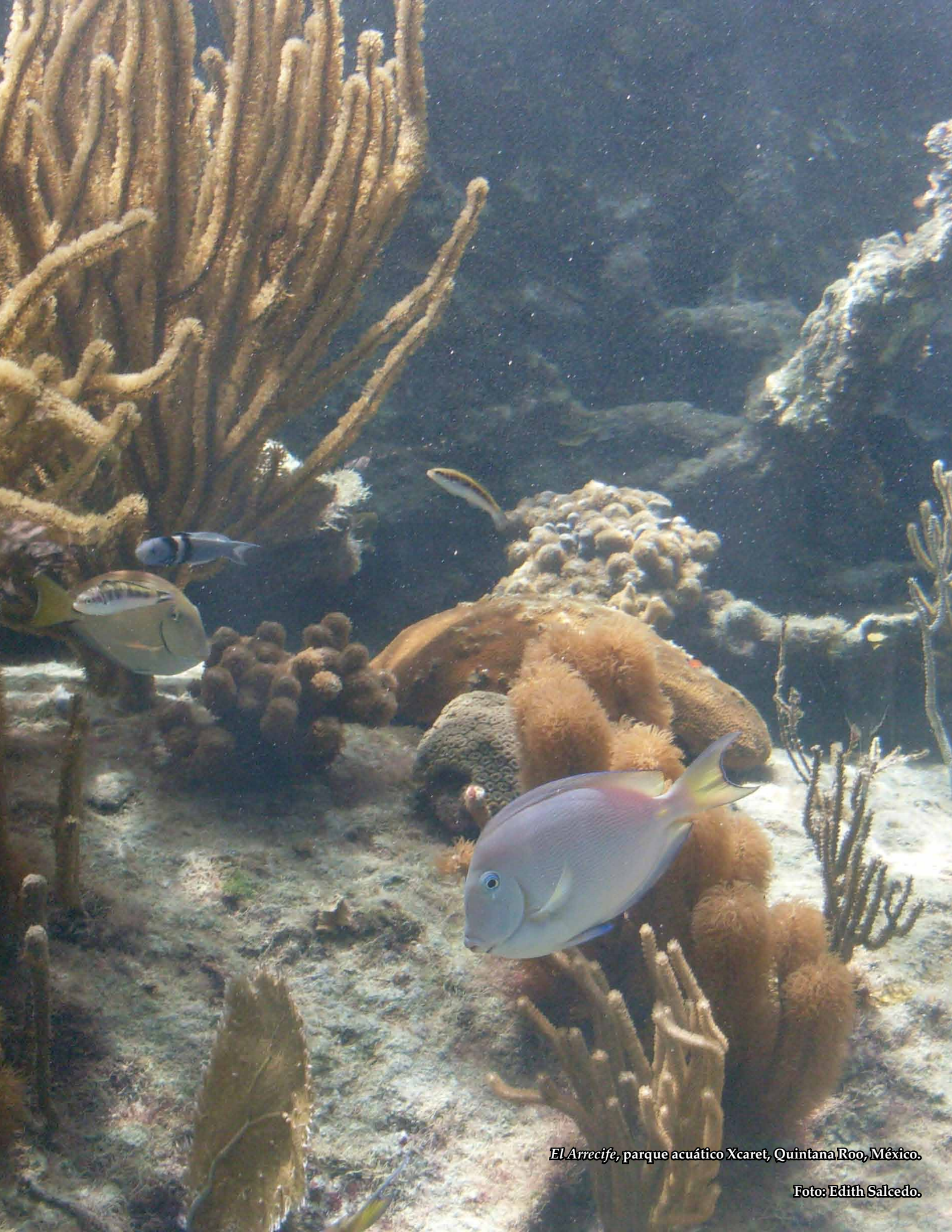

El Arrecife, parque acuático Xcaret, Quintana Roo, México.

Foto: Edith Salcedo.

Application of an Integrated Water Quality Index in the Argentine Andean Piedmont

• Emilie Lavie* •
Universidad Paris-Diderot, Francia
*Corresponding Author

• José A. Morábito • Santa E. Salatino •
Instituto Nacional del Agua, Argentina

Abstract

Lavie, E., Morábito, J. A., & Salatino, S. E. (July-August, 2014). Application of an Integrated Water Quality Index in the Argentine Andean Piedmont. *Water Technology and Sciences* (in Spanish), *5*(4), 23-37.

This paper presents the results from the application of the Water Quality Index (WQI) developed by the Canadian Council of Ministers of Environment in order to synthetically and graphically characterize water quality in large basins using a set of biological, physical and chemical parameters. This index allows the investigator to choose the parameters that are most important in a zone and that are also representative of the different water uses. This study presents the results obtained from an irrigation water quality database pertaining to two watersheds in the Argentine Andean foothills. The parameters and limits considered are based on those proposed by the General Irrigation Department of the province of Mendoza, an international agency (FAO), French water agencies (AE) and the country of Morocco whose environment is very similar to that of the one analyzed. It is concluded that the methodology leads to an overvaluation of the WQI Factor 1 and makes it possible to a) manipulate the results by including more / less favorable parameters in the construction of the index; b) modify this factor to decrease its weight in the calculation of the index and c) compare water quality among different irrigation sites and / or catchment basins, regardless of the limits detected.

Keywords: Irrigation, Mendoza, pollution, water quality index.

Resumen

Lavie, E., Morábito, J. A., & Salatino, S. E. (julio-agosto, 2014). Aplicación de índices integradores de calidad hídrica al piedemonte andino argentino. Tecnología y Ciencias del Agua, *5(4), 23-37.*

Este trabajo presenta los resultados de la aplicación del Water Quality Index (WQI) del Canadian Council of Ministers of Environment, con el objeto de caracterizar de manera sintética y gráfica la calidad del agua, considerando un conjunto de parámetros biológicos, físicos y químicos en grandes cuencas. Este índice deja a criterio del investigador la elección de aquellos parámetros que resulten importantes para la zona y que además sean representativos de los distintos usos del agua. Se presentan aquí los resultados obtenidos a partir de una base de datos de calidad de agua de riego de dos cuencas del piedemonte andino argentino, considerando diferentes parámetros y límites sugeridos por el Departamento General de Irrigación de la provincia de Mendoza, un organismo internacional (FAO), las agencias de agua (AE) francesas y un país como Marruecos, cuyo entorno medioambiental es muy similar al analizado. Se concluye que la metodología lleva a una sobrevaloración del Factor 1 del WQI y permite a) manipular los resultados al incluir en la construcción del índice parámetros más/menos favorables; b) modificar dicho factor para disminuir su peso en el cálculo del índice, y c) no obstante todas las limitaciones detectadas, resulta útil para la comparación de la calidad del agua entre distintos sitios y/o cuencas regadías.

Palabras clave: *índice de calidad del agua, riego, contaminación, Mendoza.*

Introduction

Previous works by Singh, Malika, Mohan, & Sinha (2004) and Simeonov *et al*., (2003), Boyacıoğlu, Gündogdub, & Boyacıoğlu (2013) state that surface waters are the sources of water most vulnerable to pollution because they are easily accessible to wastewater discharges. Together, natural processes as well as anthropogenic influences determine the quality of surface water. In addition, the combination of aridity, which favors the salinization of soils and water,

and the presence of urban centers with highly dense populations that generate significant industrial and agricultural activities makes the Andean piedmont of Mendoza, Argentina, one of the most vulnerable environments in the world (along with Teheran in Iran, Damascus in Syria and Urumqi, China).

In order to evaluate the impact of human activity on the water resources in the different oases in the Argentine depression (Figure 1), researchers from the National Water Institute and the School of Agrarian Sciences at the UNCuyo, based in Mendoza, have been performing physical, chemical and biological monitoring of the water in the Mendoza and Tunuyan Rivers basins. While the results obtained (Morábito *et al*., 2005, 2007 y 2009; Lavie, 2009; Lavie, Morábito, Salatino, Bermejillo, & Fillipini, 2010) are interesting, the parameters have only been analyzed individually and it has not been possible to present a simple cartography to those responsible for water management that makes it possible to see —in an integrated manner— the spatial variation in the quality from the sources of pollution to the furthest locations, for the different water uses (domestic, urban and agricultural irrigation and industrial uses). This would make it possible to propose new legal frameworks adapted to the real situation with pollution, modifying the existing regulations.

The objective of this study is to present a graphic representation of the quality of water for both basins using an integrated index that includes the set of physical, chemical and biological parameters registered in the existing database and also analyze the differences in the results obtained when applying the proposed water quality index. As a result of an exhaustive literature search, the Water Quality Index by the Canadian Council of Ministers of Environment (CCME) was chosen. This index has the advantage of allowing the investigator to select the parameters that are important in the region and representative of the different water uses. For example, the bacteriology may not be included in an index used to analyze the quality of irrigation water, while it would be indispensable to evaluate the quality of water used for human and/or animal consumption. Likewise, salinity could be a secondary parameter to evaluate rivers located in wet regions where rainwater is a key supply source for agriculture, while it would be a central parameter for the case of water used for irrigation in the Cuyo oasis region.

Given the above and based on an irrigation water quality database (river and channel networks), this work presents a discussion of the results obtained with the following four integrated quality indices:

1. WDI-DGI index defined based on the critical values (maximum permissible limits) proposed by the General Department of Irrigation (DGI, Spanish acronym) of the province of Mendoza.
2. WQI-FAO index selected given the importance of this international organization in all areas of agriculture.
3. WQI-AE, chosen among the indices used in the UE and defined according to the criteria from the capacity guide for the quality of water used in irrigation, by the French water agencies (AE).
4. WQI-MA, in order to compare the results obtained in the oasis of Mendoza with those from Morocco, whose environment is very similar.

Scientific Context and Methodology

Water Quality Index (WQI)

Constructing a synthetic index for global/integral water quality is not an easy task since the relevant parameters are different from one region to another (for example, mineralization). Therefore, defining an index that contains only one certain group of parameters is not an entirely rational criterion. On the other hand, it could be interesting to include parameters based on a particular water usage. Since all

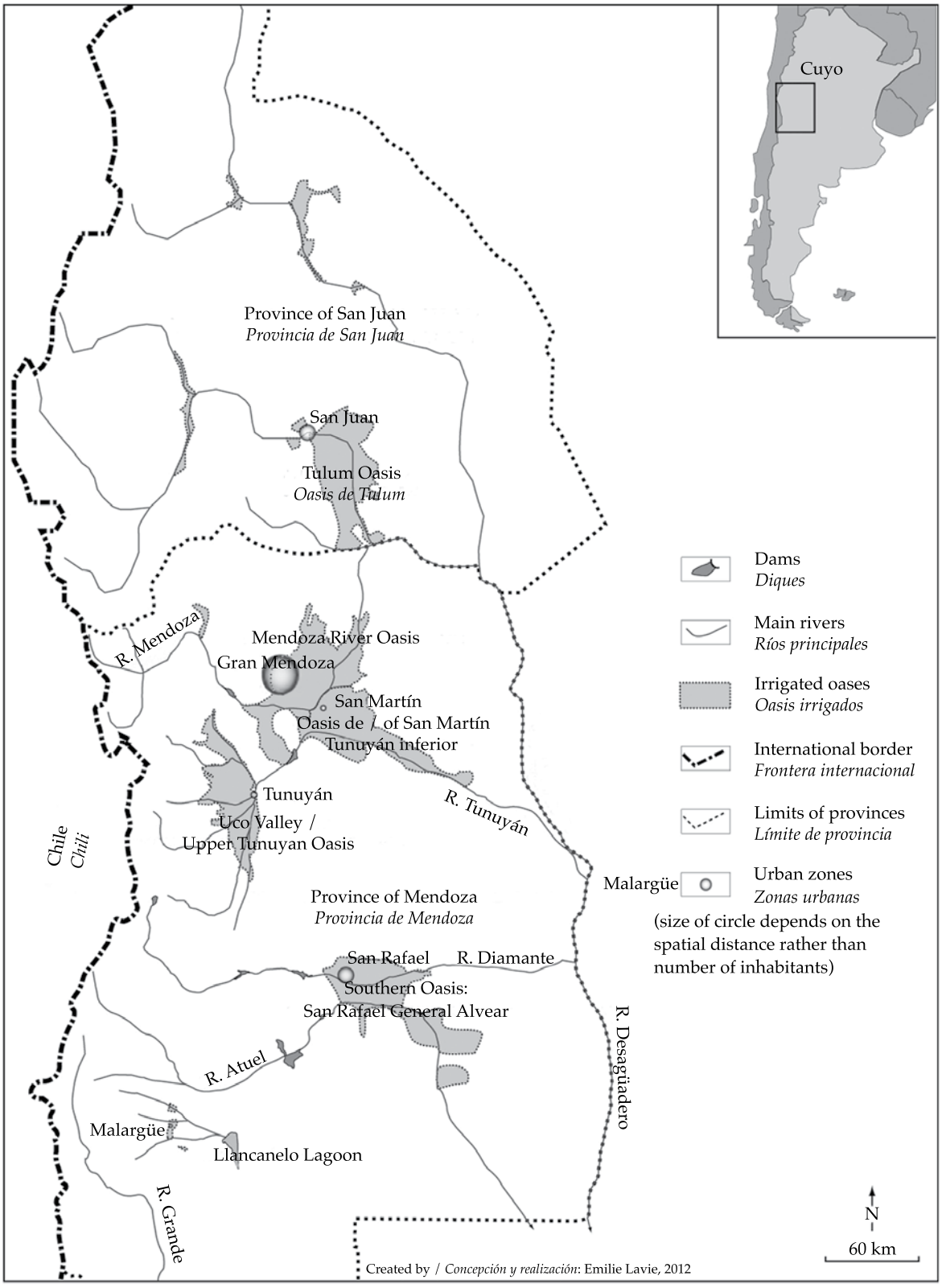

Figure 1. The oases in the Cuyo depression.

humans have a the same vulnerability with respect to water, a global water quality index could be proposed that would be applicable to human, animal and domestic uses. It would be more difficult to construct an index to evaluate the quality of water for irrigation since the various crops react differently to the negative impact of the different parameters (for example, salinity or toxic ions). Nevertheless, different classifications have been proposed worldwide, such as those by the FAO, for example (Ayers & Westcot, 1994).

During the literature review, global water quality indices were analyzed, such as the *SEQ-eau* by French agencies (Agences de l'eau); the Biologique Global Normalisé index (IBGN); the Afnor 1992 guideline (in Archaimbault & Dumont, 2010) used to rate the biological quality of rivers; the *Indice de Qualité Physique et Chimique* (IPQB) (Hébert, 2005) and its equivalent in Quebec, Canada; and the *Water Quality Index* by the United States Washington State Department of Ecology (Hallock, 2002). In addition, Chang, Chen, & Ning, 2001; Kumar and Alappat, 2004; Pesce and Wunderlin, 2004; Boyacioğlu, 2007; Boyacioğlu *et al.*, 2013; Singh, Nath, Prasad and Nema, 2008, and Golge, Yenilmez and Aksoy, 2013 have made some interesting contributions to the application of integrated water quality indices.

The present work selected the *Water Quality Index* by the Canadian Council of Ministers of Environment (CCME, 1999; Alberta Environment, 1995; Hébert, 2005; Khan, Tobin, Paterson, Khan, & Warren, 2005; Lumb, Halliwell, & Sharma, 2006; Guzmán-Colis *et al.*, 2011). This choice was based in part on the use of this index being practical in the absence not only of a database with only biological data (as in the majority of the indices cited) but also physical-chemical data. Another reason is the advantage it offers by permitting the investigator to choose the parameters to be included in the index, based on well-founded reasons. Other indices analyzed use fixed parameters that are not representative in the case of their application to the Andean situation, which is characterized by intense agricultural use. It is important to note that the WQI cannot be used globally since it would not be possible to compare with other similar ones obtained for other basins. Nevertheless, it does make it possible to propose synthetic sub-indices corresponding to the particular objective (Hébert, 2005; Khan *et al.*, 2005).

For the selection of the *Water Quality Index*, the authors proposed the following seven stages:

1. The selection of parameters important to rivers, the environment and human use.
2. Establishing objectives to increase water quality requirements (adoption of pollution regulations, for example).
3. Determining comparable registry dates (that the databases for the different rivers have identical temporal scales).
4. Calculation of the percentage of parameters that do not meet the prefixed target levels (F1 factor):

$$F1 = \left(\frac{\text{Number of parameters that do not meet desirable levels}}{\text{Number of total parameters}} \right) \times 100$$

5. Calculation of the percentage of results that do not meet prefixed target levels (factor F2):

$$F2 = \left(\frac{\text{Number of results that do not meet desirable levels}}{\text{Number of total results}} \right) \times 100$$

6. Calculation of factor F2, in stages:

a) The magnitude observed in the tests of each of the deviations not in accordance:

$$\text{Deviation}_i = \left(\frac{\text{Value of the result outside target level}_i}{\text{Desirable level}_j} \right) - 1$$

b) Divide the sum of these deviations by the total number of results:

$$snce = \frac{\sum_{i=1}^{n} \text{deviation}_i}{\text{Total number of results}}$$

c) Calculate factor F3:

$$F3 = \left(\frac{snce}{0.01\, snce + 0.01} \right) \times 100$$

7. Calculation of the WQI (values between 0 and 100):

$$WQI = 100 - \left(\frac{\sqrt{F1^2 + F2^2 + F3^2}}{1.732} \right)$$

Based on the WQI, the Canadian Council of Ministers of Environment (CCME) determined five categories for classifying water from a particular river (Table 1).

The Context of the Cuyo Rivers

In the region of Cuyo (Argentina), the depression between the Andes (west) and the Cordoba and San Luis mountains (east) (Figure 1) is an arid-semiarid region where agricultural and urban development is possible only because of the existence of the Andes' rivers which are supplied by glaciers located at roughly 6 000 masl. Since before colonization, these rivers were diverted for agricultural irrigation and domestic use (agro-alimentation). Anthropic activity in the arid region of Cuyo is concentrated in a half dozen of "oases." Some of the largest are the North Oasis (Mendoza and lower Tunuyan Rivers, approx 2 000 km^2) and the Centro Oasis (upper Tunuyan River, roughly 1 000 km^2). The latter is also known as the Valley of Uco, where the largest expansion of cultivated area over the last 20 years has occurred for the purpose of high quality viniculture (cv Malbec).

The Mendoza and Tunuyan river basins are supplied by the melting of Andean glaciers, rainfall mostly in summer, and especially by the melting of snow accumulated in the central Andes, the latter constituting the majority of the volume (85%) (Abraham *et al.*, 2007). Both rivers converge in irrigated plains composed of their respective alluvial fans forming the North Oasis of Mendoza (Mendoza and lower Tunuyan Rivers). The upper Tunuyan River and its systems of rivers and tributaries make up the Centro Oasis and the irrigated region known as the Valley of Uco (some 100 km south of the city of Mendoza), location of the departments of San Carlos, Tunuyan and Tupungato. In the Centro Oasis, the irrigated agricultural area is located upstream from three cities, outside of the area of urban and industrial anthropic effects. The North Oasis, in the irrigation area located downstream, receives the full impact of the anthropic pollution produced by the population in Gran Mendoza (more than 1 million inhabitants) and its industries (Figure 2). No less important is the fact that part of the surface water infiltrates into the recharge areas and feeds the respective underground aquifers which are also vulnerable to pollution.

Table 1. Water quality categories according to WQI (CCME, 1999).

Rating	WQI Range	Definition
Excellent	95-100	Water quality is very close to natural or desirable levels
Good	80-94	Water quality is rarely different than natural or desirable levels
Acceptable	65-79	Water quality is sometimes different than natural or desirable levels
Marginal	45-64	Water quality is often different than natural or desirable levels
Poor	0-44	Water level is almost always different than natural or desirable levels

Database (INA-UNCuyo)

The Andean Regional Center (Centro Regional Andino (CRA, Spanish acronym)) of the National Water Institute (INA, Spanish acronym), in conjunction with the School of Agrarian Sciences (FCA, Spanish acronym) of the National University of Cuyo (UNC, Spanish acronym) have been monitoring the quality of water through monthly sampling (since 2003 in the Mendoza River and 2007 in the upper Tunuyan River). There are therefore 5 years of sampling in common for the two rivers (2007-2011), totaling 10 monthly records per year. (In winter (June and July) the irrigation network does not supply water and most of the crops are dormant, so cleaning and maintenance is performed on the channels. Samples are not taken in January as well, during summer vacation). The points included in the databases corresponding to the sampling sites were selected to characterize the quality of the irrigation water and to identify the possible causes of pollution.

Eight points were selected from the Mendoza River (Figure 2) —three in the river (RI, RII and RIII) and five in the irrigation channel network (CI through CV). Point RI corresponds to the site where the waters from the Mendoza River are diverted towards the irrigation oasis (base value). Virtually no water circulates in the river between that point and point RII located in the middle of the basin at the level of the resurgence of the aquifer supplying the river. Point RIII corresponds to the outlet of the oasis and a treatment plant for domestic discharges (Paramillos) is located between the two points (RII and RIII), which occasionally produces discharges.

In terms of the network of channels, point CI is located downstream from the Gran Mendoza (final point of the Cacique Guaymallén channel-collector) and serves as a reference for CII (the Campo Espejo treatment plant is located between these two points, with occasional discharges into the irrigation network) and for CV (the Pescara drain collector for industrial discharges enters between these two points). Point CIII corresponds to the end of the network and was recently revetted. It has very low vulnerability to anthropic pollution and the quality of its water is similar to that of RI. Lastly, CIV, located on the right banks of the river, is the only point which receives pollution only from agriculture (fertilizers, compost and phytosanitary products).

Four sampling points were selected in the Tunuyan River: point LT, the highest, on the Las Tunas dike in the Las Tunas River, a tributary of the Tunuyan; point VU, Valley of Uco dike at the inlet to the oasis on the upper Tunuyan River; point Y, the Yaucha Stream and point A, the Aguanda Stream. Sixteen percent of the available volume in the Valley of Uco dike is diverted to the upper sub-basin for irrigation (50 000 ha in the region known as the Valley of Uco). The rest is stored downstream in the El Carrizal dike and used to irrigate the lower sub-basin (lower Tunuyan River, 84 000 ha of irrigation) which contains vid, stone, fruits and vegetable crops (Chambouleyron *et al*., 2002). Downstream from the agricultural sectors is the city of Tunuyan. Most of the water from the river and the streams mentioned is concentrated here, in addition to that from the resurgence of the phreatic aquifer. The sampling sites selected here were Costa Anzorena (CA) located before the river enters the El Carrizal Reservoir and the Tiburcio Benegas (TB) dike, at the diverter located downstream from the El Carrizal dike. The area of influence of the lower Tunuyan River is composed of irrigated land in eastern Mendoza.

The registries from the databases correspond to the following parameters:

1. Physiochemical and heavy metals: pH, electrical conductivity at 25°C (EC), chemical oxygen demand (COD), sodium adsorption ratio (SAR), chlorides, sodium, potassium, calcium, magnesium, carbonates and bicarbonates, nitrates, phosphates, phosphorus, lead, copper, zinc and chromium (the latter was only analyzed for the Mendoza River). Records also exist of

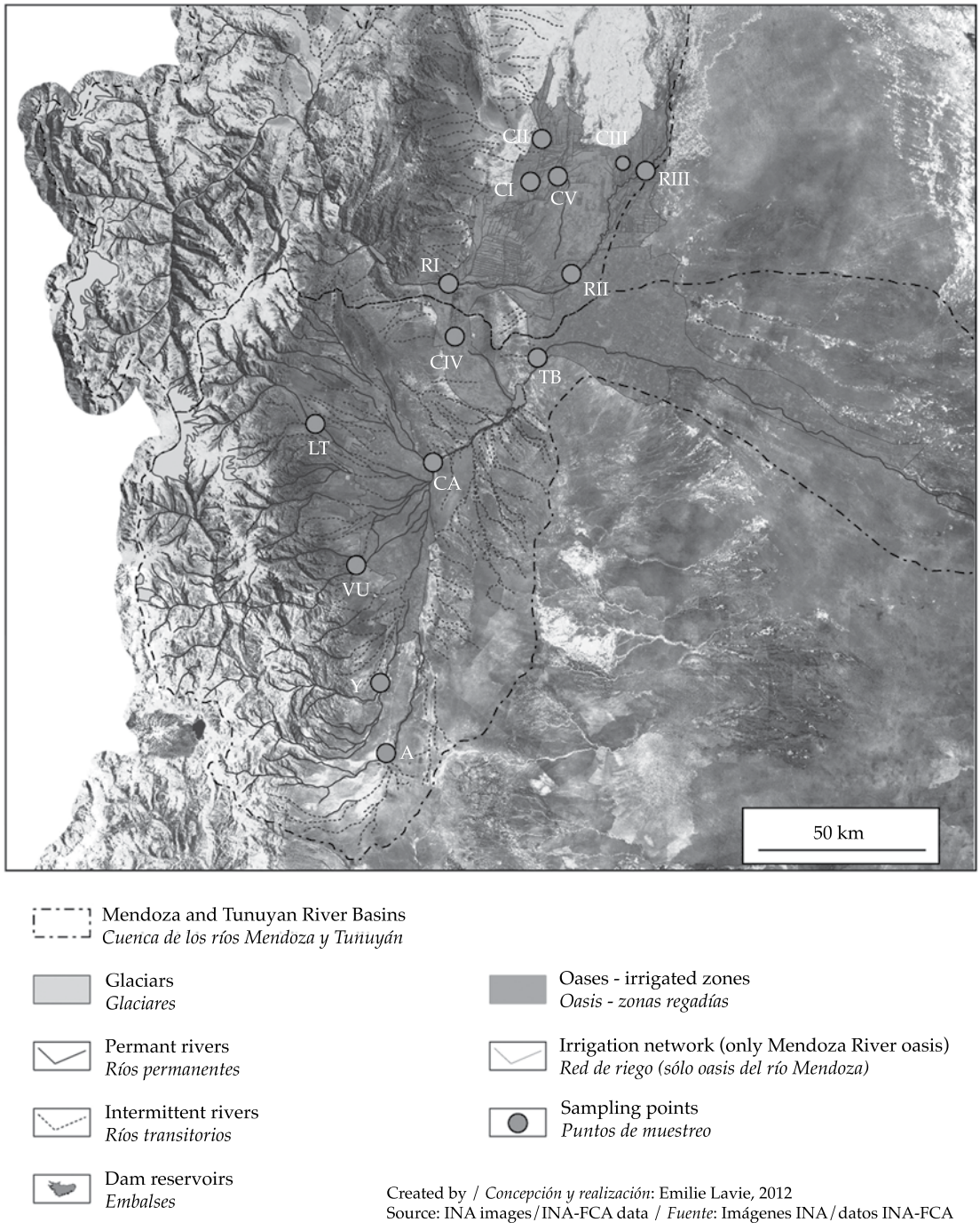

Figure 2. Mendoza and Tunuyan River Basins: geography and sampling points.

10-minute sedimentable solids (SS10), total solids (TS), total fixed solids (TFS) and total volatile solids (TVS).

2. Biological: dissolved oxygen (DO), mesophilic aerobic bacteria (MAB) and coliforms (total and fecal).

Water temperature and flow were also measures in all the samplings.

Water Quality Indices (WQI)

Given the number of studies about synthetic qualitative indices and limits, norms and recommendations, it is difficult to propose a scientifically acceptable index. This work presents the use of the WQI (CCME) method corresponding to several classification objectives. The original purpose was to obtain an index of the capacity of irrigation water for agricultural uses according to the available database. In the province of Mendoza, the water is managed by the General Irrigation Department (DGI, Spanish acronym). The existing regulation (Resolution 778/96) establishes maximum limits (permissible and tolerated) for discharges into the irrigation network and was therefore chosen as a reference (WQI-DGI). In order to compare the results, the indices developed based on FAO (WQI-FAO) recommendations by the French Water Agencies (WQI-AE; MEDD and Agences de l'Eau, 2003) were selected. Lastly, there was interest in applying an existing norm from a country with a very similar environment, in which there is a large amount of irrigation, such as Morocco (WQI-MA, Ministry of Energy, Water and Environment, SEEE, 2007, available online).

WQI-DGI

Table 3 presents the parameters selected by the French water agencies (AE) to construct the WQI. Different classifications exist in France with various permissible limits depending on the different water uses (irrigation, human consumption, animal, etc.)

WQI-AE

El cuadro 3 permite analizar los parámetros seleccionados por las agencias del agua de Francia (AE) para la construcción del WQI. En este país existen distintas clasificaciones, cuyos límites permitidos varían en función de los distintos usos del agua (riego, consumo humano y animal, etcétera).

WQI-FAO

The WHO has also developed water quality recommendations for water for human use, and the FAO has proposed quality guidelines for irrigation. These recommendations are more difficult to use than official national norms since they are composed of three guidelines having different limits: use without restriction, use with restrictions (low to high) and not possible to use (Ayers & Westcot, 1994). Since the water in Mendoza is naturally saline, the guidelines for low to high restrictions was chosen to construct the WQI-FAO, in which the limits are quite high and therefore the quality of the rivers would be *good*. It is worth noting that, with the exception of pH, only mineralization is considered. There is no mention of biological parameters, heavy metals or solids (Table 4). The SAR has not been taken into account since it would be necessary to select a limit for each level of electrical conductivity and changing the limit is not possible using the methodology.

WQI-MA

The parameters used to calculate the index proposed based on the Moroccan norms (Table 5) includes bacteriology (fecal coliforms), salinity (electrical conductivity, chlorides, sodium and sulfates), heavy metals (lead, copper and zinc) and a physical parameter of the temperature (it appears that turbidity is not used in this country).

It is not feasible to include all the databases used to calculate the WQI since approximately 750 samples are available with 6 to 12 parameters having been analyzed, depending on the index. Table 6 shows the parameters, results and factors used to calculate the WQI-DGII and the resulting rating.

Table 2. WQI-DGI Parameters and limits.

Parameters	Unit	Selected limit
Temperature	°C	30
pH	-	6.5 - 8.2
Electrical conductivity (EC)	µS/cm a 25 °C	900
Sodium Adsorption Relation (SAR)	-	6
Sodium (Na^+)	mEq/l	6.52
Chlorides (Cl^-)	mEq/l	5.65
Sulfates (SO_4^{2-})	mEq/l	5.21
Nitrates (NO_3^-)	mEq/l	45
Phosphates (PO_4^{3-})	mEq/l	0.4
Fecal coliform	u/100 ml	200
Chemical oxygen demand (COD)	mg/l O_2	75
Sedimentable soidum in 10 min	ml/l	0.5

Reference: Resolution 778/96 of the DGI contains maximum allowable and tolerable limits. For the WQI-DGI, only the former was used.

Table 3. WQI-AE parameters and limits.

Parameters	Unit	Selected limit
Dry solid residuals at 105 °C	mg/l	3 500
Chlorides (Cl^-)	mEq/l	19.77
Lead (Pb)	mg/l	2
Copper (Cu)	mg/l	5
Zinc (Zn)	mg/l	5
Total coliform	u/100 ml	1 000
Fecal coliform	u/100 ml	100

Results

The cartographic representation of the two study basins —Mendoza and Tunuyan Rivers— shows the values of the WQI index obtained based on the Canadian CCME methodology and calculated based on the different parameters registered in the database corresponding to measurements of the rivers and the channel network (Figures 3a to 3d).

Figure 3a (WQI-DGI) corresponds to the index obtained based on discharge norms and it appears to be of some concern. While the quality of 4 of the 5 points located upstream of the anthropic activities is *excellent* to *good*, the quality at VU is only *acceptable* even though the anthropic pressure it receives is minimal. Point LT only has one parameter over the limits (phosphates), and the points having *good* quality (RI, A and Y) have two high parameters each. The points with *acceptable* quality (CI, CII, VU, CA and TB) correspond to sites with medium pollution levels and have 5 parameters (phosphates, fecal coliforms, sulfates, SAR and EC) that exceed the permissible limits proposed by the DGI for discharges. Points CV and RIII are very polluted and have *poor* quality, with 5 to 6 parameters having very high values (all the above plus COD and solids). The WQI-DGI index enables distinguishing between points with few problematic parameters and those with many quality problems. Nevertheless, its application involves a possible overrating of factor 1 (percentage of parameters outside the limits).

The WQI-DGI shows the impact of the anthropogenic activities on the water quality very well, with the exception of point VU,

Table 4. WQI-FAO parameters and limits.

Parameters	Measurement unit	Limit selected
pH	-	6.5 - 8.4
Electrical conductivity (CE)	µS/cm at 25 °C	3 000
Chlorides (Cl^-)	mEq/l	10
Sodium (Na^+)	mEq/l	9
Nitrates (NO_3^-)	mg/l	30
Bicarbonates (HCO_3^{--})	mEq/l	8.5

Table 5. WQI-MA parameteres and limits.

Parameters	Measurement unit	Limit selected
Temperature	°C	35
pH	-	6.5 - 8.4
Electrical conductivity (CE)	µS/cm at 25 °C	12 000
Chlorides (Cl^-)	mg/l	9.9
Sodium (Na^+)	mg/l	3
Sulfates (SO_4^{2-})	mEq/l	5.2
Lead (Pb)	mg/l	5
Copper (Cu)	mg/l	2
Zinc (Zn)	mg/l	2
Fecal coliform	u/100 ml	1 000

which has fecal coliforms and high salinity in the basin —due to the presence of extensive livestock and the natural supply of sulfates (from the presence of gypsum in the basin), respectively. Sites CI, CII (in the Mendoza River) and CA and TB (in the Tunuyan River) have been classified as *acceptable* quality and the quality at points CV and RIII —victims of domestic and industrial discharges— is *marginal*, although together their volumes make up less than 20% of the water at RI. It is worth clarifying that sites RII, CIII and CIV have not been included in the analysis because they do not have records of nitrates or phosphates (and therefore are not comparable). The results show an increase in EC, phosphates and bacteriology as the water travels downstream, which can be attributed to industrial, agricultural and urban activities registered in the area. In the Tunuyan River, the index does not reflect an improvement in quality between sites CA (before the reservoir) and TB (diverter dike in the lower basin), in spite of the decantation and dilutions occurring in the El Carrizal dike. On a spatial level, the values of the WQI-DGI index show differences in the anthropic impact upstream and downstream and coincide with that found by Morábito *et al*. (2005, 2007 and 2009), Lavie (2009), Lavie, Morábito, & Salatino (2008) and Lavie *et al*. (2010) .
ábito, & Salatino (2008) y Lavie *et al*. (2010).

The results obtained with the WQI-AE (Figure 3b) had fewer contrasts. Two points have *excellent* quality (LT and RI with ratings of 98 and 99/100, respectively), no parameters exceeded the limit selected and 5 points had *good* quality (VU, A, Y, TB and CIII) with ongoing problems with total and fecal coliforms but with relatively low values. This bacteriological presence could be caused by the livestock activity upstream from points Y, A and VU, and by other occasional sources of pollution affecting lower points in both basins (TB and CIII). The remaining points have *acceptable*

Table 6. Model table used to determine the WQI: results from WQI-DGI.

Site	Factor 1			Factor 2			Factor 3				WQI	Range
	Number of parameters that did not comply with the maximum level	Total number of parameters	Factor 1: % of parameters not in complaince with the maximum level	Number of results not in compliance with the maximum level	Total number of results	Factor 2: % of results not in complaince with the maximum level	Sum of the standard deviation of results not in compliance	Total number of results	Magnitude (cfc)	Factor 3: magnitude of deviation of the test values from the maximum levels		
RI	2	12	**16.7**	103	431	**23.9**	26.3	431	0.06	**5.8**	83	Good
RIII	5	12	**41.7**	129	262	**49.2**	701.4	262	2.68	**72.8**	62	Marginal
CI	5	12	**41.7**	147	391	**37.6**	990.1	391	2.53	**71.7**	67	Acceptable
CII	5	12	**41.7**	190	445	**42.7**	818	445	1.84	**64.8**	65	Acceptable
CV	7	12	**58.3**	213	446	**47.8**	87 686	446	196	**99.5**	56	Marginal
Final value for the Mendoza River											67	Acceptable
VU	5	12	**41.7**	137	438	**31.3**	143.9	438	0.33	**24.7**	70	Acceptable
LT	1	12	**8.3**	28	425	**6.6**	22.7	425	0.05	**5.1**	94	Good
A	2	12	**16.7**	48	452	**10.6**	232.9	452	0.52	**34.0**	88	Good
Y	2	12	**16.7**	45	451	**10.0**	48.3	451	0.11	**9.7**	89	Good
CA	5	12	**41.7**	154	445	**34.6**	616.4	445	1.39	**58.1**	68	Acceptable
TB	4	12	**33.3**	133	392	**33.9**	254.4	392	0.65	**39.4**	72	Acceptable
Final value for the Tunuyan River											80	Good

quality with bacteriological problems (with higher values) and are located downstream from the domestic and industrial discharges (CI, CII, CV, CA, RII and RIII). In this case, the presence of sulfates is not the determinant, but rather the weight of 2 of the 7 bacteriological parameters included in constructing the index (fecal coliforms are included in total coliforms and therefore its weight in factor 1 is doubled). Factor 1 seems to play an important role in the calculation, while factors 2 and 3 (which take into account the percentage of each record and the amount that exceeds the permitted limit) indicate the points with real pollution resulting in the water classification changing from *good* to *acceptable*.

To construct the WQI-FAO, the "light to moderate" restriction was chosen since the limits corresponding to "use without restrictions" would have resulted in a *poor* classification. Nevertheless, the result obtained was not sufficiently satisfactory given that all the sites were classified as *excellent* water quality (even CII and CV in the Mendoza River), as can be seen in Figure 3c. Actually, and empirically known by the famers, the Mendoza water is suitable for irrigation and have some restrictions in certain sectors. The WQI-FAO is the index which most highlights the importance of the selection of maximum limits and of the parameters used in its calculation.

Lastly, the WQI-MA (Figure 3d), constructed based on the Moroccan norms, makes it possible to see a clear distinction in water quality between the sampling sites affected and those not affected by anthropic pressures. Two points do not have any problematic parameters and are classified as *excellent* quality —LT (99/100) and Y (100/100). The points located upstream of the anthropic activity (VU, A and RI) or those

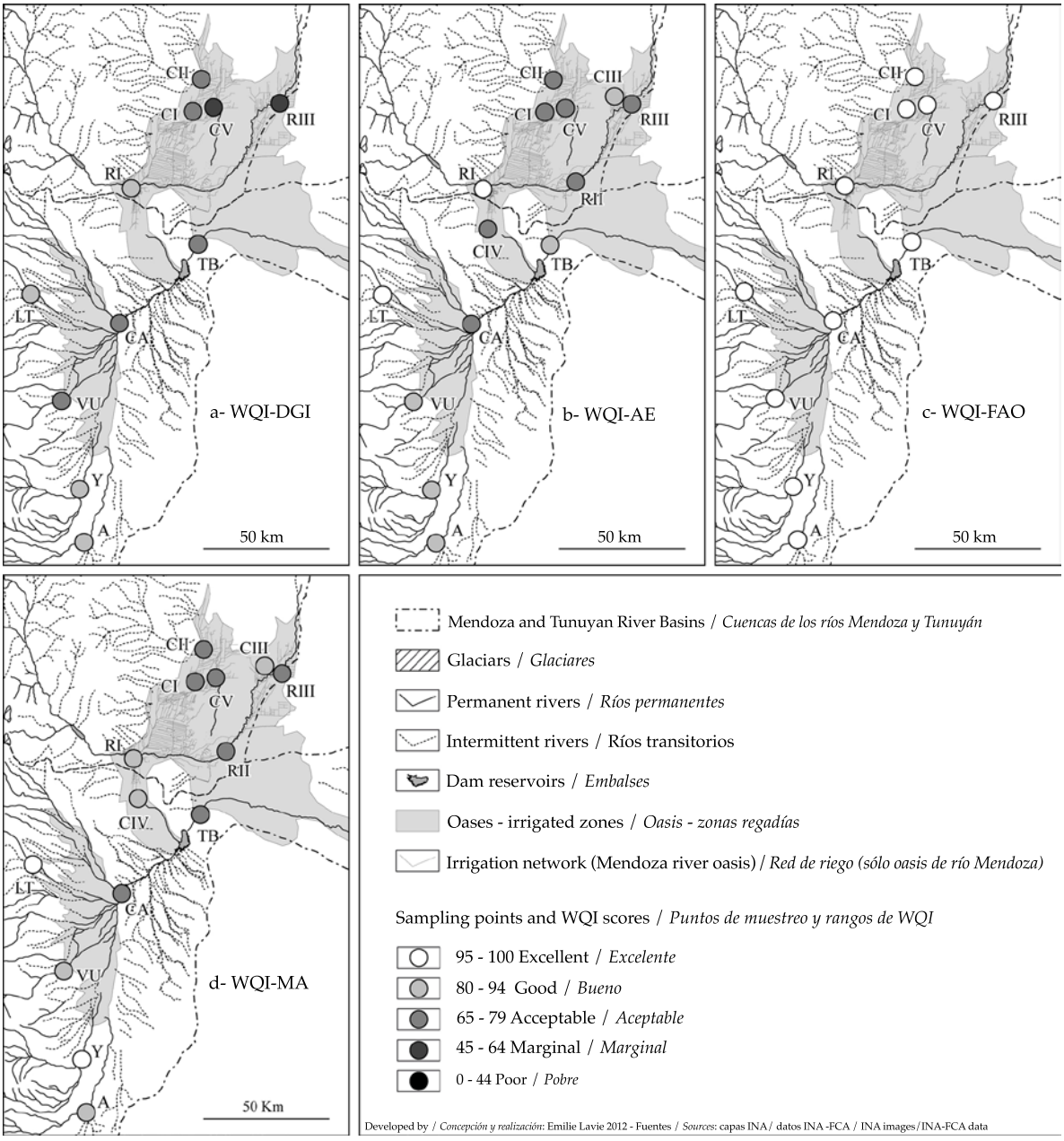

Registries corresponding to sites RII, CIII and CIV were not included in the WQI-DGI and WQI-FAO, since nitrate and phosphate data were not available.

Figura 3. Rangos de WQI para cada punto de muestreo.

protected from pollution (CIII and CIV) have only 1 or 2 high parameters (salinity, sulfates and/or sodium and/or fecal coliforms) and are classified as *good* quality. The remaining points, located downstream of anthropic activities, have sulfates, sodium and fecal coliforms and therefore were classified as *acceptable* quality. The parameters chosen for this index are very well balanced —heavy metals, mineralization and bacteriology (even though solids are not included). Nevertheless, as in the other indices, the WQI-MA shows a clear overrating of factor

1, as was reported by Hebert (2005). In the case of the Mendoza basins, the WQI-MA index better reflects the difference between water in the upper portion (with virtually no anthropic activity) and that in the lower portion (with the greatest impact from the different uses). Nevertheless, two exceptions exist —sites CIII and CIV which do not receive industrial or urban pollution, even though they are located in the oasis of the Mendoza River, and receive only agricultural discharges with *good* quality water. Therefore, it can be stated that the index developed based on the Moroccan norms permits higher levels of urban and industrial pollution.

Discussion

The use of the methodology proposed to classify the water in the Mendoza and upper Tunuyan Rivers provides results that confirm values and trends found in previous studies. It also enables distinguishing differences in quality between the sites located upstream (sources) with nearly no anthropic pollution from those downstream with records of higher pollution levels. While the selection of the parameters for constructing the proposed index (WQI) affects the final result, it enables the investigator to combine them so that the characterization of the water is most similar to the reality of each case study.

The results of the present work coincide with those obtained by authors such as Hebert (2005), in which the calculation clearly reflects factor 1 (number of problematic parameters) rather than the difference between the results and the maximum limits of the parameters. As can be seen from the results obtained, the selection of the parameters is highly related to the weight of factor 1 in the calculation of the quality index (duplication of microbiological pollution from combining fecal and total coliforms and/or from the impact of sodicity when adding the SAR variable to the sodium cation). In addition, if the calculation of the index includes parameters that do not represent a decrease in quality, no matter how much the parameters are multiplied by themselves, factor 1 will be bounded, which will result in an index with a higher quality even if the water quality is actually lower.

Conclusion

One of the objectives of the study was to identify a way in which to synthetically present a set of qualitative parameters that enable classifying the quality of water for irrigation in the areas of influence of the Mendoza and upper Tunuyan Rivers. The use of spatial cartography was also proposed to complement the presentation of previous results based on the visualization of the temporal variation and the size of the records for each parameter in the databases. As was highlighted by Boyacıoğlu *et al*. (2013), the CCME's WQI "showed that information produced based on water quality data variation and correlations can be of great value for water managers to develop realistic action plans." In fact, an interesting contribution by our work can be seen in Figure 3. A manager, administrator or investigator can quickly see the spatial variation in quality in a graphic form, as well as the importance of the selection of the parameters and the limits that best represent the reality of the basin, in accordance with the use of the water to be evaluated.

After selecting the *Water Quality Index* (WQI) proposed by the Canadian Council of Ministers of Environment (CCME), which allows the investigator to select the parameters involved according to their importance to each specific case study and the maximum permissible limits (norms) desired, it was possible to compare the classifications resulting from the application of four different indices. Based on the results, it can be concluded that the methodology overrates factor 1 and makes it possible to manipulate the results by including in the construction of the index the parameters most and least favorable to defining a class of water. Thus, Hebert (2005) proposes modifying

this factor (replacing it with a middle value between factors 1 and 2) decreasing its weight in the calculation. Regardless of all the limitations detected, the methodology is useful to compare the quality of the water among different sites and/or basins in irrigation regions.

Acknowledgements

Assisting in this article: Rocío Hernández Rosa Medina, Susana Miralles, Cora Dediol, Silvia Andre, Susana Campos, Alicia Stocco, Dora Genovese, José Maffei, Leandro Mastrantonio, Adriana Bermejillo and María F. Filippini of the School of Agrarian Sciences, National University of Cuyo, Argentina. We would also like to thank Víctor Burgos and Noelia Ortiz for their support with applying the GIS.

Received: 04/10/12
Accepted: 29/10/13

References

Abraham, E., Abad, J., Lora-Borrero, B., Salomón, M., Sánchez, C., & Soria, D. (Mayo, 2007). Caracterización y valoración hidrológica de la cuenca del río Mendoza mediante elaboración de modelo conceptual de evaluación. *Actos del Congreso Argentino del Agua (*14 p.) Tucumán: Comisión Nacional del Agua.

Alberta Environment (1995). *Alverta River Water Quality Index*. Recuperado de http://environment.alberta.ca/177.html#methodology.

Archaimbault, V., & Dumont, B. (2010). L'indice Biologique Global Normalisé (IBGN), principes et évolution dans le cadre de la Directive cadre européenne sur l'eau. *Sciences, Eaux et Territoires*, *1*, 36-39.

Ayers, R. S., & Westcot, D. W. (1994). Water Quality for Agriculture. Publication for FAO. *FAO Irrigation and Drainage Paper*, *29*(rev. 1). Recuperado de http://www.fao.org/DOCREP/003/T0234E/T0234E00.HTM.

Boyacioğlu, H. (2007). Development of a Water Quality Index Based on a European Classification Scheme. *Water SA*, *33*, 101-106.

Boyacioğlu, H., Gündogdub, V., & Boyacioğlu, H. (2013). Investigation of Priorities in Water Quality Management Based on Correlations and Variations. *Marine Pollution Bulletin*, *69*, 48-54.

CCME (1999). Recommandations canadiennes pour la qualité de l'eau. Recuperado de http://www.ec.gc.ca/ceqg-rcqe/English/ceqg/water/default.cfm#agr.

Chang, N., Chen, H. W., & Ning, S. K. (2001). Identification of River Water Quality Using the Fuzzy Synthetic Evaluation Approach. *Journal of Environmental Management*, *63*, 293-305.

Golge, M., Yenilmez, F., & Aksoy, A. (2013). Development of Pollution Indices for the Middle Section of the Lower Seyhan Basin (Turkey). *Ecological Indicators*, *29*, 6-17.

Guzmán-Colis, G., Thalasso, F., Ramíres-López, E. M., Rodríguez-Narciso, S., Guerrero-Barrera, A. L., & Avelar-González, F. J. (2011). Evaluación espacio-temporal de la calidad del agua del río San Pedro en el Estado de Aguascalientes, México. *Revista Internacional de Contaminación Ambiental*, 89-102.

Hallock, D. (2002). A Water Quality Index for Ecology's stream Monitoring (17 pp). Internal publication No. 02-03-052. Washington: Washington State Department of Ecology. Recuperado de http://www.ecy.wa.gov/biblio/0203052.html.

Hébert, S. (2005). *Comparaison entre l'indice de la qualité générale de l'eau du Québec (IQBP) et l'indice de qualité des eaux du CCME (IQE) pour la protection de la vie aquatique, Québec, ministère du Développement durable, de l'Environnement et des Parcs, Direction du suivi de l'état de l'environnement* (11 pp). Envirodoq no ENV/2005/0265, Collection n°QE/170. Montral: Ministerio del Desarrollo Sustentable. Recuperado de http://www.mddep.gouv.qc.ca/eau/eco_aqua/vie-aqua/Comparaison.pdf.

Khan, A. A., Tobin, A., Paterson, R., Khan H., & Warren R. (2005). Application of CCME Procedures for Deriving Site-Specific Water Quality Guidelines for the CCME Water Quality Index. *Water Quality Research Journal of Canada*, *40*(4), 448-456.

Kumar, D., & Alappat, B. J. (2004). Selection of the Appropriate Aggregation Function for Calculating Leachate Pollution Nindex. *ASCE Pract. Period. Hazard. Toxic Radioact. Waste Management*, *8*, 253-264.

Lavie, E. (2009). *Activités anthropiques et qualité de l'eau dans l'oasis de Mendoza (Argentine) : diagnostic, enjeux et durabilité* (385 pp). Tesis de doctorado en Geografía. Burdeos: Universidad de Burdeos.

Lavie, E., Morábito, J. A., & Salatino, S. E. (2008). *Problèmes de pollution phosphatée de l'eau d'irrigation en zones aval d'oasis : le cas de la quatrième zone agricole irriguée de l'oasis du rio Mendoza, Argentine*. XIII° World Water Congress of the IWRA (International Water Resource Association), Montpellier. Francia, 1-4 Sept.

Lavie, E.,Morábito, J., Salatino, S., Bermejillo, A., & Filippini, M. F. (2010). Contaminación por fosfatos en el oasis bajo riego del río Mendoza. *Rev. FCA UNCuyo*, *42*(1), 169-184.

Lumb, A., Halliwell, D., & Sharma, T. (2006) Application of CCME Water Quality Index to Monitor Water Quality: a Case Study of the Mackenzie River Basin, Canada. *Environmental Monitoring Assessment*, *113*(1-3), 411-429.

MEDD et Agences de l'Eau (2003). Système d'évaluation de la qualité de l'eau des cours d'eau (SEQ-Eau) Recuperado de http://rhin-meuse.eaufrance.fr/IMG/pdf/grilles-seq-eau-v2.pdf.

Morábito, J., Salatino, S., Medina, R., Zimmermann, M., Filippini, M., Bermejillo, A., Nacif, N., Campos, S., Dediol, C., Pizzuolo, P., Genovese, D., & Mastrantonio, L. (2005). Calidad del agua en el área regadía del río Mendoza (Argentina). *Revista de La Facultad de Ciencias Agrarias, Centro de Ediciones Académicas*, *37*(1), 1-23.

Morábito, J., Salatino, S., Medina, R., Zimmermann, M., Filippini, M., Bermejillo, A. *et al*. (2007). Calidad del agua en el área regadía del río Mendoza: temperatura, pH, iones solubles y sólidos. *Revista de La Facultad de Ciencias Agrarias UNCuyo*, *39*(1), 9-20.

Morábito, J., Salatino, S., Filippini, M., Bermejillo, A., Medina, R., Zimmermann, M., Nacif, N., Campos, S., Dediol, C., Mastrantonio, L., Hernández, R., Genovese, D., & Stocco, A. (2009). Evaluación de la calidad del agua en áreas de regadío del río Tunuyán Superior (Prov. de Mendoza) para un aprovechamiento racional y sustentable (1era parte). Chubut, Argentina: Conagua Trelew.

Pesce, S. F., & Wunderlin, D. A. (2004). Use of Water Quality Indices to Verify the Impact of Cordoba City (Argentina) on Suquia River. *Water Resources*, *34*, 2915-2926.

SEEE (Secrétariat d'Etat auprès du Ministère de l'Energie, des Mines, de l'Eau et de l'Environnement) (2007). *Chargé de l'Eau et de l'Environnement. Normes de qualité – eaux destinées à l'irrigation*. Recuperado de http://www.eau-tensift.net/fileadmin/user_files/pdf/publications/3_Irrigation.pdf.

Simeonov, V., Stratis, J. A., Samara, C., Zachariadis, G., Voutsa, D., Anthemidis, A., Sofoniou, M., & Kouimtzis, Th. (2003). Assessment of the Surface Water Quality in Northern Greece. *Water Resources*, *37*,. 4119-4124.

Singh, K. P., Malika, A., Mohan, D., & Sinha, S. (2004). Multivariate Statistical Techniques for the Evaluation of Spatial and Temporal Variations in Water Quality of Gomti River (India) - A Case Study. *Water Research*, *38*, 3980-3992.

Singh, R. P., Nath, S., Prasad, S. C., & Nema, A. K. (2008). Selection of Suitable Aggregation Function for Estimation of Aggregate Pollution Index for River Ganges in India. *Journal of Environment Engineering – ASCE*, *134*, 689-701.

Institutional Address of the Authors

Dra. Emilie Lavie

Universidad Paris-Diderot
PRES Sorbonne-Paris-Cité
UMR CNRS-8586 PRODIG Francia
5 rue T. Mann, cc7001 75205 Paris
Cedex 13, France
Teléfono: +33 (157) 277 271
emilie.lavie@univ-paris-diderot.fr

Ing. José A. Morábito

Instituto Nacional del Agua (INA)
Centro Regional Andino (CRA)
Programa de Riego y Drenaje
Belgrano Oeste 210, piso 3, oficina 324
5500 Ciudad de Mendoza, Argentina
Teléfono: +54 (261) 4286 993
jmorabito@ina.gov.ar

Facultad de Ciencias Agrarias
Universidad Nacional de Cuyo, Argentina

Ing. Santa E. Salatino

Instituto Nacional del Agua (INA)
Centro Regional Andino (CRA)
Programa de Riego y Drenaje
Belgrano Oeste 210, piso 3, oficina 324
5500 Ciudad de Mendoza, Argentina
Teléfono: +54 (261) 4286 993
ssalatino@ina.gov.ar

Click here to write the autor

Tunuyan River at the Costa Anzorena sampling point, Argentina.

Photo: Emilie Lavie.

Aggregation Methodology to Estimate Hydraulic Conductivity in Unsaturated Heterogeneous Soils

• Erik Zimmermann* • Pedro Basile •
Universidad Nacional de Rosario, Argentina
*Corresponding Author

Abstract

Zimmermann, E., & Basile, P. (July-August, 2014). Aggregation Methodology to Estimate Hydraulic Conductivity in Unsaturated Heterogeneous Soils. *Water Technology and Sciences* (in Spanish), *5*(4), 39-54.

This study presents the validation of an aggregation methodology proposed to obtain hydraulic conductivity equivalents for a homogeneous porous media in unsaturated heterogeneous soils. The first step in this proposal is to numerically model flow in the unsaturated zone of a heterogeneous area, with a highly detailed discretization and parameterization based on suitable pedotransfer functions. The second stage involves calibrating the equivalent parameters from the wet front model based on the results from the first phase and comparing with those proposed by the aggregation methodology. The procedure was applied to 68 soil profiles characteristic of the southern province of Santa Fe (Argentina). The results obtained validate the aggregation methodology proposed for a large sampling of textural compositions, hydraulic properties and antecedent moisture contents. For the series of soils analyzed, estimates of saturated hydraulic conductivity would be acceptable with weighting up to effective saturations of 50%, with a margin of error limited to 10%.

Keywords: Heterogeneous unsaturated soils, hydraulic conductivity, aggregation methodology.

Resumen

Zimmermann, E., & Basile, P. (julio-agosto, 2014). Metodología de agregación para estimar conductividades hidráulicas en suelos heterogéneos insaturados. Tecnología y Ciencias del Agua, *5(4), 39-54.*

Se presenta la validación de una metodología de agregación, propuesta para obtener conductividades hidráulicas equivalentes de un medio homogéneo en suelos heterogéneos no saturados. Para ello se propone, en una primera etapa, una modelación numérica del flujo en la zona no saturada, en el dominio heterogéneo discretizado con alto grado de detalle y parametrizado mediante funciones de pedotransferencia adecuadas. En una segunda etapa se calibran los parámetros equivalentes del modelo de frente húmedo con los resultados alcanzados en la primera etapa, comparándolos con los propuestos en la metodología de agregación. El procedimiento se aplica a 68 perfiles típicos de suelos que caracterizan el sector meridional de la provincia de Santa Fe (Argentina). Los resultados alcanzados validan la metodología de agregación propuesta para un numeroso muestreo de composiciones texturales, propiedades hidráulicas y contenidos de humedad antecedente. Para las series de suelos analizadas, serían aceptables las estimaciones de conductividades hidráulicas saturadas mediante ponderación hasta saturaciones efectivas del orden del 50%, con un rango de errores acotados al 10%.

Palabras clave: *suelos heterogéneos no saturados, conductividad hidráulica, metodología de agregación.*

Introduction

Numerical models are typically used to predict the movement of water and solutes in the unsaturated zone (USZ). The results of their application are only reliable if the properties of the porous medium are known. This is the primary limitation of current complex models, which are advanced by very little is known about the parameters they include. Works involving the continuous calibration of hydrological models have demonstrated the high sensitivity of underground processes (which are observable in the system through the phreatic levels) and surface hydrological processes (which are observable through runoff volumes) to hydraulic parameters that characterize the unsaturated zone (Zimmermann, 2003). These parameters

also influence the calculation of erosion and sediment deposit processes at the basin scale (Basile, Riccardi, Zimmermann, & Stenta, 2010).

The characterization of the unsaturated medium requires knowledge of conductivity $K(\theta)$ and retention $\psi(\theta)$ curves, or diffusivity $D(\theta)$, where q is the volumetric moisture contents, $K(\theta)$ is the unsaturated hydraulic conductivity, $\psi(\theta)$ is the soil matric potential and $D(\theta)$ is the diffusivity coefficient. A large number of laboratory tests and field methods have been designed to measure the hydraulic functions of the soil, but most of the methods are relatively expensive and difficult to conduct.

Indirect methods exist to estimate the hydraulic properties of soil that vary in terms of methodology and complexity. Three main groups can be distinguished: methods based on the distribution of pore sizes, inverse methods and pedotransfer functions.

Pedotransfer functions (PTF) offer a methodology to describe hydraulic properties using the textural composition of soil and other available information (for example, the distribution of particles sizes, apparent density, organic matter contents, etc.). Many pedotransfer functions exist as equations and/or are implemented as informatics codes adjusted to different edaphological information bases. PTF have been used in previous works to calculate hydraulic properties of silty soil representative of a plains regions in Argentina based on granulometric information and physio-chemical parameters available in the soil cards developed by the National Farming Technology Institute (Instituto Nacional de Tecnología Agropecuaria; INTA, Spanish acronym). PTF have been included in *SoilPar* and *Rosetta* codes, along with regression equations between hydraulic and physical parameters (Zimmermann & Basile, 2007).

Based on comparisons between parameters obtained with PTF applications and those adjusted in mathematical hydrologic models, it was possible to conclude that of the codes used, the *Rosetta* program (Schaap, Leij, & Van Genuchten, 1999) provided the best estimate for the study region (Zimmermann & Basile, 2011).

The following phase of the work consisted of the hydraulic characterization of soils with heterogeneous compositions. The soils do not have homogeneous mediums but rather the profiles are stratified into horizons and are also combined, forming associations and consociations. Therefore, in order to simplify the approach to the model, a weighting methodology was proposed to estimate the representative parameters, from a hydraulic perspective, equivalent to a homogenous medium (Zimmermann *et al*., 2008). This was done in order to use said parameters in simplified infiltration models, such as that proposed by Green and Ampt (moisture front).

The objective of the present work is to validate this weighting methodology by comparing the results obtained with a mathematical model based on the solution to the Richards equation, which considers the heterogeneity of each soil profile. This is described below.

Numerical Model Used for Flow Simulation in the USZ

The flow model used for the simulations, called *SOLUM*, is based on the Richards equation and developed specifically for this work in order to estimate the redistribution of moisture in the unsaturated zone (USZ) and the water volumes exchanged with the atmosphere and the aquifer. This is part of a more general model developed to simulate the movement of surface flow in the saturated and unsaturated zone in plains areas, call the Hydrological Simulation of Plains Areas, or *SHALL* (Spanish acronym; Simulación Hidrológica de Áreas de Llanura) (Zimmermann & Riccardi, 2000). In the model, the flow equation in the USZ is solved in terms of the volumetric moisture content, q, to directly identify one of the variables of hydrological balance. Only vertical flow is considered. The equation of movement in

terms of the volumetric moisture content and analogous to the Fick law of diffusion is:

$$q = -D(\theta)\frac{\partial\theta}{\partial z} - k(\theta) + \int_0^{zr} S(\theta)dz \qquad (1)$$

where q is the Darcy velocity of unsaturated flow; θ is the volumetric moisture contents; z is the vertical coordinate; zr the radicle depth; $K(\theta)$ the unsaturated hydraulic conductivity, $D(\theta)$ the diffusivity coefficient of the porous medium, product of the unsaturated conductivity $K(\theta)$ times the gradient of the retention curve ($d\Psi/d\theta$), and $S(\theta)$ is sink term which, in the case of cultivated soils, represents the rate of extraction of water by the roots of the plants. The model assumes the heterogeneity of the soil, providing different parameters that govern the retention curves and hydraulic conductivity for different soil strata. The application of the model in this work consisted of the simulation of the infiltration processes from a rainfall event, and therefore the sink term was not included. In the equation, a negative value of q denotes downward flow (since q is positive when flow is in the positive z direction, upward). For vertical flow, the continuity equation establishes that:

$$\frac{\partial\theta}{\partial t} = -\frac{\partial q}{\partial z} \qquad (2)$$

The unsaturated porous medium is represented discretely using a set of cells that extend vertically from the surface to the phreatic level. To solve equations (1) and (2), an explicit numerical scheme in finite differences is proposed. The scheme is centered in space and is progressive over time. The exchange flows are evaluated on the cell boundaries and moisture content is estimated in the centers of the cells. Using this discretization scheme (Figure 1), the *momentum* equation is:

$$q_j^n = -D\left(\theta_j^n\right)\frac{\theta_{j-1/2}^n - \theta_{j+1/2}^n}{\Delta z} - k\left(\theta_j^n\right)$$

$$\theta_j^n = \frac{\theta_{j+1/2}^n + \theta_{j-1/2}^n}{2} \qquad (3)$$

The continuity equation solved for the term at the level n+1 is

$$\theta_{j+1/2}^{n+1} = \theta_{j+1/2}^n - \frac{\Delta t}{\Delta z}\left(q_j^n - q_{j+1}^n\right) \qquad (4)$$

where j and n represent the spatial and temporal discretization indices, respectively. The calculation sequence is as follows: a) beginning with initial moisture content conditions θ_{0j} in the profile; b) solve the *momentum* equation (3) for the thickness of the USZ ,determining the exchange flows between cells: c) solve the continuity equation (4), determining the moisture contents of the profile in the next time step and d) repeat step b) until arriving at the ending time of the simulation. The solution code was written entirely in *FORTRAN*. For the scheme proposed, a stability and convergence analysis was performed, comparing these results with known analytical solution problems and other techniques and numerical schemes, validating consistency for all situations (Zimmermann, 1998). As a complement, a stability analysis was performed, observing the behavior of the dimensionless numbers (Courant & Péclet) in critical moisture situations, programming alerts in the source code for situations in which

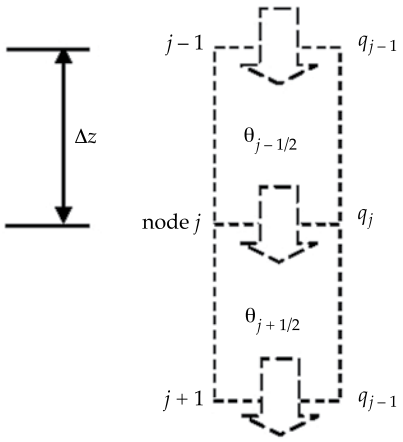

Figure 1. Discretization of the USZ in vertical cells.

the numbers fall outside numerical stability. As contour conditions, the solutions of the above equations are proposed, with some of the identified unknowns. The imbibition as an upper boundary condition was solved using the numerical scheme as an infiltration model. In the cell constituting the upper contour, the following conditions must be met:

$$q_1^n = \text{máx}\left(-D\left(\theta_{1/2}^n\right)\frac{\theta_s - \theta_{1/2}^n}{\Delta z} - k\left(\theta_{1/2}^n\right); -i^n\right) \quad (5)$$

where i^n is the intensity of effective rainfall, calculated according to the intensity of precipitation not intercepted by vegetation, during the temporal discretization interval n and θ_s is the volumetric moisture content of saturation. The first term in (5) represents the infiltration capacity and the second the water available for infiltration. Dewatering is foreseen as an upper boundary condition, although for this work it was not considered in the application. The cells included in the aquifer layer with moisture saturation were considered as a lower boundary condition. The set of saturated cells depends on the phreatic level, which is dynamically updated in the general model.

To complete the solution of the problem, it is necessary to know soil parameters such as the curves related to hydraulic conductivity versus moisture $K(\theta)$, matric potential versus moisture $\psi(\theta)$ and diffusivity versus moisture $D(\theta)$. The present work adopted the Brooks-Corey relations represented by the following equations:

$$S_e = \frac{\theta - \theta_r}{\theta_s - \theta_r} = \begin{cases} \left(\frac{\psi_c}{\psi}\right)^{\lambda} & \text{si} \rightarrow |\psi| \geq |\psi_c| \\ 1 & \text{si} \rightarrow |\psi| < |\psi_c| \end{cases} \quad (6)$$

where θ_r is the moisture content corresponding to residual saturation: λ is a parameter that depends on the distribution of pore sizes: ψ_c is the critical suction (entering air pressure) and S_e is the effective saturation. To calculate the relative hydraulic conductivity, $K_r = K(\theta)/K_s$, where K_s is the saturated hydraulic conductivity. The equation proposed by Corey is used (1977):

$$K_r = \frac{K}{K_s} = S_e^{\left(\frac{2}{\lambda}+3\right)} \quad (7)$$

Equations (6) and (7) are parametrized for each one of the cells, by which the USZ domain is divided. This enables representing heterogeneous stratified medium such as those in this study. The hysteresis loops between dry and wet were not taken into account.

Pedotransfer Functions Used

To estimate the hydraulic properties for each stratum, PTF were applied, consisting of a set of equations relating hydraulic soil properties with physical and granulometric parameters of the soil samples. Many PTF currently exist which have been included in informatics codes, such as the *SoilPar* (Acutis & Donatelli, 2003) and *Rosetta* (Schaap *et al*., 1999). Previous works (Zimmermann & Basile, 2011) used different procedures to calculate hydraulic properties of silty soils based on granulometric information and physical-chemical parameters available from soil cards from the INTA. PTF functions included in the *SoilPar* and *Rosetta* codes were used, along with regression equations between hydraulic and physical parameters, given by a set of authors. The mean weighted hydraulic parameters were calculated for basins in the region and the predictions were compared with values obtained from the calibration of the *SHALL* mathematical hydrological model (Zimmermann, 2003).

Based on the results obtained, it was possible to conclude that, among the codes used, the *Rosetta* program provided the best estimate of the hydraulic parameters calibrated for the study region, providing information

related to textural composition, apparent density and two points on the retention curve (permanent wilting and field capacity). The code mentioned to evaluate the hydraulic parameters for each stratum of soil analyzed was then employed, with which the retention curves and hydraulic conductivity mentioned previously were obtained.

Application to Soils from the Province of Santa Fe (Argentine wet plain)

The southern area of the province of Santa Fe (Argentina), subject of this study (Figure 2), has a rainfall of the order of 1 000 mm and mean annual temperature of 17°C. The available soil maps for Santa Fe, developed by the INTA, classify the soil in the region from a textural perspective as silty loam, silty clay loam and silty clay. Information related to 68 profiles for soil series types was extracted from the available soil cards. These were representative of the soils present in the southern Santa Fe area. Between 3 and 8 horizons were detailed in each profile in the series, depending on depth and stratigraphy. The textural composition and other biophysical parameters —such as organic matter contents, cation exchange capacity, pH, etc.— were published in these cards. The set of horizons for all the series studied totaled 434 soil samples, considering that, on average, each series of soils was discretized by between 6 and 7 horizons.

Calculation of Parameters by Soil Series

With the information from the cards pertaining to each type of profile or soil series, calculation forms were constructed and filled in with textual and physical-chemical characteristics for each series. With this information, using intrinsic PTF from the *SoilPar* program, apparent densities, moisture at field capacity (CC), permanent wilting point (PWP) and other matrix tension were obtained. Then, the PTF included in the *Rosetta* program were applied, resulting in the following hydraulic properties per horizon or stratum for each series: saturated hydraulic conductivity, K_s; saturation moisture, θ_s; residual moisture, θ_r; pore connectivity, λ and critical suction ψ_c.

For the modeling of the USZ, a spatial discretization interval of 0.05 m was considered, which provides sufficient detail to calculate the moisture profiles in the region of analysis. To characterize the properties of each cell, a linear interpolation routine was used for adjusted parameters for each stratum. The zone covered by the modeling domain was 3.5 m deep, and taking into account the discretization step, resulted in 70 vertical cells for each of the soil series studied.

Initial and Simulated Boundary Conditions

The boundary and initial conditions are important factors in the simulations because they influence the results obtained. The upper boundary condition was taken as described earlier, that is, the pre-established flow condition associated with the infiltration capacity. A phreatic level of 3.5 m deep was used as the lower boundary condition. This depth will not greatly change the phenomena studied on the surface and will reflect a common situation among the hydrological systems studied.

The initial condition was established considering the following criteria: a) the alteration in the moisture profile is significant from the top surface layers to a depth near the radicle length of the crops present in the systems studied and b) the depth of the moisture profile is barely altered by external environmental conditions. As a situation compatible with the fixed lower boundary, an equilibrium moisture profile was established up to 1 m deep (1 m approximately represents the radicle depth). Above 1 m of depth, the variation in the moisture profile was established linearly (arbitrary and simplified) between the profile equilibrium and the different moisture conditions preset for the analysis: between 40 and 90% of effective saturation (from 0.4 to 0.9 of *Se*). Figure 3 shows the conditions adopted.

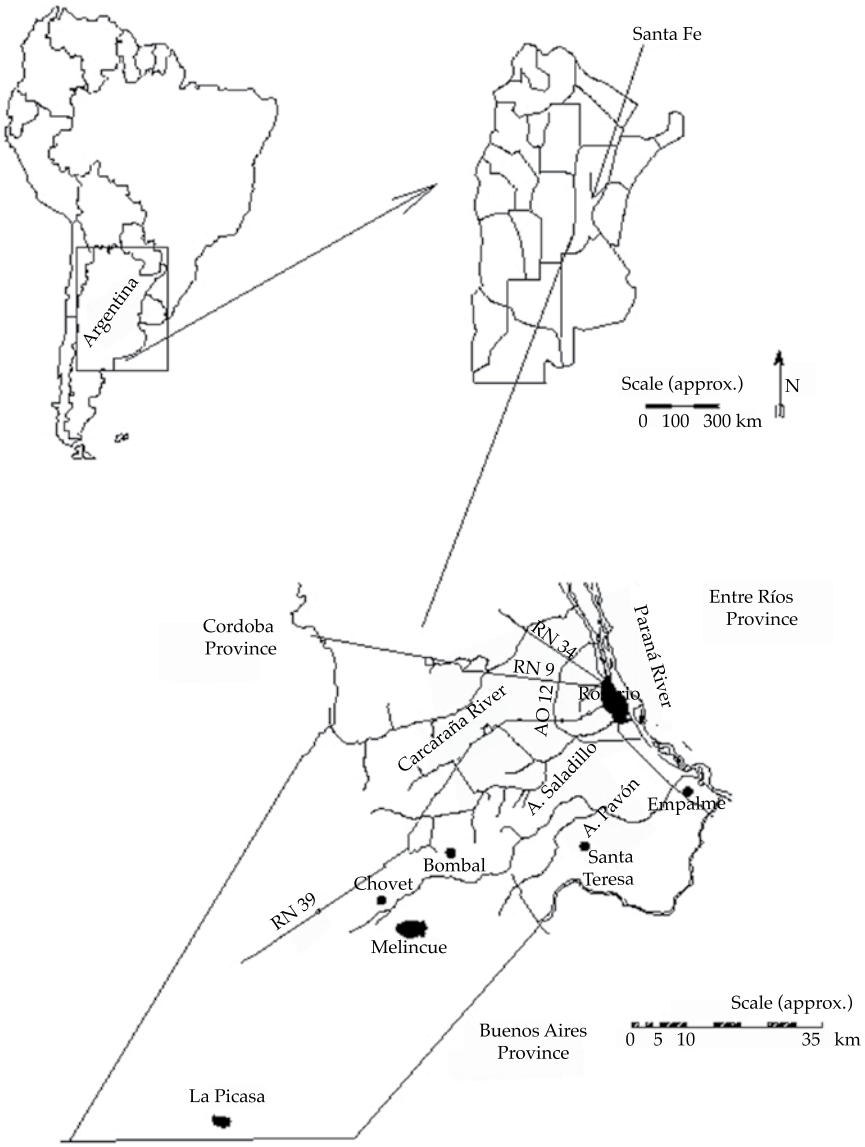

Figure 2. Study area: Southern portion of Santa Fe.

Simulations Performed

Simulations were performed assuming each profile had waterlogged conditions on the surface resulting from constant and highly intense precipitation (70 mm/h) for 12 hours. Under these conditions, 68 soil profiles were analyzed for each case. The analysis included the evolution of the depth of the moisture profiles over time and, primarily, the infiltration rate in the upper contour. For example, figures 4 and 5 present two profiles with different characteristics and therefore different hydraulic behavior. The textural characteristics are presented in Table 1. These figures show the moisture profiles at different times during the simulation for the "El Perdernal" and "Roldan" series selected and for extreme initial moisture conditions. Together they represent saturation moisture contents (θ_s) and saturated hydraulic

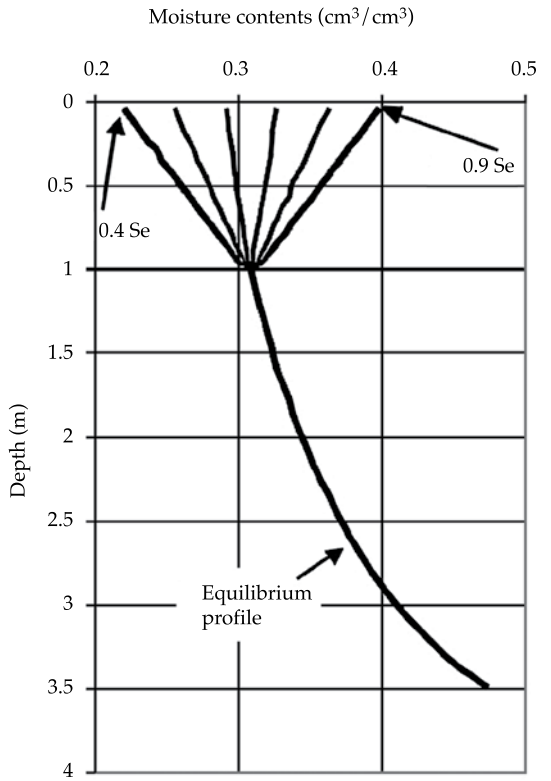

Figure 3. Moisture profiles to establish initial conditions.

conductivities (K_s) according to depth (using linear interpolation between assigned values for each stratum).

The El Pedernal series is located in the southeast portion of the province, developed from light silty loam sediments with large portions of sand (roughly 18%). This results in a relatively high saturated hydraulic conductivity (roughly 1 cm/h). In the simulation, the moisture front reaches depths of over 2 m at 48 hours, and its pattern was nearly uniform. The first stratum had large clay contents and retarded flow at greater depths, as can be seen in Figure 4. The Roldan series, with deficient drainage, is in the southeast portion of the province, near the city of Rosario. It had a similar clay content (roughly 30%) at different depths. The saturated hydraulic conductivities were on the order of 0.4 cm/h. In general, the moisture front at 48 hours reached 1 to 1.5 m, depending on the initial moisture conditions.

Simplified Approach to Modeling Events

The *SOLUM* model can provide a detailed description of the distribution of the moisture contents of the soil profile and the exchange flows between the surface and the phreatic level. Nevertheless, a considerable amount of information and time is required to execute the simulations. Such detailed results is often not needed for modeling of rain events, but rather knowledge of the exchange flows in the land surface (infiltration) is sufficient. The dilemma to be solved consists of finding "equivalent and unique parameters" for a stratified soil that make it possible to reasonably calculate the infiltration rates of the land surface. The term "unique" refers to an equivalent homogeneous medium. In this way, a simple methodology can be applied to evaluate infiltration. Therefore, this work proposes the objective of synthesizing the heterogeneities of the soil into values representative of the hydraulic properties of the set. In particular, using the simplified moisture front model (Green & Ampt), it will attempt to obtain values for the hydraulic conductivity K_e and the potential suction at the moisture front ψ_{fe}, both equivalent to homogeneous soil, that produce the same infiltrated volume as the stratified and heterogeneous soil.

Green and Ampt Method as a Loss Algorithm

The method represents a simplification of the real phenomenon, which approximates the advance of moisture in the soil profile based on the moisture front, with permanent waterlogged conditions on the surface. The soil is considered to be homogeneous and deep. The front is a flat plane (flow in the form of a "piston") which divides the soil with an initial moisture, θ_i, from the saturated soil with a moisture content equal to the saturation, θ_s, and a potential suction ψ_f in the advancing front.

For vertical movement, using the mass continuity equation and the Darcy law (generalized for unsaturated flow) between

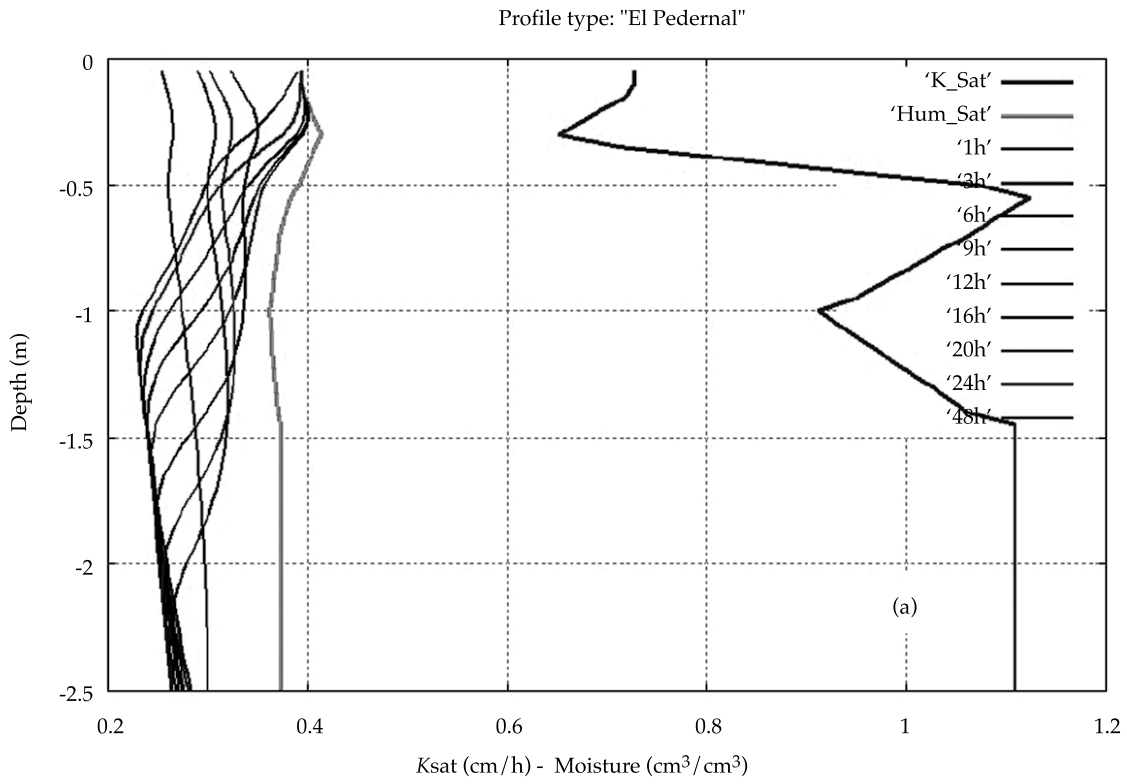

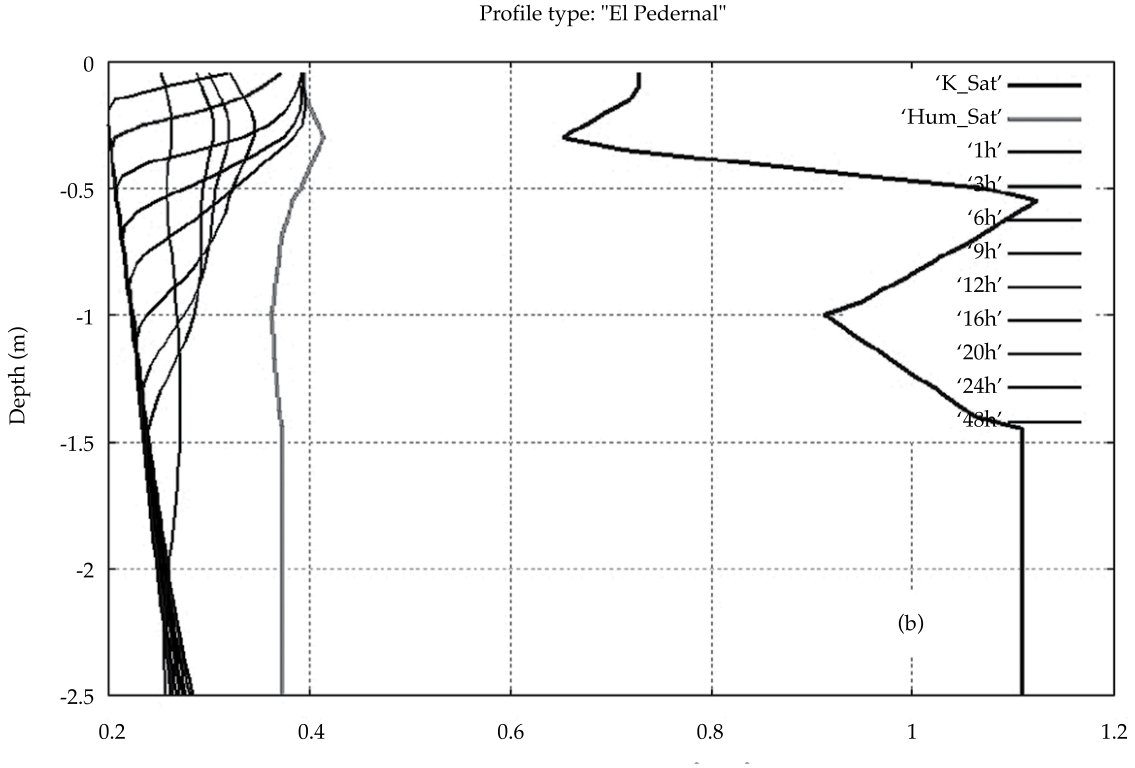

Figure 4. Profiles for different simulation times. "El Pedernal" series: a) initial *Se* = 0.9; b) initial *Se* = 0.4.

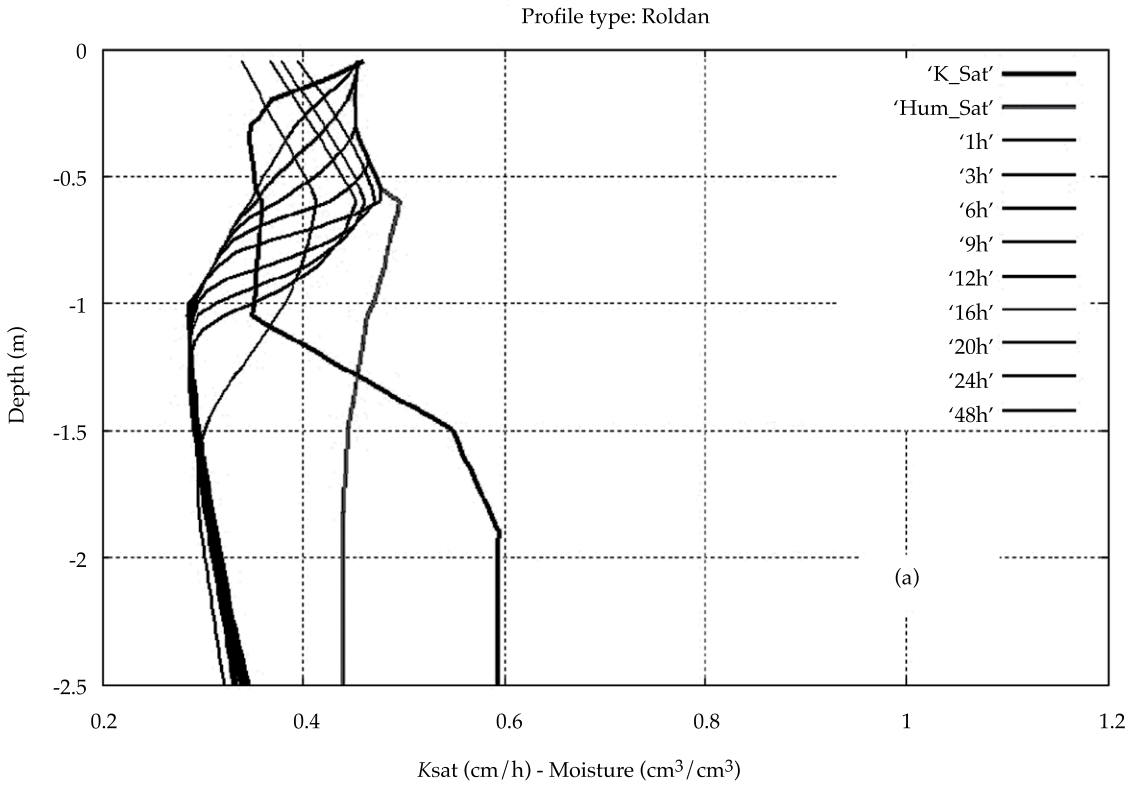

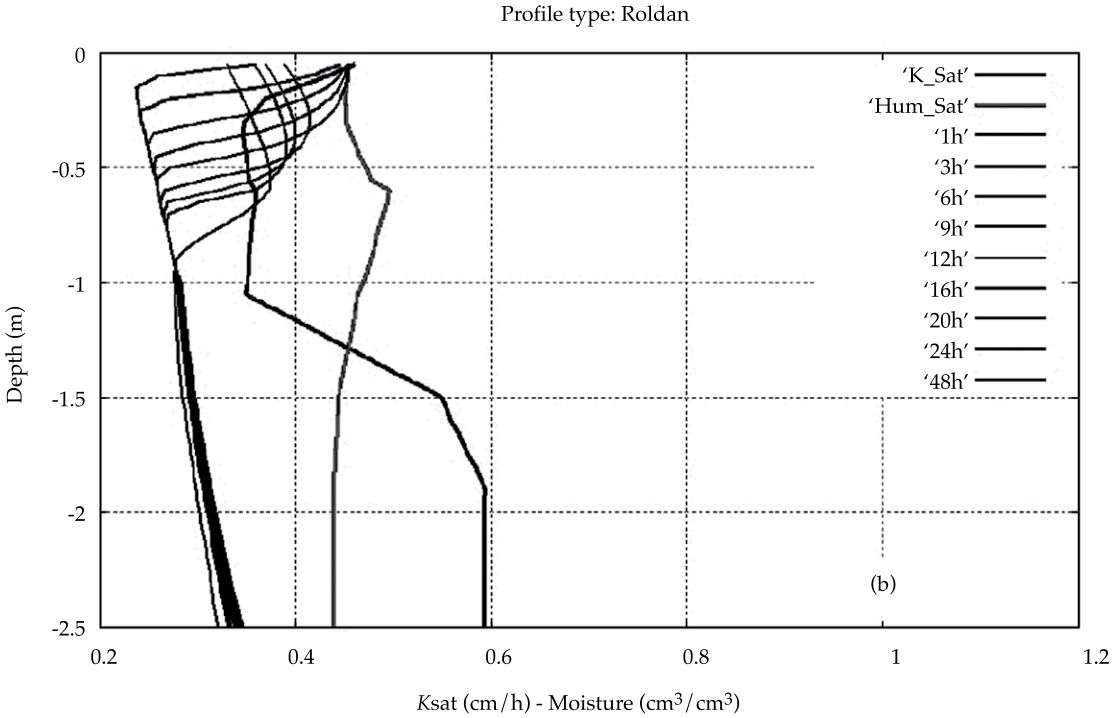

Figure 5. Profiles for different simulation times. "Roldan" series: a) initial *Se*= 0.9; b) initial *Se* = 0.4.

Table 1. Textural composition of the strata for the series analyzed.

Depths (m)		Thickness (m)	Sand (%)	Clay (%)
Serie El Pedernal				
	< 0.26	0.26	15.9	14.8
0.26	0.40	0.14	12.2	17.3
0.40	0.60	0.20	13.3	7.6
0.60	0.80	0.20	18.5	8.1
0.80	1.15	0.35	22.6	9.2
1.15	1.70	0.55	17.8	7.6
% weighted by thickness			**17.6**	**9.9**
Roldan series				
-	0.12	0.12	2.2	23.7
0.12	0.25	0.13	2.4	26.3
0.25	0.38	0.13	3.0	28.6
0.38	0.80	0.42	2.2	50.7
0.80	1.30	0.5	3.3	33.1
1.30	1.75	0.45	3.3	19.8
1.75	2.10	0.35	4.0	18.4
% weighted by thickness			**3.1**	**30.1**

the waterlogged surface and the moisture front's advance point, we get a formulation of the infiltration rate f as well as the rate of accumulated infiltrated water depth F over time:

$$f(t) = K\left(\frac{\psi_f \Delta\theta}{F(t)} + 1\right) \quad (8)$$

$$F(t) = Kt + \psi_f \Delta\theta \, ln\left(1 + \frac{F(t)}{\psi_f \Delta\theta}\right) \quad (9)$$

where K is the vertical hydraulic conductivity of the soil; ψ_f, the suction potential at the moisture front; $\Delta\theta$ the difference between saturation and initial moisture contents $\Delta\theta = \theta_s - \theta_i$ and t is time. The application of this method requires calculating the hydraulic conductivity K and the suction potential ψ_f.

Obtaining equivalent K_e and ψ_{fe} parameters

First, the *SOLUM* method was proposed to evaluate the infiltration rate in the surface strata resulting from a precipitation with sufficient intensity and duration to exceed the infiltration capacity of the set. While the model enables identifying the moisture distribution at each moment and throughout the soil profile, the information of greatest interest that synthesizes the movement of moisture in the profile is the infiltration curve corresponding to the first stratum. With the temporal distribution of infiltration for the surface cell $f_1(t)$, the equivalent K_e and ψ_{fe} parameters are adjusted for the function $f(t)$, evaluated with equation (8), and the $f_1(t)$ is calculated using a calibration algorithm specifically proposed in the present work.

Calibration Algorithm

To calculate the equivalent K_e and ψ_{fe} parameters, a fitting algorithm needed to be designed, which was included in the computational code of the *SOLUM* program. A hybrid calibration algorithm was proposed which combines a "gross fit" in the restricted

domain of the parameters along with a "fine fit" algorithm based on the gradient method.

The preliminary investigation evaluated the objective function in a grid traced over the region of the parametric validity, subdivided in intervals of 100 parts.

The algorithm of the gradient for the detailed search for the optimum is based on the definition of a multi-dimensional objective function (OF) (OF = $y(\mathbf{x})$, where $\mathbf{x}$ is the vector of parameters). Basically, the algorithm is based on a possible base point $\mathbf{x}^0(x_1, x_2,...x_n)$ with which OF = $y(\mathbf{x}^0)$ and the gradient of the OF, ∇y are evaluated. To construct the gradient, the partial derivatives are estimated using incremental quotients of the type:

$$\frac{\partial y}{\partial x_i} \approx \frac{y\left(x_1, x_2, .., x_i + \Delta x_i, ..x_n\right)}{\Delta x_i} - \frac{y\left(x_1, x_2, .., x_i, ..x_n\right)}{\Delta x_i} \quad (10)$$

for $i = 1, 2,\ldots n$, where Δx_i is a small value with respect to the value of x_i. The gradient provides a vector that determines the directions of the optimum of the OF. A new point in the multi-dimensional space is selected whose OF $y(\mathbf{x}^1)$ comes close to the optimum sought. Generically, it can be expressed as:

$$\mathbf{x}^{k+1} = \mathbf{x}^k \pm \nabla y \Delta h \quad (11)$$

The sign of the second member is positive if the search is towards a maximum, and vice versa. The search step Δh, which represents the distance at point x^k, must meet the restrictions imposed on the parameters. The search processes ends when, in two successive iterations, the difference between the calculated OF is less than a pre-established tolerance and/or a previously set maximum number of iterations is surpassed. In the particular case of this study, there are two parameters ($x_1 = K_e$; $x_2 = \psi_{fe}$) and the objective function was considered to be the root square mean error (RSME) of the differences between the infiltration rate in the surface cell, $f_1(t)$, and the $f(t)$ evaluated with equation (8). To implement the algorithm, it was developed with a subroutine in *FORTRAN* which was incorporated in the main body of the *SOLUM* model.

Weighting Methodology

In parallel, an aggregation methodology was proposed to obtain equivalent parameters per soil series, based on the parameters calculated for each horizon (Zimmermann *et al.*, 2008). This is the methodology to be validated in the present work. The criteria were: a) the harmonic mean of the conductivities of each stratum (equation (12)) were calculated for the weighted saturated vertical hydraulic conductivity, K_p and b) for the potential suction at the weighted moisture front ψ_p, the weighted average was adopted for the thickness of each stratum (equation (13)):

$$K_p = \frac{L}{\sum_{i=1}^{N} \frac{e_i}{K_i}} \quad (12)$$

$$\psi_p = \frac{1}{L} \sum_{i=1}^{N} \psi_i e_i \quad (13)$$

where K_i and ψ_i are the parameters for the thicknesses e_i, N is the total of horizons in the series and L is the total thickness. These were obtained as described earlier. For each stratum, the hydraulic conductivity K_i was considered to be equal to the saturated conductivity, and the suction potential at the moisture front, ψ_i was estimated as follows ((Muñoz-Carpena & Gowdish, 2005):

$$\psi_i = \frac{2\lambda + 3}{2\lambda + 2} \frac{\psi_c}{2} \quad (14)$$

where the critical suction of each stratum ψ_c, the pore connectivity λ and the saturated conductivity K_s were obtained using the PTF

included in the *Rosetta* program, as mentioned previously.

Comparative between both Methodologies

The parameters obtained with the weighted methodology proposed (K_p and ψ_p) were compared with the parameters resulting from the calibration (K_e and ψ_{fe} equivalents), after modeling with the *SOLUM* program.

Integrations of the weights in the comparisons were presented as an alternative, taking into account different depths (L, in equations (12) and (13)). An initial depth of 2.5 m was first adopted, according to the integration of nearly the entire profile (considering that the depth of the phreatic level proposed by the simulations was 3.5 m).

The values of K_p (on the x axis) and K_e (on the y axis) are shown in Figure 6 for the series analyzed (68) and the different initial moistures considered and integrated up to 2.5 m deep. As can be seen, the determination coefficients obtained (and shown in the upper left angle of each figure) are relatively low.

Next, the top strata were considered in the integrations for the weighting, approximately horizons "A" and "B" up to a depth of 0.50 m.

The values of K_p (estimated) and K_e (adjusted) are shown in Figure 7 for the different series and initial moistures considered. The determination coefficients obtained (and shown in the upper left angle of each figure) are considerably higher than the previous ones.

This suggests that, for the purpose of characterizing the infiltration process in the land surface, considering the top soil horizons to parametrize the hydraulic properties of the set provides better results. In other words, it can be stated that the top strata are the ones that dominate the infiltration process below the surface.

For a more detailed analysis of the effect of antecedent moisture conditions, an average hydraulic conductivity value was obtained for the 68 series of soils analyzed for both the adjusted values as well as for the values estimated with weighting. This was done in order to obtain a value representative of the set of soils analyzed, although this average has no other application except for the analysis proposed in this part of the work.

Figure 8 shows the comparison of adjusted and weighted average values of hydraulic conductivity for all the series of soils in function of the initial moisture contents. Here it can be seen that the adjusted average values of K_e are asymptotic to similarly weighted values K_p for moisture content near saturation.

Inverse or harmonic weighting was used to obtain equivalent conductivities when the flow circulates transversally through a stratified saturated soil (Custodio & Llamas, 1983). In the case analyzed, the medium is not saturated and, therefore, the results will come close to the weighting methodology when the saturation hypothesis is valid. Figure 8 presents a logical result, which also makes it possible to analyze the degree of acceptation that can be provided to the weighting formula.

For example, for the series of soils analyzed, the estimates would be acceptable for the saturated hydraulic conductivities derived from weighting up to 50% of effective saturation with the range of errors up to 10%.

In addition, in the region analyzed, given that moisture contents at depths up to horizon "B" in most of the cases were over 50% of effective saturation, because of the "humidity" of the climate, it can be stated that the weighting methodology is adequate to represent the hydraulic conductivities of the strata set.

Conclusions

This study validated an aggregation methodology to obtain hydraulic conductivities equivalent to a homogeneous medium in unsaturated heterogeneous soils. The procedure consisted of two stages. In the first stage, a numerical modeling of flow in the unsaturated zone was proposed, specifically for this work, in the discretized heterogeneous domain with a high degree of detail and parametrized using suitable

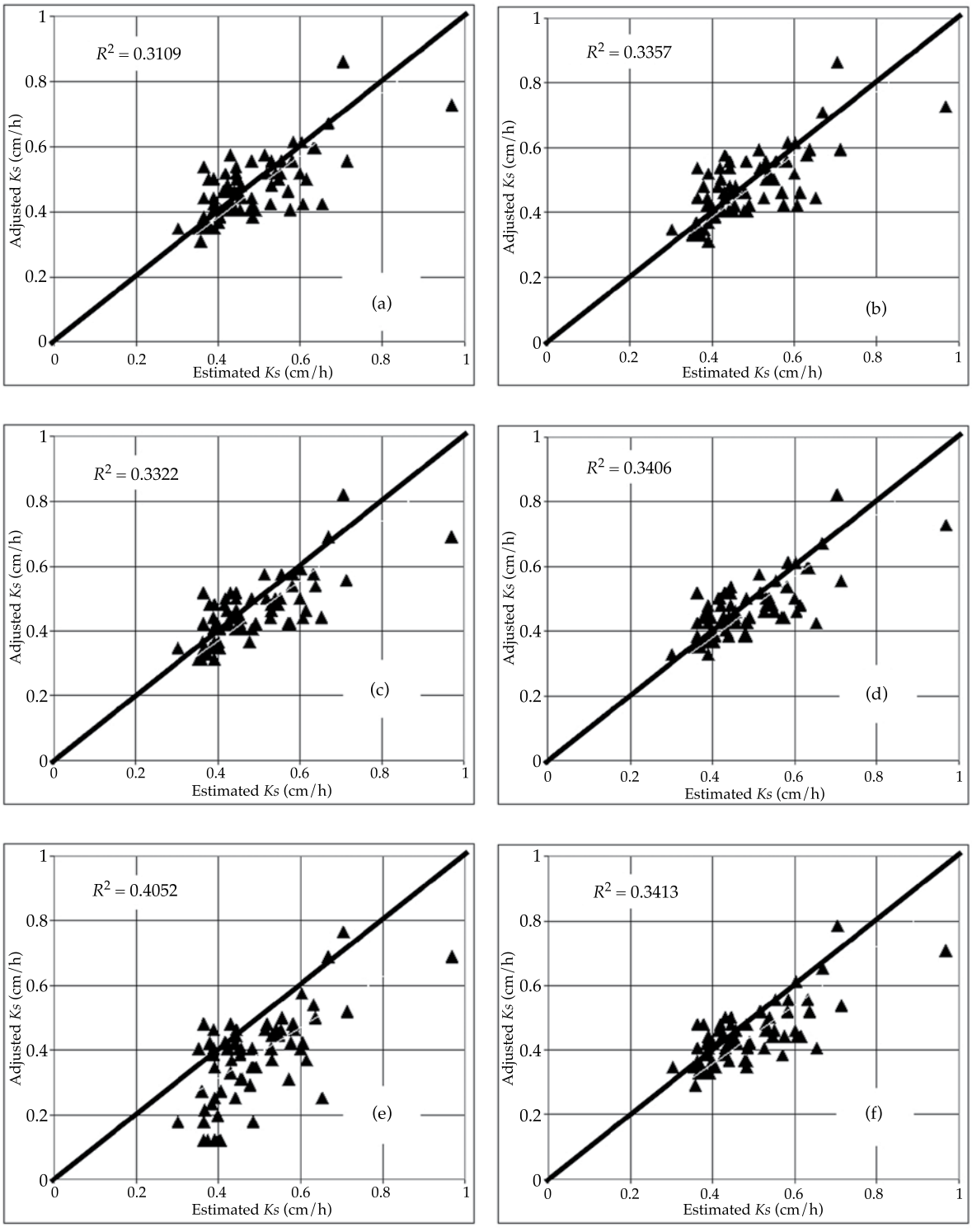

Figure 6. Comparison between weighted K_p at a depth of 2.50 m (x-axis) and adjusted K_e (y-axis) for different initial *Se*: a) 0.40, b) 0.50, c) 0.60, d) 0.70, e) 0.80 and f) 0.90, respectively.

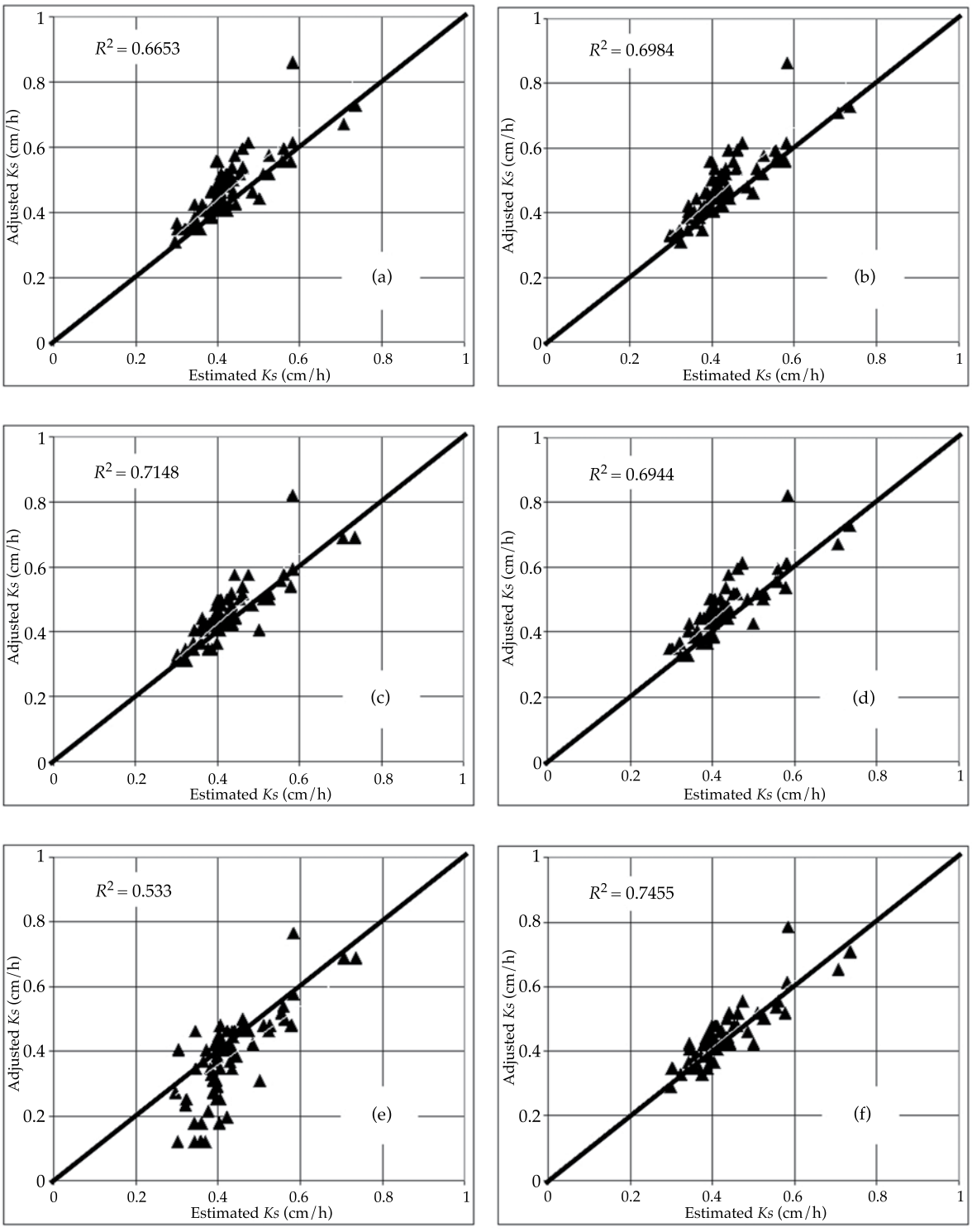

Figure 7. Comparison between weighted *Kp* at a depth of .50 m (x-axis) and adjusted *Ke* (y-axis) for different initial *Se*: a) 0.40, b) 0.50, c) 0.60, d) 0.70, e) 0.80 and f), 0.90, respectively.

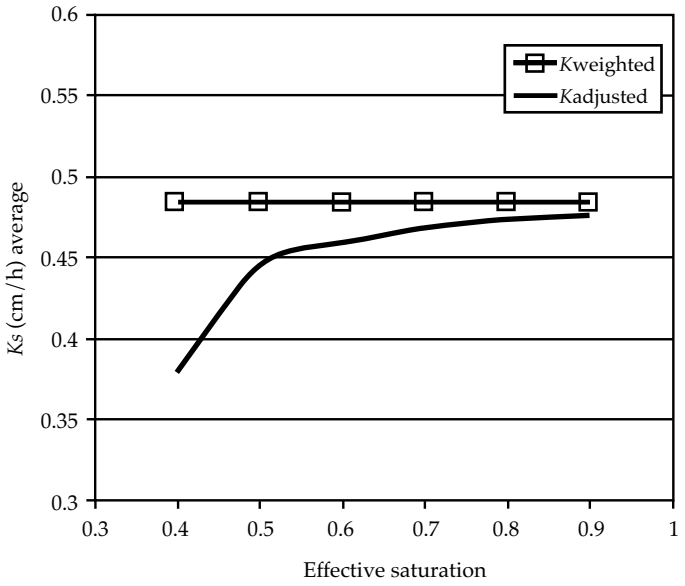

Figure 8. Comparison of average values of *Kp* and *Ke* for all the soils series in function of initial moisture.

pedotransfer functions. The second stage consisted of calibrating the equivalent parameters of the moisture front model with the results from the first stage, comparing them with those from the aggregation methodology. The procedure was applied to 68 soil profile types which characterize the southern sector of the province of Santa Fe, Argentina. The results validate the aggregation methodology proposed for a numerous sampling of textural compositions, hydraulic properties and antecedent moisture contents. For the characterization of the infiltration process in the land surface, the best results are provided by weighting the top soil horizons to parametrize the hydraulic properties of the set. It can be stated that the top strata are those that dominate the infiltration process below the surface.

The calibrated hydraulic conductivity values were observed to be asymptotic to the similarly weighted values for moistures near saturation. Considering that the harmonic weighting proposed is used to obtained equivalent conductivities when the flow circulates transversally through a stratified saturated soil, the results will be better when the saturation hypothesis is valid. For the series of soils analyzed, the estimates would be acceptable for saturated hydraulic conductivities obtained through weighting up to effective saturations of 50% with a range of error up to 10%.

Received: 26/09/12
Accepted: 17/01/14

References

Acutis, M., & Donatelli, M. (2003). SoilPar 2.00: Software to Estimate Soil Hydrological Parameters and Functions. *Europ. J. Agronomy, 18*, 373-377.

Basile, P. A., Riccardi, G., Zimmermann, E., & Stenta, H. (2010). Simulation of Erosion-Deposition Processes at Basin Scale by a Phisically-Based Mathematical Model. *International Journal of Sediment Research, 25*(2), 91-109.

Corey, A. (1977). Mechanics of Heteregeneous Fluids in Porous Media (150 pp.). Fort Collins: Water Resources Publications.

Custodio, E., & Llamas, R. (1983). *Hidrología subterránea* (2350 pp.). Segunda edición. Vol. 1. Barcelona: Editorial Omega.

Muñoz-Carpena, R., & Gowdish, L. (2005). *Aplicación del método de infiltración de Green-Ampt con redistribución de*

humedad del suelo entre encharcamientos. Estudios de la zona no saturada del suelo. Vol. VII. En F. J. Samper-Calvete & A. Paz-González (Eds.). La Coruña, España: Tórculo Artes Gráficas.

Schaap, M. G., Leij, F. J., Van Genuchten, M. Th. (1999). A Bootstrap Neural-Network Approach to Predict Soil Hydraulic Parameters. In M. Th. Van Genuchten, F. J. Leij, & L. Wu (Eds.). *Proceedings of the International Workshop on Characterization and Measurements of the Hydraulic Properties of Unsaturated Porous Media* (pp. 1237-1250). University of California, Riverside.

Zimmermann, E. (1998). *Esquema explícito para la resolución de la ecuación de Richards* (pp. 258-266). Congreso Nacional del Agua. Vol. 2. Santa Fe, Argentina.

Zimmermann, E., & Riccardi G. (2000). *Modelo de simulación hidrológica superficial y subterránea para áreas de llanura* (pp. 169-178). Vol. II. XIX Congreso Latinoamericano de Hidráulica. IAHR Div. LA, Córdoba, Argentina.

Zimmermann, E. (2003). Modelo hidrológico superficial y subterráneo desarrollado para la simulación de sistemas de llanura. 2. Estrategias para la calibración. *Journal of Earth Sciences. Boletín Geológico y Minero*, *114*(2), 159-169.

Zimmermann, E., & Basile, P. (2007). *Funciones hidráulicas de suelos limosos: regresiones no lineales con propiedades físicas y granulométricas*. XXI Congreso Nacional del Agua y IV Simposio de Recursos Hídricos del Cono Sur, Tucumán, Argentina.

Zimmermann, E., Scuderi, C., Riccardi, G., Stenta, H., Basile, P., García, M., & Rentería, J. (2008). *Asignación de parámetros hidráulicos de suelos utilizando composición textural, características físicas y estratigráficas*. XXIII Congreso Latinoamericano de Hidráulica, IAHR Div. LA, Cartagena de Indias, Colombia.

Zimmermann, E., & Basile, P. (2011). Estimación de parámetros hidráulicos en suelos limosos mediante diferentes funciones de pedotransferencia. *Tecnología y Ciencias del Agua*, *2*(1), 99-116.

Institutional Address of the Authors

Dr. Erik Zimmermann
Dr. Pedro Basile

Departamento de Hidráulica
Facultad de Ciencias Exactas, Ingeniería y Agrimensura
Universidad Nacional de Rosario
Consejo de Investigaciones Científicas y Técnicas (CONICET).
Riobamba 245 bis (2000)
Rosario, Argentina
Teléfono y fax: +54 (341) 4808 541
erikz@fceia.unr.edu.ar
pbasile@fceia.unr.edu.ar

Click here to write the autor

Diagnostic Algorithms to Detect Faults in Pipelines

• Lizeth Torres • Cristina Verde* • Rolando Carrera • Raúl Cayetano •
Universidad Nacional Autónoma de México
*Autor de correspondencia

Abstract

Torres, L., Verde, C., Carrera, R., & Cayetano, R. (July-August, 2014). Diagnostic Algorithms to Detect Faults in Pipelines. *Water Technology and Sciences* (in Spanish), *5*(4), 55-76.

This paper presents the design of an online diagnostic system (functioning while the transportation system remains in operation) to detect, identify and rebuild pipeline faults based on redundant relations and state observers. The faults include those occurring in measurement instruments, pumps, and unknown extractions from the pipeline. The algorithms that compose the diagnostic system were developed from nonlinear partial differential equations that characterize the behavior of the fluid according to the principle of conservation of mass and momentum. These equations were approximated in space using the Finite Differences Method. In order to distinguish between the different types of faults and reconstruct their behaviors, the diagnostic system operates in stages. The first one —which is called Fault Detection and Isolation— aims to isolate each fault symptom with the help of a set of redundant relations that are deduced from the nominal model of the pipeline, i.e., in normal conditions. This first stage simplifies the second, called Fault Reconstruction, which is composed of observation algorithms that estimate the temporal evolution of the isolated faults. The overall diagnostic system is validated through a series of experiments carried out in a pilot hydraulic pipeline at the Engineering Institute, UNAM. This pipeline is approximately 200 m long and was implemented and built specifically to carry out tests to monitor pipelines.

Keywords: Diagnostic systems, fault detection, hydraulic pipelines, pipeline monitoring.

Resumen

Torres, L., Verde, C., Carrera, R., & Cayetano, R. (julio-agosto, 2014). Algoritmos de diagnóstico para fallas en ductos. Tecnología y Ciencias del Agua, *5(4), 55-76.*

Se presenta el diseño de un sistema de diagnóstico basado en relaciones redundantes y observadores de estado —que funciona manteniendo al sistema de transporte en operación— para la detección, identificación y reconstrucción de fallas en ductos, tales como: anomalías en los instrumentos de medición, bombas y extracciones desconocidas. Los algoritmos se desarrollaron a partir de ecuaciones diferenciales parciales no lineales que caracterizan el comportamiento del fluido —considerando el principio de conservación de masa y momento— y que fueron discretizadas en el espacio utilizando el Método de Diferencias Finitas. Con la finalidad de discernir entre los diferentes tipos de fallas y de reconstruir el comportamiento de éstas, el sistema de diagnóstico opera por etapas. La primera etapa, llamada de Detección y Aislamiento de Fallas, tiene como objetivo aislar el síntoma de la falla con ayuda de un conjunto de relaciones redundantes deducidas a partir del modelo nominal del ducto. Esta etapa de aislamiento simplifica la segunda etapa: Reconstrucción de la Falla, en la que algoritmos de observación estiman la evolución temporal de la falla aislada. El sistema completo de diagnóstico se validó mediante una serie de experimentos realizados en un modelo hidráulico piloto de aproximadamente 200 m de largo, instrumentado y construido específicamente para llevar a cabo pruebas de monitoreo de ductos en el Instituto de Ingeniería de la Universidad Nacional Autónoma de México.

Palabras clave: *tuberías hidráulicas, detección de fallas, monitoreo de ductos, sistemas de diagnóstico.*

Introduction

The automated surveillance and monitoring of pipes is an engineering challenge given the catastrophic consequences that can be caused by pipes in poor condition, including the loss of human life and environmental damages with high ecological impacts. In general, the objectives of a real-time automated monitoring system consist of locating the presence of a fault as quickly as possible with minimal instrumentation and costs.

With SCADA (Supervisory Control and Data Acquisition) systems, which operate in real time to register pressures and flows at specific points in piping networks, automated locators of faults have been implemented using physical and virtual sensors designed according to calculation and identification algorithms (Stoianov, Lama, Sam, Timur, & Csail, 2007; Korbicz, Koscielny, Kowalczuk, & Cholewa, 2004; Makar & Chagnon, 1999). The anomalies of most interest for real-time locating include pump and servovalve faults, leaks in the body of pipes and obstructions. If the pipes are underground or in water, the inspection is more difficult. In addition, when it is not possible to suspend operations of the pipe the diagnostics must be made considering dynamic phenomena associated with the fluid in question. It is simpler to detect faults of considerable magnitude than small faults since the sensors do not always have the sensitivity required to indicate small deviations and the noise in the measurements affects the precision of the estimates.

In terms of the design of the algorithms used to detect and locate a leak in pipes, different static behavior models have been used (Billmann & Isermann, 1987; Carrera & Verde, 2001). Recently, these models have been successfully applied to the case of pipes with non-uniform topographic profiles (González, Verde y Torres, 2013). In spite of their simplicity, the main disadvantage of these models is that they cannot be used if the fluid is not in somewhat static conditions.

As an alternative, Brunone and Ferrante (2001) formulated a methodology based on the behavior of the pressure wave reflected from its point of origin when reaching a leak. In these conditions, the time it takes for the wave to arrive enables determining the position of the leak. Wang, Lambert, Simpson, & Vtkovsky (2005) also studied the characteristics of the pressure wave and reported that it attenuates in function of the position of the leak. Meanwhile, Mpesha, Chaudry, & Gassman (2001), and Covas, Ramos, & De Almeida (2005) developed methods based on the frequency response of the piping, whose dynamic response can be obtained by causing periodic transients by opening and closing a valve. If there are leaks in the pipe, the frequency response of the pressure shows additional resonant peaks. Based on the frequency of these peaks, the position of the leak can be calculated. Ferrante and Brunone (2003) also found an approach involving frequency and solved the water hammer equations using the impulse response method. Using harmonic analysis of the solution, they concluded that the position and the size of a leak can be identified based on transitory pressure.

When precise analytical models are available, symptoms of faults in complex systems can be obtained using very affordable software, with tools developed by the automated control community (Isermann, 2011). The key to generating symptoms of faults is to identify incoherence in the system by measuring and evaluating a residual whose value is zero in normal conditions, where a deviation from this will occur during abnormal events. Said incoherency can be obtained using mathematical models with the help of filters or parity relations (Chow & Willsky, 1984), by estimating parameters (Isermann & Muenchhof, 2011), and using observation techniques (Chen & Patton, 1999). The tools directly or indirectly exploit the behavior of the system by substituting the multiplicity of physical sensors with algorithms that are executed in real time. For more details about Fault Detection and Isolation (FDI), see Verde, Gentil and Morales (2012). In particular, the detection of faults in process instrumentation has been widely addressed with the idea proposed by Frank (1990) of using a bank of observers with specific tasks. Recently, some general techniques to estimate faults have been presented by Zhang (2011) and Boulkroune, Galvez-Carrillo and Kinnaert, (2011).

The above discussion motivated the development of the present work, whose primary contribution is a diagnostic system

that generally considers faults in measuring instruments and pumps as well as leaks in pipes. The system uses an algorithm that can distinguish among different faults in real-time based on five residuals and a bank of dynamic high-gainobservers to reconstruct the evolution of the detected fault.

Preliminaries in the Diagnostics of Faults

In the FDI community, a fault is defined as an unallowable deviation of at least one property characteristic of a system (Isermann, 2006). These deviations can occur in sensors, actuators or in the components of the process. The real-time monitoring of a process with the ability to detect and isolate faults and evaluate their importance and seriousness is known as a fault diagnostics system. These systems involve three tasks (Patton, Frank, & Clarke, 2000).

- Detection of the fault: make a binary decision about the state of the system according to the nominal operating conditions. For example, establish whether an abnormal event is present in the process.
- Isolation of faults: determine the type of fault present, for which a symptom must be present, such as stipulating which sensor, actuator or component has abnormal conditions.
- Identification or reconstruction of the fault: calculate the size and type of the fault, including its temporal evolution.

The basic idea of detection is the use of knowledge models with redundancy to verify that the current behavior of the system is consistent with the nominal model established. One of the advantages of the redundancy of information is that it can be evaluated simply by means of a process, under well-characterized operating conditions, and without the need for additional physical instrumentation. Nevertheless, an adequate model of the behavior of the system must exist. Figure 1 describes the detection principle, comparing models and identifying incoherence as a consequence of the fault. To generate analytical redundancy, the most common dynamic model of the concentrated parameters is the spatial representation of states:

$$\dot{x}(t) = f\left(x(t), u(t)\theta(t)\right)$$
$$y(t) = h\left(x(t)\right) \qquad (1)$$

where $x(t) \in R^n$ are the states of the system; $u(t) \in R^m$ are the exogenous inputs or control signals; $y(t) \in R^p$ are the outputs and measurable process variables and $\theta(t) \in R^{n\theta}$ represents the physical parameters of the system (such as length, elasticity, friction, etc.)

Supposing that the model (1) and the input vector $u(t)$ are known, the output $\hat{y}(t)$ can be calculated. And if the output is also known through measurements $y(t)$, the same information is available twice and there is redundancy. In abnormal modeling conditions, the measured output $y(t)$ is incoherent with the calculated output $\hat{y}(t)$ and the redundancy is lost. The equations that can be obtained with the model and the measurements with redundancy are known as analytical redundancy relations and these enable generating residuals $r(t)$ with the following property (Gertler, 1991):

$$r\left(t\right) = \begin{cases} 0 & \text{normal condition} \\ \neq 0 & \text{abnormal condition} \end{cases} \qquad (2)$$

Thus, $r(t)$ different than zero denotes an error in the mathematical model, and with the help of the residuals symptoms are determined for each fault by means of decision functions. Figure 1 describes this detection principle for generating residuals and symptoms.

In most of the applications, no residual exists $r(t)$ that is sensitive to only one fault and robust with respect to the other faults and to the uncertainties in the model. In this condition, residual patterns must be obtained to isolate the faults by specifically analyzing the model's

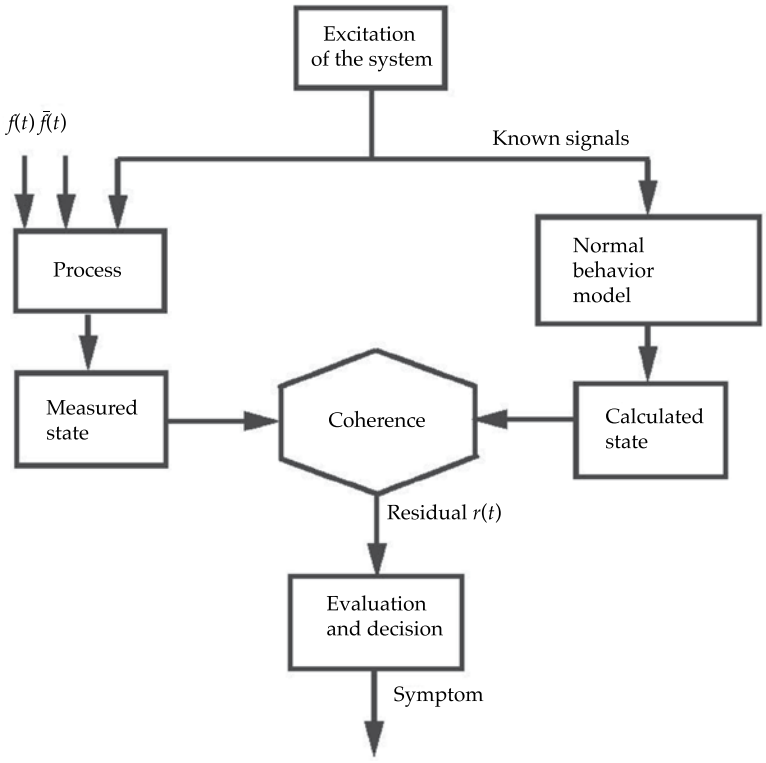

Figure 1. Beginning of obtainment of residual $r(t)$ and symptom of faults where $f(t)$ are the faults of interest and $\tilde{f}(t)$ denotes disturbances and noise.

equations and the behavior resulting from the faults.

The stage of reconstructing a fault once it has been determined to be present is mainly based on algorithms to calculate parameters and observe states. Techniques to calculate parameters are appropriate if the faults are associated with changes in the parameters of the model; that is, since the faults in the dynamic system are reflected by the physical parameters. The idea of this approach is to reconstruct the faults by calculating parameters of mathematical models (Ljung, 1999).

The observer technique is suitable if the faults produce changes in actuators, sensors or non-measurable state variables. Recently, the reconstruction of faults has been proposed using observer of the model (1) in abnormal conditions, in which the vector $x(t)$ is extended with the parameters associated with the faults. That is, the extended vector is considered to contain the parameters associated with the faults $\theta(t)\in R^{n_\theta}$, resulting in:

$$x_e(t)\rightarrow\begin{bmatrix}x(t)\\ \theta(t)\end{bmatrix} \tag{3}$$

where $x_e(t)\in R^{n+n_\theta}$ denotes the extended space. A property of this type of calculation is that it enables jointly calculating parameters and states. This advantage led to the selection of the observation algorithms for reconstructing the faults in the case of pipes.

Observation Algorithm

Definition 1. *An observer of states is a dynamic algorithm whose objective is to calculate the variables of a process* $\hat{x}(t)$ *using model (1), the available measurements* (u(t) *and* y(t)) *and an*

error correction term between measurements and calculations, which ensures the convergence of the states. Given that the observers calculate states using software, they are also called virtual sensors (Besançon, 2007).

The block diagram of an observer connected to a process has the structure shown in Figure 2, where the calculation error I$e(t) = y(t) - \hat{y}(t)$ corresponds to the difference between the measured output $y(t)$ of the process and the estimated output $\hat{y}(t)$. The objective of the observer is to make the error $e(t)$ converge at zero when time approaches infinity. In practice, the error should be sufficiently small over a short time period.

An important contribution of non-linear observer theory was reported by Gauthier, Hammouri and Othman (1992). These authors presented the design of an observer, called high gain, for non-linear systems composed of a linear dynamic term and a non-linear term with a triangular shape and bounded, which is affected by the inputs (Khalil, 2002). The tuning of the observer, in this case, is performed by adjusting only one parameter, λ, while the convergence is ensured by the single solution of the Lyapunov equation (Bornard & Hammouri, 1991).

Appendix A describes the generic algorithm for the high-gain observer proposed by Gauthier *et al.*, and used with fluid and fault models to reconstruct the parameters of the scenarios involving faults in pipes and instrumentation.

Dynamic Fluid Model

Assuming that the distribution of velocity is uniform, the flow is dimensionless and the density and area of the liquid are constant, the dynamic of a fluid in a closed horizontal pipe without lateral intakes is governed by the movement and continuity equations:

$$\frac{\partial H(z,t)}{\partial t} + \frac{b^2}{gA_r}\frac{\partial Q(z,t)}{\partial z} = 0 \qquad (4)$$

$$\frac{1}{A_r}\frac{\partial Q(z,t)}{\partial t} + g\frac{\partial H(z,t)}{\partial z} - \frac{fQ(z,t)|Q(z,t)|}{2\phi A_r^2} = 0 \qquad (5)$$

with $(z,t) \in (0,L) \times (0, \infty)$ as coordinates of time (s) and space (m). The parameters involved in the set (4) and (5) are listed in Table 1.

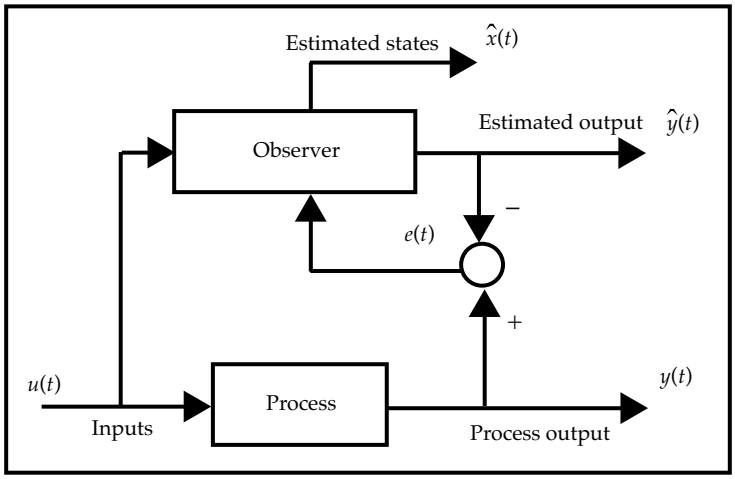

Figure 2. Calculation with observer of states.

Table 1. Parameters and physical variables of the fluids model.

Symbol	Parameter/variable	Unit
g	Gravity	(m/s^2)
b	Velocity of the pressure wave	(m/s)
ϕ	Diameter	(m)
L	Length	(m)
A_r	Area	(m^2)
f	Friction coefficient	-
$Q(z,t)$	Flow	(m^3/s)
$H(z,t)$	Pressure load	(m)

Since an analytical solution of system (4) and (5) does not exist, numerical methods must be used to obtain an approximate solution. Some of these solutions can be found in Chaudhry (1987), Wylie and Streeter (1983), and Torres, Besançon and Georges (2008). In this work, the finite differences method is used because of its simplicity, and because the structure of the models resulting from the finite dimension are Hessenberg systems (Bernard, Sallet, & Sciandra, 1998), a desired characteristic for estimating the states of a fluid $H(z,t)$ and $Q(z,t)$, with high gain-observers.

Finite Models

To obtain a finite dimension model based on the set (4) and (5), boundary conditions need to be defined that express the temporal profiles $H(z,t)$ and $Q(z,t)$ at the boundaries of the pipes, that is, the pipe's spatial coordinates $z = 0$ and $z = L$. In addition, the initial conditions need to be defined that express the spatial profiles of the fluid and initial pressure ($t = 0$), that is:

$$H(z,0) = H^0(z), Q(z,0) = Q^0(z) \qquad (6)$$

As upstream and downstream boundary conditions, ($z = 0$) and ($z = L$), respectively, Dirichlet conditions are used, expressed as 1) upstream water pressure, $H(0,t) = H_e(t)$; 2) downstream water pressure $H(L,t) = H_s(t)$; 3) upstream flow, $Q(0,t) = Q_e(t)$; 4) downstream flow $Q(L,t) = Q_s(t)$.

Various finite differences approaches exist (for example, see Leveque, 2007). Therefore, the spatial partial derivatives by first-order finite differences will be discussed next.

$$\frac{\partial H(z,t)}{\partial z} \approx \frac{\Delta H_i(t)}{\Delta z_i} = \frac{H_i(t) - H_{i+1}(t)}{\Delta z_i}$$

$$\frac{\partial Q(z,t)}{\partial z} \approx \frac{\Delta Q_i(t)}{\Delta z_i} = \frac{Q_i(t) - Q_{i+1}(t)}{\Delta z_i}$$

and the time derivative are defined as:

$$\frac{\partial H(z,t)}{\partial t} \cong \frac{\partial H_i(t)}{\partial t} := \dot{H}_i$$

$$\frac{\partial Q(z,t)}{\partial t} \cong \frac{\partial Q_i(t)}{\partial t} := \dot{Q}_i$$

where index i denotes the discretized spatial section. To reduce the presentation of the model, the variable t is omitted in unnecessary cases and the following notation is used:

$$H(z,t) \cong H_i(t) := H_i \text{ upstream pressure in section } i$$

$$Q(z,t) \cong Q_i(t) := Q_i \text{ flow in section } i$$

Thus, in each section i of the pipe, the set of fluid equations is transformed into:

$$\dot{H}_{i+1} = a_2 \frac{Q_i - Q_{i+1}}{\Delta z_i} \qquad (7)$$

$$\dot{Q}_i = a_1 \frac{H_i - H_{i+1}}{\Delta z_i} + \mu Q_i |Q_i| \quad (8)$$

with $a_i = gA_r$, $a_2 = \frac{b^2}{gA_r}$ y $\mu = -\frac{f}{2\phi A_r}$

In addition, to consider the effect of a leak at position z_f in equations (7) and (8), the extraction flow must be included:

$$Q_f(z_f, t) = H_f(t)\sigma_f \sqrt{H(z_f, t)} \quad (9)$$

where $\sigma_f = \sqrt{2g} A_f C_f \geq 0$; A_f is the area of the orifice; C_f is the discharge coefficient; and H_f is the Heaviside function which represents the occurrence of a leak at instant t_f.

For the case of various leaks, n_f is defined as the total number of leaks in a pipe; $k = 1,...,$ n_f as the identifier of each leak, and $Q_{f_k}(z_{f_k}, t)$ as the flow of the leak associated with k. Thus, the presence of a leak k at instant t_{fk} is described by $H_{f_k}(t)$, where the coefficient σ_{fk} and its position z_{fk} characterize each event. When an extraction Q_{fk} is present between sections Δz_i and_Δz_{i-1}, the conservation of mass is expressed as $Q_i - Q_{i+1} - Q_{f_k} = 0$. Therefore, at each leak point, the relation of flows between section

$$\frac{\Delta Q_i}{\Delta z_i} = \frac{Q_i - Q_{i+1}}{\Delta z_i}$$

is replaced by:

$$\frac{\Delta Q_i}{\Delta z_i} = \frac{Q_i - Q_{i+1} - Q_{f_k}}{\Delta z_i}$$

with Q_{f_k} expressed by (9). Thus, the pipe with extractions is described as:

$$\dot{Q}_i = \frac{a_1}{\Delta z_i}(H_i - H_{i+1}) + \mu Q_i |Q_i| \quad (10)$$

$$\dot{H}_{i+1} = \frac{a_2}{\Delta z_i}(Q_i - Q_{i+1} - Q_{f_k}) \quad (11)$$

for $i = 1,...,$ n and with exogenous variables $H_1 = H_e$ and $H_{n+1} = H_s$, which are the boundary conditions.

Diagnostic System for the Pipe

Based on the analytical flow model (10) and (11) with $Q_{f_k} = 0$, and considering flow and pressure loads at the ends of the duct as the only measurements available, that is H_1, H_{n+1}, Q_1 and Q_n, the development of the diagnostic algorithms for five abnormal scenarios is presented next:

- E1: fault in the pump upstream.
- E2: fault in the pump downstream or in the storage system.
- E3: fault in the flow sensor upstream.
- E4: fault in the flow sensor downstream.
- E5: leak at an unknown position in the pipe.

Figure 3 shows the diagnostics of faults, proposed and developed according to two stages: 1) detection and isolation and 2) reconstruction. The first consists of five redundant relations to isolate the faults. The second stage is designed using dynamic observers and reconstructs the fault once it is identified. It is worth noting that only one observer is activated based on the symptom identified.

Detection and Isolation of Faults

To obtain residuals for the fault scenarios (E1-E5), the nominal model (10) and (11) is used, considering the faults as additive elements in sensors, pumps and leaks.

The most widely used residual is very simple and is generated based on the flow difference:

$$r_1 = Q_e - Q_s \quad (12)$$

which is zero if the pipe operates normally and deviates from zero when there are leaks in the pipe or there is an error in one of the flow measurements; that is, r_1 deviates from zero in scenarios E3, E4 and E5.

Considering a pipe of length L in permanent state, based on (10) and (11), the relation:

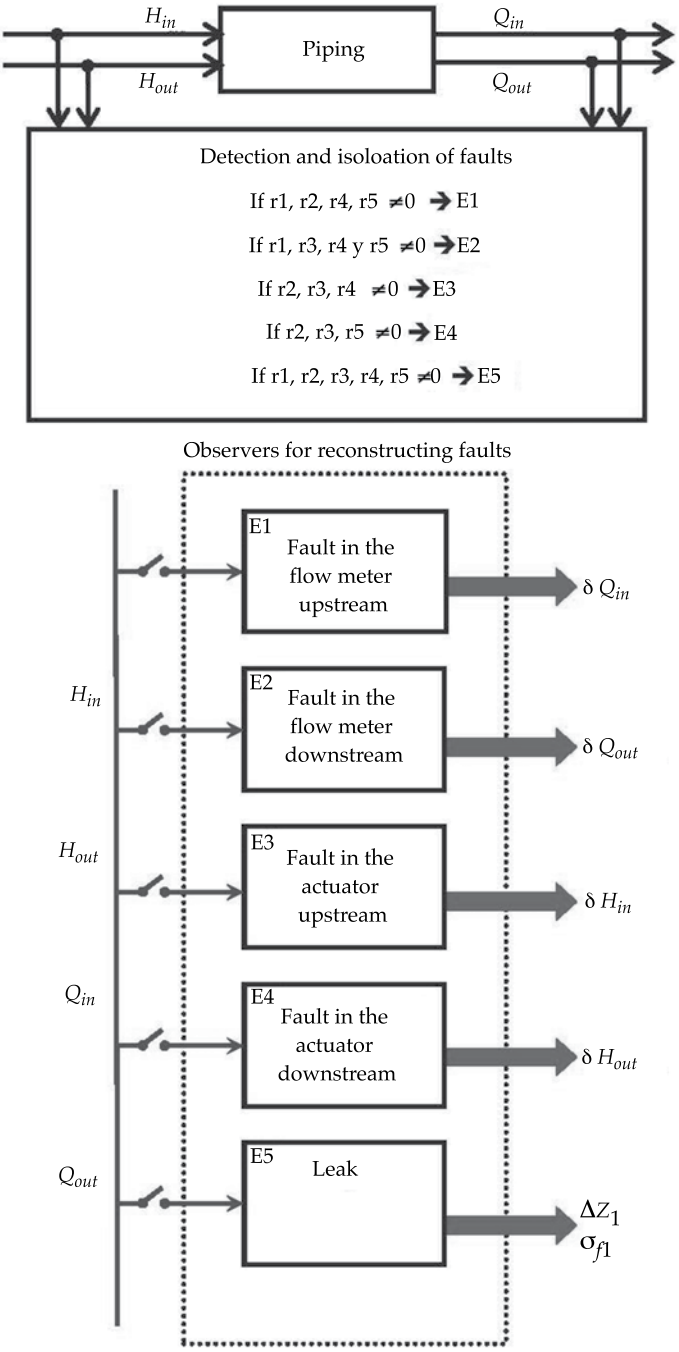

Figure 3. Diagnostics of faults for piping.

$$r_2 = \mu Q_e |Q_e| + \frac{a_1}{L}(H_e - H_s) \qquad (13)$$

equals zero in normal conditions and deviates from zero with four fault scenarios: E1, E1, E3 and E5.

Since (13) does not depend on the flow measurements downstream, Q_s, it is not sensitive to the measurements of that variable. Likewise, because of the symmetry of the model, the residual:

$$r_3 = \mu Q_s |Q_s| + \frac{a_1}{L}(H_e - H_s) \quad (14)$$

equals zero when the pipe has no leaks and the information about the pressures and the flow downstream are correct. Whereas its value deviates from zero when there is a leak or there is an error in any of the measurements mentioned. Since r_3 does not depend on Q_e, it is insensitive to input flow measurements.

With the help of residuals (12-14) the first three rows of the fault matrix (17) are obtained, where a deviation in one variable is preceded by δ and • denotes a residual different than zero, with the corresponding abnormality in the column. From this matrix it can be seen that if only one scenario is assumed to be present, it is possible to detect which flow sensor is damaged in both leak and normal conditions. On the other hand, errors in H_e and H_s cannot be isolated since both residuals, r_2 and r_3, are sensitive to both errors.

Considering the discretized model with two sections of equal sizes, the following system of equations is obtained:

$$\dot{Q}_e = \mu Q_e |Q_e| + \frac{a_1}{L/2}(H_e - H_f)$$

$$\dot{H}_f = \frac{a_2}{L/2}(Q_e - Q_s - Q_f)$$

$$\dot{Q}_s = \mu Q_s |Q_s| + \frac{a_1}{L/2}(H_f - H_s)$$

and eliminating the unknown variable H_f results in the integro-differential equation:

$$r_4 = Q_e - \mu Q_e |Q_e| + \alpha_1 \int_{t_0}^{t} (Q_e - Q_s) d\tau - \alpha_2 H_e \quad (15)$$

With $\alpha_1 = \frac{a_1 a_2}{0.25L}$ and $\alpha_2 = \frac{a_1}{0.5L}$. Therefore, r_4 equals zero given deviations in the downstream pressure, H_s, and leaks in the body of the pipe. Because of the symmetry of the model, we have the residual equation:

$$r_5 = Q_s - \mu Q_s |Q_s| - \alpha_1 \int_{t_0}^{t} (Q_e - Q_s) d\tau - \alpha_2 H_s \quad (16)$$

which does not depend on the input pressure H_e. Adding the two new residuals (15) and (16) to the matrix of abnormal case signatures, we have:

	δQ_e	δQ_s	δH_e	δH_s	Q_f
r_1	•	•			•
r_2	•		•	•	•
r_3		•	•	•	•
r_4	•	•	•		•
r_5	•	•		•	•

(17)

This matrix shows that all the residuals are sensitive to the presence of the leak (last column) and theoretically any of them could be used to diagnose it. Nevertheless, since not all the residuals respond to a leak in the same way, the use of the one whose magnitude is most sensitive is recommended. For the measurements of flow volumes and action signals associated with pressures, a different residual pattern is obtained for each scenario with abnormal conditions and, therefore, all the faults considered can be isolated.

Algorithms for Reconstruction of Faults

As a second stage to reconstruct the five faults, the non-linear model for the corresponding fault is used, in which the parameters θ(*t*) associated with the faults are additional states according to vector (3) and can be estimated using non-linear observation algorithms. This work uses the high-gainobservation algorithm described in Appendix A.

The algorithm for the discretized model of the fluid (10) and (11) is given the form:

$$f(x(t), u(t), \theta(t)) = F(x_e(t), u) + Gy(t)$$

Obtaining:

$$\dot{x}_e(t) = F(x_e(t), u(t)) + G(y(t)) \quad (18)$$

where the vector of the extended states, $x_e(t)$, is defined by state $x(t)$ and the parameters $\theta(t)$ to be estimated that are associated with the fault in question, while the inputs vector is given by:

$$u(t)=\left[u_1(t),u_2(t)\right]^T=\left[H_e(t),H_s(t)\right]^T,$$

consisting of the pressures at the ends of the pipe. In the case of operating the pipe with constant pressures or slow dynamics, $u(t) = u_0$ is assumed.

For the design of the non-linear observers, the variables that can be measured are considered to be the flows at the ends of the piping. That is:

$$y=h\left(x_e(t)\right)=\left[Q_e\,Q_s\right]^T \tag{19}$$

Nevertheless, both measurements are not needed in all cases of reconstructing faults, therefore the measured variables used are defined for each fault scenario.

Reconstruction of a Leak in a Pipe

Assuming that the instrumentation is in good condition, the objective now is to calculate the position and coefficient of a leak in a pipe. With (10) and (11), when a leak is occurring, the model should be divided into at least two sections with different flows, before and after the leak. Therefore, a finite dimension model of the fluid that represents at least both sections is needed.

The following system of equations is proposed:

$$\begin{aligned}\dot{Q}_e&=\mu Q_e\,|Q_e|+\frac{a_1}{\Delta z_1}\left(H_e-H_f\right)\\ \dot{H}_f&=\frac{a_2}{\Delta z_1}\left(Q_e-Q_s-\sigma_f\sqrt{H_f}\right)\\ \dot{Q}_s&=\mu Q_s\,|Q_s|+\frac{a_1}{\Delta z_2}\left(H_f-H_s\right)\end{aligned} \tag{20}$$

where the position of the leak is given by the size of the first section $\Delta z_1 \in [0, L]$, while the size of the second section is $\Delta z_2 = L - \Delta z_1$.

To complete the model, two additional states associated with the parameters of an unknown extraction or leak are added to the vector of the states of the system (20), for example:

$$x(t)=\left[Q_e\;H_f\;Q_s\right]^T$$

$$\theta(t)=\left[\Delta z_1\;\sigma_f\right]^T$$

thereby creating the augmented vector (3). Taking into account that these parameters are constant, their derivatives are set to zero, therefore:

$$\dot{\Delta}z_1=0,\;\dot{\sigma}_f=0$$

Following the procedure for the high-gain observer described in Appendix A, for the vector of the states:

$$x_e(t)=\left[Q_e\;H_f\;Q_s\;\Delta z_1\;\sigma_f\right]^T$$

the parameters associated with the leak can be reconstructed by calculating q(*t*) based on the observer:

$$\begin{bmatrix}\dot{\hat{Q}}_e\\ \dot{\hat{H}}_f\\ \dot{\hat{Q}}_s\\ \dot{\hat{\Delta}}z_1\\ \dot{\hat{\sigma}}_f\end{bmatrix}=\begin{bmatrix}\mu\hat{Q}_e\,|\hat{Q}_e|+\frac{a_1}{\hat{\Delta}z_1}\left(H_e-\hat{H}_f\right)\\ \frac{a_2}{\hat{\Delta}z_1}\left(\hat{Q}_e-\hat{Q}_s-\hat{\sigma}_f\sqrt{\hat{H}_f}\right)\\ \mu\hat{Q}_s\,|\hat{Q}_s|+\frac{a_1}{L-\hat{\Delta}z_1}\left(\hat{H}_f-H_s\right)\\ 0\\ 0\end{bmatrix}-K(.)\begin{bmatrix}\hat{Q}_e-Q_e\\ \hat{Q}_s-Q_s\end{bmatrix} \tag{21}$$

whose convergence gain is expressed as:

$$K(.)=\begin{bmatrix} 2\lambda & 0 \\ -\frac{\lambda^2\hat{\Delta}z_1^2}{a_1}\hat{H}_f & 0 \\ 0 & 3\lambda \\ 0 & \frac{3\lambda^2\left(L-\hat{\Delta}z_1\right)}{a_1} \\ 0 & \Pi \end{bmatrix}$$

$$\Pi=-\frac{3\lambda}{\sqrt{\hat{H}_f}}-\frac{3\lambda^2\hat{\sigma}_f\left(L-\hat{\Delta}z_1\right)}{2a_1\hat{H}_f}$$

$$-\frac{\lambda^3\hat{\Delta}z_1\left(L-\hat{\Delta}z_1\right)}{a_1a_2\sqrt{\hat{H}_f}}$$

where λ is a design parameter to adjust the convergence time of the estimated values to the real values (see appendix). This observer is conceived considering (19) as the vector of outputs vector; that is, the measurements of the flows at both ends.

Reconstruction of Faults in Flow Meters

For fault scenarios involving flow meters, these are assumed to be biased additives, known as *offsets*, therefore the fault models are reduced to:

$$\tilde{Q}_e=Q_e+\delta Q_e$$

$$\tilde{Q}_s=Q_s+\delta Q_s$$

Substituting these models in (10) and (11) for only one section of length *L*, two extended models are obtained:

- For faults in the sensor upstream:

$$\dot{\tilde{Q}}_e=\mu\left(\tilde{Q}_e-\delta Q_e\right)\left|\tilde{Q}_e-\delta Q_e\right|+\frac{a_1}{L}\left(H_e-H_s\right)$$

$$\dot{\delta Q}_e=0$$

with $x_e(t)=\left[\tilde{Q}_e\ \delta Q_e\right]^T$

- For faults in the sensor downstream:

$$\dot{\tilde{Q}}_s=\mu\left(\tilde{Q}_s-\delta Q_s\right)\left|\tilde{Q}_s-\delta Q_s\right|+\frac{a_1}{L}\left(H_e-H_s\right)$$

$$\dot{\delta Q}_s=0$$

with $x_e(t)=\left[\tilde{Q}_s\ \delta Q_s\right]^T$.

In this pair of models, the unknown variables $\dot{\delta Q}_e=0$ and $\dot{\delta Q}_s=0$, respectively, represent the dynamic constant of the bias to be calculated. The discretized finite model with only one section is selected since the flow throughout the duct is in a permanent state without extractions.

Following the procedure described in Appendix A, the equation for the high-gain observation algorithm designed for the case of a fault in a flow meter upstream is reduced to:

$$\begin{bmatrix} \dot{\hat{\tilde{Q}}}_e \\ \dot{\hat{\delta Q}}_e \end{bmatrix}=\begin{bmatrix} \mu\left(\hat{\tilde{Q}}_e-\hat{\delta Q}_e\right)\left|\hat{\tilde{Q}}_e-\hat{\delta Q}_e\right|+\frac{a_1}{L}\left(H_e-H_s\right) \\ 0 \end{bmatrix}$$

$$-K(.)\left[\hat{\tilde{Q}}_e-\tilde{Q}_e\right] \qquad (22)$$

with the gain:

$$K(.)=\begin{bmatrix} 2\lambda \\ \frac{-\lambda^2}{\Omega}+2\lambda \end{bmatrix}$$

$$\Omega=\mu\left|\hat{\tilde{Q}}_e-\hat{\delta Q}_e\right|+\mu\hat{\tilde{Q}}_e\,\mathrm{sign}\left(\hat{\tilde{Q}}_e-\hat{\delta Q}_e\right)$$

$$-\mu\hat{\delta Q}_e\,\mathrm{sign}\left(\hat{\tilde{Q}}_e-\hat{\delta Q}_e\right)$$

Assuming that $\left(\hat{\tilde{Q}}_e-\hat{\delta Q}_e\right)>0$, the gain is reduced to:

$$K(.)=\begin{bmatrix} 2\lambda \\ \frac{-\lambda^2}{2\mu\left(\hat{\tilde{Q}}_e-\hat{\delta Q}_e\right)}+2\lambda \end{bmatrix}$$

In this case, the design of the observer uses only the flow measurement upstream, $y = h(x_e(t)) = Q_e$.

Reconstruction of Faults in a Pumping System

In the case of faults in the pumping system or storage system at the ends of a pipe, the fault models considered are:

$$\tilde{H}_e = H_e + \delta H_e$$

$$\tilde{H}_s = H_s + \delta H_s$$

To design the observers that calculate pressure faults at the ends, a discretized model with at least two spatial sections is needed, similarly to the reconstruction of a leak. For the case of faults upstream, the model considered for the design of the observation algorithm is:

$$\dot{Q}_e = \mu Q_e |Q|_e + \frac{a_1}{\Delta z_1}\left(\tilde{H}_e - \delta H_e - H_f\right)$$

$$\dot{H}_f = \frac{a_2}{\Delta z_1}\left(Q_e - Q_s\right)$$

$$\dot{Q}_s = \mu Q_s |Q_s| + \frac{a_1}{\Delta z_2}\left(H_f - H_s\right)$$

$$\delta\dot{H}_e = 0$$

Given the symmetry, for a fault in the pressure downstream, the observer is based on the model:

$$\dot{Q}_e = \mu Q_e |Q_e| + \frac{a_1}{\Delta z_1}\left(H_e - H_f\right)$$

$$\dot{H}_f = \frac{a_2}{\Delta z_1}\left(Q_e - Q_s\right)$$

$$\dot{Q}_s = \mu Q_s |Q_s| + \frac{a_1}{\Delta z_2}\left(H_f - \tilde{H}_s + \delta H_s\right)$$

$$\delta\dot{H}_s = 0$$

The high gain observation algorithm designed for the fault in the pumping system upstream is given by:

$$\begin{bmatrix} \dot{\hat{Q}}_e \\ \dot{\hat{H}}_f \\ \dot{\hat{Q}}_s \\ \delta\dot{\hat{H}}_e \end{bmatrix} = \begin{bmatrix} \mu\hat{Q}_e|\hat{Q}_e| + \frac{a_1}{\Delta z_1}\left(\tilde{H}_e - \hat{H}_f - \delta H_e\right) \\ \frac{a_2}{\Delta z_1}\left(\hat{Q}_e - \hat{Q}_s\right) \\ \mu\hat{Q}_s|\hat{Q}_s| + \frac{a_1}{\Delta z_2}\left(\hat{H}_f - H_s\right) \\ 0 \end{bmatrix} - K(.)\begin{bmatrix} \hat{Q}_e - Q_e \\ \hat{Q}_s - Q_s \end{bmatrix} \quad (23)$$

which is conceived considering the flow measurements at both ends as the output vector, for example, equation (19). Supposing that the flow satisfies the condition $\hat{Q}_e > 0$, the reduced gainof the observer is expressed as:

$$K(.) = \begin{bmatrix} 2\lambda & 0 \\ 0 & \frac{\Delta z_2\lambda^2}{a_1} - \frac{4\mu\hat{Q}_s\Delta z_2\lambda}{a_1} \\ 0 & 2\lambda \\ \Theta & -\frac{\Delta z_2\lambda^2}{a_1} + \frac{4\mu\hat{Q}_s\Delta z_2\lambda}{a_1} \end{bmatrix}$$

$$\Theta = -\frac{\Delta z_1\lambda^2}{a_1} + \frac{4\mu\hat{Q}_e\Delta z_1\lambda}{a_1}$$

Physical Pilot Model

The experimental installation to detect leaks is a 40-cell steel pipe 4 inches in diameter in the shape of a spiral on a vertical plane, as shown in Figure 4. The flow input is in the lower part and its output in the upper portion. There is a 10 000 liter cistern of potable water, a 7.5 HP hydraulic pump and step valves at the input and output. Flow and pressure sensors are located at both ends of the pipe. A 1-inch diameter valve is located approximately in the middle of each horizontal pipe to simulate leaks.

The pipe has a physical length when measured directly from one point to another,

Figure 4. Side view of the pilot installation.

but the presence of elbows throughout the piping causes the pressure to fall more than that corresponding to the real length. Therefore, it is necessary to determine the length equivalent to a straight installation of the pipe. The equivalence is thereby obtained between the spiral pipe measuring 169.43 m and a straight pipe measuring 200.17 m.

The piping also has six valves (V1, V2, V3, V4, V5, V6) used to emulate leaks. Two are servovalves to perform repetitive experiments, and are located at 11.535, 49.825, 80.355, 118.365, 148.925 and 186.945 m, respectively, from the feed point. The values for the parameters of the installation are reported in Table 2.

The installation has three options to measure flow with three types of sensors: propeller, ultrasound and Coriolis force. These sensors are located at the beginning and the end of the pipe.

Table 2. Parameters of the test pipes (physical model).

Symbol	Value	Unit
b	1 497	(m/s)
ϕ	0.1047	(m)
L	200.16	(m)
f	2.785×10^{-2}	-

Monitoring, Control and SCADA Data Acquisition System

This system is mainly composed of two elements: hardware and software. The first consists of a personal computer connected to a data acquisition model via a TCP protocol, which is physically connected to the sensors, servovalves and the pump's actuator. The second consists of the application program developed in *LabVIEW*©.

The hardware: personal computer with Windows and tools to connect the *LabVIEW*© software with a modular data acquisition system with the *Modbus* (Beckhoff BK9000) protocol via a local Ethernet network. The communication between the application and the modular system is handled by an OPC server, which is the intermediary between the program and the input-output records via TCP communication. The acquisition models use a 4-terminal system with cable, with which all the sensors and actuators, having different types of signals, can be directly connected to the corresponding module.

The software: an acquisition and monitoring system for the integrated pipe using the L*abVIEW*© platform from the company National Instruments©. This is a general purpose programming system composed of libraries and functions and tools for developing specific designs for data acquisition and instrument control. The L*abVIEW*© programs are called virtual instruments because their appearance and operations can imitate commonly used instruments. Functionally, the system developed reads information from flow and pressure sensors, manages the opening of the servovalves and regulates the speed of the pump's motor. Depending on the application,

there is the option to only register data from one experiment for later processing offline, or the option to detect a leak in real-time with one of the detection methods developed by the Engineering Institute, as is the case of the algorithms validated in the present work.

Importance of Sensors to Calculate the Position of the Leak

The precise location of a leak not only depends on the method of detection and location but also on the type of measuring instruments. Figure 5 shows the estimate of the position of a leak located at 49.8 m for a fully (100%) open valve. The same calculation algorithm was used but with different flow sensors. It can be seen that, in addition to registering different locations, the standard deviations are notably different, causing uncertainty with regard to the location of the leak. The Coriolis force sensor was found to perform better.

Experimental Results

In order to evaluate the performance of the fault diagnostics system for pipes, various experiments were conducted which generated an extraction as well as alterations in the readings recorded by the flow and pressure sensors.

The unknown extraction event, or leak, was created by opening valve V4 to 150 s. The effect of the leak can be seen in the behavior of the flows shown in Figure 6. After the event, they deviate from the point of operation even though the pressure seems to remain constant, given that the flow from the leak is less than 8% and its effects on the load are not perceivable. This figure also shows the measured signals

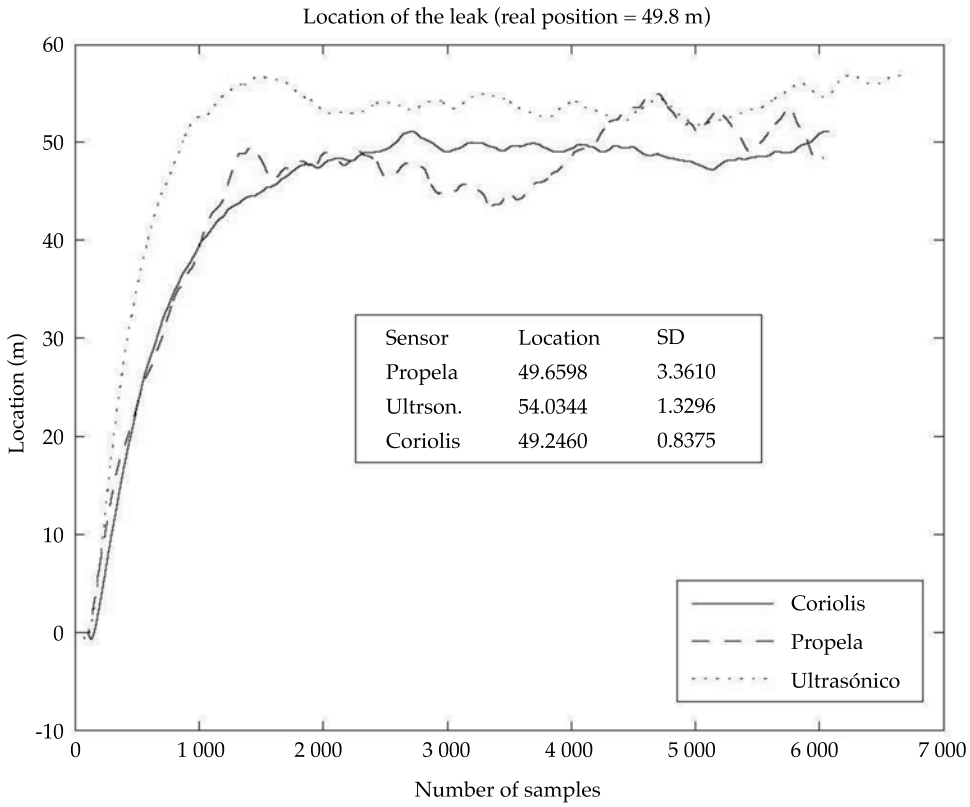

Figure 5. Deviation in the estimate of the position of hte leak, according tot he type of flow sensor.

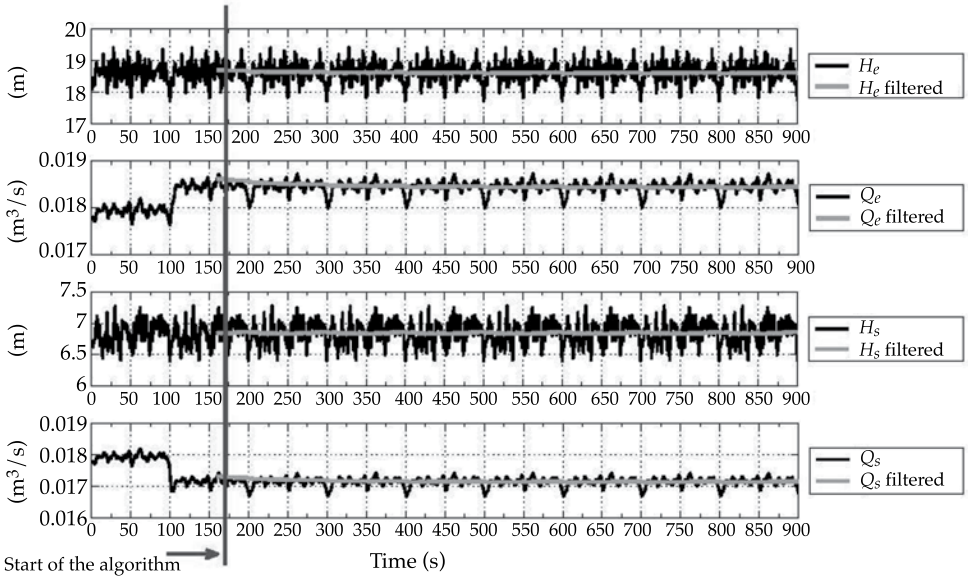

Figure 6. Measured flow signals and pressures at the ends of the pipe with extraction as of 100 s.

from the pressure at the ends of the piping used by the observers to conduct the calculations. In the graphs, filtered values were superimposed on the real measurements in order to improve the results of the calculation. The filtering was performed using a first-order low-pass filter with a cutoff frequency of w = 0.01 rad/s and a unity gain.

Isolation of Faults

Considering the real data from the pilot piping, Figures 7 and 8 show the evolution of three residuals (r_1, r_2, r_4) given abnormal scenarios. Figure 7 corresponds to the case of an extraction initiated at 100 s, in which it was demonstrated that the three residuals were different than zero once the extraction was present, as predicted by the fault signature matrix (17). Figure 8 shows the different scenarios. The top portion corresponds to the response of the residuals to a deviation in the flow meter downstream and the bottom portion the response to an error in the pumping system upstream. In both cases, the two sets of residuals responded according to the fault matrix (17) and, therefore, the fault can be isolated using logical conditions, as long as there is only one fault.

Reconstruction of Faults

Depending on the nature of the fault, once it is detected and isolated using the logical conditions given in the matrix (17), the reconstruction and value of the fault time is determined using the observation algorithm corresponding to the scenario identified. Next, the experimental results from the reconstruction observers are presented for the following three fault scenarios:

- E5: reconstruction of the leak f_k with algorithm (21).
- E3: reconstruction of the bias δQ_e in the flow meter upstream with algorithm (22).
- E1: reconstruction of the pumping fault with algorithm (23).

The evaluation of the performance of the locator with experimental data is based on the flow and pressure measurements shown in Figure 6.

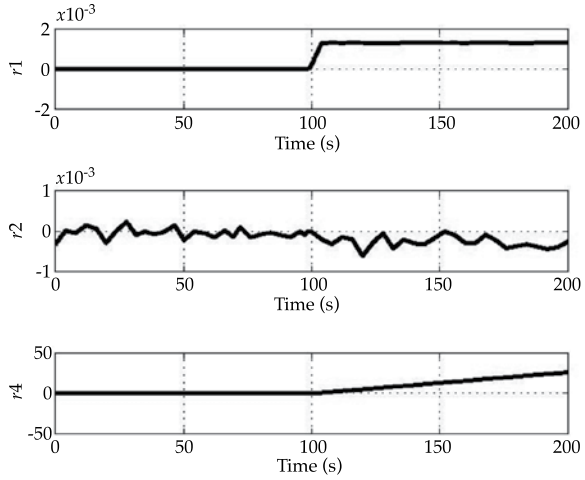

Figure 7. Evolution of residuals $r_1(t)$, $r_2(t)$ and $r_4(t)$, with an extraction produced at 100 s.

Fault scenario in the flow meter downstream with a bias of 50%

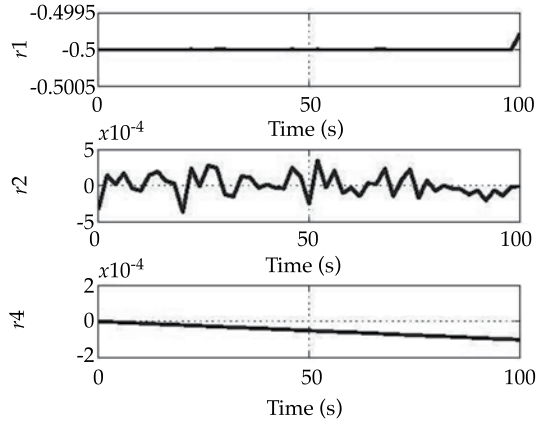

Fault scenario in the pumping system upstream with bias of 40%

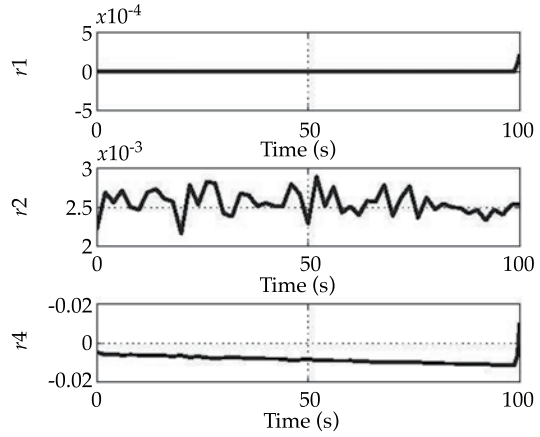

Figure 8. Evolution of residuals $r_1(t)$, $r_2(t)$ and $r_4(t)$ given two fault scenarios.

Calculation of a Leak

The observer for the calculation of leak (21) was started at time t = 160 s, once the generator of residuals identified that the symptom was due to an unknown extraction. It is worth mentioning that the observer only operates adequately in the presence of a leak, otherwise the convergence of the error cannot be guaranteed (Torres, Verde, Besançon, & González, 2012).

Figure 9 shows the evolution of the estimator of the position, performed by the observer for different values of λ, observing that the convergence time decreases when the value of λ increases. Nevertheless, the measurement noise also increases with an increase in λ. Figure 10 shows the calculation of the position of the leak when the convergence parameter is fixed at λ = 3 for two different cases —with and without filtered signals. In both figures, the values calculated are shown to be close to the real value of the real position of the leak.

Calculation of Bias in a Flow Meter

To evaluate the observer for the reconstruction of faults in the flow sensor upstream (22), a constant signal of 3 x 10^{-3}m^3/s was added to the measurements upstream. The observer was initialized at time t = 0 s in the experiment shown in Figure 6; that is, when there was no presence of a leak. The initial conditions chosen for the observer were different than for the real pipe, and it was tuned with λ = 2. The input signals were filtered with two different cutoff frequencies, whose values are shown in Figure 11, where the result of the calculation can also be seen. It is notable that if filters are not used in the inputs then the calculation of the parameters will inherit their noise. It is also interesting that the cutoff frequency chosen

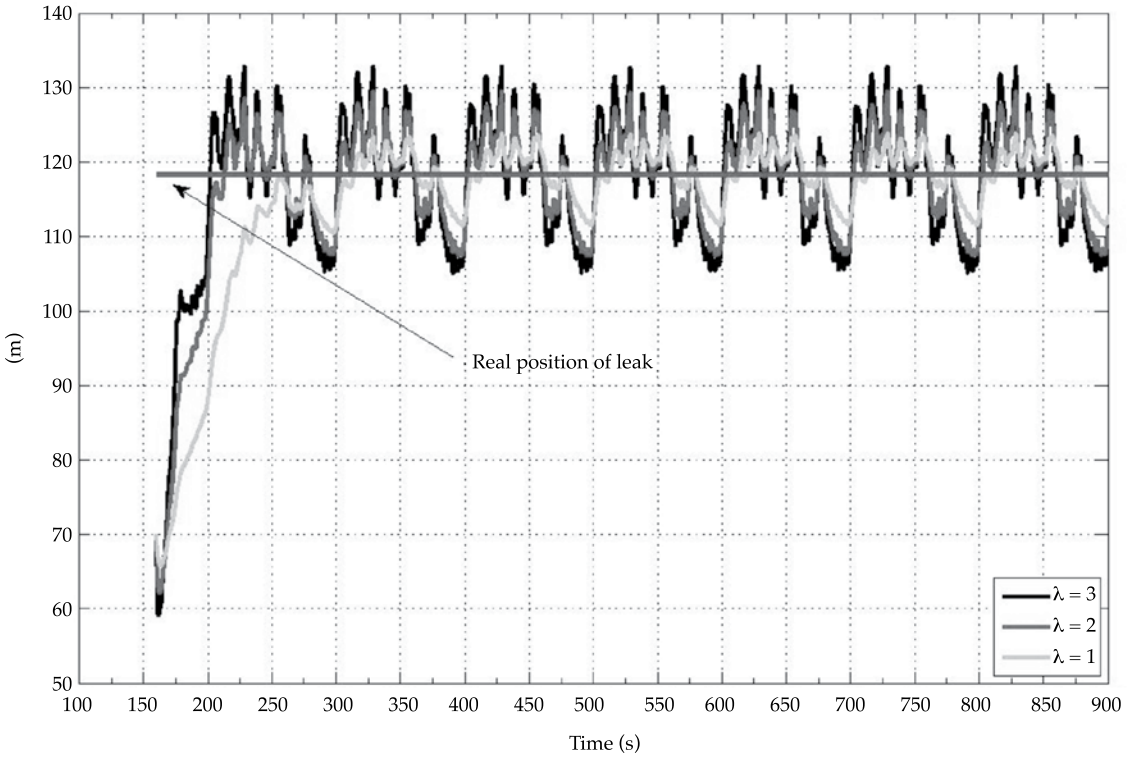

Figure 9. Estimate with different values of λ.

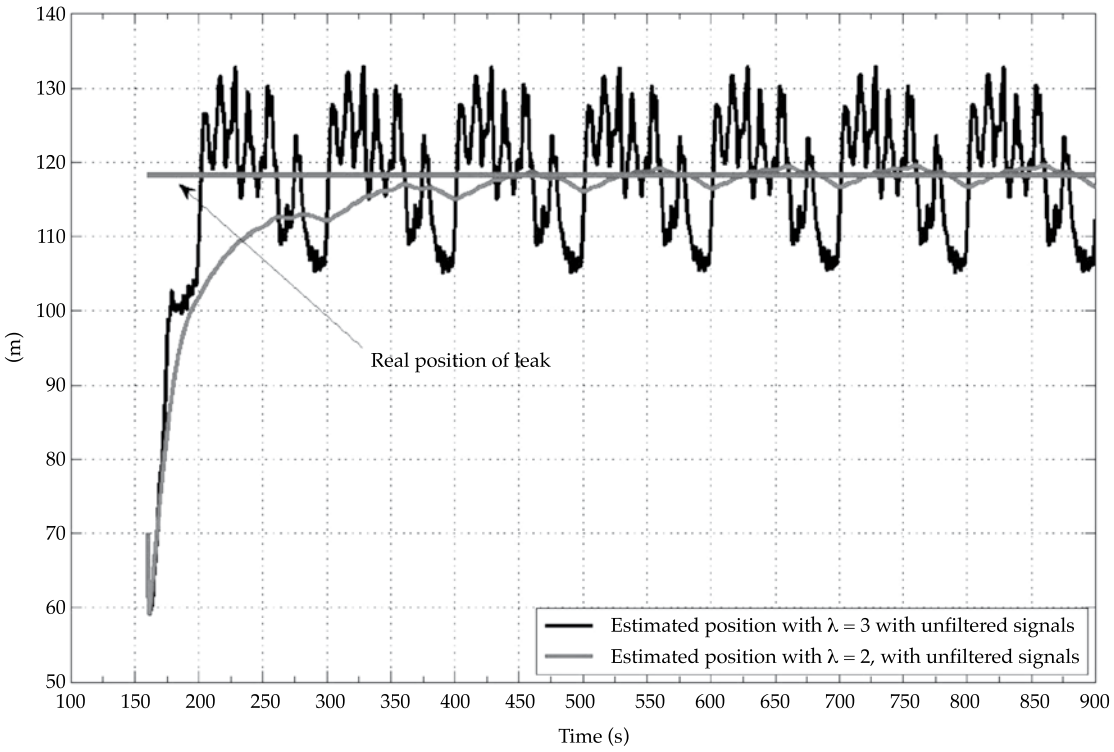

Figure 10. Estimate of the position with/without filter.

for the filters influences the calculations and, therefore, this factor must be taken into account during the calibration of the estimator.

Las señales de entrada se filtraron con dos diferentes frecuencias de corte, cuyos valores se muestran en la figura 11, donde también se puede apreciar el resultado de la estimación. Es notable que si no se utilizan filtros en las entradas, la estimación del parámetro hereda el ruido de éstas. También es interesante que la frecuencia de corte elegida para los filtros incide en la estimación, por lo que hay que tener en cuenta este factor durante la calibración del estimador.

Calculation of Pump Faults

To evaluate the observer for faults in the pumping system (23), a constant signal of 1.6×10^{-3} m. was added to the measurement of pressure upstream. The observer was initialized when there were no extractions. The initial conditions for the observer were different than those chosen for the pipe, and it was sintonizó with $\lambda = 1$. Figure 12 shows the results of a good calculation by the observer with and without filters.

Conclusions

This article presented a robust system to diagnose faults in pipes by implementing a pilot model from the Engineering Institute at the UNAM. This system is currently programmed in *LabVIEW*© for data acquisition and in *MATLAB*© for the diagnostics and reconstruction of faults. The originality of this system is its capacity to detect, isolate and reconstruct different types of faults in ducts, a novel and key contribution of the present work.

The principal characteristics of this monitoring system are that it is composed of two stages with specific tasks. The objective of the first stage is to distinguish among five

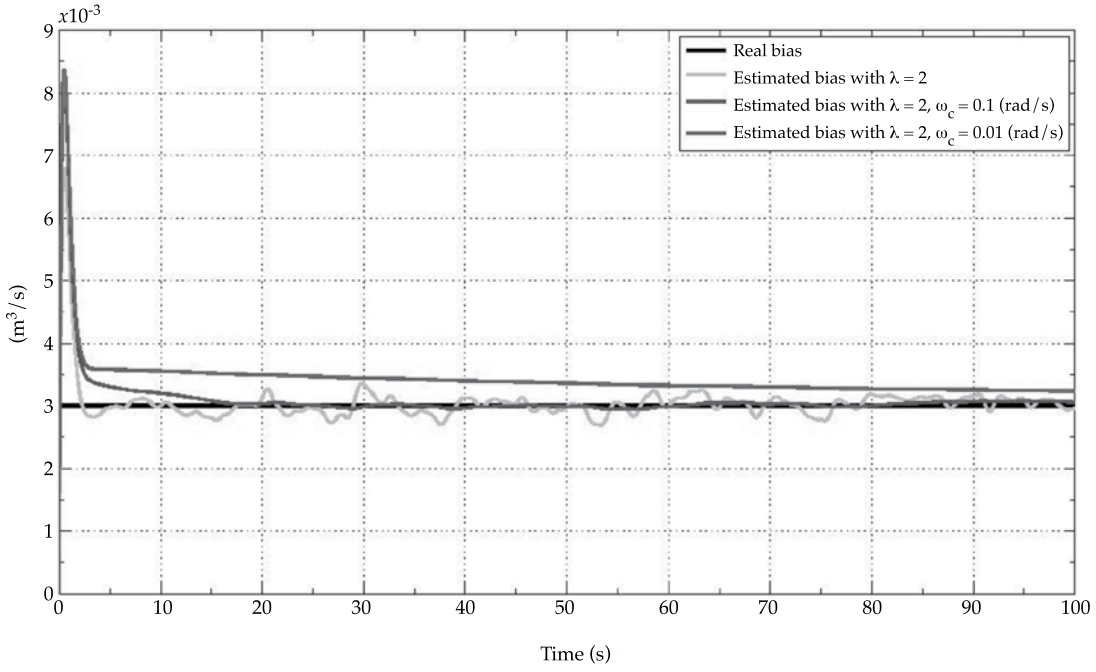

Figure 11. Estimate of *offset* in the flow meter upstream.

fault scenarios the one that represents a leak in a pipe. This task is performed using redundant relations obtained from the fluid transport model of the pipe. The second stage consists of the task to reconstruct the evolution over time of the fault that was identified. The results of the evaluation of the diagnostic system using experimental data were satisfactory, making its implementation in real ducts viable.

Appendix

Design of a high-gain observer

Gauthier *et al.* (1992) demonstrated that for any system represented by (1) which possess the property of being transformed into the following triangular shape:

$$\dot{\xi}(t) = A\xi(t) + \varphi(\xi(t), u_0)$$
$$y(t) = C\xi(t) \qquad (24)$$

a high-gain observer can be designed with:

$$A = \begin{bmatrix} 0 & 1 & \cdot & \cdot & 0 \\ 0 & 0 & 1 & \cdot & \cdot \\ \cdot & \cdot & \cdot & \cdot & 0 \\ \cdot & \cdot & \cdot & \cdot & 1 \\ 0 & \cdot & \cdot & \cdot & 0 \end{bmatrix}$$

$$\varphi(\xi(t), u_0) = \begin{bmatrix} \varphi_1(\xi_1(t)) \\ \varphi_2(\xi_1(t), \xi_2(t)) \\ \vdots \\ \varphi_{n-1}(\xi)_1(t, \ldots, \xi_{n-1}(t)) \\ \varphi_n(\xi_1(t), \ldots, \xi_n(t)) \end{bmatrix}$$

$$C = \begin{bmatrix} 1 & 0 & 0 & \ldots & 0 \end{bmatrix} \qquad (25)$$

The design procedure for an observer, given the particular case of a model in space of states (18) with constant inputs u_0, which compactly expresses the finite model for the transport of

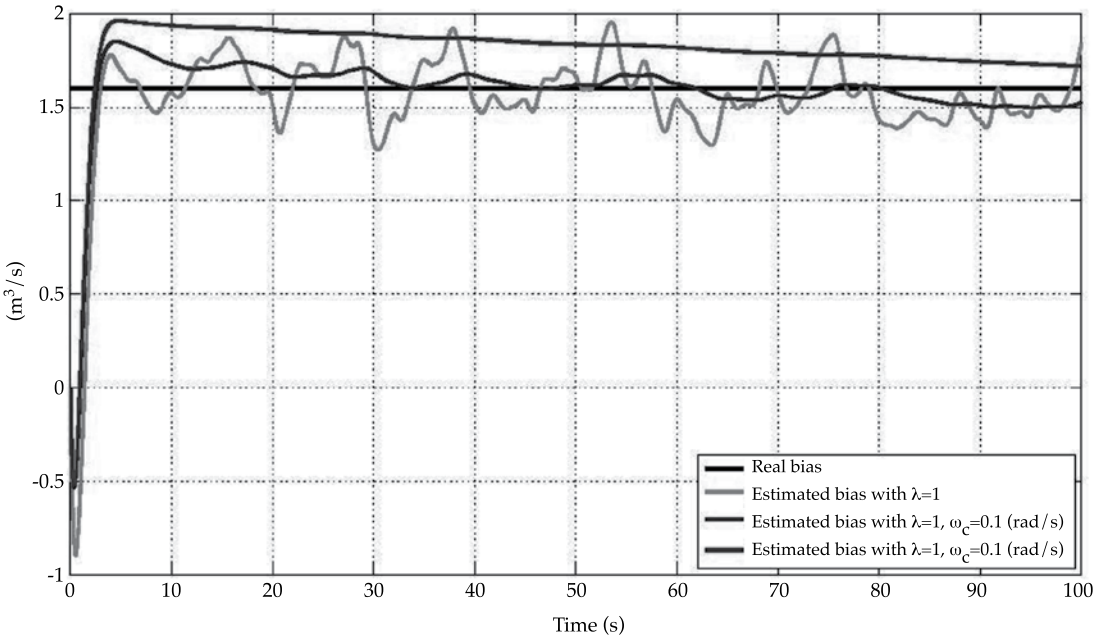

Figure 12. Estimate of the error in the pressure sensor upstream.

fluid in a pipe given by equations (10) and (11) consists of the following steps:

Step 1: apply the non-linear transformation $\Phi(x_e(t)) = \xi(t)$ to system (18) using the following change in coordinates:

$$\xi(t) = \begin{bmatrix} \xi_1(t) \\ \xi_2(t) \\ \vdots \\ \xi_n(t) \end{bmatrix} = \begin{bmatrix} h(x_e(t)) \\ L_f h(x_e(t)) \\ \vdots \\ L_f^{n-1} h(x_e(t)) \end{bmatrix}$$

where L_f is the Lie derivative of the output $h(x_e(t))$ with respect to operator f (for more information see Isidori, 1995).

Step 2: construct the structure of the observation algorithm

$$\dot{\hat{\xi}}(t) = \underbrace{A\hat{\xi}(t) + \varphi\left(\hat{\xi}(t), u(t)\right)}_{\text{Transformed system}} \underbrace{-S^{-1}C^T\left(C\hat{\xi}(t) - y(t)\right)}_{\text{Correction term}} \quad (26)$$

which is nothing other than a copy of the model of the transformed system and a correction term that ensures the convergence of the algorithm with matrix S, the design parameter.

Step 3: Return observer (26) to the original coordinates, obtaining:

$$\dot{\hat{x}}(t) = f\left(\hat{x}_e(t), u_0(t)\right) + K\left(\hat{x}_e(t)\right)\left[C\hat{x}_e(t) - y(t)\right] \quad (27)$$

where the gain of the correction term:

$$K\left(\hat{x}_e(t)\right) = \left[\frac{\partial \Phi}{\partial \hat{x}_e}\left(\hat{x}_e(t)\right)\right]^{-1} S^{-1}C^T$$

includes the matrix S, which is symmetrical, positive, and ensures the convergence of the observer, where the unique solution of the following matricial equation is:

$$-\lambda S + A^T S + SA - C^T C = 0 \quad (28)$$

And $\lambda > 0$ is a design parameter and the matrices A and C are given in the canonic model (24).

Note: Gauthier et al. (1992) demonstrated that the calculation error converges exponentially at zero if the parameter λ selected is sufficiently large. In addition, the tuning of the observer is reduced to the calibration of this simple parameter and the selection of a large value of λ ensures a quick convergence of the calculations to real values, thus the name high gain. Nevertheless, a very high gain produces overtakes in the convergence and amplification of the noise. Therefore, the selection of the gain should take these factors into account.

Received: 04/02/13
Accepted: 16/11/13

References

Bernard, O., Sallet, G., & Sciandra, A. (1998). Nonlinear Observers for a Class of Biological Systems: Application to Validation of Phytoplanktonic Growth Model. *IEEE Transactions on Automatic Control*, *43*(8), 1056-1065.

Besançon, G. (2007). *Nonlinear Observers and Applications*. Berlin: Springer.

Billmann, L., & Isermann, R. (1987). Leak Detection Methods for Pipelines. *Automatica*, *23*(3), 381-385.

Bornard, G., & Hammouri, H. (1991). A High Gain Observer for a Class of Uniformly Observable Systems. *Proceedings of the 30th IEEE Conference on Decision and Control*, Brighton.

Boulkroune, B., Galvez-Carrillo, M., & Kinnaert, M. (2011). *Additive and Multiplicative Fault Diagnosis for a Doubly-Fed Induction Generator*. IEEE International Conference on Control Applications. Denver.

Brunone, B., & Ferrante, M. (2001). Detecting Leaks in Pressurized Pipes by Means of Transients. *Journal of Hydraulic Research*, *39*(5), 539-547.

Carrera, R., & Verde, C. (2001). Localizador automático de fugas en un ducto. *Ingeniera Hidráulica en México*, *16*(2), 139-151.

Chaudhry, M. H. (1987). *Applied Hydraulic Transients*. New YorkÑ Van Nostrand Reinhold Company.

Chen, J., & Patton, R. J. (1999). *Robust Model-Based Fault Diagnosis for Dynamic Systems*. Norwell, USA: Kluwer Academic Publishers.

Chow, E., & Willsky, A. (1984). Analytical Redundancy and the Design of Robust Failure Detection Systems. *IEEE Transactions on Automatic Control*, *29*(7), 603-614.

Covas, D., Ramos, H., & De Almeida, A. B. (2005). Standing Wave Difference Method for Leak Detection in Pipeline Systems. *Journal of Hydraulic Engineering*, *131*(12), 1106-1116.

Ferrante, M., & Brunone, B. (2003). Pipe System Diagnosis and Leak Detection by Unsteady-State Test-1: Harmonic Analysis. *Advanced Water Resources*, *26*(1), 95-105.

Frank, P. (1990). Fault Diagnosis in Dynamic Systems Using Analytical and Knowledge-Based Redundancy. *Automatica*, *26*(2), 459-474.

Gauthier, J. P., Hammouri, H., & Othman, S. (1992). A Simple Observer for Nonlinear Systems-Applications to Bioreactors. *IEEE Transactions on Automatic Control*, *37*(6), 875-880.

Gertler, J. (1991). *Analytical Redundancy Methods in Fault Detection and Diagnosis* (pp. 9-21). Baden-Baden: IFAC-1st SAFEPROCESS.

González, O., Verde, C., & Torres, L. (2013). Leak Estimation Method for Complex Pipelines with Extractions. *Journal of Pressure Vessel Technology* (en revisión).

Isermann, R. (2006). *Fault Diagnosis System*. Berlin: Springer.

Isermann, R. (2011). *Fault-Diagnosis Applications: Model-Based Condition Monitoring: Actuators, Drives, Machinery, Plants, Sensors, and Fault-Tolerant Systems*. Berlin: Springer.

Isermann, R., & Mnchhof, M. (2011). *Identification of Dynamic Systems: An Introduction with Applications*. Berlin: Springer.

Isidori, A. (1995). *Nonlinear Control Systems*. London: Springer.

Khalil, H. K. (2002). *Nonlinear Systems*. Upper Saddle River, USA: Prentice Hall.

Korbicz, J., Koscielny, J., Kowalczuk, Z., & Cholewa, W. (2004). *Fault Diagnosis: Models, Artificial Intelligence, Applications*. Berlin: Springer Verlag.

Leveque, R. J. (2007). *Finite Difference Methods for Ordinary and Partial Differential Equations*. Philadelphia: SIAM.

Ljung, L. (1999). *System Identification Theory for the User*. Upper Saddle River, USA: Prentice Hall.

Makar, J., & Chagnon, N. (1999). Inspecting Systems for Leaks, Pits, and Corrosion. *American Water Works Association Journal*, *91*, 36-46.

Mpesha, W., Chaudry, M. N., & Gassman, S. (2001). Leak Detection in Pipes by Frequency Response Method. *Journal of Hydraulic Engineering*, *127*, 137-147.

Patton, R., Frank, P., & Clarke, B. (2000). *Issues of Fault Diagnosis for Dynamic Systems*. London: Springer.

Stoianov, I., Lama, N., Sam, M., Timur, T., & Csail, M. (2007). *Pipenet : A Wireless Sensor Network for Pipeline Monitoring* (pp. 264-273). IEEE 6th International Symposium on Information Processing in Sensor Networks, Cambridge.

Torres, L., Besançon, G., & Georges, D. (2008). A Collocation Model for Water Hammer Dynamics with Application to Leak Detection. *Proceedings of the 47th IEEE Conference on Decision and Control*, Shangai.

Torres, L., Verde, C., Besançon, G., & González, O. (2012). High Gain Observers for Leak Location in Subterranean Pipelines of Liquefied Gas. *International Journal of Robust and Nonlinear Control*, *24*(6), 1127-1141.

Verde, C., Gentil, S., & Morales, R. (2013). *Monitoreo y diagnóstico automático de fallas en sistemas dinámicos*. México, DF: Trillas-Instituto de Ingeniería, UNAM.

Wang, X. J., Lambert, M., Simpson, A., & Vtkovsky, J. (2005). Leak Detection in Pipelines Using the Damping of Fluid Transients. *Journal of Hydraulic Engineering*, *128*(7), 697-711.

Wylie, E. B., & Streeter, V. L. (1983). *Fluid Transients in Systems*. Englewood Cliffs, USA: Prentice-Hall.

Zhang, X. (2011). Sensor Bias Fault Detection and Isolation in a Class of Nonlinear Uncertain Systems Using Adaptive Estimation. *IEEE Transactions on Automatic Control*, *56*(5), 1220-1226.

Institutional Address of the Authors

Dra. Lizeth Torres
Dra. Cristina Verde
M.I. Rolando Carrera
Ing. Raúl Cayetano

Instituto de Ingeniería
Universidad Nacional Autónoma de México
Ciudad Universitaria
Apdo. Postal 70-472
04510 México, D.F., México
Teléfono: +52 (55) 5623 3684
ftorreso@ii.unam.mx
verde@unam.mx
rcarrera@unam.mx

Click here to write the autor

Low-Frequency Climate Variability in the Non-Stationary Modeling of Flood Regimes in the Sinaloa and Presidio San Pedro Hydrologic Regions

• Jesús López-de la Cruz* • Félix Francés •
Universitat Politècnica de València, España
*Corresponding Author

Abstract

López-De La Cruz, J. & Francés, F. (July-August, 2014). Low-Frequency Climate Variability in the Non-Stationary Modeling of Flood Regimes in the Sinaloa and Presidio San Pedro Hydrologic Regions. *Water Technology and Sciences* (in Spanish), *5*(4), 77-97.

Stationarity has been a main premise in the study of the components in the hydrological cycle and the corner stone in the frequency analysis of extreme events. Stationarity is also a common hypothesis and practice in planning and managing water resources. Based on this assumption, statistical methods have been used to extract data related to all the hydrological indicators used to develop estimates. These estimates can be refined from year to year as the recorded data increase. Over recent years, a variety of studies have shown that hydrological records present some type of Stationarity, such as changes and trends, leading experts to question the stationary hypothesis at the basin level. The effects of human intervention (such as changes in land use and reservoirs), the effect of low-frequency climate variability (for example, El Niño-Southern Oscillation, Pacific Decadal Oscillation) and climate change caused by increased gasses in the atmosphere are among the primary mechanisms that have emerged as inducers of changes in the hydrological cycle of basins and in the magnitude and frequency of extreme floods. The objective of the present study is to develop a framework for the analysis of frequency under non-stationary conditions using Generalized Additive Models for Location, Scale and Shape (GAMLSS). Two different approaches to non-stationarity statistical modeling were applied to annual instantaneous peak flow records from the Sinaloa and Presidio San Pedro hydrological regions in the Pacific northwestern Mexico. These models include the model with temporal trends in parametric distribution parameters and the model with forced low-frequency climate variability. The results from the trend model show the ability of models to describe the variability in flood regimes. In addition, the parametric distribution parameters are observed to be highly dependent on time, which suggests a lack of stationarity in the flood regimes in the gauging stations studied. The second approach— in which the climate indices (Niño 12, Niño 3, Niño 3.4, SOI and PDO) that describe the behavior

Resumen

López-De La Cruz, J., & Francés, F. (julio-agosto, 2014). La variabilidad climática de baja frecuencia en la modelación no estacionaria de los regímenes de las crecidas en las regiones hidrológicas Sinaloa y Presidio San Pedro. Tecnología y Ciencias del Agua, *5(4), 77-97.*

El asumir estacionaridad ha sido una de las premisas principales en el estudio de las componentes del ciclo hidrológico y la piedra angular en el análisis de frecuencia de eventos extremos. La estacionaridad ha sido una hipótesis común y práctica en la planificación y gestión de recursos hídricos. A partir de ella se han usado métodos estadísticos para extraer de los datos todos los indicadores hidrológicos útiles para proporcionar estimaciones, donde estas estimaciones pueden ser refinadas año con año conforme los registros en las estaciones hidrométricas se hacen más largos. En años recientes, diversos estudios han demostrado que los registros hidrológicos presentan algún tipo de no estacionaridad, como cambios y tendencias, lo cual ha llevado a los expertos a un consenso, en el sentido de que la hipótesis de estacionaridad a nivel de cuenca se encuentra comprometida. Entre los principales mecanismos que han sido sugeridos como los inductores de cambios en el ciclo hidrológico de las cuencas y en la magnitud y frecuencia de las crecidas se encuentran los efectos de la intervención humana (p. ej., cambio de uso de suelo, embalses), el efecto de la variabilidad climática de baja frecuencia (p. ej., El Niño-Oscilación del Sur, Oscilación Decadal del Pacífico) y el cambio climático debido al incremento de los gases a la atmósfera. El objetivo del presente estudio yace en el desarrollo de un marco para análisis de frecuencia bajo condiciones de no estacionaridad por medio de los Modelos Aditivos Generalizados en Localización, Escala y Forma (GAMLSS por sus siglas en inglés). Dos diferentes aproximaciones para la modelación estadística no estacionaria fueron las aplicadas a los registros de caudales instantáneos máximos anuales en las regiones hidrológicas Sinaloa y Presidio San Pedro en el noroeste del Pacífico mexicano. Estos modelos consisten básicamente en el modelo con incorporación de tendencias temporales en los parámetros de las distribuciones paramétricas y el modelo con incorporación del forzamiento de la variabilidad climática de baja frecuencia. Los resultados en la primera aproximación muestran la capacidad de los modelos para describir la variabilidad presente en los regímenes de crecidas; asimismo, se observa la alta dependencia de los parámetros de las distribuciones paramétricas respecto del tiempo, lo cual sugiere la ausencia de estacionaridad en los regímenes de crecidas en

of low-frequency variability patterns are incorporated in the models as explanatory covariables —makes it possible to demonstrate the important role of the macro-scale phenomena that occur in the Pacific on the inter-annual variability of the flood regimes in the Pacific Mexican coast. In addition, a comparison of classic inference models between non-stationary and stationary quantiles shows that differences between stationarity and non-stationarity assumptions can be significant over long periods of time.

Keywords: Flood frequency analysis, annual peak flows, GAMLSS, low-frequency climate variability patterns, Mexican Pacific, non-stationarity.

las estaciones de aforo de estudio. En el segundo enfoque, en el cual los índices climáticos (Niño12, Niño3, Niño3.4, SOI y PDO) que describen el comportamiento de los patrones de variabilidad de baja frecuencia fueron incorporados como covariables explicativas en los modelos, permiten resaltar el importante papel de los fenómenos de macroescala que ocurren en el Pacífico, en la variabilidad interanual de los regímenes de las crecidas en la costa del Pacífico mexicano. Además, la comparación de los modelos en la inferencia de cuantiles entre los modelos no estacionarios respecto del clásico modelo estacionario muestra que las diferencias obtenidas asumiendo no estacionaridad y sus equivalentes estacionarios pueden ser importantes durante extensos periodos de tiempo.

***Palabras clave**: análisis de frecuencia de crecidas, caudales máximos anuales, GAMLSS, no estacionaridad, patrones de variabilidad climática de baja frecuencia, Pacífico mexicano.*

Introduction

The hypothesis of stationarity in hydrological time series has been one of the main premises for studies about this subject and a cornerstone for the analysis of the frequency of extreme events (Stedinger, Vogel, & Foufoula, 1993; Khaliq, Ouarda, Ondo, Gachon & Bobée, 2006; Villarini *et al*., 2009b). In fact, all of the hydraulic infrastructure existing to-date was designed based on the premise of fixed systems; in other words, in a stationary world. It has been assumed that hydrological series are stationary in terms of not having trends or periodicity (Salas, 1993). Nevertheless, various studies performed over the past decades have shown hydrological registries to have some type of non-stationarity in the form of trends (Lettenmaier & Wallis, 1994; Kundzewicz & Robson, 2004; Stahl *et al*., 2010), abrupt changes (Potter, 1976; Salas & Boes, 1980) or a combination thereof (Villarini, Serinaldi, Smith, & Krajewski, 2009a). This has led investigators to question the hypothesis of a static world that is not influenced by external forces, suggesting an urgent need for paradigm shift (Khaliq *et al*., 2006; Milly *et al*., 2008; Sivapalan & Samuel, 2009). Factors such as human intervention in basins, the effect of low-frequency climate variability and anthropogenic climate change have been reported by diverse investigators to be the main mechanisms behind changes in the hydrological cycle and in the magnitude and frequency of floods (Perreault, Haché, Slivitzky, & Bobée, 1999; Rasmussen, 1999; Zhang & Schilling, 2006; Villarini *et al*., 2009b). Matalas (1997) and Koutsoyiannis (2006) provide two reference studies related to the concept of stationarity and non-stationarity in hydrology.

A recent work which brought the topic of non-stationarity to the forefront of hydrological sciences was published Milly *et al*. (2008), who announced that "stationarity is dead" and "it should not be revived." They propose that the hypothesis of stationarity should not continue to be followed, in light of the development of new statistical procedures that enable capturing the dynamics of the evolution of probability density functions over time (Cox, Isham & Northrop, 2002; Milly *et al*., 2008; Villarini *et al*., 2009b). These authors base the urgent need for changing the paradigm on the need for tools to adapt the design and management of control and protection structures to a dynamic reality, one in which new strategies must be adopted to mitigate the risks resulting from extreme events.

Diverse approaches to modeling flood regimes under non-stationarity conditions have been proposed in the literature (Olsen, Lambert, & Haimes, 1998; Strupczewski, Singh, & Feluch *et al*., 2001b; Strupczewski, Singh, & Mitosek, 2001a; Cox *et al*., 2002; Katz, Parlange, & Naveau, 2002; Ramesh & Davison, 2002; Cunderlink & Burn, 2003; Sankarasubramanian & Lall, 2003; Yi, Bardossy, & Brommundt, 2006; Leclerc & Ouarda, 2007). In these approaches, the parameters or moments of the distributions of a given distribution (for example, Gumbel distribution) can change over time. These include models with trends components; purely stochastic models that consider change patterns and those that consider covariables. These models have been proposed to avoid assuming the simplification of stationarity in nature, in order to take into account the dynamics existing over time that make this system obviously more complex. One of the schemes recently addressed by non-stationarity modeling is the forces to be considered in the relationship between hydrometeorological extremes and low-frequency climate variability patterns. The objective of this has been to identify the indices that describe the behavior of variables that control and improve the results of the modeling of extreme events under non-stationarity conditions. This is a line of study recommended by Khalid *et al*. (2006), in an important discussion about the different non-stationarity modeling approaches.

The main objective of the present work is to contribute to the modeling of the flood regimes of rivers in Mexico under non-stationarity conditions. The study region is located in the Mexican Pacific northwest. In particular, our interest is in statistical models, incorporating time trends and the climate-forced variability as explanatory covariables of the parameters of the parametric distributions used. Non-stationary models are implemented in *GAMLSS* models, which provide flexibility in modeling the parameters of parametric distributions incorporating explanatory covariables (Stasinopoulos & Rigby, 2007). The external covariables chosen to characterize the effect of climate variability on the study are climate indices that summarize the behavior of low-frequency climate variability patterns in the Pacific region. After implementing the two non-stationary models, a time trends model and a model that incorporates external covariables are compared to the classical stationary, according to the calculation of quantiles for an exceedance probability of 0.01 (corresponding to *Tr* of 100 years). In addition, flood predictions are performed for different exceedance probabilities based on non-stationary adjusted models in order to observe the ability of the models to serve as possible prediction tools.

Effect of Climate Variability Associated with El Niño-Southern Oscillation (ENSO)

There has been broad interest over recent decades in studying the impact of climate variability on the components of the hydrological cycle using different time scales. ENSO is the primary modular mechanism in the global climate at an inter-annual scale. In Mexico, investigators have studied the effects of climate variability on the hydroclimatology, in particular the effects of the two ENSO phases (El Niño/La Niña) on the hydrological processes in the country. El Niño recurs every 3 to 4 years and La Niña every 6 to 8 years, on average. Previous events have shown that ENSO significantly affects the rainfall behavior pattern in Mexico (Magaña & Quintanar, 1997) and significantly influences the evolution of precipitation in the central region of the country (Mosiño & Morales, 1988), affecting not only summer but also winter precipitation (Cavazos & Hastenrath, 1990). In general, during the positive phase of ENSO (El Niño events), precipitation intensifies in the northwestern and northeastern Mexico and decreases in the south (Magaña, Pérez, Conde, Gat, & Medina, 1998). Summers with El Niño events are dryer and hotter than summers with La Niña throughout nearly the entire country.

In terms of the relationship between El Niño phenomena and flow regimes, studies have shown a period with runoff below normal in the Pacific zone when El Niño events occur, primarily in summer. Therefore, even with significant winter precipitations, intense El Niño events have been related to droughts and thus water scarcity (Magaña *et al*., 1998). In terms of La Niña phenomena in the Pacific, summers are more humid, making the impact of ENSO more evident in this region.

Given the results reported, the probability distribution function of the hydrological variables is evidently affected by both ENSO phases, and given the resulting collapse of the stationarity hypothesis, statistical modeling of flood regimes is urgently needed using an approach that incorporates the effects of climate variability (Villarini *et al*., 2009a).

Case Study and Data

The present study is focused on the modeling of time series for maximum instantaneous annual gauged flows in basins located in the Sinaloa and Presidio San Pedro hydrological regions, in the Mexican Pacific northwest (Figure 1). Statistical modeling of the flood regimes in sites located in these hydrological regions is of interest since the ENSO signal may be stronger in this region, according to results reported in previous studies (Trasviña, Lluch, Filonov, & Gallegos, 2004).

After reviewing the database from the two hydrological regions, 38 hydrometric stations were selected, of which 25 pertained to the Sinaloa region and 13 to Presidio San Pedro. The time series for the maximum annual flows selected for this study contain at least 30 years of records (Table 1), which were obtained from the *BANDAS* (national surface water database; Banco Nacional de Datos de Aguas Superficiales) database. It is important to mention that the maximum annual flow events were selected considering a hydrological year of June 1 to May 31 of the following year. The top panel of Figure 2 shows the seasonal distribution of the maximum annual flow events in the gauging stations analyzed. The top left panel shows that these tend to be concentrated in winter months, autumn and the final months of summer at stations located in the Sinaloa region. A similar behavior in the temporality of the events is seen in the stations located in the Presidio San Pedro region (top right panel), where a lower recurrence of events during the summer months can be seen. In terms of the hydrological regime in each gauging station, this was evaluated based on the flow coefficient, which relates the monthly average flow and the annual average flow, thereby eliminating the real absolute factor for the different rivers. The bottom panel of Figure 2 shows a unimodal regime in the stations in the two regions, with the mode during the months of July and October. A bimodal regime with a second attenuated mode from December to February can be seen in the stations located in Sinaloa (bottom left panel). These results demonstrate the fact that the precipitations during the summer and autumn months are the primary mechanism governing the evolution of floods in the gauging stations studied.

The climate indicators used in the present work consist of the following indices: Niño12, Niño3, Niño3.4, Niño4, the Southern Oscillation Index (SOI) and the Pacific Decadal Oscillation (PDO). The time series pertaining to the climate indices were obtained from the Climate Prediction Center (CPC, Spanish acronym, http://www.cpc.ncep.noaa. gov/), which contains information on a monthly scale.

These indices provide information about the internal variability of low-frequency climate variability patterns in the Pacific region, thereby making it possible to take into account the impact that low-frequency climate variability can have on the magnitude and frequency of floods. The annual climate indices selected for use as explanatory covariables in models included the average values for the period April to September prior to the hydrological year for which the flood events were registered.

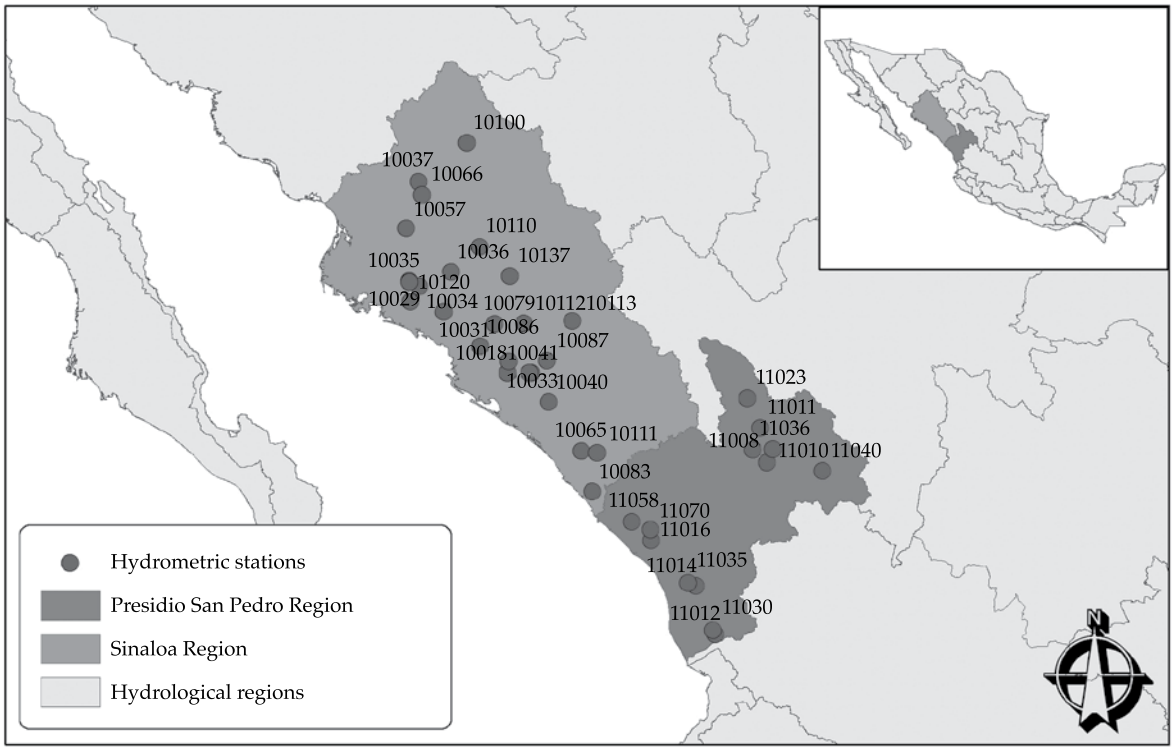

Figure 1. Location of the hydrometric stations used in the study.

Generalized Additive Models for Location, Scale and Shape (GAMLSS)

Coinciding with recent opinions by diverse authors (Milly *et al*., 2008; Villarini *et al*., 2009a) that the stationarity hypothesis pertaining to the behavior of hydrological processes is not upheld at inter-annual and decadal scales, non-stationary statistical models capable of reproducing the temporal variation of parameters of probability distribution functions need to be used. The present study uses the *GAMLSS* models proposed recently by Rigby and Stasinopoulos (2005), which provide a flexible framework for modeling time series under non-stationarity conditions. In these models, the response of the random variable Y (maximum annual instantaneous flows in this work) takes on a parametric distribution and its parameters can be modeled as a function of selected covariables, in this case: time (t_i) and climate indices (Niño12*i*, Niño3*i*, Niño3.4*i*, Niño4*i*, *SOIi* and *PDOi*).

In *GAMLSS* models, the distribution of the Y variable is not restricted, enabling the use of bias functions and high kurtosis, as well as continuous and discreet functions. The systematic part of the model makes it possible to model the location, scale, and shape parameters (related to the mean, bias and kurtosis) of the distribution of Y as linear or non-linear, parametric or non-parametric, using smoothing functions (Rigby & Stasinopoulos, 2005; Stasinopoulos & Rigby, 2007). For the *GAMLSS* models, the observation y_i (for $i = 1, 2,\ldots n$) is taken to be independent with a distribution function $F_Y = (\mathbf{y_i}\,\boldsymbol{\theta_i})$ where $\boldsymbol{\theta}_i = (\theta_{i1,\ldots,}\,\theta_{ip})$ is a vector of the p parameters of the distribution considered for location, scale and shape. Usually, p is less or equal to 4 since families of up to four parameters provide sufficient flexibility to describe the data. The

Table 1. Main characteristics of the gauging stations used in the study.

No.	Station	Code	Basin area (km^2)	Amount of registries (years)	Annual maximum mean flow volume (m^3/s)	Coefficient of variation
1	Puente Sudpacífico	10018	15 731	70 (1924-1993)	1 876.83	1.01
2	El Bledal	10027	371	59 (1938-1996)	283.52	0.91
3	Canatlán	10029	2 064	45 (1940-1984)	612.17	1.10
4	Guamúchil	10031	1 645	36 (1939-1974)	593.60	1.10
5	Palos Blancos	10033	11 409	49 (1940-1988)	1 320.70	1.34
6	Zopilote	10034	666	63 (1940-2002)	344.29	0.79
7	Naranjo	10035	2 450	45 (1940-1984)	11.89	0.28
8	Jaina	10036	8 179	61 (1942-2002)	947.12	1.19
9	Huites	10037	26 057	52 (1942-1993)	3 118.47	1.07
10	Santa Cruz	10040	8 919	57 (1944-2000)	943.26	1.17
11	Sanalona I	10041	3 657	33 (1945-1977)	487.93	1.15
12	Bamicori	10057	223	36 (1952-1987)	173.88	1.02
13	Ixpalino	10065	6 166	48 (1953-2000)	1 177.91	0.92
14	Choix	10066	1 403	50 (1956-2005)	293.14	0.97
15	Badiguarato	10079	1 018	41 (1960-2000)	1 003.93	1.64
16	El Quelite	10083	835	33 (1961-1993)	463.26	0.94
17	Pericos	10086	270	33 (1961-1993)	230.97	0.68
18	Tamazula	10087	2 241	38 (1963-2000)	559.49	0.73
19	Urique II	10100	4 000	35 (1968-2002)	297.03	0.60
20	Toahayana	10110	5 281	32 (1957-1988)	944.59	0.73
21	Piaxtla	10111	5 307	47 (1958-2004)	1 266.19	1.24
22	Guatenipa II	10112	8 252	37 (1969-2005)	1 550.19	0.84
23	La Huerta	10113	6 149	31 (1970-2000)	858.16	0.64
24	Guasave	10120	9 245	31 (1975-2005)	685.10	1.03
25	Tecusiapa	10137	3 773	47 (1958-2004)	952.70	1.08
26	San Felipe	11008	2 008	63 (1943-2005)	126.46	1.31
27	Refugio Salcido	11010	1 052	63 (1944-2006)	122.01	1.03
28	Peña del Águila	11011	2 616	53 (1954-2006)	91.30	1.27
29	San Pedro	11012	25 800	64 (1944-2007)	1 835.92	0.74
30	Acaponeta	11014	5 092	62 (1946-2007)	2 087.90	1.18
31	Baluarte II	11016	4 653	56 (1948-2003)	2 944.76	1.07
32	Caborca	11023	643	56 (1950-2005)	95.30	1.29
33	El Bejuco	11030	334	43 (1959-2001)	182.69	0.60
34	La Ballona	11035	451	47 (1961-2007)	439.17	0.87
35	El Pueblito	11036	1 810	46 (1961-2006)	172.48	1.53
36	Vicente Guerrero	11040	1 868	46 (1962-2007)	52.91	0.99
37	Siqueiros	11058	5 614	52 (1956-2007)	116.22	1.03
38	Las Tortugas	11070	863	36 (1971-2006)	497.85	0.99

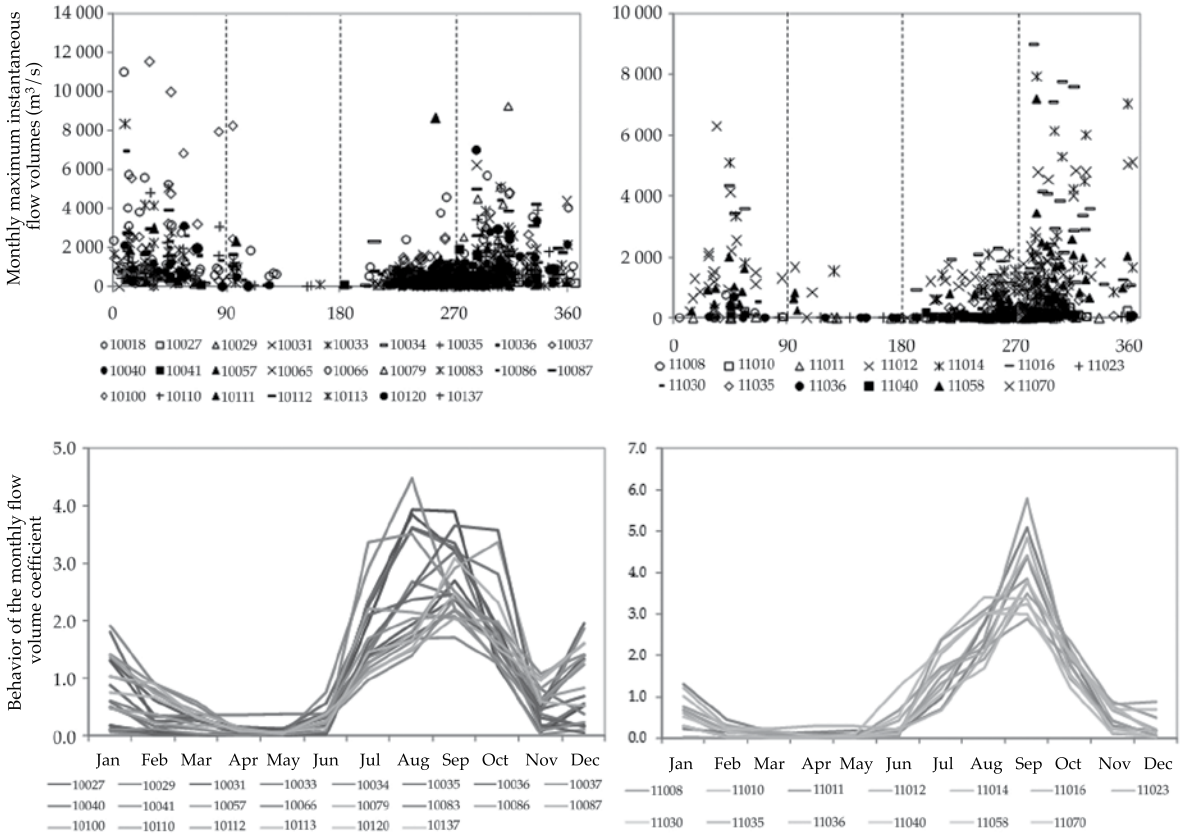

Figure 2. Seasonal distribution of the annual maximum flow volumes (upper panel) and behavior of the monthly flow volume coefficient (bottom panel).

parameters of the distribution are related to the explanatory covariables through $gk(\cdot)$ for $k = 1,2...p$, known as the monotone link function. In this work, the link functions considered are the identity and logarithm. *GAMLSS* models are diverse, and ours in particular is based on the semi-parametric additive formulation, which is given by:

$$g_k(\boldsymbol{\theta}_k) = \mathbf{X}_k\boldsymbol{\beta}_k + \sum_{j=1}^{m}\mathbf{h}_{jk}(x_{jk}) \qquad (1)$$

donde $\boldsymbol{\theta}_k$ es un vector de longitud n; $\boldsymbol{\theta}_k^T = \{\beta_{1k},...\beta_{mk}\}$ es un vector de parámetros de longitud m; $\mathbf{X}_k$ es una matriz de covariables de orden where $\boldsymbol{\theta}_k$ is a length vector n; $\boldsymbol{\theta}_k^T = \{\beta_{1k},...\beta_{mk}\}$ is a vector of length parameters m; $\mathbf{X}_k$ is a matrix of covariables on the order $n \times m$; $\boldsymbol{h}_{jk}(\boldsymbol{x}_{jk})$ represents the additive terms in the model, where $\boldsymbol{h}_{jk}$ is a smoothing function which evaluates the covariable vector $\boldsymbol{x}_{jk}$ (Stasinopoulos & Rigby, 2007). In this study, the parameters of the distribution functions selected for the study are considered to be a function of time and indicators of climate. Incorporating smoothing terms in the models (equation (1)) provides the advantage of being able to identify nonlinearities in the dependency when modeling the parameters of the distributions as a function of the covariables. In this study, the smooth dependency is based on mathematical formulation of cubic splines (Rigby & Stasinopoulos, 2005; Stasinopoulos & Rigby, 2007) which have shown good results in the works of Villarini *et al*. (2009b) and Villarini, Smith and Napolitano (2010). For the use of cubic splines, degrees of freedom need

to be defined taking into account that when the degrees of freedom approach zero the cubic splines tend to be a linear function. The degrees of freedom are selected according to that proposed by Stasinopoulos and Rigby (2007), using the Akaike information criterion and the Bayesian criterion by Schwarz. Therefore, the linear parametric model is a particular case in which there are no additive terms with smooth dependency. Then, we have a model of the form:

$$\mathbf{g}_k(\theta_\mathbf{k}) = \mathbf{X}_k\boldsymbol{\beta}_k \qquad (2)$$

where $\boldsymbol{X}_k\boldsymbol{\beta}_k$ is a combination of linear estimates. This model is considering the limit when the smooth dependency is included. Another particular case is when all the parameters of the distributions are independent of the explanatory covariables, then the model for the parameters $\boldsymbol{\theta}_\mathbf{k}$ is simplified to a stationary model where $g_k(\boldsymbol{\theta}_\mathbf{k})$ is constant.

The criterion by Stasinopoulos and Rygby (2007) was followed as a methodology for the selection and discrimination of the explanatory covariables to describe the parameters of the distributions. They recommend determining the best model for θ_1, then for θ_2, up to θ_n, comparing the different models based on Akaike information criterion and the Bayesian criterion. With these criteria, the final models provide a balance between precision and complexity, trying to avoid over-parameterization of the models. It is important to mention the degrees of freedom in the cubic splines were not greater than *Ln(n)* in any of the cases. This is because an increase in the complexity of the model is related to the extraction of information from the data. (To better understand the theory, adjust and selection of the model, see Rigby and Stasinopoulos (2005), and Stasinopoulos and Rygby (2007).)

After defining the functional dependency among the parameters of the distributions and each selected covariable, and the degrees of freedom when smooth dependency is assumed via cubic splines, the distribution function $F_Y(y_i$ $\theta_i)$ is selected according to the highest value of the maximum verosimilitude. In this work, five distribution functions used in the analysis of flood frequencies were selected (Table 2): Gumbel (GU), Lognormal (LNO), Weibull (WEI), Gamma (GA) and Generalized Gamma (GG). The first four contain two parameters and the last one three (Stedinger *et al.*, 1993; Escalante & Reyes, 2002).

In the absence of statistics to evaluate the quality of the fitof the set of models selected, conformity with the recommendations by Rigby and Stasinopoulos (2005) was verified using an analysis of normality and independence of the residuals for each model. To this end, the first four statistical moments of the residuals, the autocorrelogramand the Filliben coefficients were analyzed. The graphs of the residuals versus response, *q-q plot* and *q-q plot* without trends, were inspected visually. This ensures that the models selected adequately explore the systematic part, the white noise (random signal) being the information remaining (residual). All the calculations were performed with the GAMLSS package (Rigby & Stasinopoulos, 2005; Stasinopoulos & Rigby, 2007), implemented in the *R* platform (*R* Development Core Team, 2008).

Results

*Implementation of the **GAMLSS** Models*

This section presents and analyzes the results obtained from the modeling of the flood regimes in the study stations under non-stationarity conditions. Three different types of models were implemented: a) trends, b) covariables and c) stationary.

Modeling of Flood Regimes Incorporating Time Trends: Trends Model

The first approach to modeling the flood regimes under non-stationarity conditions consisted of implementing models in which time was incorporated as a single explanatory

Table 2. Summary of the probability density functions used to model annual maximum flow series.

	Probability density function	Moments of the distribution
Gumbel	$f_Y(y\|\theta_1,\theta_2)=\frac{1}{\theta_1}\left\{-\left(\frac{y-\theta_1}{\theta_2}\right)-\exp\left[-\frac{(y-\theta_1)}{\theta_2}\right]\right\}$ $-\infty<y<\infty,\ -\infty<\theta_1<\infty,\theta_2>0$	$E[y]=\theta_1+\Upsilon\theta_2\cong\theta_1+0.5772\theta_2$ $\mathrm{Var}[y]=\pi^2\theta_2^2/6\cong 1.64493\theta_2^2$
Lognormal	$f_Y(y\|\theta_1,\theta_2)=\frac{1}{\sqrt{2\pi\theta_1}}\frac{1}{y}\exp\left\{-\frac{[log(y)-\theta_1]^2}{2\theta_2^2}\right\}$ $y>0,\ \theta_1>0,\ \theta_2>0$	$E[y]=w^{1/2e^{\theta_1}}$ $\mathrm{Var}[y]=w(w-1)e^{2\theta_1}$, where $w=\exp(\theta_2^2)$
Weibull	$f_Y(y\|\theta_1,\theta_2)=\frac{\theta_2 y^{\theta_2-1}}{\theta_1^{\theta_2}}\exp\left\{-\left(\frac{y}{\theta_1}\right)\right\}$ $y>0,\ \theta_1>0,\ \theta_2>0$	$E[y]=\theta_1\Gamma\left(\frac{1}{\theta_2}+1\right)$ $\mathrm{Var}[y]=\theta_1^2\left\{\Gamma\left(\frac{2}{\theta_2}+1\right)-\left[\Gamma\left(\frac{1}{\theta_2}+1\right)\right]^2\right\}$
Gamma	$f_Y(y\|\theta_1,\theta_2)=\frac{1}{(\theta_2^2\theta_1)^{1/\theta_2^2}}\frac{\frac{1}{y\theta_2^2}-1\exp\left[\frac{y}{(\theta_2^2\theta_1)}\right]}{\Gamma\left(\frac{1}{\theta_2^2}\right)}$ $y>0,\ \theta_1>0,\ \theta_2>0$	$E[y]=\theta_1$ $\mathrm{Var}[y]=\theta_2^2\theta_1^2$
Generalized Gamma	$f_Y(y\|\theta_1,\theta_2,\theta_3)=\frac{\|\theta_1\|y^{\theta_1\theta_3-1}}{\Gamma(\theta_3)\theta_2^{\theta_1\theta_3}}\exp\left\{-\left(\frac{y}{\theta_2}\right)^{\theta_1}\right\}$ $y>0,\ -\infty<\theta_1<\infty,\ \theta_2>0$ y $\theta_3>0$	$E[y]=\theta_1\Gamma\left(\Omega+\frac{1}{\theta_3}\right)/\left[\Omega^{1/\theta_3\Gamma(\Omega)}\right]$ $\mathrm{Var}[y]=\theta_1^2\left\{\Gamma(\Omega)\Gamma\left(\Omega+\frac{2}{\theta_3}\right)-\left[\Gamma\left(\Omega+\frac{1}{\theta_3}\right)\right]^2\right\}/\left\{\Omega^{2/\theta_3[\Gamma(\Omega)]^2}\right\}$ $\Omega=1/(\theta_2^2\theta_3^2)$

covariable. Table 3 summarizes the time trends models adjusted to the 38 flood time series for the study sites. Based on this, a description of the inter-annual variability present in the flood regimes over time was attempted. The distribution of the adjusted models is not the same for the entire time series. It is worth noting that the Gamma and Lognormal distributions best described the behavior of the flood regimes given the distributions used in the study. In terms of the dependence and the type of dependency of the parameters of the distributions over time, θ_1 was observed to be strongly dependent on time in most of the smoothing models. A strong dependency was also observed with θ_2, though it was clearly observed to be less. It is important to mention that both a smooth as well as linear dependency can be seen. Overall, it can be said that in the sites studied (34 stations) there is a strong dependence on time, where 15 sites were shown to be dependent on the two parameters while only four sites were shown to be totally independent of the parameters.

The modeling of the time series of annual maximum flows using time as an explanatory covariable of the parameters of the parametric distributions show the ability of adjusted models to capture the variability exhibited in the flood regimes. Figure 3 shows the results of the modeling of the maximum annual flows with the non-stationary time trend model in six sites representative of the 38 analyzed. In Figure 3, a similarity in the variation over

Table 3. Summary of the adjusted trends models and type of dependency between time and the parameters of the distribution as well as of the statistics for the residuals of the models and the Filliben correlation coefficient: *cs*(·) indicates that the dependency is modeled using cubic splines, "t" indicates linear dependency and "--" means the parameter is independent of time (stationary).

Station	Distribution	θ_1	θ_2	Mean	Variance	Filliben Correlation Coefficient	AIC	SBC
10018	LNO	*cs(t)*	*cs(t)*	0.0163	1.0142	0.9914	1113.74	1 136.22
10027	LNO	*cs(t)*	*cs(t)*	0.0009	1.0172	0.9955	782.77	803.55
10029	LNO	--	*cs(t)*	-0.0551	1.0201	0.9948	655.49	666.21
10031	GA	--	*cs(t)*	-0.0146	1.0053	0.9807	518.49	527.82
10033	LNO	*cs(t)*	*cs(t)*	-0.0036	1.0203	0.9946	771.51	790.63
10034	WEI	*cs(t)*	--	-0.0014	1.0187	0.9969	862.75	875.62
10035	LNO	*cs(t)*	*cs(t)*	0.0137	1.0225	0.9855	188.83	206.89
10036	LNO	*t*	--	5.518*e*-17	1.0166	0.9794	925.52	931.86
10037	LNO	*cs(t)*	*cs(t)*	0.0002	1.0196	0.9493	933.04	952.56
10040	LNO	*cs(t)*	*cs(t)*	0.0197	1.0174	0.9892	838.33	858.76
10041	LNO	*cs(t)*	--	-1.660*e*-14	1.0312	0.9943	463.31	472.29
10057	GA	*cs(t)*	--	-0.0116	1.0198	0.9732	433.64	443.14
10065	GA	*cs(t)*	--	0.0005	1.0220	0.9870	766.50	777.73
10066	LNO	*cs(t)*	*cs(t)*	-0.0009	1.0204	0.9812	642.90	662.03
10079	LNO	*t*	--	2.397*e*-16	1.0250	0.9717	635.09	640.24
10083	GA	*cs(t)*	*cs(t)*	0.0076	1.0362	0.9899	483.25	498.22
10086	GA	*t*	--	0.0062	1.0347	0.9865	416.93	421.42
10087	WEI	*cs(t)*	*cs(t)*	0.0403	1.0897	0.9772	542.74	559.12
10100	WEI	--	*t*	-0.0058	1.0855	0.9828	461.64	466.31
10110	WEI	--	--	-0.0003	1.0343	0.9833	501.42	504.35
10111	LNO	--	--	1.078*e*-16	1.0217	0.9879	755.92	759.62
10112	LNO	*t*	--	-4.548*e*-17	1.0277	0.9691	614.64	619.47
10113	GA	*cs(t)*	--	-0.0031	1.0318	0.9892	468.29	476.89
10120	GA	*cs(t)*	*cs(t)*	-0.0083	1.0116	0.9887	461.37	475.72
10137	GA	*cs(t)*	*cs(t)*	-0.0031	1.0174	0.9889	741.31	759.81
11008	GA	--	*t*	-0.0092	1.0058	0.9819	720.97	727.45
11010	GA	*cs(t)*	*cs(t)*	-0.0151	0.9930	0.9952	730.97	752.40
11011	WEI	--	--	-0.0067	1.0055	0.9526	566.32	570.26
11012	LNO	cs(t)	--	1.760*e*-14	1.0158	0.9836	1 059.72	1 072.67
11014	LNO	*cs(t)*	*cs(t)*	0.0132	1.0162	0.9893	1 045.79	1 067.06
11016	GA	--	*cs(t)*	-0.0376	0.9684	0.9467	1 006.16	1 018.31
11023	WEI	--	*t*	-0.0124	1.0100	0.9864	615.72	621.79
11030	WEI	*t*	*t*	0.0079	0.9806	0.9816	512.17	519.22
11035	GA	*cs(t)*	*cs(t)*	-0.0041	1.0230	0.9822	631.01	649.08
11036	LNO	--	--	1.461*e*-17	1.0222	0.9496	538.57	542.23
11040	GA	--	*cs(t)*	-0.0393	0.9728	0.9805	456.79	467.77
11058	LNO	*cs(t)*	--	-1.563*e*-14	1.0196	0.9914	830.82	842.53
11070	GA	*cs(t)*	--	0.0211	1.0439	0.9519	497.99	507.49

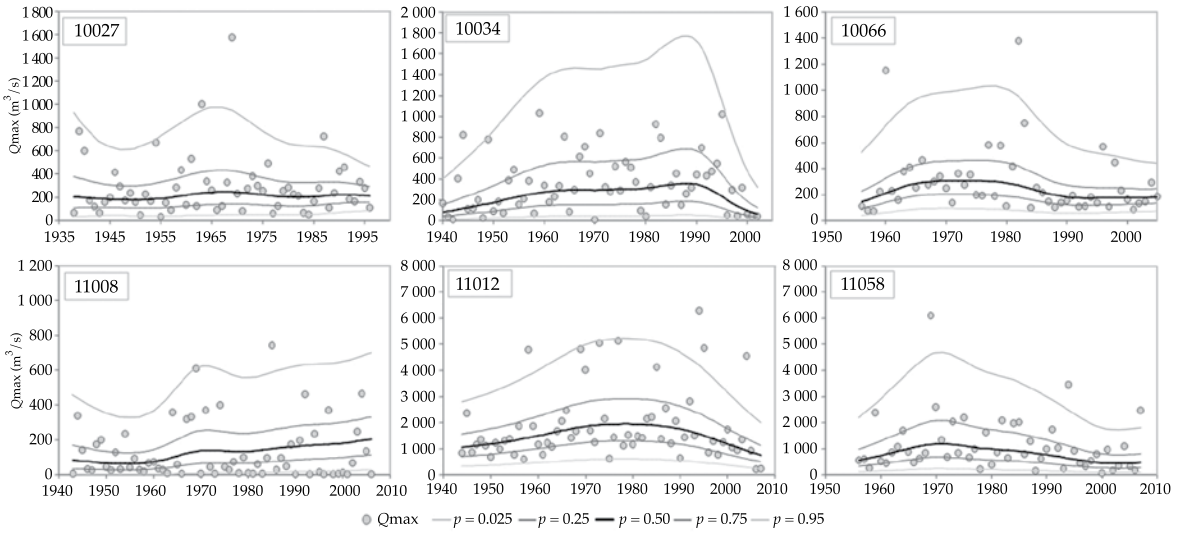

Figure 3. Summary of the results obtained with the trends model at six representative stations. The results show the quantiles calculated for different non-exceedance probabilities (0.025, 0.25, 0.50, 0.75, 0.95).

time of the quantiles calculated for different probabilities can be seen, with no exceedance in the stations closer to the coast (10027, 10034, 11012 and 11058). These show a pattern of increasing magnitude in the floods from 1940-1970, after which a decreasing trend was identified. Nevertheless, this is not generalized pattern, considering that in some of the stations it begins in the 1980s (10034 and 11012) while in others (10027 and 10011058) it lasts until the 1970s. In terms of the behavior in stations located in the innermost part of the study region, the results are somewhat different than the stations mentioned above. Analyzing the stations presented in Figure 3 (10066 and 11008), an increasing trend in the magnitude in floods can be seen after the 1950s, while a decrease can be seen in station 10066 between the late 1980s and the 1990s. An aspect to be highlighted in the results obtained from the implementation of the trends models is that the temporal variability in the quantiles is more significant for the highest quantiles (0.75 and 0.99) and less significant for the middle (quantile 0.5).

As a way to evaluate the effectiveness of the adjustment of the models implemented with this approach, the normality of the residuals for each model was verified. Table 3 presents a summary of the statistical moments of the residuals as well as the calculation of the Filliben correlation coefficient for the quantiles, which overall did not present any significant deviations from normal. In addition to the review of the statistical moments of the residuals, the *q-q plot* quantile graphs without trends were verified, which show the deviations of the observations of the sample with respect to the normal line, such that if the sample were from a normal population, the points should vary around 0 and with no particular pattern, remaining within the confidence level (95%). Otherwise, the residuals would not present normality.

Among the points to be noted in the implementation of this first non-stationary model is that the parameters of the distributions selected were strongly dependent on time. The non-linearity of this relation is also notable. This is established due to the need to incorporate mathematical smoothing formulas to model the dependency of the parameters on time. It is important to mention that the degrees of freedom were determined, respecting the

parsimony principle, in the adjustment of the models, assuming smooth dependency in the parameters. These were reduced when not significantly affecting the effectiveness of the adjustment of the models.

The modeling of the maximum annual flows under non-stationarity conditions in this first scenario has enabled us to reconstruct the quantiles for different non-exceedance probabilities, modeling the parameters of the parametric distribution using time as an explanatory covariable. The analysis of the graphs show that, in general, the adjusted models adequately describe the variability observed in the maximum annual flow series. In addition, with these models a high percentage of time series clearly deviate from the supposition of stationarity, observing that the mean as well as variance of the distributions are obviously affected by changes in the parameters over time.

Modeling of Flood Regimes Incorporating Effects of Climate Variability: Covariables Model

The implementation of the time trend models in the previous section clearly shows the deviations from the supposition of stationarity in the behavior of flood regimes in the gauged stations studied. In this section, non-stationary models are implemented using climate indices as explanatory covariables of the parameters. These models are implemented in order to explore the feasibility of adequately describing the non-stationarity observed in the time trend models using climate indicators selected in this study.

Over recent years, the study of the influence of ENSO (El Niño-Southern Oscillation) on hydrological processes has been a focus of diverse investigations. ENSO represents the dominant oceanic-atmospheric phenomena in the tropical Pacific (Cane, 1992). The results from these studies (Amarasekera, Lee, Williams & Eltahir, 1997; Jain & Lall, 2001; Poveda *et al*., 2002; Zhang, Xu, Jiang, & Wu, 2007) have shown that the extreme phases of this phenomenon may be highly related to increased episodes of floods and droughts in different regions of the world.

Table 4 presents a summary of the models obtained, incorporating the effects of low-frequency climate variability. This table shows the distribution functions with the best fit, as well as the significant covariables for each parameter. In general, the results from the models selected show the statistical significance of the climate indices as explanatory covariables for the evolution of the flood regimes at the study sites. In particular, it is worth noting the greater significance of indices Niño3.4, Niño4 and PDO as covariables, among the six indices used. In terms of the dependency represented by these models, Table 4 shows that parameter θ_1 is strongly dependent on climate indices, while the dependency is less for parameter θ_2, where 18 sites were shown to be independent of the climate indices. In terms of the results for parameter θ_3, total independence was observed with models in which the GG distribution was the distribution with the best fit, which could indicate that climate variability had no influence on higher-order moments. In terms of the type of dependency, Table 4 does not show any generalized pattern, and it is worth noting only the need to incorporate dependency using mathematical smoothing formulas. This is an important point of the analysis since it highlights the need to assume non-linearity when modeling flood regimes, incorporating climate indices as covariables.

Figure 4 summarizes the results from the implementation of the non-stationary models with the incorporation of external covariables (in addition to time) for six representative stations. The models tend to adequately reproduce the inter-annual variability of the flood regimes. In fact, the best description of the results were obtained with the time trend models. In terms of the review of the normality of the residuals for the adequate adjustment of the models, they adjusted reasonably well according to the observation of the statistical moment of the residuals, as well as in the graphics of the quantiles. Figure 5 presents the

Table 4. Summary of the models with external covariables and type of dependency between climate indices and the parameters of the distributions as well as the Filliben correlation coefficient for the residuals of the models: *cs*(·) indicates that the dependency is modeled using cubic splines, "t" indicates linear dependency and "--" means the parameter is independent of climate indices (stationary).

Station	Distribution	θ_1	θ_2	θ_3	Filliben corr coef
10018	LNO	Niño3 + *cs*(Niño3.4) + Niño4	--		0.9876
10027	LNO	*cs*(Niño3) + Niño3.4	SOI		0.9950
10029	LNO	*cs*(Niño 12) + Niño 3 + Niño4	--		0.9859
10031	GA	*cs*(PDO)	--		0.9949
10033	LNO	--	PDO		0.9788
10034	GG	Niño3.4 + *cs*(Niño4)	Niño4	--	0.9915
10035	LNO	Niño3.4 + Niño4 + IOS + PDO	--		0.9747
10036	LNO	--	PDO		0.9896
10037	LNO	*cs*(Niño3.4) + Niño4	--		0.9647
10040	LNO	Niño3 + *cs*(PDO)	--		0.9774
10041	LNO	*cs*(Niño3.4) + *cs*(PDO)	Niño3		0.9891
10057	GA	*cs*(Niño3.4)	PDO		0.9921
10065	GG	--	Niño4 + SOI	--	0.9907
10066	LNO	*cs*(Niño3.4) + *cs*(Niño4)	--		0.9818
10079	LNO	--	--		0.9768
10083	GA	--	--		0.9829
10086	GA	*cs*(Niño4)	--		0.9833
10087	WEI	Niño4 + IOS + PDO	*cs*(Niño3.4) + PDO		0.9873
10100	GG	*cs*(Niño4) + IOS + PDO	*cs*(Niño3) + Niño3.4	--	0.9793
10110	WEI	--	--		0.9833
10111	LNO	*cs*(Niño3.4)	*cs*(SOI)		0.9913
10112	LNO	--	--		0.9832
10113	GA	--	--		0.9856
10120	GG	*cs*(Niño3.4) + Niño4	PDO	--	0.9963
10137	GA	--	--		0.9727
11008	GA	Niño12 + *cs*(Niño4)	*cs*(PDO)		0.9953
11010	GG	*cs*(Niño3.4) + IOS	--	--	0.9943
11011	WEI	*cs*(Niño12)	--		0.9677
11012	LNO	*cs*(Niño3.4)	*cs*(Niño12) + cs(SOI)		0.9894
11014	LNO	Niño3 + *cs*(Niño3.4)	*cs*(Niño3.4)		0.9848
11016	GA	*cs*(Niño3.4)	Niño4 + SOI		0.9808
11023	GA	Niño3.4 + *cs*(IOS)	--		0.9875
11030	WEI	PDO	Niño12 + *cs*(Niño3) + Niño4		0.9839
11035	GA	Niño12 + Niño3 + PDO	*cs*(Niño3)		0.9834
11036	LNO	Niño12 + *cs*(PDO)	--		0.9839
11040	GG	Niño3	PDO	--	0.9957
11058	LNO	*cs*(Niño3.4) + Niño4	Niño3.4		0.9887
11070	GA	Niño3.4 + *cs*(Niño4)	Niño4 + *cs*(PDO)		0.9786

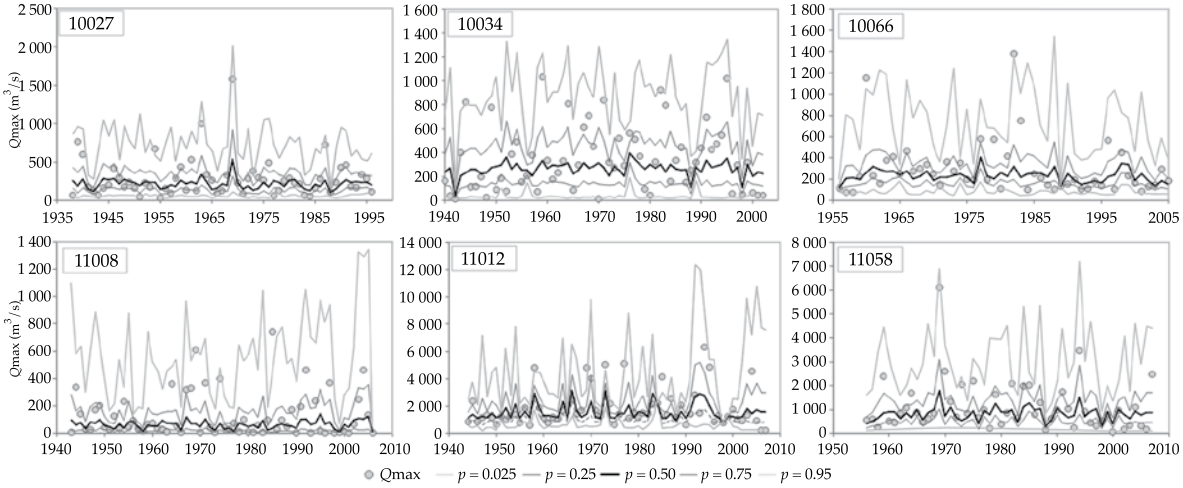

Figure 4. Summary of the results obtained using the external covariables model at six representative stations. The results show the calculated quantiles for different non-exceedance probabilities (0.025, 0.25, 0.50, 0.75, 0.95).

graphs for the *q-q plot* quantiles without trends, obtained from the review of the normality of the residuals.

Returning to the inspection of the results in Figure 4, the calculation of the middle quantile (with an exceedance probability of 0.50) tended to be less affected by climate variability. Nevertheless, the effects are significant in the calculation for the higher quantiles. Another point to be noted is that in spite of an adequate fit of the models, some noise in the results of the model can be observed, which reflects the non-linearity in the response of the flood regimes to natural climate-forced variability.

Comparison Between Non-Stationary and Stationary Models

The main objective of the study of floods in operational hydrology is to calculate growth events for an exceedance probability defined *a priori* in order to obtain flood maps, design protection measures or establish flood risk management plans. In fact, in Mexico and many parts of the world, legislation related to the risk of floods is based on the analysis of the frequency of floods to calculate design floods associated with different time periods (for example, 20, 50 and 100 years). These return periods are related to the need for sound structures.

Figure 6 shows the results from the analysis of the frequency of floods in stationary conditions and non-stationarity conditions for an exceedance probability of 0.01 (that is, a return period of 100 years). The graphs show the problem with assuming stationarity in the calculation of the flood events. As can be observed, the non-stationary models indicate the existence of important periods during which the flood calculated under non-stationarity is above that obtained with the stationary model. Focusing on the analysis of the results for station 10027, based on the trend model, the flood for an annual exceedance probability of 0.01 for 58 years of records has ranged from a minimum value of 640.40 m^3/s in 1996 to a maximum of 1 730.52 m^3/s in 1966. Based on the covariables model, the minimum value was 295.51 m^3/s in 1988 and the maximum was 3 508.08 m^3/s in 1969.

Analyzing the results from the modeling of the flood events in the non-stationary scenario with the covariables model and the stationary

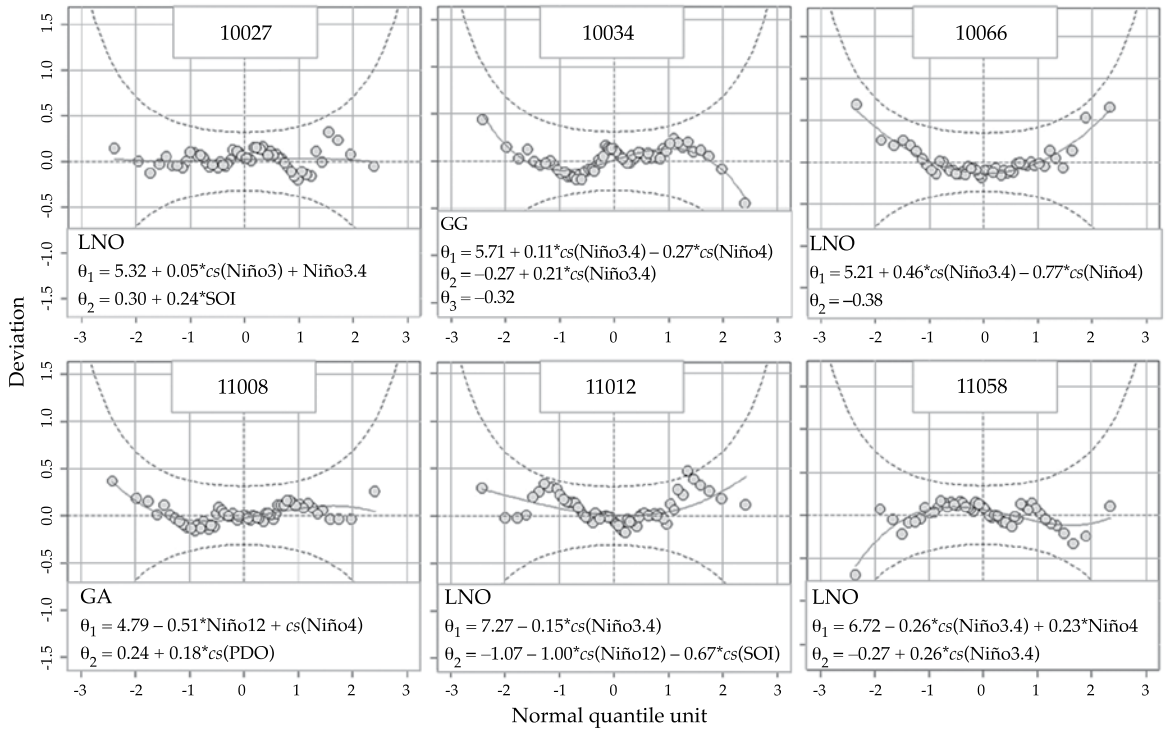

Figure 5. The *q-q plots* without trends of the residuals of models with external covariables for the representative stations analyzed. The two dotted lines correspond to confidence limits for 95%.

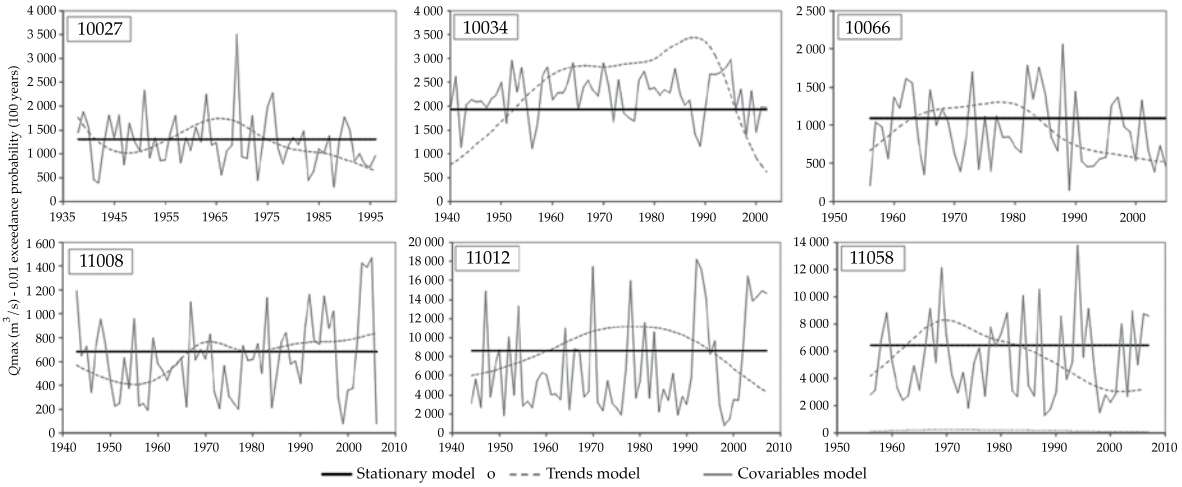

Figure 6. Quantiles calculated for maximum annual floods with 0.01 exceedance probability for the six representative stations, based on the three different models implemented.

scenario for station 10027 shown in Figure 7, the median tends to be underestimated in the stationary model for high negative values for index Niño3.4, while the model overestimates the median for high positive values. These values are more significant for

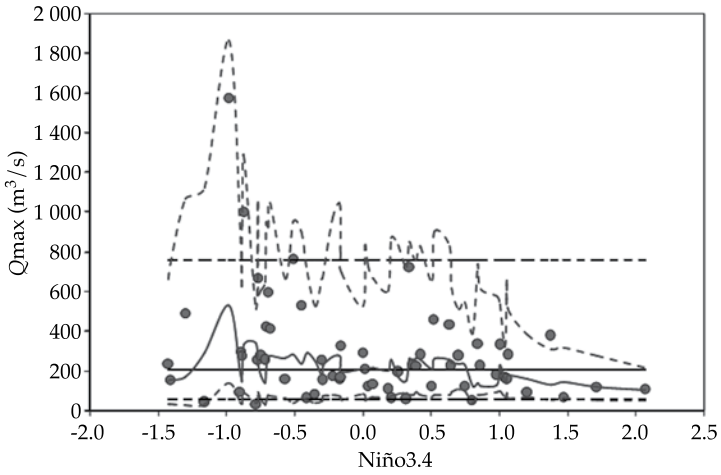

Figure 7. Calculation of the median and percentiles for 5 and 95%, with the stationary model (black line) and the covariables model (gray line) for station 10027, for the Niño 3.4 index

the 95th percentile, as can be seen in Figure 7. It is important to mention that a complex relationship can be seen between the climate index and the maximum annual flow values, which may reflect that only a part of the variability in the flood regimes is explained by the low-frequency patterns. This undoubtedly leads to the need to consider the effects of anthropogenic factors on flood regimes, through changes in basins (such as changes in land use) or through changes directly in the hydrological cycles as a result of the construction of reservoirs.

In general, the results presented in this section show that the inferences related to flood events under non-stationarity conditions may change significantly. These results strengthen the recent questioning about the stationarity hypothesis and lead us to suggest the possible collapse of the hypothesis of stationarity in the study of floods.

Concepts Related to Flood Period and Risk in the Non-Stationary Context

In general, the results obtained in the modeling of flood regimes under non-stationary conditions lead us to suggest the need to use alternative models to account for the dynamic of nature instead of the classical analysis of flood frequencies. Nevertheless, in a non-stationary world, concepts regarding return periods and risk need to be redefined because of changes that will occur in the probability density function over time (Sivapalan & Samuel, 2009; Salas & Obeysekera, 2013).

Figure 8 shows the calculation of the return period under non-stationarity conditions based on the non-stationary statistical models adjusted for the time series of the flood at station 10027. As can be seen, the exceedance probability changes from year to year and therefore a framework needs to be defined to extend the concept related to return period and risk, since in this context their current definition lose their meaning.

Evaluation of the Non-Stationary Covariables Model for Prediction

This section evaluates covariable models as predictive tools. The non-stationary model with covariables is considered since trend models cannot adequately describe the future behavior flood events. This is because time trends can change over the short- and long-

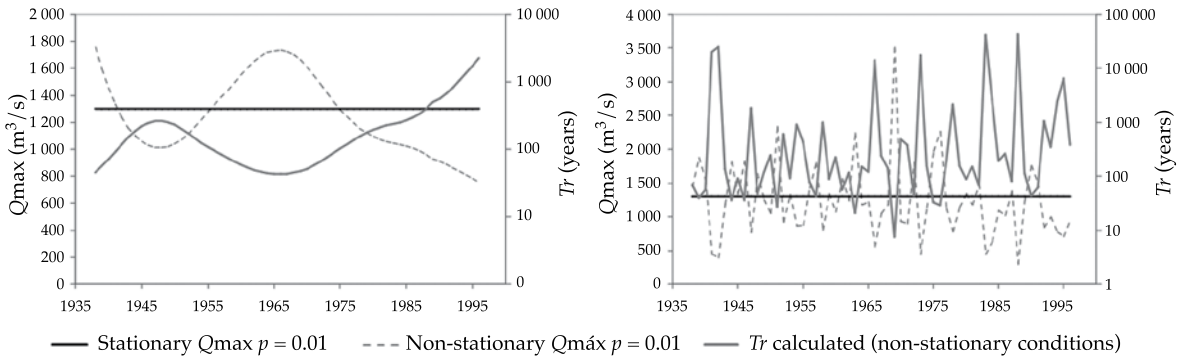

Figure 8. Calculation of the return period under non-stationary conditions with the trends model (left) and the covariables model (right) for station 10027.

term. The prediction is made based on the last date of records for each one of the stations using the adjusted models.

Figure 9 shows the results obtained from the use of the models with covariables as tools to predict floods for different exceedance probabilities. As can be seen, the climate indices that characterize the behavior of the low-frequency patterns can be very helpful to capture the changes in the frequency of floods in the study stations. Undoubtedly, the models that incorporate additional covariables, besides time, are a more attractive option than models that incorporate time trends. This is because trend models can ignore changes in the frequency of floods over the prediction period.

It is important to take into account that the indices used to characterize the impact of climate variability are limited in their ability to represent additional physical processes, which can affect the frequency of floods. Therefore, in spite of their usefulness, the prediction values obtained must be considered very carefully. Also important to consider is that the indices that describe the behavior of low-frequency variability patterns are a simplification of the overall circulation of the atmosphere.

Discussion

The study has examined the non-stationarity of the distribution of maximum annual flows registered at 38 gauging stations located in the hydrological regions of Sinaloa and Presidio San Pedro (Mexican Pacific). Two models were implemented under non-stationarity conditions —time trend and covariable models. The non-stationary models were developed using GAMLSS models which have flexibility in the probabilistic modeling of the time series of maximum annual flows in a non-stationary context. The can also model the dependency of the parameters of the distributions on explanatory covariables. The implementation of the time trend model in which time was the only covariable enabled identifying that the flood regimes in a significant number of study stages deviated significantly from the supposition of stationarity. Analyzing the type of dependency observed in the modeling of the parameters as a function of time presented both linear dependency as well as non-linear dependency cases, according to smoothing formulas.

The application of the non-stationary models, incorporating the effects of climate variability, exhibited the significant influence that ENSO can have on the inter-annual variability of flood regimes. It is particularly worth noting that the high flood values at the study stations are related to the negative phase of ENSO (La Niña events) while low flood values tend to be related to the positive phase

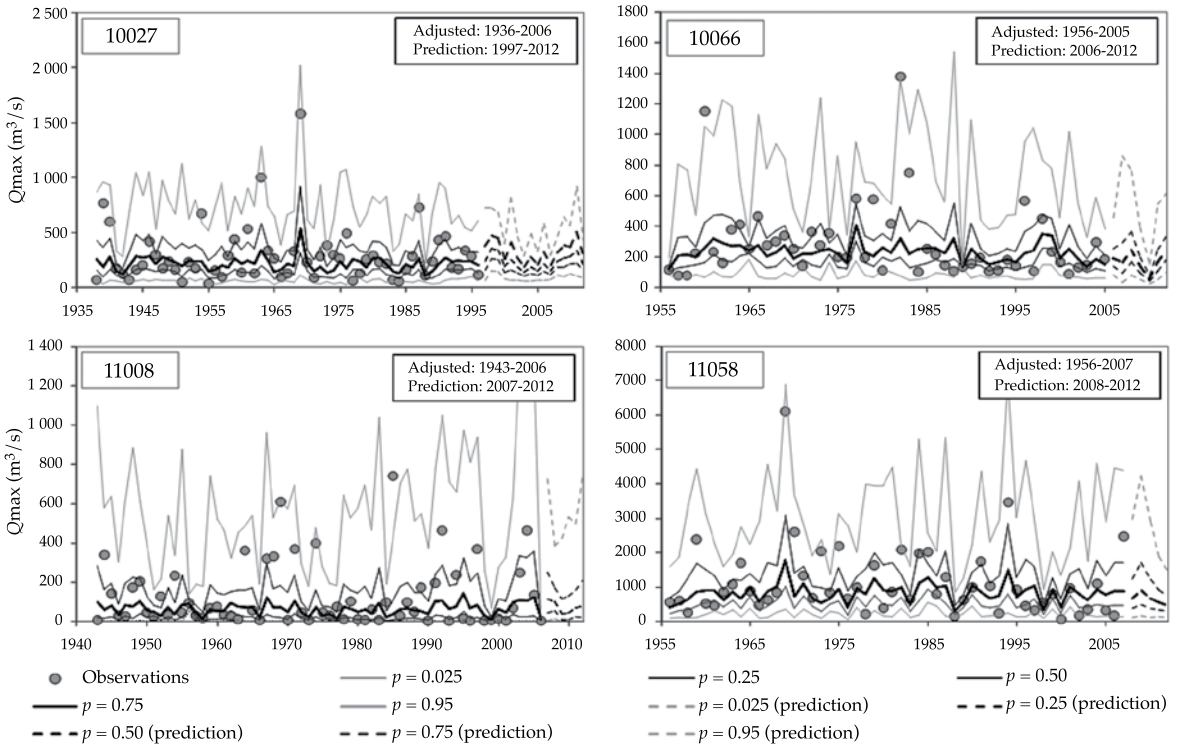

Figure 9. Results from the modeling of maximum annual floods for stations 10027, 10066, 1008 and 11058 with the covariables model. The results in the period of fit of the models are shown in solid lines, while the prediction period with solid lines.

(El Niño). The results show that by simply incorporating the effects of climate variability using climate indices, the non-stationarity observed in the behavior of the flood regimes can be reasonably described.

The non-stationary models showed that the trends and effects of climate variability affect the mean and the variance of the distributions. An important point to highlight is that the models involving smoothing formulas (cubic splines) tend to better reproduce the dispersion of the floods since they are more flexible. Nevertheless, these types of models, that provide good fit and flexibility, are highly sensitive to changes in the evolution of predictive variables and, therefore, should be used with caution. Another point worth noting in the use of smoothing formulas is that the Akaike criterion tends to provide very complex models while the Vayesian criterion provides simpler ones. Therefore, for the optimization of the degrees of freedom in the models it is important to follow a procedure which complies with the parsimony principle since the increase in the complexity of the model is related to the extraction of information from data.

The results of the analysis of the frequency of floods with non-stationary models showed that, for a flood even with an annual exceedance probability of 0.01 (corresponding to a period of 100 years), the variations obtained with the classical stationary model were very significant, with extensive periods in which the value calculated under non-stationary conditions was greater than that with stationarity. These results have a significant effects on the hydrological practice and provide evidence

that the simplification of stationarity can lead to assuming greater risks when planning the design of hydraulic structures.

The implementation of non-stationary models as prediction tools shows that the models with covariables are a better alternative than trend models since the short- and long-term trends can change due to the effect of climate variability and human activities. Nevertheless, it is important to consider that factors in the production of runoff exist that are not taking into account by covariable models. Therefore, the use of models as a prediction tool requires more exhaustive work.

A variance analysis among the climate indices is necessary given the high multi-collinearity that can exist among the climate indicators used since the describe the same phenomenon, making it possible to obtain models that are adjusted to the parsimony principle. In addition, it is important to mention that this study does not consider anthropogenic factors (for example, changes in land use, construction of reservoirs) that can affect flood regimes. More exhaustive studies should be performed to incorporate these effects. Finally, although among the parametric distributions used the Gamma and Lognormal seemed to provide acceptable results, additional distributions need to be included in future studies, such as the Generalized Extreme Value Distribution or the distributions of two populations, such as the TCVE (Two Components Extreme Value).

Final Conclusions

The stationarity hypothesis in the study of floods was found to be compromised and alternative statistical methods need to be implemented that enable taking into account the impact of anthropogenic and climate factors on the probability distribution functions. Though ENSO is not caused by climate change, an important question is whether the ENSO events in a climate change scenario will be more intense and frequent. Given the results, a key task is incorporating the effects of anthropogenic factors, given evidence showing that the impacts of these factors have intensified over recent decades. Although the potential of using climate indices as explanatory covariables of the variability in flood regimes is evident in the study stations, these investigations must go hand-in hand with the best of those being conducted by meteorologists for the prediction of the indices, in order for them to serve as a useful prediction tool in the medium- and long-range. Also important to take into account is the fact that the indices that describe the behavior of low-frequency variability patterns are a simplification of the overall circulation of the atmosphere and, therefore, the prediction values should be interpreted with caution. Lastly, although the results show the influence of ENSO on the frequency and intensity of flood regimes in the Mexican Pacific northwest, these results cannot be extrapolated to other regions in Mexico since ENSO presents significant spatial variation, according to the results reported in previous studies about the influence of ENSO in North America.

Acknowledgements

This development of this work was financed by the Consejo Nacional de Ciencia y Tecnología de México (Conacyt). The authors wish to thank Mikis Stasinopoulos, Robert Rigby and Calliope Akantziliotou for making the *GAMLSS* available. Thank you to James A. Smith and Gabriele Villarini for the meetings held during the second author's visit to Princeton University, United States, who contributed to the development of the present work.

Received: 07/12/11
Accepted: 26/03/14

References

Amarasekera, K. N., Lee, R. F., Williams, E. R., & Eltahir, E. A. (1997). ENSO and the Natural Variability in the Flow of Tropical Rivers. *Journal of Hydrology*, *200*, 24-39.

Cane, M. A. (1992). Tropical Pacific ENSO Models: ENSO as a Mode of the Coupled System (pp. 377-386). In K. Trenberth (Ed.). *Climate System Modeling*. Cambridge: Cambridge University Press.

Cavazos, T., & Hastenrath, S. (1990). Convection and Rainfall over Mexico and their Modulation by the Southern Oscillation. *International Journal of Climate*, *10*, 337-386.

Cox, D. R., Isham, V. S., & Northrop, P. J. (2002). Floods: Some Probabilistic and Statistical Approaches. *Philosophical Transactions. Series A, Mathematical, Physical, and Engineering Sciences*, *360*, 389-408.

link, J., & Burn, D.H. (2003). Non-Stationary Pooled Flood Frequency Analysis. *Journal of Hydrology*, *276*, 210-223.

Escalante, C., & Reyes, L. (2002). *Técnicas Estadísticas en Hidrología*.

Jain, S., & Lall, U. (2001). Floods in a Changing Climate: Does the Past Represent the Future? *Water Resources Research*, *36*, 3641-3652.

Katz, R. W., Parlange, M. B., & Naveau, P. (2002). Statistics of Extremes in Hydrology. *Advances in Water Resources*, *25*, 1287-1304.

Khaliq, M. N., Ouarda, T. B. M. J., Ondo, J. C., Gachon, P., & Bobée, B. (2006). Frequency Analysis of a Sequence of Dependent and / or Non-Stationary Hydro-Meteorological Observations: A Review. *Journal of Hydrology*, *329*, 534-552.

Koutsoyiannis, D. (2006). Nonstationarity versus Scaling in Hydrology. *Journal of Hydrology*, *324*, 239-254.

Kundzewicz, Z., & Robson, A. (2004). Change Detection in Hydrological Records — A Review of the Methodology. *Hydrological Sciences Journal*, *49*, 7-19.

Leclerc, M., & Ouarda, T. (2007). Non-Stationary Regional Flood Frequency Analysis at Ungauged Sites. *Journal of Hydrology*, *343*, 254-265.

Lettenmaier, D. P., & Wallis, J. R. (1994). Hydro-Climatological Trends in the Continental United States. *Journal of Climate*, *7*, 586-607.

Magaña, V., & Quintanar, A. (1997). *On the Use of a General Circulation Model to Study Regional Climate. Numerical Simulations in the Enviromental and Earth Sciences*. (pp. 39-48). García, F. Cisneros, G., Fernández-Equiarte, A. y Álvarez, R. (Editores). Cambridge: Cambridge University Press.

Magaña, V., Pérez, J. L., Conde, C., Gay, C., & Medina, S. (1998). El fenómeno de El Niño y la Oscilación del Sur (ENOS) y sus impactos en México. *Atmósfera*. México, DF: Universidad Nacional Autónoma de México.

Matalas, N. C. (1997). Stochastic Hydrology in the Context of Climate Change. *Climatic Change*, *37*, 89-101-101.

Milly, P. C. D., Betancourt, J., Falkenmark, M., Hirsch, R. M., Kundzewicz, Z. W., Lettenmaier, D. P., & Stouffer, R. J. (2008). Stationarity is Dead: Whiter Water Management? *Science*, *319*, 573-574.

Mosiño, P., & Morales, T. (1988). Los ciclones tropicales, El Niño y las lluvias en Tacubaya. *Geofis. Int.*, *27*, 61-82.

Olsen, J. R., Lambert, J. H., & Haimes, Y. Y. (1998). Risk of Extreme Events under Nonstationary Conditions. *Risk Analysis*, *18*, 497-510.

Perreault, L., Haché, M., Slivitzky, M., & Bobée, B. (1999). Detection of Changes in Precipitation and Runoff over Eastern Canada and U.S. Using a Bayesian Approach. *Stochastic Environ. Res. Risk Assess.*, *13*, 201-216.

Potter, K. W. (1976). Evidence for Nonstationarity as a Physical Explanation of the Hurst Phenomenon. *Water Resources Research*, *12*, 1047-1052.

Poveda, G., Veléz, I., Mesca, O., De Hoyos, C., Mejía, F., Barco, O., & Correa, P. (2002). Influencia de fenómenos macroclimáticos sobre el ciclo anual de la hidrología colombiana: cuantificación lineal no lineal y percentiles probabilisticos. *Meteorología Colombiana*. *6*, 121-130.

Ramesh, N. I., & Davison, A. C. (2002). Local Models for exploratory Analysis of Hydrological Extremes. *Journal of Hydrology*, *256*, 106-119.

Rasmussen, P. F. (1999). Bayesian Estimation of Change Points using General Linear Model. *Water Resources Research*, *37*, 2723-2731.

Rigby, R. A., & Stasinopoulos, D. M. (2005). Generalized Additive Models for Location, Scale and Shape. *Journal of the Royal Statistical Society: C-App.*, *54*, 507-554.

Salas, J. D. (1993). Analysis and Modelling of Hydrologic Time Series. In Maidment, D. (Ed.). *Handbook of Hydrology* (pp. 19.11-19.72). New York: McGraw-Hill.

Salas, J. D., & Boes, D. C. (1980). Shifting Level Modeling of Hydrologic Series. *Adv. Water Resour.*, *3*, 59-63.

Salas, J. D., & Obeysekera, J. (2013). Revisiting the Concepts of Return Period and Risk for Nonstationary Hydrologic Extreme Events. *ASCE J. Hydrol. Eng.* *19*(3), 554-568.

Sankarasubramanian, A., & Lall, U. (2003). Flood Quantiles in a Changing Cli

mate: Seasonal Forecasts and Causal Relations. *Water Resources Research*, *39*, 12.

Sivapalan, M., & Samuel, J. M. (2009). Transcending Limitations of Stationarity and the Return Period: Process-Based Approach to Flood Estimation and Risk Assessment. *Hydrological Processes*, *23*, 1671-1675.

Stahl, K., Hisdal, H., Hannaford, J., Tallaksen, L. M., Van Lanen, H. A., Sauquet, E., Demuth, S., Fendekova, M., & Odar, J. J. (2010). Streamflow Trends in Europe: Evidence from a Dataset of Near-Natural Catchments. *Hydroloy and Earth System Sciences*, *7*, 5769-5804.

Stasinopoulos, D. M., & Rigby, R. A. (2007). Generalized Additive Models for Location Scale and Shape (GAMLSS). *R. Journal of Statistical Software*, *23*, 1-46.

Stedinger, J. R., Vogel, R. M., & Foufoula, G.E. (1993). Frequency Analysis of Extreme Events. In *Handbook of Hydrology* (pp. 18.11-18.65). New York: McGraw Hill.

Strupczewski, W. G., Singh, V. P., & Mitosek, H. T. (2001a). Non-Stationary Approach to At-Site Flood Frequency Modelling, III. Flood Analysis of Polish Rivers. *Journal of Hydrology*, *248*, 152-167.

Strupczewski, W. G., Singh, V. P., & Feluch, W. (2001b) Non-Stationary Approach to At-Site Flood Frequency

Modelling I. Maximum Likelihood Estimation. *Journal of Hydrology*, *248*, 123-142.

Trasviña, A., Lluch, C. D., Filonov, A. E., & Gallegos, A. (2004). *Oceanografía y el Niño* (pp. 69-1002). México, DF: UNAD.

Villarini, G., Smith, J. A., & Napolitano, F. (2010). Nonstationary Modeling of a Long Record of Rainfall and Temperature over Rome. *Advances in Water Resources*, *33*, 1256-1267.

Villarini, G., Serinaldi, F., Smith, J. A., & Krajewski, W. F. (2009a). On the Stationarity of Annual Flood Peaks in the Continental United States during the 20th Century. *Water Resources Research*, *45*, 1-17.

Villarini, G., Smith, J. A., Serinaldi, F., Bales, J., Bates, P. D., & Krajewski, W. F. (2009b). Flood Frequency Analysis for Nonstationary Annual Peak Records in an Urban Drainage Basin. *Advances in Water Resources*, *32*, 1255-1266.

Yi, H., Bardossy, A., & Brommundt, J. (2006). Non-Stationarity Flood Frequency Analysis Southern Germany. *Proceedings of the 7th International Conference on HydroScience and Engineering*, Philadelphia, USA.

Zhang, Q., Xu, C., Jiang, T., & Wu, Y. (2007). Possible Influence of ENSO on Annual Maximum Streamflow of the Yangtze River, China. *Journal of Hydrology*, *333*, 265-274.

Zhang, Y., & Schilling, K. (2006). Increasing Streamflow and Baseflow In Missisipi River Since the 1940's: Effect of Lans Use Change. *Journal of Hydrology*, *324*, 412-422.

Institutional Address of the Authors

Dr. Jesús López-de la Cruz

Universitat Politècnica de València
Instituto de Ingeniería del Agua y Medio Ambiente (IIAMA)
Despacho Becarios Hidráulica-Hidrología
Edificio 4E, primera planta, C/ Camino de Vera, s/n,
46022 Valencia, España
Teléfono: +34 (963) 877 000
jeslpede@pograd o.upv.es

Dr. Félix Francés

Universitat Politècnica de València
Instituto de Ingeniería del Agua y Medio Ambiente (IIAMA)
Edificio 1 Central, planta 1
Escuela Técnica Superior de Ingenieros de Caminos Canales y Puertos
Código numérico 4E
Camino de Vera s/n
46022 Valencia, España
Teléfono: +34 (963) 877 000
ffrances@hma.upv.es

Click here to write the autor

Aqueduct in the Mexican Institute for Water Technology, Juitepec, Morelos, Mexico.

Photo: Rafael Espinoza Méndez.

Relation between Specific Capacity and Transmissivity with Non-linear Flow and Partial Penetration Well

• Armando O. Hernández-Valdés* •
Instituto Superior Politécnico José Antonio Echeverría, Cuba
*Autor de correspondencia

Abstract

Hernández-Valdés, A. O. (July-August, 2014). Relation between Specific Capacity and Transmissivity with Non-linear Flow and Partial Penetration Well. *Water Technology and Sciences* (in Spanish), *5*(4), 99-113.

Specific capacity has been used by several authors, including the author of the present work, to estimate the Darcian transmissivity of an aquifer, given the lack of data related to these systems because of the costs involved in conducting pumping tests to determine transmissivity. Several factors can cause significant errors in this estimate. This work presents the analytical expressions and results from pumping tests in order to demonstrate the error magnitudes, especially when non-linear fluid is present around pumping wells, in the case of a partial penetration well, or there are recharge effects or caves that quickly stabilize the levels of the wells during pumping. In the first two cases the Darcian transmissivity of the aquifer is underestimated, whereas in the latter it is overestimated. Results from a pumping test using two satellites, or observation wells are also shown. Although this is an uncommon situation, interpretation is possible based on one of the proposals above to calculate hydrogeological properties under a non-linear flow regime. Errors in determining the storage coefficient and the use of an inadequate specific capacity parameter to estimate transmissivity were found.

Keywords: Non linear regime, partial penetration, specific capacity-transmissivity, well hydraulics.

Resumen

Hernández-Valdés, A. O. (julio-agosto, 2014). Relación gasto específico y transmisividad con flujo no lineal y pozo de penetración parcial. Tecnología y Ciencias del Agua, *5*(4), *99-113.*

El gasto específico ha sido utilizado por numerosos autores, incluido el del presente trabajo, para estimar la transmisividad darciana del acuífero, dada la carencia de datos de estos sistemas y de los costos que implican la realización de ensayos de bombeo para determinarla. Existen numerosos factores que pueden incidir en errores significativos de dicha estimación. En este trabajo se presentan expresiones analíticas y resultados de ensayos de bombeo para demostrar las magnitudes de los errores, sobre todo cuando hay presencia de flujo no lineal en los alrededores del pozo de bombeo, si es de penetración parcial o hay efectos de recarga o cavernas que provocan en los pozos una rápida estabilización de los niveles durante el bombeo. En los dos primeros casos, las estimaciones subvaloran la transmisividad darciana del acuífero y en el último se sobrevalora este parámetro. Se muestran los resultados de una prueba de bombeo con dos satélites o pozos de observación, situación poco frecuente, pero que permite realizar la interpretación utilizando una de las variantes propuestas anteriormente para calcular las propiedades hidrogeológicas con régimen no lineal de flujo, donde se evidencia el error que se comete en la determinación del coeficiente de almacenamiento y el uso de un inadecuado gasto específico para estimar la transmisividad.

Palabras clave: *régimen no lineal, penetración parcial, gasto específico-transmisividad, hidráulica de pozos.*

Introduction

Many authors have often used specific capacity data (*Qs*) (relation between pumping flow volume and drawdown, or the decrease produced by this) to calculate the transmissivity of aquifers given the lack of pumping tests to provide a more detailed characterization of aquifer systems. The main reason for this is the cost of pumping tests and the ease of determining Qs during the construction of a well or when it is gauged.

Although *Qs* is not constant for each pumping well and cannot be used to calculated the transmissivity of an aquifer, to a certain extent it enables qualitatively evaluating the

constructive quality of the well and the aquifer characteristics of the geological formation in which it is located, as will be seen later. In addition, if optimization techniques are desired, in which minimum level restrictions are imposed on pumping wells, as is necessary in coastal aquifers, then a correction can be applied to the simulated drawdown at points corresponding to pumping wells, in function of the specific capacity. This procedure is used by Cabrera-Estupiñán (2010).

Pérez (2001) states: "specific capacity is a function of time and flow volume, and can only be considered to be constant in the case of linear flow throughout the entire aquifer, in a well with no structure, which is not very likely, since in aquifers where the flow on the well face could be linear the need for a structure would be nearly certain, unless it is formed out of jacket and rack. On the other hand, for cases in which a structure in the well is not needed, the flow is most likely not linear on the well face. That is, the probability that the specific flow volume is constant is very small. Nevertheless, it can be used as a relative fertility index, although not with the certainty with which it has been used to-date."

In general, specific capacity has been used to quantitatively characterize wells and aquifers in different hydrogeological basins, but without associating it with hydrogeological properties of the corresponding aquifers, as reported by Capucci *et al*. (2001).

Next, the factors influencing the magnitudes of *Qs* will be discussed as well as how they influence calculating transmissivity based on the specific capacity. Nevertheless, works exist that only consider variation over time due to the increase in the radius of influence, such as in Chenini, Silvain and Ben-Mammou (2008).

Specific Capacity and Factors that Affect It

Many efforts have been aimed at trying to find a correlation between transmissivity T_D and specific capacity Q_s, defined by the relation between the pumping flow volume and the drawdown produced in the corresponding well.

According to Pérez (2001) and Walton (1970), the drawdown in pumping wells and, therefore, the specific capacity (Q_s) depend on various factors:

$$Q_s = \frac{Q}{S_p} = \frac{Q}{A*Q + B*Q^2 + D*Q^{(n)}} \qquad (1)$$

- Pumping time (A).
- Non-linear flow near the pumping well (B).
- Losses due to the structure of the pumping well (D).

In addition to the above, additional factors to be included are:

- Partial penetration
- Filtration surface in free aquifers
- Effects of interference between wells and impermeable boundaries or recharge effects.
- Heterogeneity and anisotropy of the geological medium, etc.

Although what Aitchison- Earl and Smith indicate is true, that the specific capacity decreases as time and pumping flow volume increase, it must be specified that the effect of pumping time is only reflected in the linear drawdown component, and its variation is more significant when pumping begins and lessens after several hours of pumping, when the Jacob approximation $u \leq 0.01$ would be applicable $u = \frac{r^2 * E}{4 * T_D * t}$ where E is the storage coefficient, t is pumping time, r is the well radius and T_D is the transmissivity of the aquifer. In relation to the increases in flow volume, it is important to mention that they significantly affect specific capacity since these increases influence both the turbulent component of drawdown as well as losses due to the structure and partial penetration effects.

The study by Knopman and Hollyday (1993) confirms the large amount of variables that influence specific capacity. They also evaluate the statistical behavior of those variables in a considerable number of wells with specific capacity data, but do not propose mathematical expressions that relate this with transmissivity.

Lari, Knochenmus and Bowman (1998) indicate that the large variability in the relation between transmissivity and specific capacity in the study region may be caused by losses due to the well structure, its penetration into the aquifer and the influence of fractures in the connection.

Meanwhile, El-Naga (1994) shows that a logarithmic correlation between transmissivity and specific capacity fits better than a linear correlation since they are both lognormal distributions and the transmissivity of the aquifer matrix is affected by fracturing and karstification. As will be demonstrated later, a good correlation does not necessarily imply that the calculation of the parameters will be good.

The WRI Report 87-4034 (2008) indicates important limitations when calculating transmissivity based on specific capacity, considering that the effective radius of a pumping well can be substantially much larger than the nominal radius, since many wells found in karst formations can be drilled in caverns, which would result in high specific capacity and, therefore, high transmissivity would be calculated. Meanwhile, the presence of turbulent flow and losses due to the pumping well structure can cause a larger drawdown, as can partial penetration, reducing both parameters. The report mentions that the above effects can offset the calculation errors, which is true for evaluating mean transmissivity values but not for spatial variability. In addition, it reports that pumping time is not known in many cases and nearly all of the drawdown occurs in a few minutes.

The present work will analyze the effects of the non-linear flow regime in areas near pumping wells and the effect of the wells' partial penetration into the aquifer. This coincides with the report mentioned above and theoretically and practically demonstrates several points presented therein.

Relation between Specific Capacity and Transmissivity T_D to a Linear Regime in the Area Around a Pumping Well

a) Total Penetration Well

According to the formula known as Dupuit-Thiem:

$$S_p = 0.366 * \frac{Q}{T_D} * \log\left[\frac{r_o}{r_p}\right] \quad (2)$$

Solving for T_D and changing the units we get:

$$T_D\left(\mathrm{m}^2/\mathrm{d}\right) = 0.366 * 86.4 * \log\left[\frac{r_o}{r_p}\right] * \frac{Q(lps)}{S_p} \quad (3)$$

The above equation can be expressed in other units, such as those used in many works referenced, as follows:

$$T_D\left(p^2/d\right) = 0.366 * \frac{3.7853 * 86.4 * (3.28)^3}{60} \log\left[\frac{r_o}{r_p}\right] * \frac{Q(gpm)}{S_p(p)} \quad (3a)$$

For a pumping well 50 cm in diameter and a radius of influence of 370 m, equation (3) is rewritten as:

$$T_D\left(m^2/d\right) = 100 * \frac{Q(lps)}{S_p} = 100 * Q_s\left(lps/m\right) \quad (4)$$

In Cuba, the above expression has frequently been used to calculate Darcy hydraulic transmissivity, although it depends on pumping time, among other factors.

For the above diameter and radius of influence values in equation (3), we get:

$$T_D\left(p^2/d\right) = 224 * \frac{Q(gpm)}{S_p(p)} = 224 * Q_s\left(gpm/p\right) \quad (4a)$$

For a radius of influence of r_o = 1 250 m, from the two previous equations we get:

$$T_D\left(m^2/d\right) = Factor_{RL} * \frac{Q(lps)}{S_p} = 117 * Q_s\left(lps/m\right) \quad (5)$$

$$T_D\left(p^2/d\right) = 260 * \frac{Q(gpm)}{S_p(p)} = 260 * Q_s\left(gpm/p\right) \quad (5a)$$

The above shows that pumping time affects specific capacity, which decreases as time increases, but the variation is more significant for short pumping times.

In equations (4a) and (5a), the coefficient obtained is in the range of the formulas used by Abbott and Dehay (2008), who employed the Parkhurst, Christenson and Breit formula (1996) T = 242 Q/s, reporting that the values calculated with the above relation are 1.1 to 4.3 times greater than for transmissivity obtained through pumping tests.

The WRI Report 87-4034 (2008) used the relation T = 270 Q/s, indicating that the coefficient is between 170 and 370 for that zone, with an average value of 270. This coefficient is shown to be highly variable and aquifers with caverns such as the one studied are shown to create high specific capacities that can lead to very large transmissivity calculations, while the effect of turbulent flow results in very low transmissivity calculations. Both of these will be analyzed and analytically justified in the present work.

b) Partial Penetration Well

From the expression for the relation between transmissivity T_D and specific capacity, Q_s, in partial penetration wells with linear regimes, we have the following, where the first three are cited by Perez (2001):

- From Glee (1930)

$$T_D = \frac{Q}{Sp_p} * \frac{86.4}{2\pi}\left\{\left[\frac{1}{Fp}\ln(\pi x)\right] + \ln\left(\frac{\alpha * Fp}{4x}\right) + 0.1\right\}.$$

- Babouchkine
- $T_D = \frac{Q}{Sp_p} * \frac{86.4}{2\pi}\left\{\left[\frac{1}{Fp}\ln(2ax)\right]\right\}$, donde a (1.32-1.6).
- Schneebeli (1966)

$$T_D = \frac{Q}{Sp} * \frac{86.4}{2\pi}\left[\frac{\ln(4x)}{Fp} + \ln\left(\frac{\alpha * Fp}{4x}\right)\right].$$

- Author $T_D = \frac{Q}{Sp} * \left[116.2 * Fp^{-0.368}\right]$ (obtained from equation (20) for a linear regime).

In the above expressions, $Fp = hs/m$, $\alpha = r_o/r_p$ y $x = hs/2r_p$, where hs is the penetration of the well into the aquifer (m); m is the thickness of the aquifer; r_p is the radius of the pumping well and r_o is the radius of influence.

Table 1 presents the results from evaluating the above expressions for the same magnitudes of the parameters, where similar results are obtained, except for the case of Babouchkine.

Both the effect of partial penetration of the pumping wells and the non-linear flow that can be produced around them result in greater decreases than those produced if the regime were linear and the penetration of the well were total. In the simulation of local effects in a regional model, both factors can be simulated by grid refinement and with a heterogeneous medium (Cabrera-Estupiñán & Hernández-Valdés, 2011).

Relation between Specific Capacity and Darcy Hydraulic Transmissivity with the Non-linear Regimen around Pumping Wells

Two situations often occur:

a) Total penetration well

For this analysis, it is considered important to introduce expressions that determine

Table 1. Partial penetration factor with linear regime.

Fp	Glee	Babouchkine		Author	Schneebeli
		a = 1.32	*a* = 1.6		
0.4	233.77	191.69	198.30	162.77	240.70
0.5	194.24	153.35	158.64	149.94	199.51
0.6	167.88	127.79	132.20	140.21	172.05
0.7	149.06	109.54	113.31	132.48	152.43
0.8	134.94	95.84	99.15	126.12	137.72
0.9	123.96	85.19	88.13	120.77	126.27
1	115.17	76.67	79.32	116.18	117.12

drawdown at any distance from a pumping well at a constant flow in a homogeneous and isotropic medium (Pérez, 2001):

$$S = S_D + S_T = 0.183\frac{Q}{T_D}\log\left(\frac{2.246T_D t}{r^2 E}\right) + \left(\frac{Q}{2\pi T_T}\right)^2 \frac{1}{r} \qquad (6)$$

Or its equivalent:

$$S = 0.366\frac{Q}{T_D}\log\left(\frac{r_0}{r}\right) + \left(\frac{Q}{2\pi T_T}\right)^2 \frac{1}{r} \qquad (6a)$$

Where $r_0 = \left(\frac{2.246T_D t}{E}\right)^{1/2}$ and is known as the radius of influence.

The distance measured from the center of the pumping well, from which a linear flow regime can be considered, is determined by the Darcy's radial (r_D), defined by Pérez (2001):

$$r_D = \frac{Q}{0.1\pi}\left[\frac{T_D}{T_T^2}\right] \qquad (7)$$

Equation (6a) for the pumping well in function of r_D is expressed as follows:

$$S_p = \frac{Q}{T_D}\left\{0.366\log\left(\frac{r_0}{r_p}\right) + \frac{1}{40\pi} * \left[\frac{r_D}{r_p}\right]\right\} \qquad (8)$$

In expressions (6), (6a) and (8), the first addend from the right represents the Darcy drawdown component and the second represents the turbulent components, where Q is the pumping flow volume; S, the drawdown; $T_D = mK_D$ is the Darcy transmissivity; $T_T = mK_T$, the turbulent transmissivity, where m is the aquifer thickness; E the storage coefficient; t the pumping time and r is the distance from the observation well to the center of the pumping well.

From the above equations and based on Darcy's hydraulic conductivities $K_D = \frac{T_D}{m}$ and turbulence $K_T = \frac{T_T}{m}$, and given the equations $K_D = \frac{gk}{\nu}$ and $K_T^2 = \frac{g\sqrt{k}}{C}$, where ν is the kinematic viscosity of the fluid and g is the acceleration of gravity, the hydrological properties characteristic of the aquifer could be obtained: intrinsic or geometric permeability (k) and equivalent roughness of the porous or fissured medium (C).

The representation of equation (5a) as a semilog S *vs* log(r) graph would behave as indicated in Figure 1.

To obtain the same drawdown in the pumping well with a linear flow regime, the slope of the semi-logarithmic graph in Figure 1 would be $\Delta S'_{r10} > \Delta S_{r10}$, which implies that the corresponding transmissivity which simulates the effect of the non-linear regime is less than that of the aquifer $T'_D < T_D$.

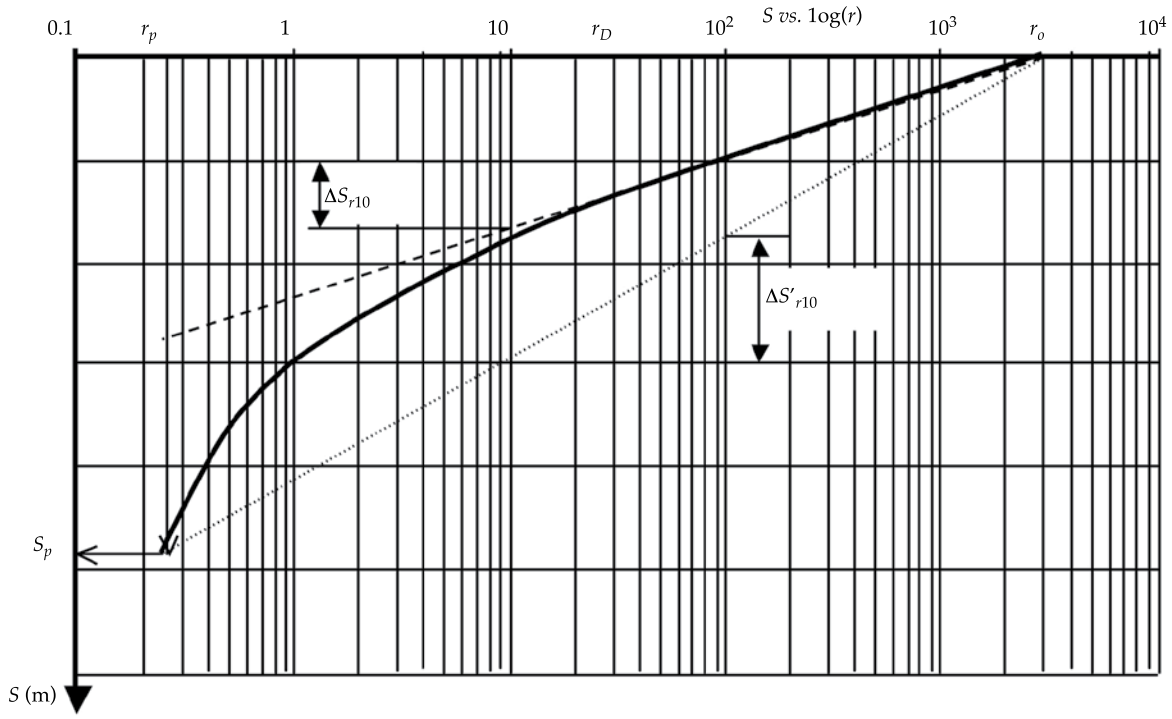

Figure 1. *S* vs. log(*r*) graph for the nonlinear regime near the pumping well.

$$S_p = 0.366 \frac{Q}{T_D} \log\left(\frac{r_o}{r_p}\right) \quad (9)$$

By matching equations (8) and (9), the relation between the real transmissivity of the aquifer and the transmissivity calculated based on the specific capacity is obtained if there is a non-linear flow component $\left(\frac{r_D}{r_p} > 1\right)$:

$$T_D = \left[1 + \frac{0.366 * \log\left(\frac{r_o}{r_p}\right)}{40 * \pi} * \left(\frac{r_D}{r_p}\right)\right] * T'_D \quad (10)$$

Solving for T_D in equation (8), we get:

$$T_D\left(\frac{m^2}{d}\right) = \frac{Q(lps)}{S_p(m)} * (\text{Factor}_{RNL}) \quad (11)$$

Substituting $r_p = 0.25$ m and for a radius of influence of $r_0 = 1\,250$ m, we get:

$$\text{Factor}_{RNL} = \left[117 + 0.688 * \frac{r_d}{r_p}\right] \quad (12)$$

Note that for the linear regime, $\frac{r_d}{r_p} = 1$, therefore Factor_{RNL} coincides with the linear regime corresponding to equation (5).

b) Partial Penetration Well

The use of partial penetration wells is the most frequent situation for pumping wells. Therefore, the effects of the non-linear regime more frequently occur due to larger gradients near the pumping wells, which implies a larger drawdown.

Figure 2 shows a scheme representative of a partial penetration well used by Hernández-Valdés (1984) to calculate drawdown in this

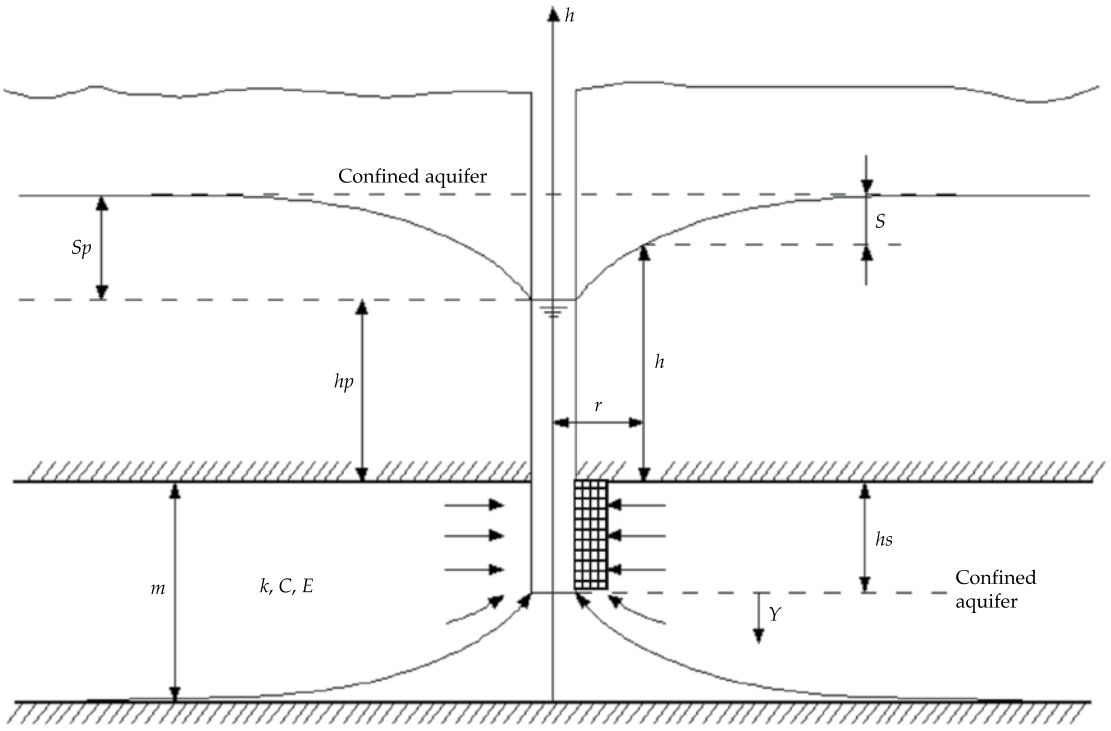

Figure 2. Representation of a partial penetration well.

type of well for a non-linear flow regime. The hypothesis was that the low line of current was parabolic with its vertex at the wall of the well and intercept at the impermeable bottom of the aquifer, at twice the distance of the thickness of the aquifer. Therefore, the thickness of the aquifer would vary according to the penetration of the pumping well, from its wall to as much as two times its thickness.

Based on the scheme presented in Figure 2, in the said work the equation that enables determining the drawdown in the pumping well is obtained by integration, considering a non-linear flow regime that complies with the binomial law for the relation between velocity and the hydraulic gradient (Perez, 2001):

$$I = \frac{U}{K_D} + \frac{U^2}{K_T^2} \qquad (13)$$

Between the pumping well and the distance of twice the thickness of the aquifer (2 m), the continuity equation takes the form:

$$Q = A * U = 2\pi r \left[h_s + \frac{(m - h_s)}{\sqrt{2m}} * r^{\frac{1}{2}} \right] * U \qquad (14)$$

Where U is the apparent mean velocity.

Considering $I = \frac{dh}{dr}$, solving for U in equation (14), substituting in equation (13) and through integration, the difference in drawdown between the pumping well and the distance of twice the thickness of the aquifer can be determined with the expression:

$$\left[S_{pp} - S_{2m} \right] = \int_{h_{pp}}^{h_{2m}} dh = \int_{r_p}^{h_{2m}} \frac{Q dr}{2\pi K_D r \left[h_s + \frac{(m - h_s)}{\sqrt{2m}} * r^{\frac{1}{2}} \right]}$$

$$+ \int_{r_p}^{r_{2m}} \frac{Q^2 dr}{4\pi^2 K_T^2 r^2 \left[h_s + \frac{(m - h_s)}{\sqrt{2m}} * r^{\frac{1}{2}} \right]^2} \qquad (15)$$

The thickness is constant from the distance of twice the thickness of the aquifer (2 m) to the radius of influence (r_o), therefore the drawdown in the aquifer is determined by:

$$S_{2m}\frac{Q}{2\pi K_D m}\ln\left[\frac{r_o}{2m}\right]+\frac{Q^2}{4\pi^2 m^2 K_T^2}*\frac{(r_o-2m)}{r_o*2m} \quad (16)$$

Equation (17) is obtained from the integration of equation (15) with the substitution of equation (16) and using the dimensionless variables.

Solving for T_D in the equation obtained from the drawdown, we have:

$$T_D\frac{Q}{Sp_p}*\frac{1}{2\pi}\left\{\left[\ln\left(\left(\frac{4x}{Fp}\right)\left(Fp+(1-Fp)\left(\frac{Fp}{4x}\right)^{\frac{1}{2}}\right)^2\right)\right.\right.$$

$$\left.\left.\left(\frac{1}{Fp}+0.0375*\frac{\left((1-Fp)^2*\beta\right)}{Fp^3*x}\right)\right]+\ln\left(\frac{\alpha*Fp}{4x}\right)+\frac{0.025*\beta}{x*Fp^2}\right.$$

$$*\left\{\left[\left(Fp^2-4.5*Fp+3\right)+\left(\frac{2*x*Fp}{\left(Fp+(1-Fp)\left(\frac{Fp}{4x}\right)^{\frac{1}{2}}\right)}\right)\right]\right.$$

$$\left.-1.5*(1-Fp)\left(\frac{4x}{Fp}\right)^{\frac{1}{2}}*\left[1+\frac{(1-Fp)\left(\frac{Fp}{4x}\right)^{\frac{1}{2}}}{Fp+(1-Fp)\left(\frac{Fp}{4x}\right)^{\frac{1}{2}}}\right]\right\}$$

$$\left.+0.05*\beta*\left(\frac{Fp}{4x}-\frac{1}{\alpha}\right)\right\} \quad (17)$$

where $Fp = hs/m$, $\beta = r_D/r_p$, $\alpha = r_o/r_p$ and $x = hs/2r_p$, where hs is the penetration of the well into the aquifer (m); r_D is the Darcy's radial, m is the thickness of the aquifer; r_p is the radius of the pumping well and r_o is the radius of influence.

Equation (17) can be replaced by the product of Q_S and a factor that considers the non-linearity of the regime and the partial penetration (Factor $_{RNLpp}$):

$$T_D\left(m^2/d\right)=Factor_{RNLpp}*Q_s\left(lps/m\right) \quad (18)$$

An approximate expression of the Factor $_{RNLpp}$ obtained from the regression of equation (18) would be:

$$\text{Factor}_{RNLpp}=Fac_{RNL}*Fac_{RNLpp1} \quad (19)$$

$$Fac_{RNL}=\left[115.5+0.6845*\frac{r_d}{r_p}\right] \text{ y}$$

$$Fac_{RNLpp1}=\left[Fp^{-0.368*\left(r_d/r_p\right)^{0.234}}\right]$$

$$\text{Factor}_{RNLpp}=Fac_{RNL}*Fac_{RNLpp1}$$

$$=\left[115.5+0.6845*\frac{r_d}{r_p}\right]*\left[Fp^{-0.368*\left(r_d/r_p\right)^{0.234}}\right] \quad (20)$$

For the case of total penetration ($F_p = 1$), Factor $_{RNLpp}$ ≈ Factor $_{RNL}$ in equation (12).

Figure 3 shows the correlation between the factor in the analytical formula (17) and the adjusted factor represented by equation (20) for a wide range of values $Fp = hs/m$ and $\beta = r_D/r_p$.

If the coefficient that affects Qs in partial penetration wells or in those affected by a non-linear regimen given by (Factor $_{RNLpp}$) is divided by (Factor $_{RL}$), the results shown in Table 2 will be obtained, which represent the coefficient. Therefore, the transmissivity obtained from the specific capacity would be multiplied, assuming a linear flow regime and a total penetration well, in function of the penetration of the well (Fp) and the presence of a non-linear flow regime.

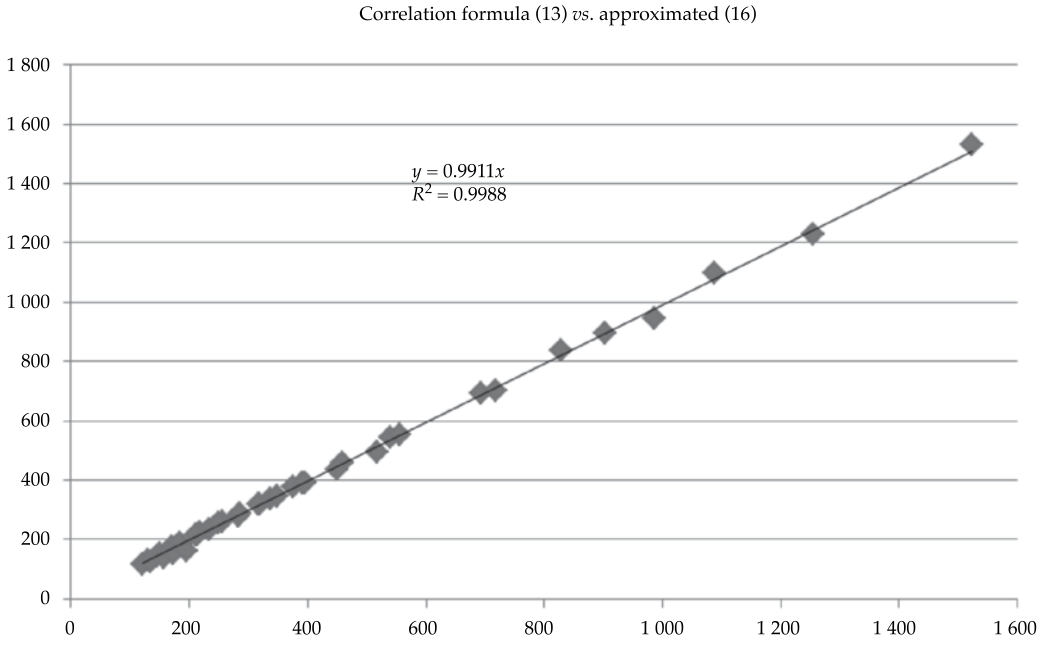

Figure 3. Correlation of the factor with partial penetration and nonlinear regime based on the analytical formula and the equation representing the adjusted factor.

Table 2. Transmissivity orrection coefficient calculated based on specific capacity *Qs*.

	Linear regime			Nonlinear regime. Relation between r_D/rp							
Fp	**Schneebeli**	**DeGlee**	**AutHor**	**4**	**20**	**40**	**80**	**100**	**240**	**320**	**400**
0.4	2.06	2.00	1.39	1.61	2.18	2.72	3.73	4.23	8.07	10.50	13.10
0.5	1.71	1.66	1.28	1.44	1.85	2.24	2.96	3.33	6.00	7.65	9.38
0.6	1.47	1.43	1.20	1.31	1.61	1.91	2.46	2.73	4.71	5.90	7.14
0.7	1.30	1.27	1.13	1.21	1.44	1.67	2.10	2.31	3.84	4.74	5.67
0.8	1.18	1.15	1.08	1.13	1.30	1.48	1.83	2.00	3.22	3.92	4.65
0.9	1.08	1.06	1.03	1.07	1.19	1.34	1.62	1.76	2.75	3.32	3.90
1	1.00	0.98	0.99	1.01	1.10	1.22	1.46	1.57	2.39	2.86	3.33

Evaluation of the application of the Above Results in Karst Aquifers in the Old Province of La Habana, Cuba

The main aquifers that supply the city of La Habana are in karst formations with different degrees of fissuring and cavernous characteristics. The application of deduced equations for non-consolidated medium in karst aquifers has raised various questions in the scientific community. Nevertheless, conceptual models that consider these geological formations to be equivalent porous mediums have been accepted in mathematical modeling at the region scale and for flow towards wells at the local scale. Nonetheless, for this latter case it is important to consider the drawdown component, which generally is present in areas around pumping wells and is due to a non-linear regime that does not comply with the Darcy Law.

To evaluate the behavior of the relation between specific capacity and transmissivity, the results from a set of pumping tests

performed in aquifers in the old province of La Habana, Cuba, are presented, primarily the coastal aquifer in southern Habana. These results were obtained by Molina-Rosabal and Ferrás-Martínez (1989) and are shown in Table 3.

The principal characteristic of the samples not selected (148) by the study cited was very rapid stabilization produced in the pumping wells (85 immediate and 63 in less than 15 minutes), which is typical of the recharge effect and may be caused by the cavernous system in this karst region. These tests resulted in a very large specific capacity, and if the transmissivity T_D of the aquifer were to be predicted by equation (5), it would be overestimated.

Figure 4 shows the behavior of the factor that relates transmissivity with specific capacity (T_D/Qs) in the 90 samples selected. Only 34% of the sample has a factor in the currently used range between 100 and 140, while 58% of the sample has a factor in the range of 80 to 160, indicating that calculations of transmissivity based on specific capacity are not reliable. The deviations demonstrate the effects of the non-linear flow regime, the losses due to the structure or the partial penetration of pumping wells. The specific cause could not be determined without additional details.

In the reference work (Molina- Rosabal & Ferrás-Martínez, 1989), data from satellite wells was included to try to determine the aquifer property indicative of a non-linear regime using the procedure proposed by Perez (2001) and modified with the procedure by Hernández-Valdés (2008). In the latter work, the author proposes that the pumping well not be used to calculate properties since causes such as partial penetration, loss due to structures and other factors can be attributed to the non-linear regime and the property characterizing it, which is actually not the case.

In five of the tests shown below the pumping well was used to determined T_T and therefore the Darcy's radial obtained could be affected by the causes mentioned above. Nevertheless, the magnitude of the relation $\left(\frac{T_D}{Q_S}\right)$, an equivalent factor, can be explained by the presence of the non-linear flow regime and/or by the presence of partial penetration of the pumping well. The cause cannot be know without other information.

Table 4 shows the results of five pumping tests with satellite wells taken from the work by Molina-Rosabal and Ferrás-Martínez (1989); well 966 in the same basin was added.

Commentaries about the Results of Pumping Tests with Satellite Wells

For the cases in which there were two observation wells (15 and 966), the following commentaries are presented:

- The first case did not present a non-linear regime between the two satellites, and therefore the pumping well was used and the closest one, located at 38 m. This implied that losses in load would be considered as a product of the non-linear flow regime, where there would be other causes and an error in the calculation of T_T would occur, resulting in the Darcy's radial being larger than the distances from the observation well, where a linear regime was not present. Therefore, according to the relation between T_D/Q_S theoretically the Darcy's radial should be 53 m when solving for rd in $Fac_{RNL} = \left[115.5 + 0.6845 * \frac{r_d}{r_p}\right]$.
- The second case shows that the specific capacity obtained from the test is affected by recharge or cavernous effects, and the drawdown that should be obtained in the pumping well would result in a four times lower specific capacity. Therefore, the corresponding relation would exist between $\left(\frac{T_D}{Q_S}\right)$ and the $Factor_{RNL}$. Figure 5 shows the calculation of the properties using the methodology proposed by

Table 3. Relation T_D/Q_s in wells in the province of La Habana.

Well	*Qs* (lps/m)	T_D(m²/d)	T_D/Qs	Well	Qs (lps/m)	T_D (m²/d)	T_D/Qs
19	324.00	52 600.00	**162.35**	1 615	75.36	8 197.00	**108.77**
86	100.00	11 900.00	**119.00**	657	3.50	324.00	**92.57**
23	12.00	3 730.00	**310.83**	715	2.43	479.00	**197.12**
85	35.00	4 360.00	**124.57**	1 100	74.00	7 313.00	**98.82**
115	14.61	3 160.00	**216.29**	1 580	22.32	3 169.00	**141.98**
98	141.00	30 800.00	**218.44**	619	45.90	4 061.00	**88.47**
95	22.00	3 800.00	**172.73**	1 784	7.04	821.00	**116.62**
97	66.00	6 700.00	**101.52**	1 023	54.38	8 657.00	**159.19**
103	42.20	10 000.00	**236.97**	22	31.16	11 331.00	**363.64**
115	109.00	15 330.00	**140.64**	1 590	9.00	1 000.00	**111.11**
132	216.00	26 800.00	**124.07**	2 077	43.70	4 353.00	**99.61**
131	121.70	12 470.00	**102.47**	1 957	33.60	2 435.00	**72.47**
133	176.60	65 800.00	**372.59**	1 627	19.92	1 878.00	**94.28**
149	154.30	17 900.00	**116.01**	1 815	9.97	1 392.00	**139.62**
6	57.00	10 000.00	**175.44**	1 662	39.01	4 872.00	**124.89**
7	12.00	1 000.00	**83.33**	1 732	43.40	7 423.00	**171.04**
10	50.00	5 600.00	**112.00**	701	0.78	72.13	**92.47**
54	14.00	2 180.00	**155.71**	1 160	40.10	12 482.00	**311.27**
56	102.00	33 000.00	**323.53**	15	1.65	373.00	**226.06**
57	2.70	289.00	**107.04**	1 393	20.40	835.00	**40.93**
60	53.50	5 490.00	**102.62**	1 192	876.00	107 271.00	**122.46**
59	59.60	5 490.00	**92.11**	1 113	1.60	752.00	**470.00**
61	15.20	1 480.00	**97.37**	690	30.76	5 424.00	**176.33**
63	154.30	17 100.00	**110.82**	814	3.03	567.00	**187.13**
67	13.50	2 670.00	**197.78**	608	3.30	500.00	**151.52**
68	34.90	4 840.00	**138.68**	519	52.60	9 686.00	**184.14**
75	123.00	14 900.00	**121.14**	507	27.45	6 375.00	**232.24**
78	53.00	7 330.00	**138.30**	503	38.80	5 564.00	**143.40**
79	287.00	18 170.00	**63.31**	494	20.70	4 598.00	**222.13**
80	8.20	1 140.00	**139.02**	1 432	55.90	4 188.00	**74.92**
81	110.00	29 200.00	**265.45**	75	16.25	2 462.00	**151.51**
83	16.14	1 335.00	**82.71**	1 681	10.80	1 282.00	**118.70**
87	40.00	2 804.00	**70.10**	1 605	1.66	740.00	**445.78**
91	142.40	17 500.00	**122.89**	1 447	5.42	530.00	**97.79**
92	7.80	1 000.00	**128.21**	1 317	13.07	1 683.00	**128.77**
94	53.96	27 902.00	**517.1**	AB2/9	49.00	7 848.00	**160.16**
93	11.50	4 950.00	**430.43**	TE-21	3.56	1 917.00	**538.48**
540	100.00	21 600.00	**216.00**	AB4/45	139.00	12 305.00	**88.53**
365	1.65	403.00	**244.24**	911	21.88	3 971.00	**181.49**
278	57.20	13 400.00	**234.27**	791	6.34	460.00	**72.56**
277	53.40	6 450.00	**120.79**	1 732	143.00	20 000.00	**139.86**
896	3.67	292.00	**79.56**	976	12.18	1 708.00	**140.23**
1	13.87	3 531.00	**254.58**	966	15.10	2 350.00	**155.63**
2	13.19	4 312.00	**326.91**	467	7.26	1 164.00	**160.33**
3	24.35	2 635.00	**108.21**	398	11.93	1 427.00	**119.61**
33	7.04	792.00	**112.50**	89	27.4	27 112	**989**
						Average	**179.3**
						Deviation	**85.0**

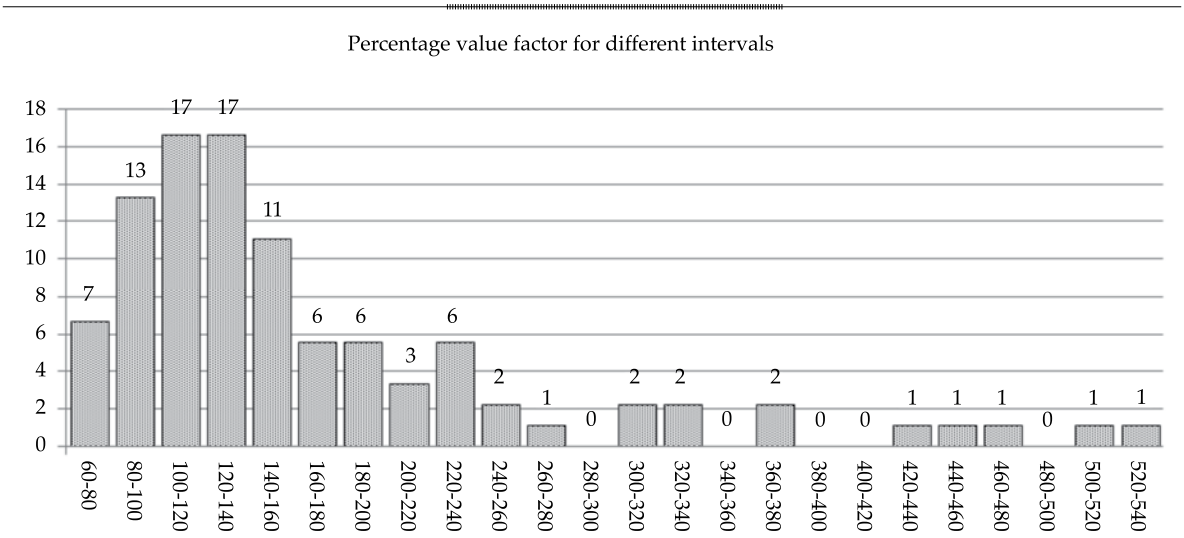

Figure 4. Percentage values for the transmissivity correlation factor with specific capacity for the 90 samples from Table 3.

Table 4. Wells from Table 3 with at least one satellite well.

Well	T_D (m²/d)	Distances (m) Wells for T_T	T_T (m²/d)	Darcy Radial (m)	Qs (lps/m)	T_D/Q_S	Factor$_{RNL}$	Observations
94	27 902	0.25 and 23.3	3 049	124	54	517	455	*Partial penetration $Fp = 0.92$
89	27 112	0.2 and 100	1 250	162	27.4	989	670	*Partial penetration $Fp = 0.8$
1160	12 482	0.25 and 15	2 538	80	40	311	335	Ok
22	11 330	0.2 and 60	1 920	72.6	31.16	363	364	Ok
966	2 900	**0.3**, **38** and 60	~~823~~	~~79~~	12.2	237	~~295~~	Calculation error for T_T
15	373	0.2, **10 and 15**	120	224	~~1.65~~ 0.438	~~226~~ 851	883	Inadequate Qs valueo

*The calculated values of the partial penetration were obtained by applying Factor$_{RNLpp}$ (20).

Hernández-Valdés (2008) and the pumping data are graphically shown.

This pumping test was conducted with a flow volume of 26 lps in a 40 cm diameter well and the drawdown was measured in two satellites located 9.7 and 15 m from the pumping well, respectively.

Calculation of Darcy's Transmissivity T_D

The procedure described by Cooper and Jacob (1946), cited by Todd (1959) is followed, obtaining the slope per ΔSt_{10} cycle from the graphic representation of S *vs.* log(t) and then determining T_D using the following expression:

$$T_D = 0.183\frac{Q}{\Delta St_{10}} = 0.183 * \frac{26 * 86.4}{1.1} = 373\ m^2/d$$

Calculation of Turbulent Transmissivity T_T

Since the fitted lines in the semi-logarithmic graphs in the previous section should be parallel, the difference in drawdown among

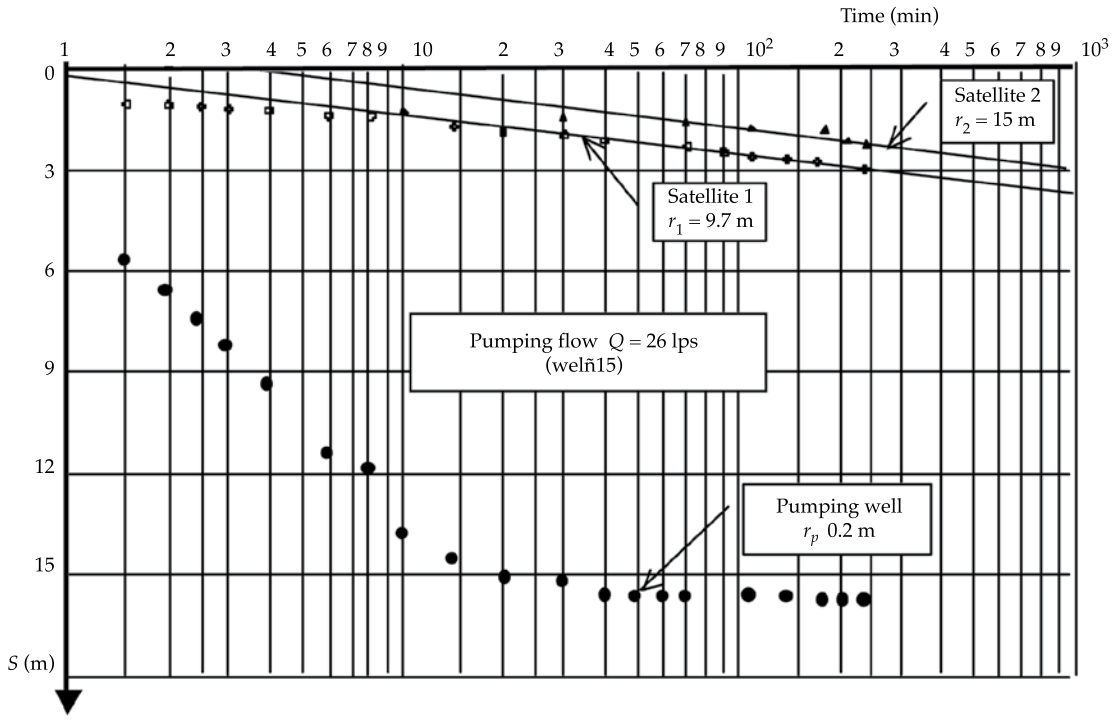

Figure 5. semi-logarithmic graph of well 15 (data from Molina-Rosabal and Ferras-Martinez, 1989).

these is determined for any time and we get the value of T_T from equation (6a).

$$T_T^2 = \frac{\frac{Q^2}{4\pi^2}\left(\frac{r_2 - r_1}{r_2 * r_1}\right)}{\left[\left(S_1 - S_2\right) - 0.366\frac{Q}{T_D}\log\left(\frac{r_2}{r_1}\right)\right]} \Rightarrow T_T = 109\, m^2/d$$

Where r_1 = 9.7 m and r_2 = 15 m are the distances from the pumping well to the observation wells; S_1 = 2.96 m and S_2 = 2.16 m are the drawdowns corresponding to the above distances for a time of 239 minutes.

Calculation of the Darcy's radial r_D

This parameter was already defined as $r_D = \frac{Q}{0.1\pi}\left(\frac{T_D}{T_T^2}\right)$ and would result in r_D = 224 m.

Determination of the Storage Coefficient E

Since the two observation wells are in the non-linear regime zone (less than the Darcy's radial), then the procedure by Jacob (Chenini *et al.*, 2008) is used to calculate E_J, obtaining from this value the storage coefficient, *E:*

$$E = \frac{2.246 T_D t_0}{r^2} * e^{\frac{QT_D}{\pi r T_T^2}} = E_J * e^{0.1\left(\frac{r_D}{r}\right)}$$

For r_1 = 9.7 m, $t_0 = 3.47 * 10^{-4}$ days and E_J = 0.0031, therefore E = 0.031.

For r_1 = 15 m, $t_0 = 1.8 * 10^{-3}$ days and E_J = 0.0069, therefore E = 0.031.

The factor that affects E_J in the equation above is the error committed by determining the storage coefficient E using the procedure proposed by Jacob in an observation well located in a non-linear flow zone.

Utilization of Factor$_{RNLpp}$ to Calculate Drawdown in Pumping Wells

Likewise, it can be said that the drawdown in the pumping well can be determined from equation (18), according to the flow (Q) and the transmissivity (T_D):

$$S_p(m) = \text{Factor}_{RNLpp} * \frac{Q(\text{lps})}{T_D(m^2/d)} \qquad (21)$$

In the proposal by Hernández-Valdés and Llanusa-Ruiz (2009), applied by Cabrera-Estupiñán (2010), to consider the drawdown as a restriction in some of the nodes representative of pumping wells when the penetration of the well is known, Factor$_{RNLpp}$ would be calculated for a pumping flow volume at maximum capacity in order to avoid iterations, since the Darcy's radial (7) depends on this factor, and to be on the safe side. This would allow for using the MADA optimization model (Cabrera-Estupiñán & Dilla-Salvador, 2011) with a semi-local refinement of the grid in the regional model of the aquifer.

Conclusions

The following conclusions can be drawn from this work:

- The calculations of transmissivity (T_D) based on specific capacity (Q_S) causes significant errors in this parameter since it can be overestimated in cases in which the pumping well levels are rapidly stabilized or underestimated when the effects of partial penetration, non-linear regimes, losses due to the structure of wells, etc. influence the magnitude of the factors that correlate them.
- The effect of non-linear flow regimes on pumping wells results in transmissivity calculations that are lower than the actual transmissivity when using specific capacity to calculate them. These will decrease as pumping flow volumes increase.
- The magnitude of the coefficient that relates T_D (m^2/d) with Q_S (lps/m) can indicate whether effects exist resulting from recharge or cavernous properties, non-linear flow regimes, partial penetration, losses due to the pumping well's structure, etc.
- To identify the real causes of increases in drawdown in pumping wells, it is necessary to know the constructive characteristics of the catchment works, the hydrogeological properties of the aquifer and the exploitation conditions to which said work is subjected.
- For different pumping flow volumes, the drawdown in pumping wells can be calculated in partial penetration wells and with the non-linear flow regime based on factor Factor$_{RNLpp}$ and transmissivity T_D, when the properties of the aquifer and the penetration factor are known.
- Pumping tests are recommended that make it possible to determine the properties of an aquifer with a non-linear regime, performing two pumping tests with different flow volumes and one observation well, or one test if two observation wells are located near the pumping well and at least one of those shows the effect of non-linear flow. The use of data from pumping wells is not advisable, except to calculate transmissivity T_D.

Received: 27/03/12
Accepted: 22/04/13

References

Abbott, M. M., & Dehay, K. (2008). *Aquifer Tests and Characterization of Transmissivity, Ada-Vamoosa Aquifer on the Osage Reservation* (10 pp.). Osage County, USA: Geological Survey Scientific Investigations Report 2008-5118. Recuperado de pubs.usgs.gov/sir/2008/5118/.

Aitchison-Earl, P., & Smith, M. (2008). *Aquifer Test Guidelines* (2nd edition). Report No. R08/25. Environment Canterbury Technical Report. Recuperado de www.ecan.govt.nz.

Cabrera-Estupiñán, E. (2010). *Sistema para la administración de la explotación del agua subterránea*. Tesis presentada en opción al grado científico de Doctor en Ciencias Técnicas. La Habana: Instituto Superior Politécnico José Antonio Echeverría.

Cabrera-Estupiñán, E., & Hernández-Valdés, A. O. (2011). Modelación del agua subterránea a escala regional con refinamiento local de la malla. Planteamiento y validación del algoritmo. *Tecnología y Ciencias del Agua, antes Ingeniería Hidráulica en México*, 2(1), 65-82.

Cabrera-Estupinán, E., & Dilla-Salvador, F. (octubre-diciembre, 2011). Modelo de administración de acuíferos: MADA. *Tecnología y Ciencias del Agua, antes Ingeniería hidráulica en México*, 2(4), 5-24.

Chenini, I., Silvain, R., & Ben-Mammou, A. (2008). A simple method to estimate Transmissibility and Storativity of Aquifer Using Specific Capacity of Wells. *J. Applied Sci., 8*(14), 2640-2643.

De Glee, G. J. (1930). *Over Groundwaterstominger Bij Water Onnttrekking Door Middle Van Put Ten*. Thesis. Delft Holland: J. Waltman.

El-Naga, A. (1994). Estimation of transmissivity from specific capacity data in fractured carbonate rock aquifer, central Jordan. *Environmental Geology*, *23*(1), 73-80.

Hernández-Valdés, A. O. (1984). Efectos de la penetración parcial e pozos con régimen no lineal. *Ingeniería Hidráulica* (ISPJAE), *5*(2).

Hernández-Valdés, A. O., & Llanusa-Ruiz, H. (2009). "La modelación matemática y la explotación de los acuíferos costeros". Congreso Internacional de Hidráulica. Cayo Santa María. Cuba.

Hernández-Valdés, A. O. (2008). *Nuevas formulaciones para determinar las propiedades hidrogeológicas con régimen no lineal*. XXIII Congreso Latinoamericano de Hidráulica, Cartagena de Indias, Colombia.

Knopman, D. S., & Hollyday, E. F. (1993). Variation in Specific Capacity in Fractured Rocks, Pennsylvania. *Ground Water*, *31*(1), 135-145.

Knochenmus, A., & Bowman, G. (MOE) (1998). *Transmissivity and Water Quality of Water-Producing Zones in the Intermediate Aquifer System*. Sarasota County, USA: Geological Survey Water-Resources Investigations Report 98-4091.

Molina-Rosabal, Y., & Ferrás-Martínez, L. (1989). *Características de las propiedades hidrogeológicas de la Cuenca Sur: Tramo Güira–Quivicán*. Trabajo de Diploma. La Habana: Facultad de Ingeniería Civil, ISPJAE.

Parkhurst, D. L., Christenson, S., & Breit, G. N. (1996). *Ground-Water-Quality Assessment of the Central Oklahoma Aquifer, Oklahoma: Geochemical and Geohydrologic Investigations* (101 pp.). Paper 2357-C. US Geological Survey Water-Supply.

Pérez, D. (2001). *La explotación del agua subterránea. Un nuevo enfoque*. La Habana: Editorial Félix Varela.

Schneebeli, G. (1966). *Hydraulique Souterraine***.** Paris: Eyrolles.

Walton, W. (1970). *Groundwater Resource Evaluation* (664 pp.). McGraw-Hill Series in Water Resources and Environmental Engineering.

WRI Report 87-4034 (2008). *Hydrogeology, Aquifer Characteristics, and Ground-Water Flow of the Surficial Aquifer System, Broward County*. Disponible en: sofia.usgs.gov/publications/wri/87-4034/spcapacity.html.

Institutional Address of the Authors

Dr. Armando O. Hernández-Valdés

Facultad de Ingeniería Civil
Centro de Investigaciones Hidráulicas
Instituto Superior Politécnico José Antonio Echeverría
Calle 114, núm. 11901 entre 119 y 127, Marianao
19390 La Habana, Cuba
Teléfonos: +53 (7) 2601 416 y 2603 636
Fax: +53 (7) 2672 013
ahernandez@cih.cujae.edu.cu

Click here to write the autor

Location of limnimetric scales on the southern shore of the Mar Chiquita lagoon, Miramar Argentina.

Image provided by Mariana Pagot.

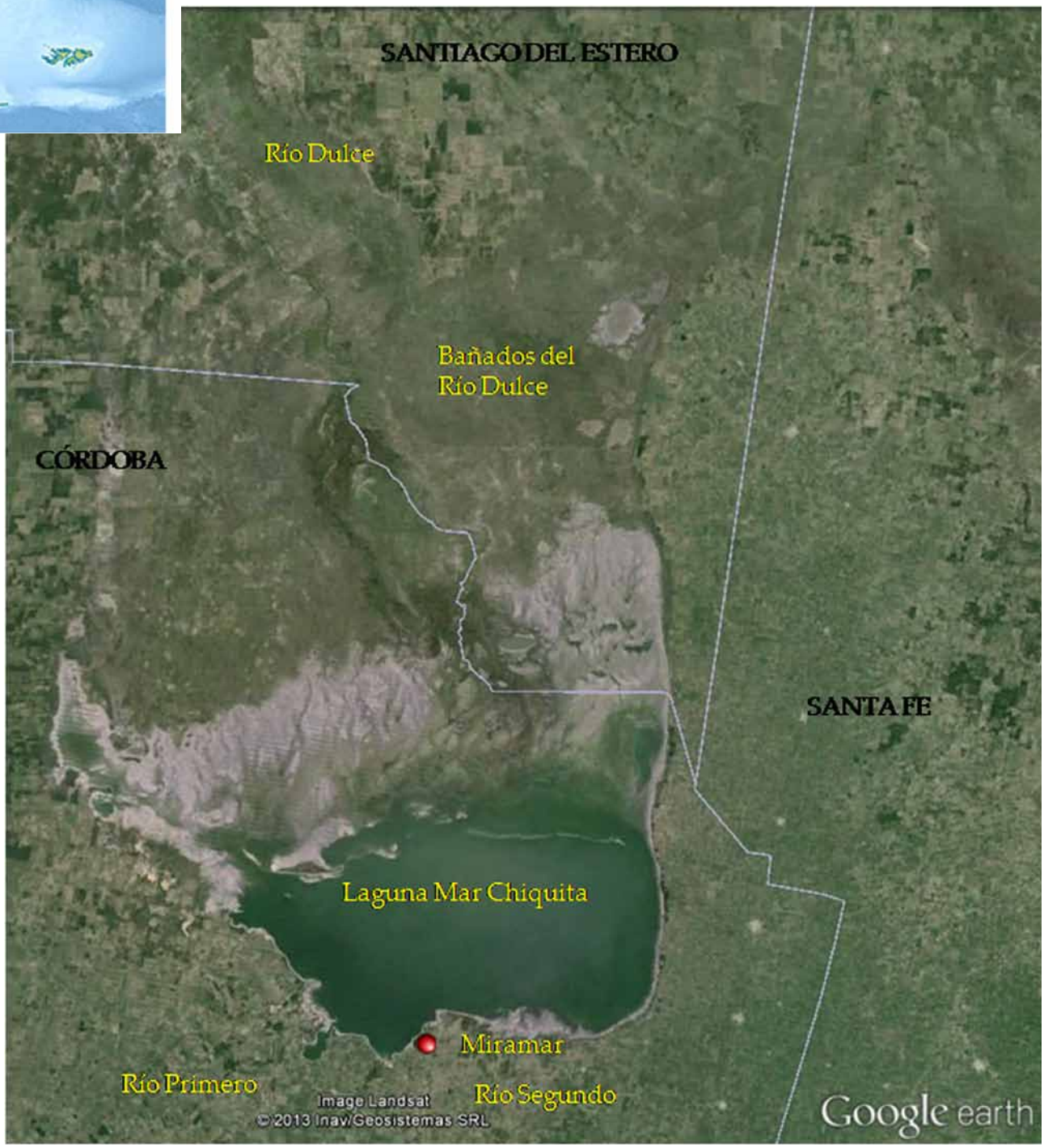

Maximum Water Level in Mar Chiquita, Lagoon, Cordoba, Argentina

• Mariana Pagot* • Gerardo Hillman • Cecilia Pozzi-Piacenza •
• Paolo Gyssels • Antoine Patalano • Andrés Rodriguez •
Universidad Nacional de Córdoba, Argentina
*Corresponding Author

Abstract

Pagot, M., Hillman, G., Pozzi-Piacenza, C., Gyssels, P., Patalano, A., & Rodriguez, A. (July-August, 2014). Maximum Water Level in Mar Chiquita, Lagoon, Cordoba, Argentina. *Water Technology and Sciences* (in Spanish), *5*(4), 115-128.

Mar Chiquita lagoon is the largest endorheic body of water in Argentina. It is located in the northeast portion of the province of Cordoba. The maximum water level is the topic of this work, which is defined using the combined effect of the historical maximum water level measured on the coast and the maximum storm elevation (considering both wind and waves) estimated for recurrences of 25, 50 and 100 years. The analysis of the series of water levels made it possible to determine the historical maximum level measured in the lagoon. This value was recorded in 2003 as a height of 71.9 meters above sea level (masl). The maximum storm level is defined by both the action of the wind and waves generated by the storm. Specific software and empirical formulas were used to obtain these estimates. To propagate the waves on the beach profile, the bathymetry of the lagoon was rebuilt using remote sensing techniques. To this end, terrain elevation data were used from space surveys derived from radar and from thematic maps based on Landsat images with the digital extraction of water contours. The results indicate that the maximum flood that could occur in Laguna Mar Chiquita, on the southern coast of the system, is 73.5 masl with a recurrence of 100 years. It is important to conduct this analysis for systems with large fluctuations in water levels, such as the one presented here.

Keywords: Mar Chiquita lagoon, maximum flood stage, remote sensing, water levels, wind, waves.

Resumen

Pagot, M., Hillman, G., Pozzi-Piacenza, C., Gyssels, P., Patalano, A., & Rodriguez, A. (julio-agosto, 2014). Elevación máxima del agua en la laguna Mar Chiquita, Córdoba, Argentina. Tecnología y Ciencias del Agua, *5(4), 115-128.*

La laguna Mar Chiquita es el mayor cuerpo de agua endorreico de la República Argentina y está ubicada al noreste de la provincia de Córdoba. El nivel de agua máximo es objeto de este trabajo y se definió con base en el efecto combinado del máximo nivel de agua histórico medido sobre la costa sur y de la máxima sobre-elevación por tormenta estimado para recurrencias de 25, 50 y 100 años. El análisis de las series de niveles de agua permitió definir el valor máximo histórico del nivel medido en la laguna. Este valor se registró en el año 2003 con una cota de 71.9 m sobre nivel del mar (snm). La máxima sobre-elevación por tormenta se definió por la acción conjunta del viento y del oleaje generado por el mismo. Para estas estimaciones se utilizaron programas específicos y formulaciones empíricas. Para propagar el oleaje sobre el perfil de playa, se reconstruyó la batimetría de la laguna, basada en técnicas de teledetección. A tal efecto se utilizaron datos de elevación del terreno, tomando relevamientos espaciales con radar y mapas temáticos derivados de imágenes satelitales ópticas, productos LandSat, basados en el proceso de extracción digital de los contornos de agua. Los resultados indicaron que la cota máxima de inundación de la laguna Mar Chiquita para la costa sur del sistema podría llegar a los 73.5 msnm para una recurrencia de 100 años. Este análisis es importante realizarlo en sistemas que presentan grandes fluctuaciones del nivel de agua, como el aquí presentado.

***Palabras clave**: laguna Mar Chiquita, cota máxima de inundación, teledetección, niveles de agua, viento, oleaje.*

Introduction

Mar Chiquita Lagoon (Figure 1) is located in the largest endorheic basin in Argentina. It represents an important habitat with a large variety of aquatic birds and other species, serving as support for these populations during critical periods of their biological cycles (especially hemispheric migrations). It is a salty lake, with an area measuring 6 500 km^2 at the beginning of this century. It is shallow (10 m maximum) and large wetlands are found in the north, where

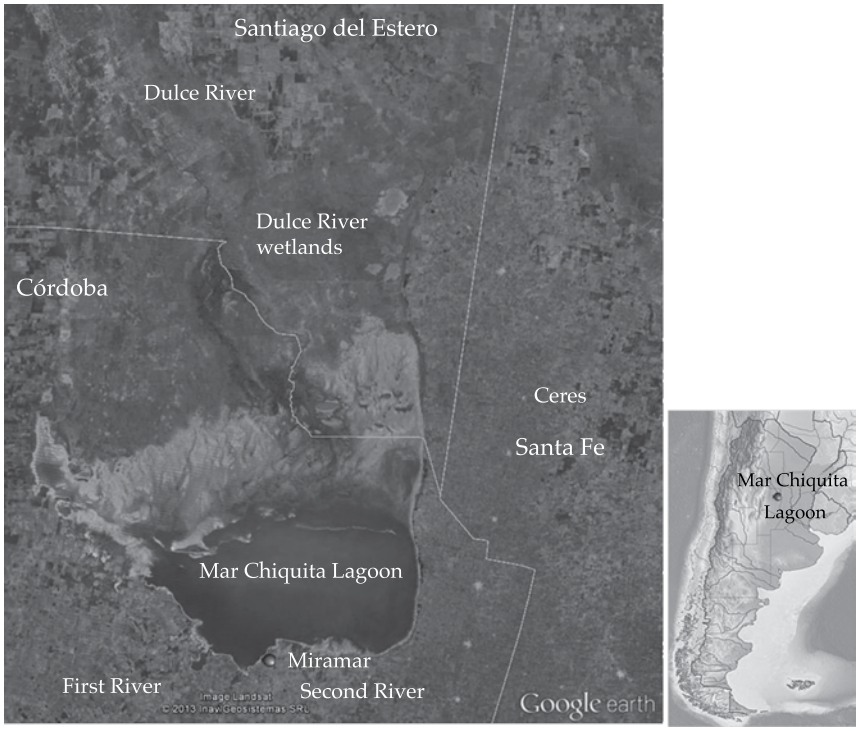

Figure 1. Mar Chiquita Lagoon System (image from April 10, 2013, Google Earth).

the Dulce (Petri) River discharges after many diversions and course changes, losing the main channel as it passes through planes with a very slight slope (0.03%). The outlets of the Suquia (first) and Xanaes (second) Rivers are in the south.

Because of these characteristics, the area was recognized in 1994 as the Mar Chiquita Provincial Nature Reserve. At the beginning of the 1990s, the wetlands pertaining to the Dulce River and Mar Chiquita Lagoon were declared a "Hemisphere Site" by the "Hemispheric Shorebirds Network." In 2002, these wetlands were added to the "Ramsar Sites" list, created by the Ramsar Convention on Wetlands, with nine countries (National Law no. 23.919/91). Finally, this comprehensive system makes up the International Network of Living Lakes (UNC-UNSE, 2007).

Many hydrological and hydrodynamic studies have been conducted continuously since 1998, primarily by researchers from the Hydraulic Laboratory of the School of Exact, Physical and Natural Sciences at the National University of Cordoba (2011). The main results have been reported by Hillman (1999 and 2003), Hillman *et al*., 2003; Pagot (1999 and 2003); Pagot, Hillman, Rodriguez, Caamaño-Nelli and Plencovich (2003); Rodriguez *et al*. (2000a, 2000b); Rodriguez, Hillman, Pagot and Caamaño- Nelli (2002); Plencovich *et al*. (2005); Plencovich (2011); Pozzi *et al*. (2005); Pozzi (2006), and Cereceda-Botella (2009), among others.

The objective of the present study was to define the elevation and maximum flood level of the southern coast of Mar Chiquita Lagoon, with return periods of 25, 50 and 100 years.

Even though the water level in the lagoon has declined continuously over the past 10 years (a 40% decrease in height), defining maximum level limits is considered important, especially to prevent floods in the area around Miramar, the only urban coastal population,

which could occur from a new rise in the water level.

Material and Methods

The maximum flood level (MFL) was defined by equation (1), according to the scheme proposed in Figure 2, as the sum of the maximum historical level (MHL) recorded and the maximum storm level (MSL) calculated for each recurrence time (T_R), or return period proposed.

To define the maximum historical level, daily and monthly data corresponding to measured and/or calculated water levels in the Mar Chiquita lagoon were analyzed.

Significant variations in the water level of the lagoon have occurred as a direct result of natural hydrological cycles, amplified by the management of the resource in the upper Dulce River basin (the lagoon's main tributary) (Pagot, 1999; Hillman, 1999; Plencovich, 2011). These variations in levels have been documented since 2001 on a daily and continuous basis with direct measurements on limnimetric on the southern coast of the Mar Chiquita lagoon (see Figure 3), across from the locality of Miramar (Figure 3). These data were provided by the Cordoba Environmental Agency through the Provincial Miramar Reserve and the Secretary of Water Resources and Coordination of the Province of Cordoba (Cordoba Environmental Agency, S.E., 2004).

The maximum storm level was calculated by first using empirical formulas applied at significant points, called "target points," selected on the southern coast of the lagoon. The results depend on the physical, geomorphological and hydrodynamic parameters, such as wind intensity, duration and direction, local bathymetry, geometry of the coast and the height and period of the wave that can be generated in the lagoon.

Figure 10 shows the points selected (S1 through S5) for the calculation of the maximum flood level (MFL), taking the level established by the MHL as the coastline.

The maximum storm level (MSL) (MSL in equation (2)) is the result of the sum of the over-height due to the wind's drag over the surface, or "Wind Set-Up" (WSU), and the over-height due to irregular incident waves on the coast, or "Run-Up" (RU), (which is the maximum vertical local increase produced on the beach slope from the effects of the irregular waves during the process of their breaking). Both are calculated for return periods (T_R) of 25, 50 and 100 years:

$$MSL_{TR} = WSU_{TR} + RU_{TR} \qquad (2)$$

The over-height from the wind (WSU) was calculated using the equations for the conservation of the amount of movement and averaged continuity in the water column (Kamphuis, 2000), in one-dimensional. The approximate value of this variable depends on the wind intensity (wind speed generated by the storm) and the local bathymetry. To calculate this, the wind intensity was

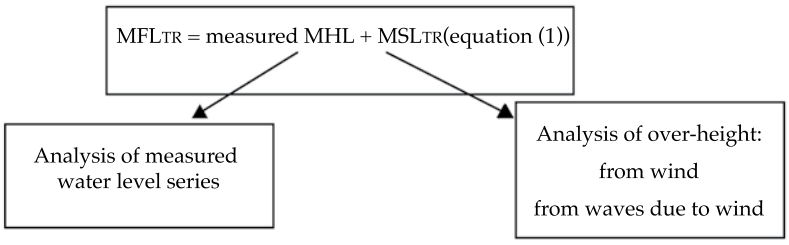

Figure 2. Methdology of the work.

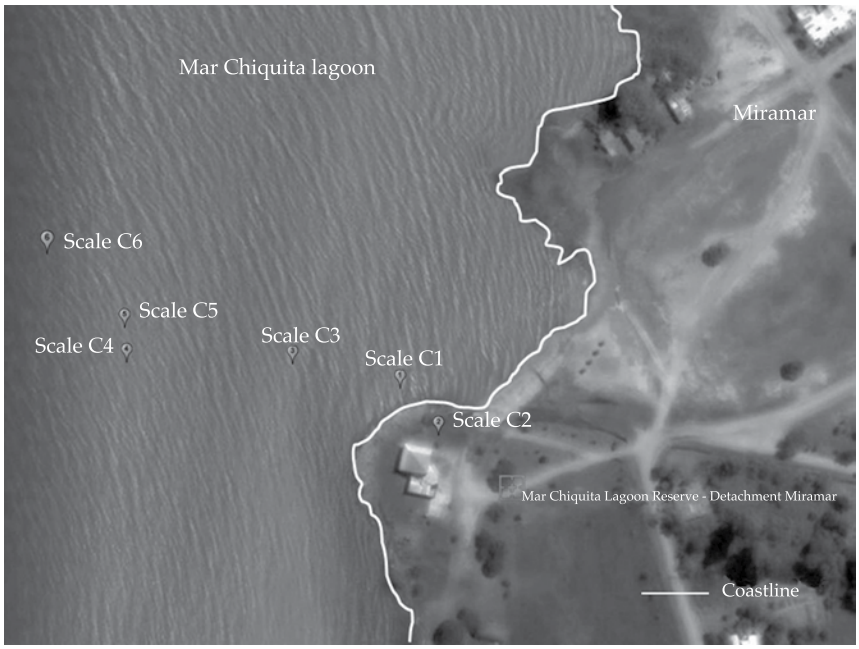

Figure 3. Location of the limnimetric scales on the southern coast of the lagoon, Miramar.

considered for each of the return periods analyzed. The local bathymetry corresponding to each target point was determined according to sections perpendicular to the coast.

The one-dimensional (1D) equation used in this work is equation (3) (Kamphuis, 2000):

$$\frac{dS}{dx} = \frac{\zeta\left(U\cos\phi\right)}{gD} \qquad (3)$$

Where, and according to the scheme in Figure 4, S is the over-height or "Wind Set-up" given by the wind (m); x is the distance based on which the over-height is calculated (m); ζ is a constant = $3.2 \cdot 10^{-6}$; U, is the wind speed (m/s); ϕ is the angle between the wind direction and direction x; d is the depth before the over-height (m); D is the depth ($d + S$) for each Δx (m).

This equation assumes stationary conditions, considering that the wind always maintains the same direction. With this hypothesis, the maximum over-height possible was calculated, which represents a conservative value in a feasibility study.

In a closed water body, such as the Mar Chiquita Lagoon, when the force of the wind produces an over-height at one end of the lagoon, the levels at the opposite end decrease (Figure 4).

To calculate the over-height due to waves, empirical formulas were used that take into account the height of the waves in deep water, the wave length of the incident wave and the slope of the beach.

Therefore, prior to the calculation of this variable, it was necessary to calculate the wave characteristics (generation and propagation) in deep waters (when the height of the wave is much less than the depth). Given the shallowness of the Mar Chiquita Lagoon, waves generated by wind was used, according to the formulas that take into account mean depth corresponding to each target point.

The present work uses the formulas for irregular waves presented in the *ACES* software (1992) and the *TIC* software (2003).

In the *ACES* program (1992), the empirical model used pertains to the works by Mase and

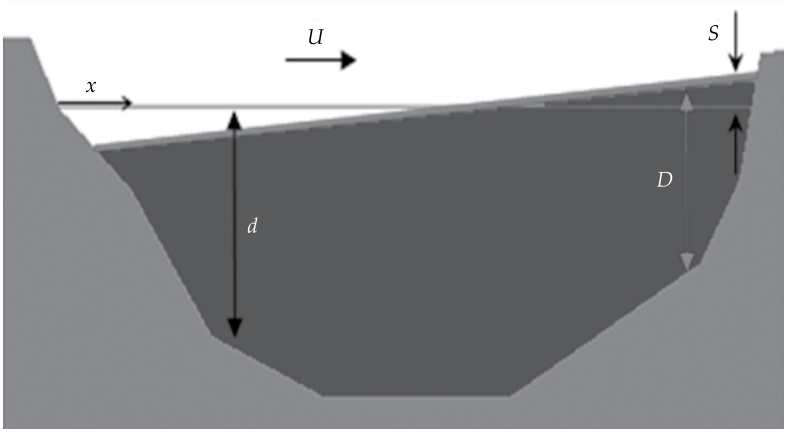

Figure 4. Over-height in a lage due to the effect of constant wind.

Iwagaki (1984) and Mase (1989). The maximum over-height is given by equation (4):

$$R_p = H_{so} a_p Ir^{b_p} \quad (4)$$

Where $_p$ is the quantile or statistical value desired (max 2% on average), R_p is the over-height of the quantile $_p$ (m): H_{so}, the significant wave height in deep waters (m); *a, b* constants which depend on the quantile value desired in the calculation; *Ir* is the Irribarren number (equation (5)):

$$Ir = \frac{\tan \beta}{\left(H_{so} / L_o\right)^{0.5}} \quad (5)$$

Where β is the mean slope of the foreshore of the beach (corresponding to the water/earth intersection) and L_o (m) is the wave length in deep waters.

In the *TIC* program (2003), the Holmann formula (1986) was used, which comes from a large series of campaigns performed in Duck Beach, North Carolina. The author found an acceptable correlation between over-height of the normalized wave with the significant incident wave height and the Irribarren number. In particular, the expression used is the one presented in equation (6):

$$\frac{R_{u2\%}}{H_s} = 0.822 \cdot I_r + 0.2 \quad (6)$$

Where $R_{u2\%}$ is the over-height due to the wave over 2% of the time.

Results

Maximum Historical Level (MHL)

To determine the MHL, the daily water level data were digitalized, which included up to the year 2011 (Figure 5). It is noteworthy that each datum measured was analyzed in a particular manner by assigning the reading to the corresponding limnimetric scale and filtering uncertain data that appeared in the original form used. These filters were applied to eliminate the errors that arose in the measurement and digitalization process of these data.

The series of monthly mean levels was completed for a period of 44 years, between 1967 and 2011 (Figure 6).

Troin, Vallet-Coulomb, Sylvestre and Piovano (2010) present a curve (Figure 7) that begins in the year 1890 and is associated with a level slightly lower than 68 masl. The same curve shows a continual decreasing cycle until 1915, followed by cycles of fluctuations between heights of 64 and 67 m during the 52 remaining years of the period without records. During 1915 and the periods 1931-1935 and

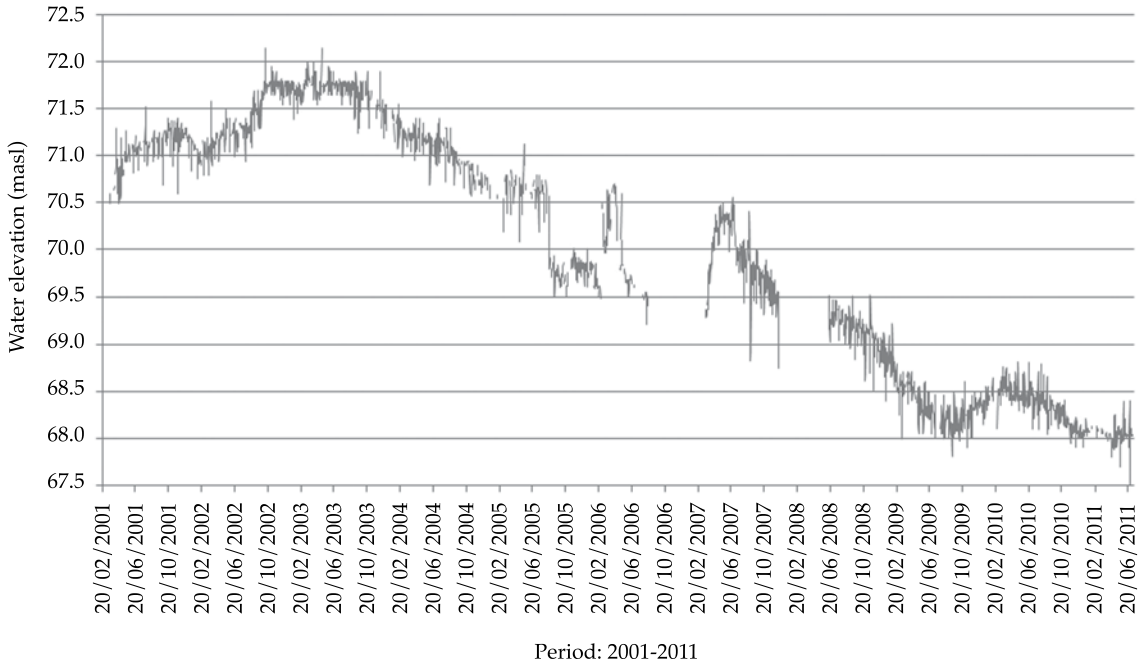

Figure 5. Daily measured water levels in the Mar Chiquita Lagoon (LH-UNC, 2011).

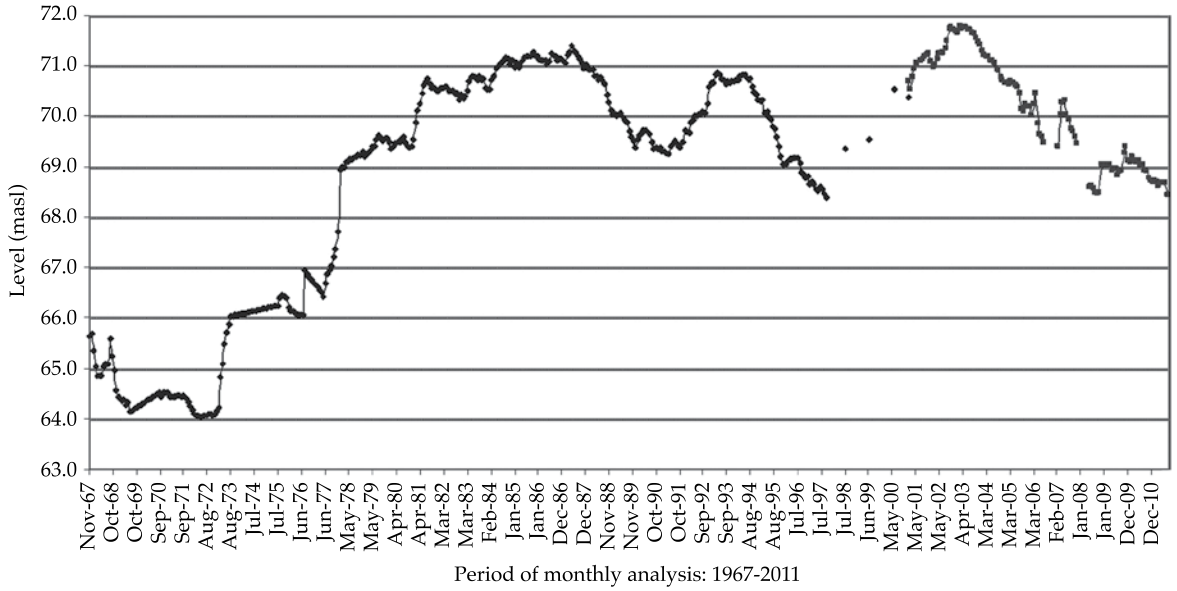

Figure 6. Monthly measured mean levels in the Mar Chiquita Lagoon (LH-UNC, 2011).

1959-1961, some increases in pulses of short durations over 67 masl are notable. Beginning in 1972, the level in the lagoon started to rise, and until the present has remained at levels over the reference value for the period of historical data without measured records.

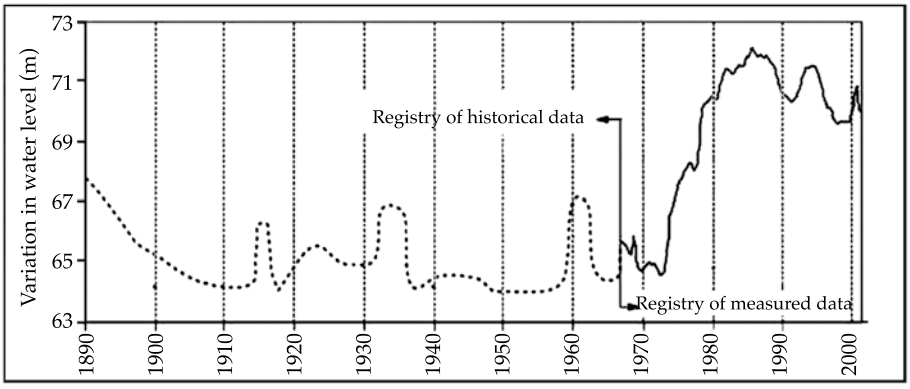

Figure 7. Variation in levels in the Mar Chiquita Lagoon between 1890 and 2000. Troin *et al.*, 2010.

The set of monthly mean data analyzed shows variations in height between 64.05 m and 71.76 masl. During the year 1973, the lagoon's level increased 2 m, from a height of 64.23 to 66.05 masl between February and October of that year. The level rose again in early 1981, exceeding 70.24 masl and in June of 1987 the lagoon reached 71.40 masl; that is, an approximate increase of 7.5 m was observed in the level over 20 years of records.

In particular, water level data were analyzed from measurements taken in 2003, the year with the most records for the available daily and monthly data series.

During that year, maximum daily values of 72.15 masl were measured. The analysis of these data with respect to the days before and after indicate variations in the water level between 0.15 and 0.35 m, respectively.

One explanation for this phenomenon is that large-scale horizontal movement of water mass in response to the wind can cause changes in water level. Von Grumbkow (1890) calculated the range of variation between +0.24 and -0.36 m high. In particular, Pozzi (2006) performed a two-dimensional modeling of this water body with northerly wind scenarios of 7 km/h, obtaining a 2 cm water level over-height on the southern coast, and an 18 cm over-height with winds of 18 km/h.

Given evidence that these over-heights are caused by the effect of wind, the compass rose was constructed for the month of May 2003 (Figure 8). The values used were corrected for height based on the records from the weather station installed at the Mar Chiquita Lagoon Reserve in Miramar, 10 m from the surface of the lagoon.

The results show that 10% of the winds are from the north-northeast, with a maximum value under 20 km/h, and 10% of the total are from the south-southeast, where winds up to 26 km/h were registered for the month of May. It is notable that during May 7 and 8 data was registered every 15 minutes, with an average wind speed of 20 km/h. Finally, is it concluded that the maximum levels registered (72.15 masl) were directly influenced by the prevailing winds on the days prior to the measurement.

Under these conditions, maximum historical level (MHL) on the Miramar coast can be considered to be equal to 71.9 masl. This value corresponds to the average of the levels measured during the first half of the year 2003

The adoption of this value is justified since the methodology used consists of applying, at a baseline level, the effect of wind associated with each return period analyzed, thereby avoiding the duplication this effect in the analysis developed by the present work.

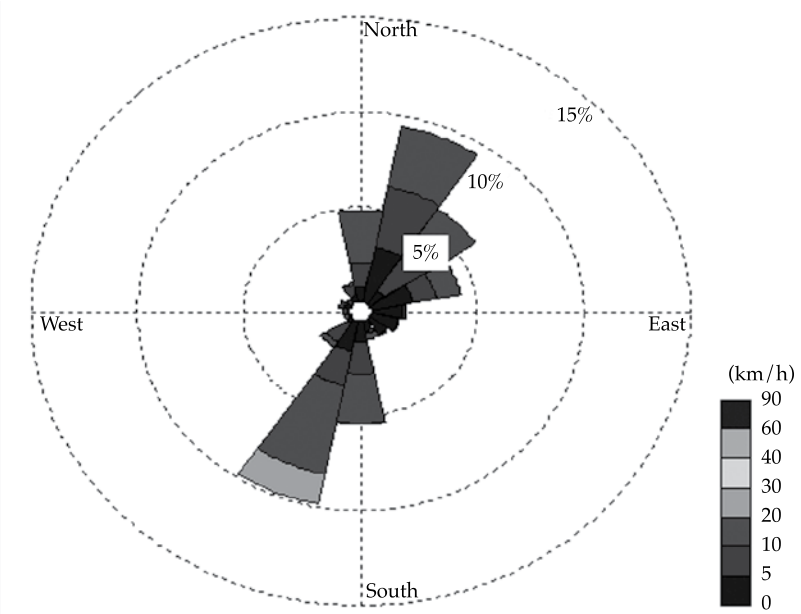

Figure 8. Wind compass rose for May 2003 in Miramar, southern coast of Mar Chiquita.

Analysis of Wind based on an Extreme Regime

The analysis of extreme regimes provides a theoretical distribution of the probability of the occurrence of winds based on data from many years. In this work, the extremes were analyzed using the total set of data available from the series from the Ceres airport (CRR), located northeast of the Mar Chiquita Lagoon.

In this work, two of the models most widely used in the analysis of extreme wind regimes were compared —Gumbel, equation (7) and Weibull, equation (8).

$$F(x) = \exp\left[-\exp\left(-\frac{x-\lambda}{\delta}\right)\right] \quad -\infty < x < \infty \qquad (7)$$

$$F(x) = 1 - \exp\left[\left(-\frac{x-\lambda}{\delta}\right)^{\beta}\right] \quad -\infty < x < \infty \qquad (8)$$

Where λ is the location parameter, δ is the scale parameters; β is the shape parameter.

The values found for the correlation coefficients (R^2) were 0.9741 for the Gumbel distribution and 0.9757 for the Weibull. The series analyzed were filtered and values over 70 km/h with a duration under 1 hour were eliminated since that is not enough time to produce a significant wave for the study presented herein. The cutoff limit was verified until obtaining the best feasible correlation coefficient.

Based on these data, the number of events per year (Γ) on which the analysis is based was calculated. The exceedance probability of an event for an assigned return period (T_R) results in equation (9):

$$Q = \frac{1}{\Gamma T_R} \qquad (9)$$

with which:

$$F = 1 - \frac{1}{\Gamma T_R} \qquad (10)$$

Therefore, for the two distributions used, the wind associated with a determined return period is given by the following formulas (Kamphuis, 2000):

Gumbel: $$W_{T_R} = \lambda - \delta \ln\left(\ln\frac{1}{F}\right) \quad (11)$$

Weibull: $$W_{T_R} = \lambda + \delta \ln\left(\ln\frac{1}{Q}\right)^{1/\beta} \quad (12)$$

The extreme wind values for return periods of 25, 50 and 100 years are shown in Table 1.

The results presented above were take from speed values from the Ceres (CRR) analysis. To be conservative, the highest wind values associated with each return period were chosen.

The design values selected from Table 1 correspond to those obtained with the Gumbel distribution. These value were applied to the most frequent directions —north (N), northeast (NE) and south (S), which also represent the most unfavorable directions for rising water levels on the southern, southwestern and western coasts of the lagoon.

Topo-bathymetric Information Pertaining to the Mar Chiquita Lagoon

To propagate the wave over the slope of the beach in each section of the coast analyzed, tele-detection techniques were used which enabled producing a precise cartography of the topo-bathymetry of the Mar Chiquita Lagoon, given the lack of measurements of this datum.

This process is based on available elevation data from the Shuttle Radar Topography Mission (SRTM) (USGS, 2004), thematic maps from LandSat satellite images and water level measurements in the lagoon.

The thematic maps were constructed for this study based on the identification of the water contour during the analysis period, which was possible to temporally replicate based on the marked decrease in water registered from 2003 to 2011.

Digital extraction of the water contours was performed, associating the areas identified with the corresponding daily water level measurements.

Thus, each digitalized area represents a closed polygon with spatial *X*-*Y* data (referenced in the official system of Argentina, Gauss Kruger Posgar94 and Datum: WGS84), while the corresponding elevation value (*Z*) associated with this polygon is assigned by the daily water level measurement on the date of acquisition of each satellite image analyzed.

The main procedure for the topographic information was performed with the *ENVI* 4.3 (ESRI, 2004) program. With the interpolation of data related to land elevation and depth of the lagoon, conventional geostatistical methods were implemented (inverse distance weighted and Kriging) to generate and represent a new regular grid of depths, according to Figure 9.

Figure 10 shows the data corresponding to the level curves used to generate the digital 3D topo-bathymetric model of the lagoon.

The grid boundaries are associated with the defined area of interest. Thus, a grid with 250 columns and 226 rows was obtained. The resulting topo-bathymetric model is presented in Figure 10.

Generation of the Wave by the Wind

The process to generate the wave is complex mainly because of the action of the wind shear stress on the water surface and the variation in pressures produced when the

Table 1. Wind speeds associated with different return periods in the CRR station for Gumbel and Weibull distributions.

Station	Distribution	Speed (km/h)		
		25 years	50 years	100 years
CRR	Gumbel	102	110	116
	Weibull	102	108	114

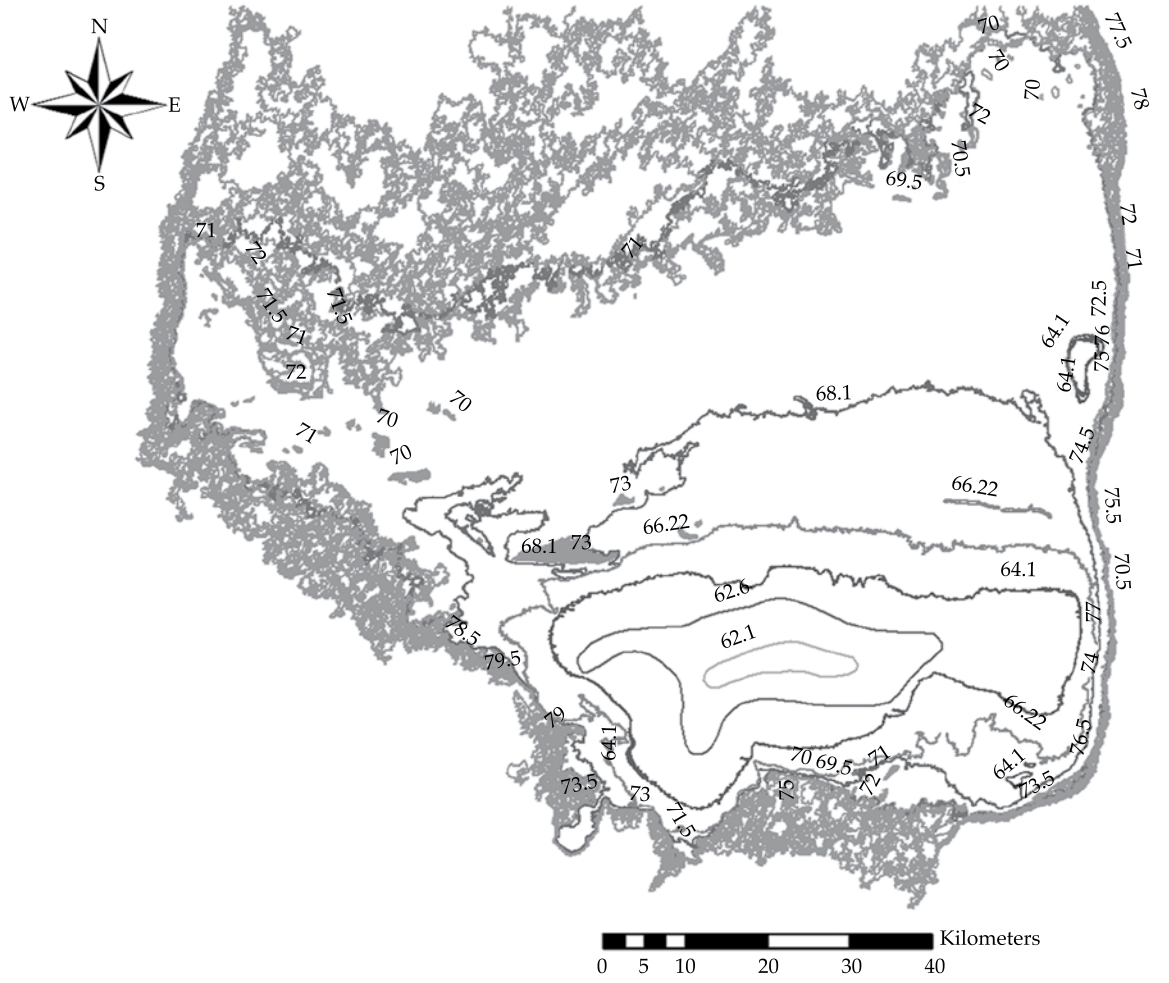

Figure 9. Level curves generated from satellite data.

first waves are formed. In general, the wave height and period are highly related to the wind speed (Kamphuis, 2000). It is thereby possible to calculate the wave conditions and reconstruct the maritime climate based on wind records. This reconstruction is called "wave hindcasting".

This work uses parametric models to determine the height and period of waves based on wind. These methods use parameters such as fetch (distance over which the wind blows over the water to generate the wave); storm duration (duration of the climatological event that generates the wave); water depth (in the zone where the wave is generated); wind intensity and direction (with respect to the fetch and the location of the defined target point).

The formulations herein are the broadest used in engineering practice (SPM, 1984; ACES, 1992). As a hypothesis, the storm was considered to last the amount of time necessary to generate the maximum wave possible for a given fetch.

As a verification test, wave generation simulations were performed with the SWAN model (2000). Constant and uniform winds were imposed as contour conditions throughout the surface of the lagoon (corresponding to each direction considered). Figure 11 presents the results with winds for a 100-year return period,

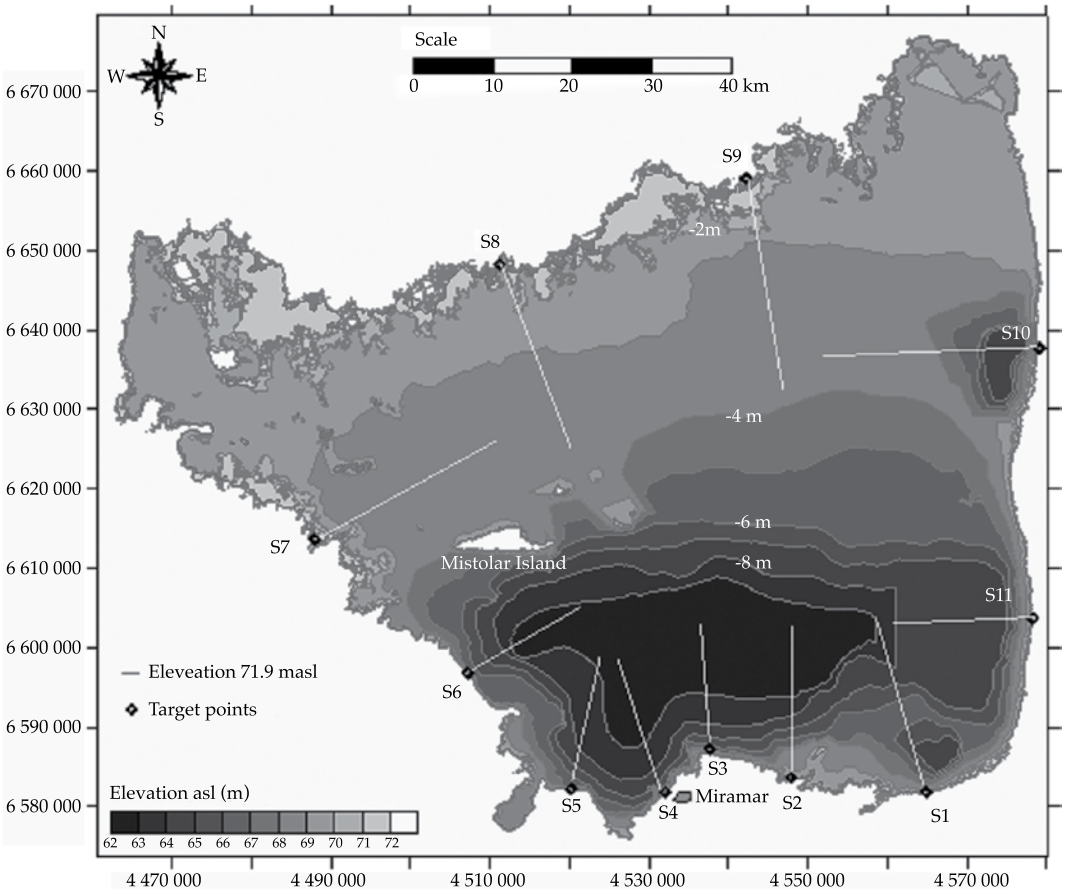

Figure 10. Digital topo-bathymetric model generated for Mar Chiquita lagoon. Target points and calculation sections.

considering a northerly wind direction. The arrows indicate the direction of the propagation of the wave generated. Good concordance is observed between the results of the SWAN model (2000) and the results obtained with empirical formulas.

The value of the over-height of waves due to wind was equivalent to the value exceeding 2% of the time (*Ru2%*), following the recommendations by the Spanish Maritime Works (ROM 02.90, 1990) for pre-design calculations.

The maximum flood height (MFH) was defined as the sum of the maximum historical level (MHL) registered and the maximum storm level (MSL), where the latter parameter was determined by the sum of the rise in level due to wind drag over the surface of the lagoon (WSU, "Wind Set- Up") and the rise due to all the effects from irregular breaking waves propagating towards the coast (RU, "Run-Up"). In particular, the latter effects were evaluated with the return periods considered. The results obtained are summarized in Table 2.

Conclusions

In this work, the maximum flood height was defined for the southern coast of the Mar Chiquita Lagoon for return periods of 25, 50 and 100 years. Measured water levels were analyzed along with the characterization and definition of over-height due to both the action of the wind and the associated wave.

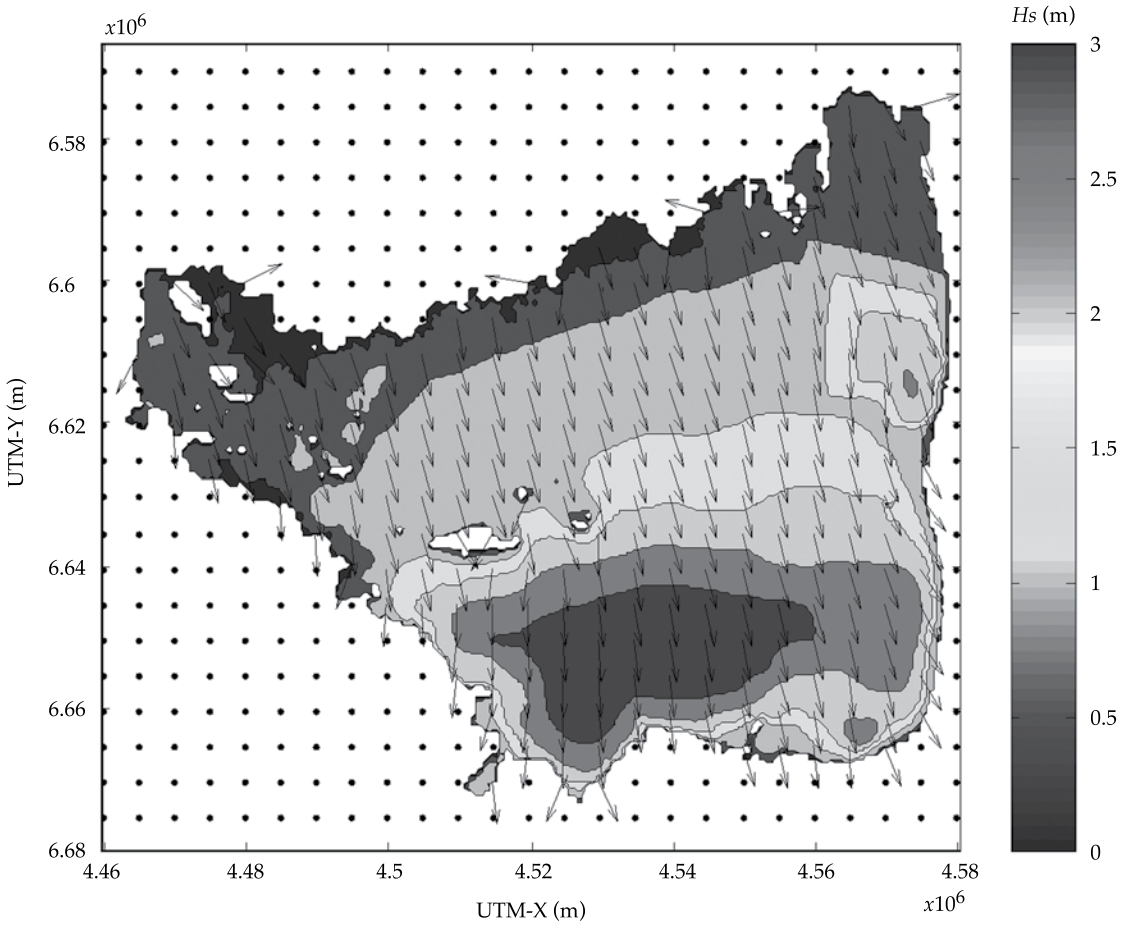

Figure 11. Generation of waves with SWAN model from northerly winds for 100 year return period.

Table 2. Maximum flood height for each target point.

Sections (Figure 10)	Maximum flood height (masl)		
	Tr (años)		
	100	**50**	**25**
S1	73.03	72.96	72.86
S2	73.07	73.00	72.91
S3	**73.51**	**73.44**	**73.30**
S4	73.48	73.41	73.27
S5	73.04	72.99	72.89

The over-height values due to wind and waves were calculated using topo-bathymetric data, defined according to tele-detection techniques. This procedure was used because of insufficient direct measurements of the morphology of this large water body. The procedure used provided an alternative to associating each digitalized level curve with

the water contour identified and the water level measured on the date of acquisition of each satellite image used.

The results show that the maximum flood heights defined for a 100-year return period correspond to target points S3 and S4, with a maximum value of 73.51 masl.

This work combined technical criteria from traditional engineering techniques involving coasts, making it possible to replicate the methodology for other water bodies, primarily those presenting complex and extensive morphologies, such as the one presented herein.

Acknowledgements

The authors wish to thank the Ministerio de Ciencia y Tecnología of the province of Cordoba which for their support of the work herein. To the Cordoba Environmental Agency (in particular, the Provincial Miramar Reserve), the Vice-Ministry of Water Resources and Coordination of the Province of Cordoba, and park ranger Pablo Michelutti, of the Miramar Reserve, for providing information.

Received: 07/06/13
Accepted: 16/11/13

References

ACES (1992). *Automated Coastal Engineering System, v 1.07*. Vicksburg, USA: US Army Corps of Engineers, Coastal and Hydraulics Laboratory-Engineer.

Research and Development Center. Waterways Experiment Station

Agencia Córdoba Ambiente S.E. (2004). *Suelos de la Provincia de Córdoba* (300 pp.). Córdoba, Argentina: Gobierno de la Provincia de Córdoba.

Cereceda-Botella, A. (2009). *Propuesta de volúmenes ambientales para el sistema Laguna Mar Chiquita*. Trabajo final de grado. Córdoba, Argentina: Facultad de Ciencias Exactas, Físicas y Naturales, Universidad Nacional de Córdoba.

Environmental System Research (ESRI) (2004). *Manual de Usuario del Programa ENVI 4.3* (pp. 750). Boulder, USA: ITT Industries, Inc.

Hillman, G. (1999). *Simulación Hidrológica del Sistema de Mar Chiquita* (pp. 490). Trabajo final de Grado. Córdoba, Argentina: Facultad de Ciencias Exactas, Físicas y Naturales de la Universidad Nacional de Córdoba.

Hillman, G. (2003). *Análisis y Simulación Hidrológica del Sistema de Mar Chiquita*. Tesis de Maestría en Ciencias de la Ingeniería, Mención Recursos Hídricos. Córdoba, Argentina: Facultad de Ciencias Exactas, Físicas y Naturales de la Universidad Nacional de Córdoba.

Hillman, G., Rodriguez, A., Pagot, M., Caamaño-Nelli, G., Pozzi, C., & Plencovich, G. (2003). Análisis de volúmenes ecológicos para la laguna de Mar Chiquita. *Cuadernos del CURIHAM* (Universidad Nacional de Rosario, Argentina), *8*(2), 185-195.

Holman, R. A. (1986). Extreme Value Statistics for Wave Run-Up on a Natural Beach. *Coastal Engineering*, *9*, 527-544.

Kamphuis, J. W. (2000). *Introduction to Coastal Engineering and Management* (pp. 437). Lyon: World Scientific Press.

Laboratorio de Hidráulica-Universidad Nacional de Córdoba (2011). *Estimación de la cota máxima de inundación para la laguna mar chiquita. Informe Final Ministerio de Ciencia y Tecnología de la Provincia de Córdoba* (94 pp.). Córdoba, Argentina: Laboratorio de Hidráulica-Universidad Nacional de Córdoba.

Mase, H. (1989). Random Wave Run-up Height on Gentle Slope. *Journal of Waterway, Port, Coastal, and Ocean Engineering*, *115*(5), 649-661.

Mase, H., & Iwagaki, Y. (1984). Run-up of Random Waves on Gentle Slopes. *Proceedings of the 19th International Conference on Coastal Engineering* (pp. 593-609), American Society Civil Engineers, Houston.

Pagot, M. (1999). *Análisis y simulación hidrológica del Sistema Bañados del río Dulce*. Trabajo Final de Grado. Córdoba, Argentina: Facultad de Ciencias Exactas, Físicas y Naturales de la Universidad Nacional de Córdoba.

Pagot, M. (2003). *Análisis y simulación hidrológica del Sistema Bañados del río Dulce*. Tesis de Maestría en Ciencias de la Ingeniería, Mención Recursos Hídricos. Córdoba, Argentina: Facultad de Ciencias Exactas, Físicas y Naturales de la Universidad Nacional de Córdoba.

Pagot, M., Hillman, G., Rodriguez, A., Caamaño-Nelli, G., & Plencovich, G. (2003) Determinación de hidrogramas ecológicos para la cuenca inferior del río Dulce con apoyo satelital. *Cuadernos del CURIHAM* (Universidad Nacional de Rosario, Argentina), *8*(2), 146-154.

Plencovich, G., Hillman, G., Pagot, M., Pozzi, C., Rodriguez, A., Caamaño-Nelli, G., & Bertoni, J.C. (mayo, 2005). *Actualización del modelado del sistema Laguna Mar Chiquita – Bañados del río Dulce, Córdoba, Argentina*. XX Congreso Nacional del Agua 2005 y III Simposio de Recursos Hídricos del Cono Sur, Mendoza, Argentina.

Plencovich, G. (2011). *Simulación hidrológica de los humedales de Mar Chiquita con apoyo satelital*. Tesis de Maestría en Ciencias de la Ingeniería, Mención Recursos Hídricos. Córdoba, Argentina: Universidad Nacional de Córdoba, Facultad de Ciencias Exactas, Físicas y Naturales.

Pozzi, C., Plencovich, G., Hillman, G., Rodriguez, A., Caamaño-Nelli, G., Michelutti, P., Salio, P., & Pagot, M.

(mayo, 2005). *Monitoreo hidroambiental de la laguna Mar Chiquita, Córdoba. Aplicación al diseño de las defensas costeras de Miramar*. XX Congreso Nacional del Agua 2005 y III Simposio de Recursos Hídricos del Cono Sur, Mendoza, Argentina.

Pozzi, C. (2006). *Simulación hidrodinámica y monitoreo del sistema Mar Chiquita (Mar de Ansenuza), Córdoba, Argentina*. Tesis de Maestría en Ciencias de la Ingeniería, Mención Recursos Hídricos. Córdoba, Argentina: Facultad de Ciencias Exactas, Físicas y Naturales de la Universidad Nacional de Córdoba.

Rodriguez, A., Hillman, G., Pagot, M., Menajovsky, S., Barbiero, S., Caamaño-Nelli, G., Chini, I., & Bernasconi, I. (2000a). *Simulación Hidrológica del Sistema de Mar Chiquita, Córdoba, República Argentina*. XVIII Congreso Nacional del Agua, CPCA, Santiago del Estero, Argentina.

Rodriguez, A., Pagot, M., Hillman, G., Caamaño-Nelli. G., Bernasconi, I., Menajovsky, S., Barbiero, S., & Chini, I. (2000b). *Simulación Hidrológica del Sistema Bañados del Río Dulce, Córdoba, República Argentina*. XVIII Congreso Nacional del Agua, CPCA, Santiago del Estero, Argentina.

Rodriguez, A., Hillman, G., Pagot, M., & Caamaño-Nelli, G. (2002). Análisis y simulación de riesgos ecológicos en un sistema hidrológico endorreico. *Revista Internacional de Desastres Naturales, Accidentes e Infraestructura Civil, Puerto Rico*, 2(1), 15.

ROM 02.90 (1990). *Recomendaciones de obras marítimas. Acciones para proyectos de obra portuaria o marítima*. Madrid: Dirección General de Puerto y Costas, Ministerios de Obras Públicas y Urbanismos.

SPM (1984). *Shore Protection Manual*. Fort Belvoir, USA: Coastal Engineering Research Center.

SWAN (2000). *Simulating Wave Near Shore Model*. Delft, The Netherlands: Delft University of Technology.

TIC (2003). *Software tutor de ingeniería de costas. Sistema de modelado costero*. Cantabria: Instituto de Hidráulica Ambiental de la Universidad de Cantabria.

Troin, M., Vallet-Coulomb, C., Sylvestre, F., & Piovano, E. (2010). Hydrological Modelling of a Closed Lake (Laguna Mar Chiquita, Argentina). *Journal of Hydrology*, *393*, 233-244.

Universidad Nacional de Córdoba (1998). *Valoración del Impacto Ambiental en la Región de Mar Chiquita y la cuenca afectada por el Canal Federal. Informe Final al Consejo Federal de Inversiones*. Córdoba, Argentina: Universidad Nacional de Córdoba.

Universidad Nacional de Córdoba-Universidad Nacional de Santiago del Estero (UNC-UNSE) (2007). *Estudio hidrológico-ambiental del sistema Mar Chiquita-Bañados y tramo inferior del río Dulce. Informe Final a la Subsecretaría de Recursos Hídricos de la Nación* (312 pp.). Córdoba, Argentina: Universidad Nacional de Córdoba-Universidad Nacional de Santiago del Estero.

U.S. Geological Survey (USGS) (February, 2004). *Shuttle Radar Topography Mission. U.S. Geological Survey. Global Land Cover Facility*. College Park, USA: University of Maryland.

Von Grumbkow, J. B. (1890). Exploración de Mar Chiquita. *Boletín del Instituto Geográfico Argentino*, 2(1), 113-115.

Institutional Address of the Authors

M.I. Mariana Pagot
M.I. Gerardo Hillman
M.I. Cecilia Pozzi Piacenza
M.I. Paolo Gyssels
M.I. Antoine Patalano
Dr. Andrés Rodriguez

Laboratorio de Hidráulica
Facultad de Ciencias Exactas, Físicas y Naturales
Universidad Nacional de Córdoba
Av. Filloy s/n
Córdoba, Argentina
Teléfono: +35 (1) 4334 446
mpagot@efn.uncor.edu

Click here to write the autor

Technical Note

Hybrid Maritime Climate Reconstruction and its Application to the Study of Sediment Transport in the Mexican Pacific Coast

• José Cristóbal Medina-González •
Grupo TYPSA, España

• Gabriel Díaz-Hernández* •
Instituto de Hidráulica Ambiental de Cantabria, España
*Corresponding Author

Abstract

Medina-González, J. C., & Díaz-Hernández, G. (July-August, 2014). Hybrid Maritime Climate Reconstruction and its Application to the Study of Sediment Transport in the Mexican Pacific Coast. *Water Technology and Sciences* (in Spanish), *5*(4), 129-138.

This study analyzes the historical maritime climate on the coast of Manzanillo (Colima, Mexico), in order to reconstruct 62-year hourly wave statistics for the coastal zone. The analysis was performed by integrating different numerical tools, instrumental measurements and statistical techniques to jointly analyze the processes associated with the propagation of waves from deep waters to the coast. This information is likely to be used to drive future detailed coastal and harbour studies. The innovative contribution of this methodology includes the integration of different numerical wave propagation models and the use of algorithms to validate wave data obtained with instruments, as well as the establishment of a hybrid technique that enables performing an historical wave reconstruction with 62 years of duration in the study zone and with efficient and competitive CPU times. The proposed methodology can be easily adopted as a tool that can be commonly used for technical coastal and port engineering consulting. As an example of the use of the wave series offered by this study, a preliminary study of the short- (days to weeks) and long-term (months, seasons, years and decades) evolution of coastal dynamics is presented for the Tepalcates channel in Manzanillo, before and after its expansion.

Keywords: Auto-classification, calibration, maritime climate, numerical modelling, wave propagation.

Resumen

Medina-González, J. C., & Díaz-Hernández, G. (julio-agosto, 2014). Reconstrucción híbrida del clima marítimo y su aplicación al estudio del transporte de sedimentos en la costa del Pacífico mexicano. Tecnología y Ciencias del Agua, *5(4), 129-138.*

El presente estudio se encarga de analizar el clima marítimo histórico en la playa de Campos en la región de Manzanillo (Colima, México), con el objetivo de trasladar la estadística histórica de 62 años de oleaje horario a la zona costera. El análisis se ha realizado mediante la integración de diferentes herramientas numéricas, medidas instrumentales y técnicas estadísticas que en conjunto analizan los procesos relacionados con la propagación del oleaje que se suceden desde las aguas profundas hasta la costa. Esta información es susceptible de ser empleada como forzamiento de estudios costeros y portuarios de detalle. La aportación innovadora de la presente metodología es la integración de distintos modelos de propagación numérica de oleaje, el uso de algoritmos de validación de los datos de oleaje obtenidos con datos instrumentales, y el establecimiento de una técnica de hibridación que permite llevar a cabo una reconstrucción histórica del oleaje horario con 62 años de duración en la zona de estudio, con tiempos computacionales eficientes y competitivos. La metodología propuesta fácilmente puede ser adoptada como una herramienta metodológica de uso habitual en consultorías técnicas de ingeniería costera y portuaria. Como ejemplo de la explotación de las series de oleaje que esta metodología ofrece, se realiza el estudio preliminar de la evolución de la dinámica litoral en el corto (días a semanas) y largo plazos (meses, estaciones, años y décadas), en la zona del canal Tepalcates, en Manzanillo, antes y después de su ampliación.

Palabras clave: *clima marítimo, propagación de oleaje, calibración, modelación numérica, auto-clasificación.*

Introduction

Coastal zones are highly valuable because of their diversity and uniqueness. Lately, the use of the Mexican coast for industrial, communications and tourism purposes has increased significantly, requiring the construction of coastal protection works to protect designated zones from the environmental agents (primarily waves) affecting them. The present study proposes a comprehensive and innovative methodology for the propagation of waves from deep waters to the coast, as information for functional design analyses and the analysis of coastal protection structures. It is directly applied to the diagnostics of the construction of the new liquid natural gas terminal (LNGT) in the Cuyutlan Lagoon, located in Manzanillo, Colima, Mexico.

This study is based on different mathematical tools which, with different hybridization, propagation and reconstruction techniques, are able to obtain long historical series of waves. This presumes high-quality forcing that can be used by semi-empirical and numerical models to study different action scenarios and alternatives for improving or modifying any study of the effect of coastal works. This work exemplifies this fact, addressing the need and importance of identifying changes on coastlines that can be produced by human actions involving the natural environmental.

Objectives

The main objective of the present study is to establish the use of a new integral methodology for the hybrid reconstruction of coastal waves from deep waters taking into account the main processes involved —transformation, local wind effects and dissipation.

This methodology is considered to be efficient. It is based on algorithms for the self-selection of representative sea states that reduce simulation computing time. It is also uses statistical techniques to reconstruct series of environmental variables that enable obtaining a middle wave regime that adequately represents reality.

The study also exemplifies the use of wave series obtained with the methodology proposed by Camus, Méndez, Medina, & Cofiño (2011a) (called technical hybrid) to understand the functioning of coastal dynamics on the Manzanillo coast, and associated coastal processes.

Proposed Hybridization Methodology

In order to quantify the possible impacts on the hydrodynamics of the coastal zone, the present study proposes the use of different statistical and numerical modeling tools and the interpretation of instrumental data to identify current and future functioning of the coast by understanding wave processes in deep water, their propagation towards the coast and interaction with it, and relationships with different coastal elements (for example, sedimentary trends at different time scales), considering different states or alternative analyses.

Specifically, the proposed methodology presents the steps shown in the diagram in Figure 1. It involves the use, treatment and adaptation of bathymetric data from the study zone, as well as the use of a database of waves in deep water with enough records to statistically characterize the maritime climate. In this case, the *GOW* database was chosen (Reguero, Menéndez, Méndez, Mínguez, & Losada, 2012), provided by the IH Cantabria, which contains 62 years of hourly data of waves, from 1948 to 2010. The hybridization technique follows the guidelines proposed by Camus *et al*. (2011a) and Camus, Méndez, & Medina (2011b) for self-selection, propagation and reconstruction of sea states, thereby meeting two key objectives: a) obtain statistics for the maritime climate in deep waters in the study zone and b) minimize the number of sea states to be numerically propagated from deep water to the coast, considering that it is not currently feasible or computationally efficient to execute an hourly 62-year wave series. This algorithm

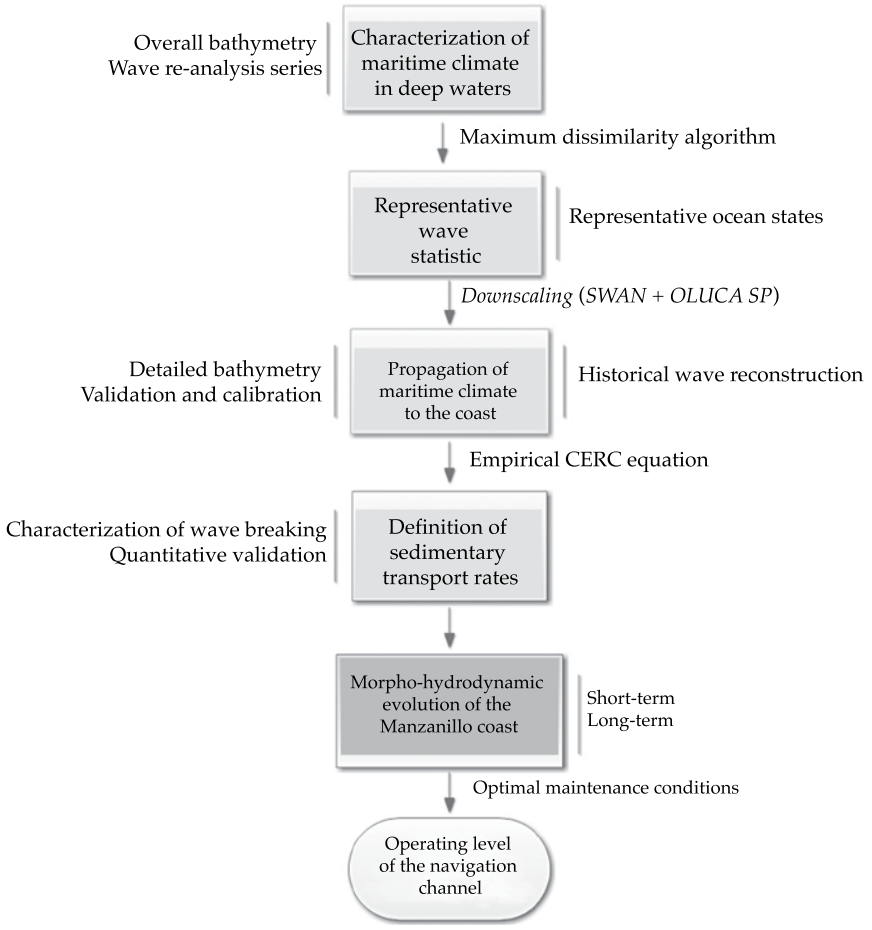

Figure 1. Flow diagram of the methodology of this work.

corresponds to the maximum dissimilarity technique (Max-Diss), which enables identifying the sea states that represent the mean behavior and extreme wave conditions at any point, with the abstraction of a reduced number of these "clusters." The present study, which is based on the recommendation by Camus *et al* (2011a), obtained 250 clusters (n = 250), which has served as forcing for the paired numerical models —the *SWAN* wave propagation model (Booij, Ris, & Holthuijsen, 1999) for propagations from deep to intermediate water and the *OLUCA* (González *et al*., 2007) model with an action zone from the intermediate water boundary to the coastline. This methodological process is called hybrid *downscaling*.

After executing the n sea states in the breaking zone, the 62 years of hourly records of waves at different points along the study coast were reconstructed taking into account the n propagation coefficients from the *GOW* database in deep waters and using the algorithm pertaining to the *Radial Basis Functions* (RBF), proposed for this purpose by Camus *et al*. (2011b) and Rippa (1999). After reconstructing the statistics for waves in the breaking zone, this wave series can be used with semi-empirical formulas (first approximation of the problem) and numerical approaches (detailed analysis of processes) to perform any type of detailed analysis related to harbour agitation, wave interaction with

natural and artificial structures, and studies of dynamic sedimentation.

For example, in the present study, if the grain size representative of the study coast and the mean slope of each zone are known, the classical empirical formula for coastal dynamics provided by CERC (USACE, 1984) can be efficiently employed to obtain sediment transport rates and trends along the coast for the hourly 62-year series.

Therefore, it is easy to see that using this methodology, along with concatenated hybrid analysis and individual processes, it is possible to compute and efficiently interpret a) the wave statistics in deep water, b) their propagation towards the coast, c) the reconstruction of the wave statistics, d) sediment transport rates and e) the hydrodynamic functioning governing the coast.

For this technical note, the present methodology was applied in the coastal zone of Manzanillo in order to obtain general data about the sedimentary dynamics at different time scales, before and after the expansion of the Tepalcates canal. It is important to mention that instrumental wave data and topo-bathymetric measurements provided by the GEIC-CFE were used to validate, calibrate and prove the veracity of each one of the steps mentioned above.

Initial Data and Study Zone

In order to apply the methodology proposed in the Manzanillo study zone, the work herein used the *GOW* (Global Ocean Waves) wave database (Reguero *et al.*, 2012) provided by IH Cantabria (Institute of Environmental Hydraulics of Cantabria, Spain) as well as topo-bathymetric data and sedimentary measurements from different field campaigns on different dates. Both were supplied by the GEIC-CFE (Department of Oceanography of the Management of Civil Engineering Studies at the Mexico Federal Electric Commission).

The study area is located in western Mexico on a 12.5 km section of the Manzanillo coast, in the state of Colima. The coastal section studied represents a strategic point and one of general interest for Mexico in terms of port operations. In 2009-2010, a new liquid natural gas regasification and storage terminal (LNGT) was built. As a result, the original width of the Tepalcates canal needed to be increased from 150 to 500 m and the depth to 15 m (dredging 16.5 million m^3 of material). In addition, two new breakwaters measuring 250 m each were built, delimiting the banks of each canal. The GEIC-CFE has been conducting topo-bathymetric follow-up of the coast since the works began, measuring the possible effects on the environment.

Results

DOW Database in Deep Water

To obtain the waves in the deep water zone of the Manzanillo coast, wave data (height of the significant wave, *Hs*, peak time period *Tp* and mean direction, q) from the GOW database corresponding to the point (lat. = 18° N, long. = 105° W) were used. The GOW database was calibrated with instrument information (all the data from the six satellite missions from 1992 to 2012). To this end, directional aggregation of quantiles was used (Mínguez, Espejo, Tomás, Méndez, & Losada, 2011), which is a non-linear calibration technique. It is important to mention that the GOW database does not contain extreme wave data generated by tropical cyclone events, as was mentioned by Ruiz-Martínez, Silva-Casarín, Pérez-Romero, Posada-Vanegas and Bautista-Godínez (2009b). This is because the *WRF-ARW 3.1.1* wind database has a medium resolution, with wind data every 0.5°. Figure 2 shows the summary of GOW data at the point in deep water.

Self-Selection of Representative Sea States

Before beginning the downscaling and simulation of the wave transformation processes involved in their propagation toward the coast the hybrid methodology was applied,

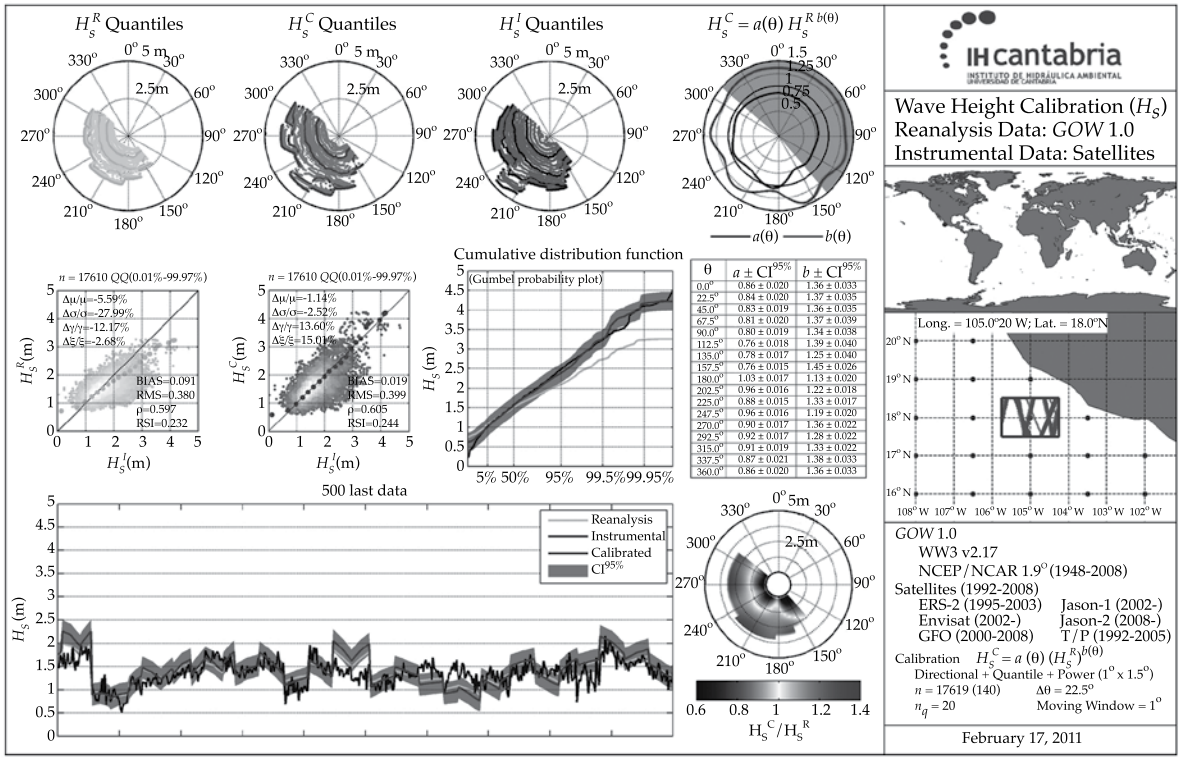

Figure 2. *GOW* series at point lat. = 18º N, long. = 150º W validated with satelite data. Source: IH Cantabria.

which combines numerical propagation models (dynamic downscaling) and mathematical classification and reconstruction methods (statistical downscaling). To this end, the maritime climate of each zone was classified according to the spatial-temporal fields of waves and wind for each zone, selecting $n = 250$ sea states at undefined depths, representative of the entire 62 years (over 534 000 sea states). The classification technique used was the maximum dissimilarity algorithm (Kennard & Stone, 1969).

Numerical Wave Propagation from Deep Water to the Coast

Using successive nested grids, the $n = 250$ sea states (already calibrated) selected from the GOW were spectrally propagated, resulting in spatial resolutions between 350 and 70 m. SWAN propagation was used with GEBCO global bathymetry (British Oceanographic Data Centre) as well as detailed bathymetric data provided by the GEIC-CFE. The adequate resolution for the general grid (5 400 m) is 0.05° and 0.003125º for the detailed grid (340 m). Two sea levels were taken into account —low tide and high tide. The results obtained for the n = 250 sea states executed provide maps of *Hs*, *Tp* and q that show the behavior of the wave as it propagates towards the coast. They also contain spectral information at different control locations at several points in the numerical domain.

Reconstruction of the Wave Series and Obtainment of Transport Rates

Based on the spectral information provided by the SWAN numerical model, the 62-

year historical reconstruction of waves was obtained at two control points —point 1 (lat. = 18.947° N, long. = 104.360° W) and point 2 (lat. = 18.967° N, long. = 104.316° W), where point 1 corresponds to the coupling point between forcings in the SWAN and OLUCA SP models and point 2 to the location of the wave data instruments provided by the GEIC-CFE.

Using interpolation (RBF), each of the spectral parameters propagated at both target points was reconstructed. This makes it possible to numerically transfer the multi-dimensional maritime climate from deep waters for the 62-year historical series.

Validation and Calibration of the Wave Statistics in Shallow Water

For the validation work, this study used the instrument information for waves provided by the GEIC-CFE, taken from a Nortek doppler model AWAC, at a depth of 15 m, between the year 2009 and 2010. This information was post-processed to obtain spectral wave statistics similar to the GOW series.

After propagating the wave to the study zone and its reconstruction at control point 1, a comparison was performed with the GOW series propagated using the hybrid approach (see Figure 3). The numerical predictions are observed to be adequately reproduced, following the maximum and minimum *Hs* trends over the time period. The numerical series also systematically overestimates this value. There are three possible explanation for this. One may be the resolution of the numerical grid, which does not adequately define the bathymetric details near the coast. It may also be a lack of waves generated by the local wind (not included in the simulation) or because of a variation in the sea level reference heights with respect to the heights from the bathymetry used.

Therefore, it is absolutely necessary to establish a calibration protocol for this numerical series, reconstructed at the control points. This is achieved with the directional treatment of quantiles proposed by Tomás, Méndez and Losada (2008) and Mínguez *et al*. (2011), which establishes that the calibration factors obtained follow a dependency based on the mean direction of the wave propagation and comply with a linear regression between source and target data. Once the *linear polynomial fitting* between both series of data is performed, the newly analyzed information is improved by applying the directional calibration proposed. With the regression analysis, the similitude between the two sources of data can be quantified by analyzing the central trends of the data as well as the dispersion (see Figure 4a).

Figure 4b shows the *Q*-*Q* plot which enables verifying whether the different parts of the middle regime of the two variables are similar, observing in this case that the medium-high branch of data in the wave regime was adequately corrected after calibration of the series reconstructed at the target point. Again, it is important to mention that the series reconstructed at the control point does not include information about cyclonic forces and therefore the methodology underestimates the waves in the extreme branch, as suggested by Ruíz- Martínez *et al*. (2009a and 2009b). Thus, a calibrated reconstruction of the complete 62-year wave series from deep water is obtained, which is very important in order to ensure the successful transfer of the wave to the coast. These differences were seen to decrease after applying the directional calibration to the reconstructed series, arriving at a trend very similar to that from the instrument information (see Figure 5).

Analysis of the Sedimentary Dynamics of the Manzanillo Coast Before and After the Works

The OLUCA model was used to analyze the sedimentary dynamics of the section of coast studied in Manzanillo. This analysis was performed considering both topo-bathymetric

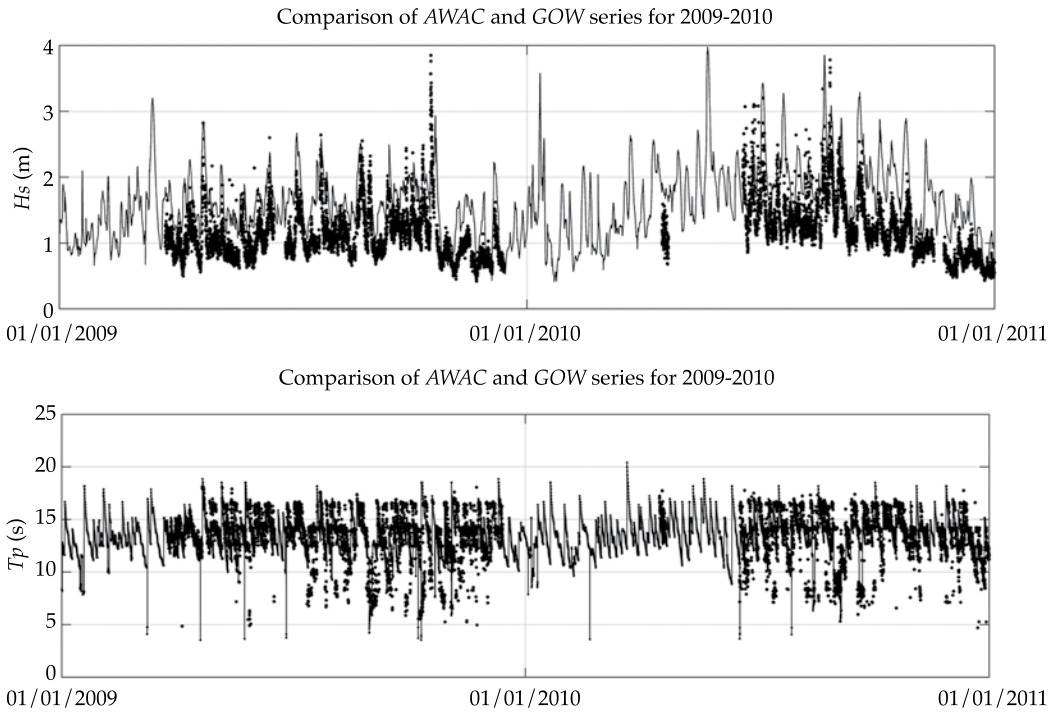

Figure 3. Validation of the *Hs* and *Tp* parameters between numerical GOW series, propagated and reconstructed at point 1 (black line) and the *AWAC* instrument series (black dots).

configurations, before and after expanding the Tepalcates canal. The wave in the breaking zone was reconstructed for the period 1948-2010 for the unmodified configuration, and the semi-empirical formula proposed by CERC (USACE, 1984) was applied, thereby obtaining annual sediment transport rates and trends along the coast. The hydrodynamic functioning governing the Manzanillo coast was identified at different time scales based on a characteristic grain size of D_{50} = 0.3 mm (GEIC-CFE). The historical coastal transport obtained was analyzed for different periods (annual, seasonal and monthly). Similar trends among them are observed, generally associated with sediment transport of 60 500 m³/year in a WNW-ESE direction along both beaches west of the canal and 52 000 m³/year east of the canal. It is interesting to observe how the mean transport on the beach east of the Tepalcates canal is 8% less than that calculated for the beach west of the canal. This may be due to the defensive action of the breakwater on the incidence of storms from the west in the first section of the eastern beach. Lastly, in order to adequately understand the behavior of the coastal dynamics obtained herein, the results were quantitatively validated by comparing different coastlines for the dates 1/12/2009 to 1/12/2010. The accumulated volume over the breakwater on the western beach was approximately 38 500 m³. No relevant differences were observed on the eastern beach, with an accumulated volume of 7 245 m³.

Conclusions

By coupling wave propagation models, the methodology proposed demonstrates a novel technique for the historical reconstruction of the maritime climate of the study coast. This methodology has been shown to be an effective and efficient alternative to feed the historical wave forcing for any type of coastal study.

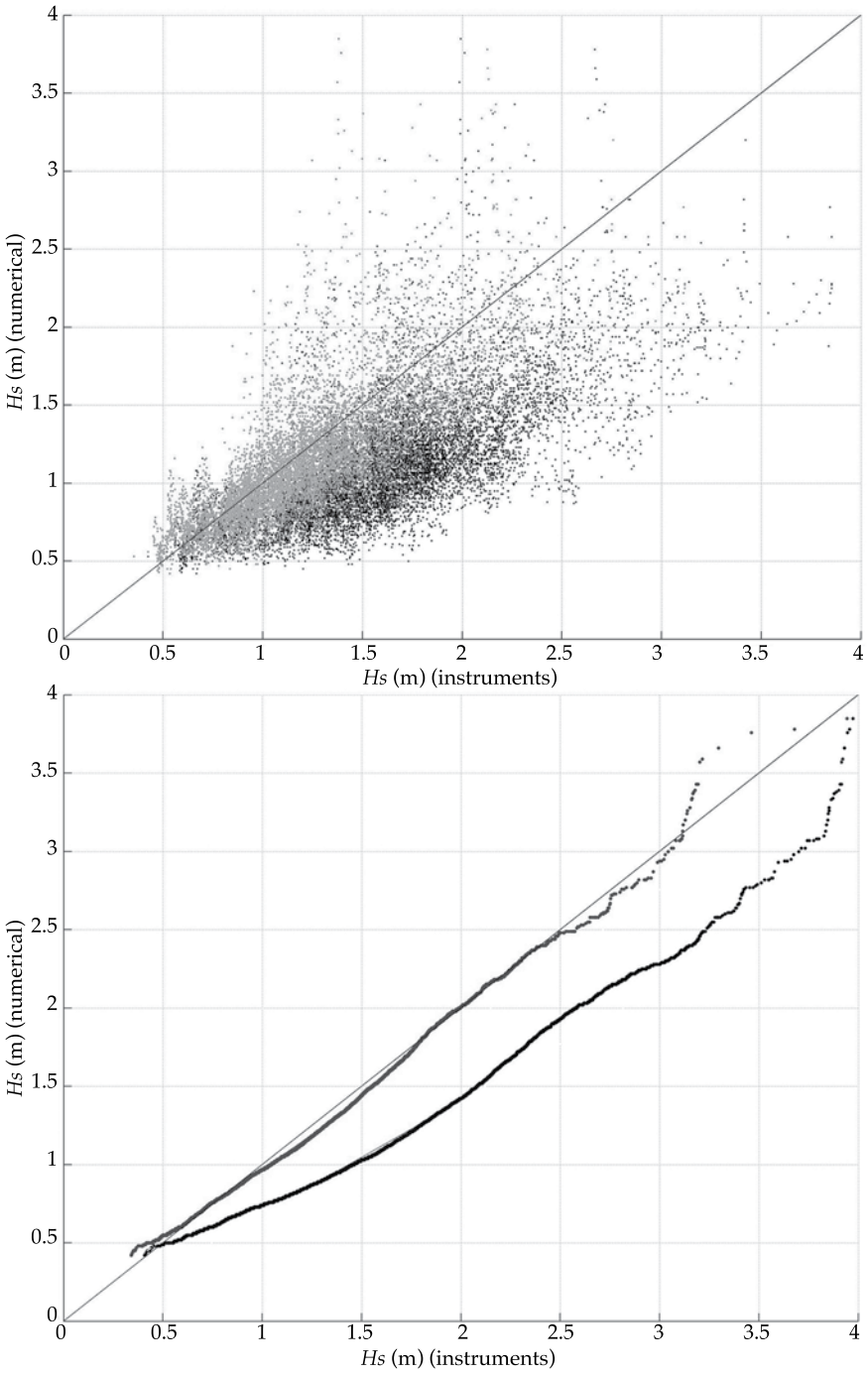

Figure 4. Results from the calibration process: a) spread diagram and b) q-q plot for uncalibrated (black dots) and calibrated (gray dots) data corresponding to the series reconstructed at point 1 for the years 2009 and 2010.

This study exemplified the use of a reconstructed wave series on the coast for a preliminary study of coastal dynamics in Manzanillo, specifically for the analysis of the beach-breakwater-canal system. Satisfactory results were obtained and were consistent

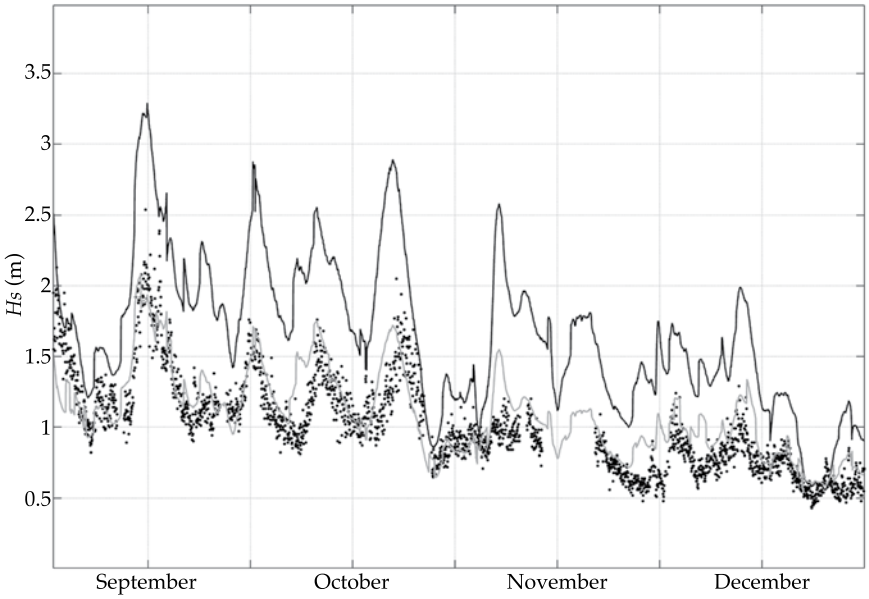

Figure 5. Comparative of the last four months of 2010 between the AWAC instrument series (black dots) and the series reconstructed at point 1 before (black line) and after (gray line) applying the calibration protocol.

with the instrument and topo-bathymetric observations performed by GEIC-CFE. The dominant wave conditions on the Manzanillo coast and the sedimentary dynamic trends in the region were defined.

Acknowledgements

The authors wish to thank the Gerencia de Estudios de Ingeniería Civil of the Federal Electric Commission for their support in performing the analysis of the coast in Manzanillo, Mexico, as well as for the information needed, professional advice and data provided during the development of this work.

Received: 06/03/13
Accepted: 11/12/13

References

Booij, N., Ris, R. C., & Holthuijsen, L. H. (1999). A Third-Generation Wave Model for Coastal Regions, Part I: Model Description and Validation. *Journal of Geophysical Research*, *104*(4), 7649-7666, doi: 10.1029/98JC026222.

Camus, P., Méndez, F. J., Medina, R., & Cofiño, A. S. (2011a). Analysis of Clustering and Selection Algorithms for the Study of Multivariate Wave Climate. *Coastal Engineering*, *58*(6), 453-462, doi:10.1016/j.coastaleng.2011.02.003.

Camus, P., Méndez, F. J., & Medina, R. (2011b). A Hybrid Efficient Method to Downscale Wave Climate to Coastal Areas. *Coastal Engineering*, *58*(9), 851-862. doi:10.1016/j.coastaleng.2011.05.007.

González, M., Medina, R., González-Ondina, J., Osorio, A., Méndez, F. J., & García, E. (July, 2007). An Integrated Coastal Modeling System for Analyzing Beach Processes and Beach Restoration Projects, SMC. *Comput. Geosci.*, *33*(7), 916-931.

Kennard, R. W., & Stone, L. A. (1969). Computer Aided Design Experiments. *Technometrics*, *11*, 137-148.

Mínguez, R., Espejo, A., Tomás, A., Méndez, F. J., & Losada, I. J. (2011). Directional Calibration of Wave Reanalysis Databases Using Instrumental Data. *J. Atmos. Oceanic Technol.*, *28*, 1466-1485.

Rippa, S. (1999). An Algorithm for Selecting a Good Value for the Parameter C in Radial Basis Function Interpolation. *Advances in Computational and Mathematical*, *11*(1999), 193-210.

Reguero, B. G., Menéndez, M., Méndez, F. J., Mínguez, R., & Losada, I. J. (July, 2012). A Global Ocean Wave (GOW) Calibrated Reanalysis from 1948 Onwards. *Coastal Engineering*, *65*, 38-55.

Ruiz-Martínez, G., Mendoza, E., Silva-Casarín, R., Posada-Vanegas, G., Pérez, D., Rivillas, G., Escalante, E., & Ruiz, F. (2009a). Caracterización del régimen de oleaje y viento de 1948-2007 en el litoral mexicano. *Revista Interdisciplinaria de Ciencia y Tecnología del Agua*, *16*(1), 51-64.

Ruiz-Martínez, G., Silva-Casarín, R., Pérez-Romero, D. M., Posada-Vanegas, G., & Bautista-Godínez, E. G. (julio-septiembre, 2009b). Modelo híbrido para la caracterización del oleaje. *Ingeniería hidráulica en México*, *24*(3), 5-22.

Tomás, A., Méndez, F. J., & Losada, I. J. (2008). A Method for Spatial Calibration of Wave Hindcast Data Bases. *Continental Shelf Research*, *28*(3), 391-398.

U.S. Army Corps of Engineers, Coastal Engineering Research Center (USACE) (1984). *Shore Protection Manual* (3rd Ed.). Washington, DC: Department of the Army, Waterways Experiment Station, Corps of Engineers, Coastal Engineering Research Center.

Institutional Address of the Authors

M.I. José Cristóbal Medina González

TYPSA-Sede Social
Gomera, 9
28703, S.S. de los Reyes
Madrid, España
jmedina@typsa.es

Dr. Gabriel Díaz Hernández

Instituto de Hidráulica Ambiental "IH Cantabria"
C/Isabel Torres núm. 15
Parque Científico y Tecnológico de Cantabria
39011 Santander, España
Teléfono: +34 (942) 201 616, extensión 1255
Fax: +34 (942) 201 860
gabriel.diaz@unican.es
www.ihcantabria.es

Click here to write the autor

Technical Note

Use of Satellite Images to Assess the Effects of Land Cover Change on Direct Runoff in the Andean Basin

• César Cano* • Andrea Andreoli • José Luis Arumi • Diego Rivera •
Universidad de Concepción, Chile
*Corresponding Author

Abstract

Cano, C., Andreoli, A., Arumi, J. L., & Rivera, D. (July-August, 2014). Use of Satellite Images to Assess the Effects of Land Cover Change on Direct Runoff in the Andean Basin. *Water Technology and Sciences* (in Spanish), *5*(4), 139-145.

The curve number method by the Natural Resources Conservation Service of the United States was used to study the effect of land cover changes on runoff in the Lirquén River Basin, Chile. The curve number was calculated using two methods: (1) classification of three LandSat images from 1987, 2003 and 2009, in combination with soil texture information and correction for the effect of the slope, and (2) the use of the runoff coefficient from daily rainfall and flow data for the periods 1985-1988, 2001-2004 and 2007-2010. The first method resulted in CN values for 1987, 2003 and 2009 of 51, 46 and 49 respectively, since mature grassland areas changed over the same years from 27.9 to 15 and 17.7%, respectively. Furthermore, the adult plantation area changed over those years from 7.2 to 22.9 and 15.4%, respectively. The results from the second method show higher curve number values during the period 1985-1989 and lower numbers during the period 2001-2004, since the runoff volume generated over this period was smaller than the other two. This is due to an increase in the adult plantation area which provides greater intercept capacity, higher evapotranspiration rates and greater storage of soil moisture.

Keywords: Curve number, LandSat images, land cover change, runoff coefficient.

Resumen

Cano, C., Andreoli, A., Arumi, J. L., & Rivera, D. (julio-agosto, 2014). Uso de imágenes de satélite para evaluar los efectos de cambio de cobertura de suelo en la escorrentía directa de una cuenca andina. Tecnología y Ciencias del Agua, *5(4), 139-145.*

El método de la curva número del Natural Resources Conservation Service de los Estados Unidos fue utilizado para estudiar el efecto del cambio de cobertura de suelo sobre la escorrentía directa en la cuenca del río Lirquén, Chile. Para calcular la curva número (CN) se utilizaron dos métodos: (1) la clasificación de tres imágenes LandSat de 1987, 2003 y 2009, en combinación con información de texturas de suelos y corrección por efectos de la pendiente, y (2) el uso del coeficiente de escorrentía proveniente de datos de caudal y precipitaciones diarias para los periodos 1985-1988, 2001-2004 y 2007-2010. Los resultados del primer método muestran que los valores de CN para los años 1987, 2003 y 2009 son de 51, 46 y 49, respectivamente, ya que existe una variación de superficie de praderas en estos años que va de 27.9 a 15 y 17.7%, respectivamente, y una variación de superficie de plantaciones adultas en los mismos años que va de 7.2 a 22.9 y 15.4%, respectivamente. Los resultados del segundo método muestran que los valores de curva número son mayores en el periodo 1985-1989 y menores en el periodo 2001-2004, ya que el volumen de escorrentía generada es menor en este periodo con respecto a los otros dos. Lo anterior se debe a una mayor superficie de plantaciones adulta que proporciona más capacidad de intercepción, una mayor tasa de evapotranspiración y un mayor almacenamiento de humedad en el suelo.

Palabras clave: *curva número, coeficiente de escorrentía, imágenes LandSat, cambio de cobertura del suelo.*

Introduction

Interest has increased over recent years in quantifying the effects of changes in land use/cover on hydrological processes (Wang & Kalin, 2010). Sullivan, Ternan and Williams (2004) report that the types of land management practiced by the farming sector —such as

shepherding, intensive agricultural practices and reductions in forest mass— have led to soil compacting, which in turn reduces infiltration, decreases groundwater recharge and increases runoff. In Chile, the hydrological behavior of *Pinus radiata* plantations has been compared to that of native vegetation, in which differences in the water balance have been found. In effect, runoff decreases in forests in the summer primarily because of less interception capacity, which in turn affects groundwater recharge (Huber, Iroumé, & Bathurst, 2008; Little, Lara, Mcphee, & Urrutia, 2009).

One of the most widely used methods for studies of water balance and runoff is the curve number (*CN*) developed by the Natural Resources Conservation Service (Yu, 1998). This method has been used widely in distinct models, including *SWAT*, *L-THIA* y *HEC-HMS* (Ali, Khan, Aslam, & Khan, 2011; Githui, Mutua, & Bauwens, 2009; Harbor, 1994) because it is easy to apply when data is scarce and it provides a simple method to determine runoff (Babu & Mishra, 2012). Another advantage is that the determination of the curve number depends on land use/cover and the type of soil as well as the topography, resulting in the method being compatible with tele-detection and geographic information systems techniques (Shi *et al*., 2007).

The objective of this study was to validate the use of satellite images to evaluate the effects of changes in ground cover and direct runoff on the Lirquen River basin, Chile. To this end, (a) curve number values needed to be obtained from the classification of satellite images for different periods; (b) they also needed to obtained from hydrometeorological records for the same periods, and (c) the curve numbers obtained need to be compared with the previous methods.

Material and Methods

The study region corresponds to the Lirquen River Basin (Figure 1a) with an area of 102 km^2. This is a sub-basin of the Biobio River Basin (36° 42′ - 38° 49′ latitude south). The maximum elevation of the Lirquen River Basin is 1 420 masl and the minimum is 330 masl. The length of the river is 16.9 km and its average slope is 16°. The annual precipitation is 2 000 mm and the average annual temperature ranges between 7 and 10°C (DGA, 2004). The study area is characterized by two soil series —Santa Barbara and Andean range. The soils corresponding to the Andean range is similar to that of the Santa Barbara series, except that they are located in sectors with large slopes (Carrasco, Millán, & Peña, 1993; CIREN, 1999). For the Santa Barbara soil series, a hydrological group was defined according to texture, infiltration rate and saturated hydraulic conductivity values for soils at depths over 100 cm (NRCS, 2007). These values were also assigned to the Andean range. The Santa Barbara series corresponds to hydrological group B, having deep soils with good drainage, loam or silty loam textures, and hydraulic conductivity values of 15 mm/h and 28 mm/h, according to the Soil Water Characteristic database (Saxton & Rawls, 2006).

LandSat™ images for the years 1987, 2003 and 2009 were used. The image for the year 1987 was geometrically corrected using the images from the years 2003 and 2009 as cartographic bases (Chuvieco, 2002). This process consisted of eliminating the geometric distortions produced by a series of factors that vary for each acquisition of images, to ensure the correct geographic referencing of each pixel in a map. Next, a topographic correction of all the images was performed by eliminating the effects of shade, a product of the topography, using the semi-empirical correction method known as C-correction (Chuvieco, 2002). Then, an atmospheric correction was performed by eliminating the spread of the electromagnetic radiation generated by gases and suspended particles in the atmosphere. This was accomplished using the method proposed by Chavez (2006). Vegetation indices were then calculated, including simple ratio (SR), normalized difference vegetation index

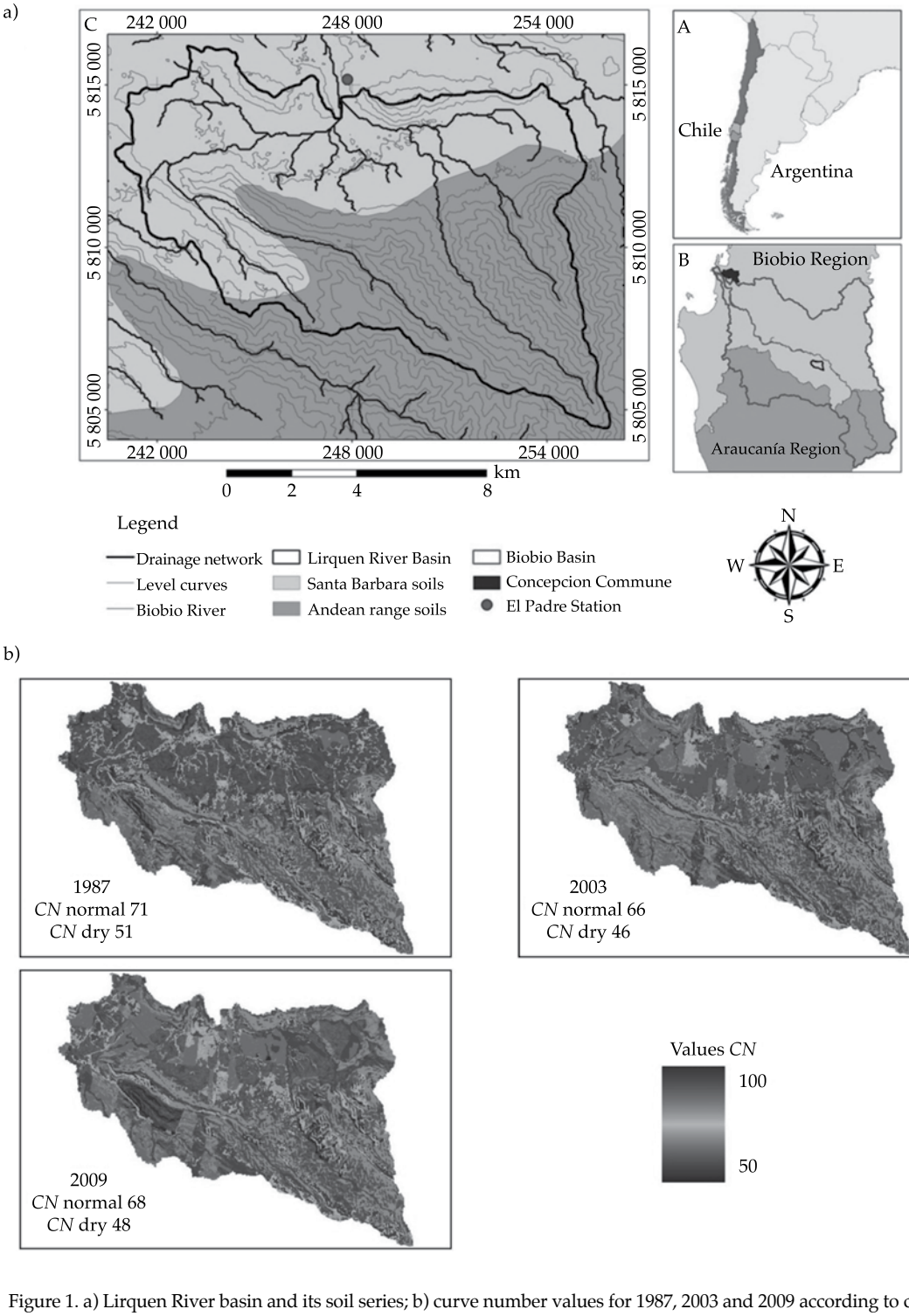

Figure 1. a) Lirquen River basin and its soil series; b) curve number values for 1987, 2003 and 2009 according to cover, hydrological groups of the soil series and correction for slope effect.

(NDVI), soil adjusted vegetation index (SAVI) and the Normalized Difference Infrared Index (NDII) (Chuvieco, 2002). Lastly, the images were classified according to the maximum verisimilitude method (Chuvieco, 2002), supported by data taken on the land and from

aerial photography, as well as information regarding land uses from the Chile Registry and Evaluation of Vegetation Resources (Catastro y Evaluación de los Recursos Vegetacionales de Chile; CONAF-CONAMA-BIRF, 1999). The classification was validated by applying the kappa method to measure the difference between the observed reality and the random expectation. A value of 0 indicates no concordance and a value of 0.8 to 1 nearly perfect to perfect concordance (Chuvieco, 2002).

Obtainment of the Curve Number Value and Runoff Coefficient

The curve number (*CN*) values were defined according to the land use/cover and hydrological type pertaining to the soil series (NRCS, 2004). Then, a correction for slope (α) (equation (1)) was applied to these values, where CN_c is the value of the corrected curve number. The effect of the slope on runoff can be summarized as: (1) decreased initial abstraction, (2) decreased infiltration rate, (3) decreased surface flow recession time and (4) increased runoff velocity:

$$CN_C \frac{CN}{\mathrm{Cos}(\alpha)} \qquad (1)$$

Next, 50 daily precipitation events were taken from the Cerro El Padre weather station (Figure 1a) for three periods: 1985-1988 (period A); 2001- 2004 (period B), and 2007-2010 (period C). These events were selected between September and May, excluding events with more snow to avoid runoff due to melting. All these precipitation events occurred in conditions of low humidity, separated according to the amount of water fallen: class 1 corresponds to precipitation over 100 mm, class 2 to precipitation over 60 and less than 100 mm and class 3 to precipitation over 40 and less than 60 mm. The growth period was defined for events occurring from September to December and the dormant period for January through May (NEH-4, 1972), since the environmental conditions of the seasons affect the physiology of the plants. To calculate the runoff volume from these events, the base flow volume was subtracted from the hydrographs. The latter was obtained using the Eckhardt method (2005), a type of low pass filter used by the theory of separation of signal processing, considering that the base flow volume is the lowest frequency component of the flow volume. The parameters of this method include a recession constant and the maximum base flow index. The latter was obtained using the Collischonn and Fan (2012) method. Then, using the rational method, curve number values for each event were calculated using runoff coefficients (Martínez, & Mongil, 2009).

Results

The results from the classification of images are shown in Table 1. This table presents the curve number values for the years 1987, 2003 and 2009 with low and normal moisture conditions in the soil and on the surface, for each type of cover. A decrease in grassland area of 28% is observed for the year 1987 and 15 and 17.7% for 2003 and 2009, respectively. An increase of 7.2% in the area of adult plantations can be observed for 1987, and 23% in 2003 and 15.4% in 2009. It must be noted that the other land covers remained constant, indicating that most of the transformation in the basin corresponded to the conversion of grassland into forests. The values for the kappa coefficient were 0.83, 0.80 and 0.79, respectively.

Table 2 shows the average values for runoff, precipitation, the runoff coefficient and the curve numbers obtained from hydrometeorological records, according to the precipitation class and periods. A comparison of the different classes between periods B with A shows that the average precipitation is higher for B than A, while the average runoff coefficient and the curve numbers are lower for B than for A. This is because of a larger area of

Table 1. Surface area (%) and CN values in low and normal moisture conditions and ground cover in the Lirquen River basin.

Soil Cover	Normal *CN* condition	Dry *CN* condition	Surface (%)		
			Year 1987	Year 2003	Year 2009
Prairie	80	60	27.91	15.01	17.67
Fern scrubland	65	45	14.34	10.37	10.22
Adult plantation	60	40	7.18	22.88	15.36
Native Renewal	55	35	41.85	45.04	45.42
Young plantation	75	55	2.71	1.14	5.59
Scrubland	70	50	2.05	1.59	1.77
Native adult forest	50	30	3.93	3.93	3.93
Water	100	100	0.04	0.04	0.04

Table 2. Average values for runoff, precipitation, runoff coefficient and curve number, according to precipitation class and period.

Class	Period	Average runoff (mm)	Average precipitation (mm)	Average runoff coefficient	Average curve number
1	A	36.8	150.2	0.190	51
	B	29.9	170.4	0.140	46
	C	103.4	275.0	0.315	49
2	A	9.1	78.3	0.114	60
	B	6.8	79.6	0.083	55
	C	5.6	71.8	0.079	56
3	A	3.0	46.7	0.065	66
	B	2.8	50.5	0.054	63
	C	4.3	52.6	0.082	64

adult plantations during period B, generating more interception capacity, evapotranspiration and moisture storage in the soil (Huber *et al.*, 2008; Sriwongsitanon & Taesombat, 2011). In addition, the largest differences in runoff coefficients between the periods occurred for rainfalls over 100 mm. Figure 1b shows the curve number values for: the classification of images from 1987, 2003 and 2009; the hydrological soil series groups; and the correction for slope. These curve number values are very similar to those obtained with the runoff coefficient for class 1 precipitation events (Figure 2), possibly because the temporal resolution of the flow volume and precipitation data overestimates the runoff volume generated for class 2 and 3 precipitation events.

Conclusions

The curve number values obtained based on classifications of satellite images, and corrected for slope, had a pattern similar to those obtained for the runoff coefficient during the same periods. This shows that satellite images are reliable tools for hydrological studies.

This study clearly demonstrates the effect of changes in land use/cover on runoff. In particular, it demonstrates that a change from grassland to adult plantations strongly decreases the generation of runoff because of a greater interception capacity, a higher evapotranspiration rate and a larger moisture retention capacity of soil in forests.

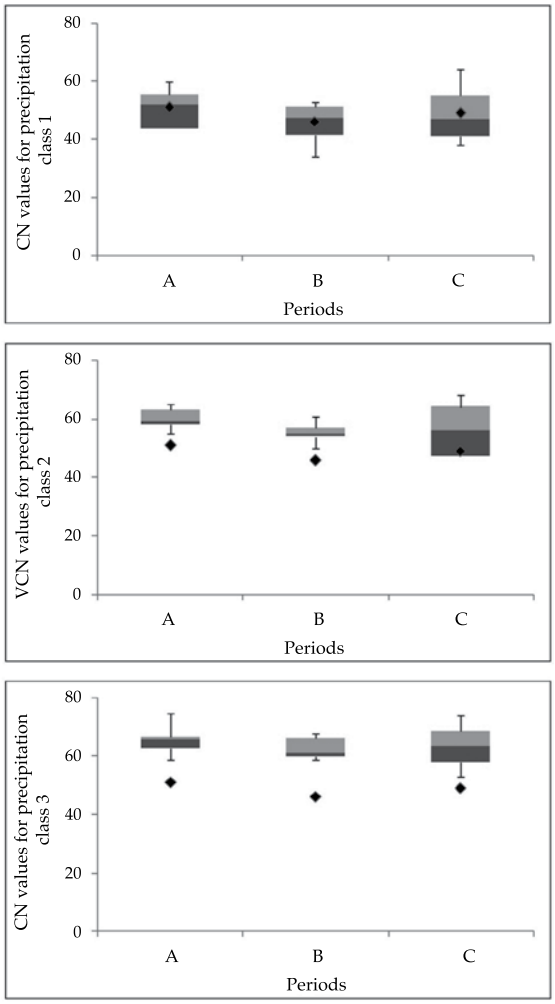

Figure 2. Comparison of curve number values between the images classified with most soil texture and slope correction (points) and the runoff coefficient method (bars) for each precipitation class.

Acknowledgements

We wish to thank the Fondecyt project number 1090774 for the support to perform this study.

Received: 02/04/13
Accepted: 22/01/14

References

Ali, M., Khan, S. J., Aslam, I., & Khan, Z. (September, 2011). Simulation of the Impacts of Land-Use Change on Surface Runoff of Lai Nullah Basin in Islamabad, Pakistan. *Landscape and Urban Planning*, *102*, 271-279.

Babu, P. S., & Mishra S. K. (November, 2012). An Improved SCS-CN Inspired Model. *Journal of Hydrology Engineering*, *17*(11), 1164-1172.

Carrasco, P., Millán, J., & Peña, L. (1993). *Suelos de la cuenca del río Biobío, características y problemas de uso* (108 pp.). Concepción, Chile: Centro EULA-Chile. Gestión de los Recursos Hídricos de la Cuenca del Río Biobío y del Área Marina Costera Adyacente, Editorial Universidad de Concepción.

Chávez, P. J. (September, 1996). Image Based Atmospheric Corrections-Revisited and Improved. *Photogrammetric Engineering and Remote Sensing*, *62*(9), 1025-1036.

Chuvieco, E. (2002). *Teledetección ambiental: la observación de la Tierra desde el espacio* (586 pp.). España: Editorial Ariel Ciencia.

CIREN (1999). *Estudio agrológico de la VIII Región* (550 pp.). Chile: Centro de información de Recursos Naturales, Ministerio de Agricultura.

CONAF-CONAMA-BIRF (1999). *Catastro y evaluación de los recursos vegetacionales nativos de Chile. Informe Nacional con Variables Ambientales* (87 pp.). Santiago, Chile: Universidad Austral de Chile, Pontificia Universidad Católica de Chile, Universidad Católica de Temuco.

Collischonn, W., & Fan, F. M. (April, 2012). Defining Parameters for Eckhardt's Digital Baseflow Filter. *Hydrological Processes*, doi: 10.1002/hyp.9391.

DGA (2004). *Diagnóstico y clasificación de los cursos y cuerpos de agua según objetivos de calidad: cuenca del río Biobío* (179 pp.). Chile: Dirección General de Aguas, Ministerio de Obras Públicas.

Eckhardt, K. (February, 2005). How to Construct Recursive Digital Filters for Base Flow Separation. *Hydrological Processes*, *19*, 507-517.

Githui, F., Mutua, F., & Bauwens, W. (October, 2009). Estimating the Impacts of Land-Cover Change on Runoff Using the Soil and Water Assessment Tool (SWAT). Case Study of Nzoia Catchment, Kenya. *Hydrological Science Journal*, *54*, 899-908.

Harbor, J. (1994). A Practical Method for Estimating the Impact of Land-Use Change on Surface Runoff, Groundwater Recharge and Wetland Hydrology. *Journal of the American Planning Association*, *60*, 95-108.

Hevia, J., Martinez, A., & Mongil, J. (2009). *Hidrología de conservación de aguas. Captación de precipitaciones horizontales y escorrentía en zonas secas* (446 pp.). Valladolid: Universidad de Valladolid, Secretariado de Publicaciones.

Huber, A., Iroumé, A., & Bathurst, J. (January, 2008). Effect of *Pinusradiata* Plantations on Water Balance in Chile. *Hydrological Processes*, *22*, 142-148.

Hundecha, Y., & Bárdossy, A. (June, 2004). Modeling of the Effect of Land Use Changes on the Runoff Generation of a River Basin through Parameter Regionalization of a Watershed Model. *Journal of Hydrology*, *292*, 281-295.

Little, C., Lara, A., Mcphee, J., & Urrutia, R. (June, 2009). Revealing the Impact of Forest Exotic Plantations on Water Yield in Large Scale Watersheds in South-Central Chile. *Journal of Hydrology*, 374, 162-170.

NEH-4 (1972). *NRCS National Engineering Handbook. Chapter 21. Hydrology, Natural Resources Conservation Service*. US Department of Agriculture.

NRCS (2004). *NRCS National Engineering Handbook, Chapter 10. Hydrologic Soil-Cover Complexes, Natural Resources Conservation Service*. Washington, DC: US Department of Agriculture.

NRCS (2007). *NRCS National Engineering Handbook, Chapter 7. Hydrologic Soil Groups, Natural Resources Conservation Service*. Washington, DC: US Department of Agriculture.

Shi, P., Yuan, Y., Zheng, J., Wang, J., Ge, Y., & Qiu, G. (January, 2007). The Effect of Land Use/Cover Change on Surface Runoff in Shenzhen Region, China. *Catena*, *69*, 31-35.

Sriwongsitanon, N., & Taesombat, W. (November, 2011). Effects of Land Cover on Runoff Coefficient. *Journal of Hydrology*, *41*, 226-238.

Sullivan, A., Ternan, J. L., & Williams, A. G. (April, 2004). Land Use Change and Hydrological Response in the Camel Catchment, Cornwall. *Applied Geography*, *24*, 119-137.

Wang, R., & Kalin, L. (November, 2010). Modelling Effects of Land Use/Cover Changes under Limited Data. *Ecohydrology*, *4*, 265-276.

Yu, B. (November, 1998). Theoretical Justification of SCS Method for Runoff Estimation. *Journal of Irrigation and Drainage Engineering*, *124*, 306-310.

Institutional Address of the Authors

Dr. César Cano

Universidad de Concepción
Facultad de Ingeniería Agrícola
Departamento de Recursos Hídricos
Chillán, Chile
ccano@udec.cl

Dr. Andrea Andreoli

Universidad de Concepción
Facultad de Ciencias Forestales
Departamento de Bosques y Medioambiente
Laboratorio de Ecología de Paisaje
Concepción, Chile

Dr. José Luis Arumi
Dr. Diego Rivera

Universidad de Concepción
Facultad de Ingeniería Agrícola
Departamento de Recursos Hídricos
Chillán, Chile

Click here to write the autor

Sumidero Canyon, Chiapas, Mexico.

Photo: Mariana Veira Huerta.

Technical Note

Runoff Curve Identification in Three Micro-Basins of the Coatan River, Chiapas, Mexico

• Homero Alonso-Sánchez • Laura Alicia Ibáñez-Castillo* •
• Ramón Arteaga-Ramírez • Mario Alberto Vázquez-Peña •
Universidad Autónoma Chapingo
*Corresponding Author

Abstract

Alonso-Sánchez, H., Ibáñez-Castillo, L. A., Arteaga-Ramírez, R., & Vázquez-Peña, M. A. (July-August, 2014). Runoff Curve Identification in Three Micro-Basins of the Coatan River, Chiapas, Mexico. *Water Technology and Sciences* (in Spanish), *5*(4), 147-155.

The curve numbers (CN) method by the Soil Conservation Service (SCS) has applications in the field of hydrology and has been widely used in many countries, including Mexico. Nevertheless, these values were obtained in United States basins and pertain to very general land use categories. Therefore, using them can result in errors. This study identified and compared the runoff curve number for three micro-basins in the Coatan River watershed, in Chiapas, for several rain events ranging from 13 to 36 events during 2011. This watershed is located in the Mexican humid tropics. On the one hand, values were used from SCS tables corresponding to the micro-basins and its events, with the respective corrections for antecedent moisture and slope. On the other hand, NC values were calculated from direct rainfall and runoff measurements. Rainfall was measured using rain gauges and runoff using water level recorders near the watershed and at its outlet. Both NC were compared, those obtained from the measurements (69 in Vega de los Gatos, 55 in Progreso and 72 in Chanjale) and those provided by SCS tables (79 for Vega de los Gatos, 79 for Progreso and 78 for Chanjale). Significant differences in means were found between these two sets of data. These results are attributed to the use of SCS tables that do not have the required land use, thereby needing to subjectively use those which are closest, resulting in accuracies.

Keywords: Runoff depth, measurement of rainfall and runoff in tropical watersheds, runoff coefficients in tropical watersheds.

Resumen

Alonso-Sánchez, H., Ibáñez-Castillo, L. A., Arteaga-Ramírez, R., & Vázquez-Peña, M. A. (julio-agosto, 2014). Identificación de curva de escurrimiento en tres microcuencas del río Coatán, Chiapas, México. Tecnología y Ciencias del Agua, *5(4), 147-155.*

La metodología de los números de curva de escurrimiento (NC) del Servicio de Conservación de Suelos (SCS) de Estados Unidos (EU) tiene aplicaciones en el campo de la hidrología y se ha extendido ampliamente a muchos países, incluyendo México; sin embargo, dichos valores fueron obtenidos en cuencas de EU y son para categorías muy generales de uso de suelo, por lo que se puede caer en errores al usarlos. En este trabajo se identificaron y compararon los números de curva de escurrimiento de tres microcuencas dentro de la cuenca del río Coatán, en Chiapas, para varios eventos de lluvia que van desde 13 hasta 36 eventos ocurridos durante 2011; dicha cuenca se encuentra en el trópico húmedo de México. Por un lado se utilizaron los valores de tablas del SCS que corresponden a las microcuencas y a sus eventos, haciendo las correcciones respectivas por humedad antecedente y por pendiente y, por otro lado, se calcularon los valores de NC a partir de medición directa de la lluvia y el escurrimiento. Las mediciones se realizaron con pluviógrafo y limnígrafo establecidos cerca de la microcuenca y a la salida de ella, respectivamente. Se compararon ambos NC, los obtenidos a partir de la medición (69 para Vega de los Gatos, 55 Progreso y 72 Chanjalé) y los de las tablas (79 para Vega de los Gatos, 79 Progreso y 78 Chanjalé) del SCS y se encontraron diferencias significativas entre sus medias. Estos resultados se atribuyen a que al usar las tablas del SCS no se tiene el uso de suelo que se requiere y se tiene que usar subjetivamente el más cercano, originando imprecisiones.

***Palabras clave**: lámina escurrida, medición de lluvia y escurrimientos en cuencas tropicales, coeficientes de escurrimientos en cuencas tropicales.*

Introduction

The runoff curve number (*CN*) procedure was developed by the United States Department of Agriculture (USDA) and the former Soil Conservation Service (USDA-SCS, 1972) as a simple procedure to calculate runoff volume generated by large storms in small farming

basins. The methodology can be applied to basins without instrumentation and the *NC* can be obtained from tables corrected for slope and antecedent moisture. Because of its simplicity, it quickly surpassed its overall objectives and was adopted for different land uses, such as for urban and forest basins (Rawls, Onstad, & Richardson, 1980; Mishra & Singh, 1999). It rapidly became one of the techniques most widely used by engineers and hydrologists (Mishra, Sahu, Eldho, & Jain, 2006). Methodologies have even been developed to automatically generate the *NC* using geographic information systems (Ferrer, Rodríguez, & Estrela, 1995). Currently, the runoff curve number method to convert rainfall into runoff is so popular that software such as *HEC-HMS* and *SWAT* included it among their most used options for the corresponding calculations (USACE, 2010; Neitsch, Arnold, Kiniry, & Williams, 2011). The method is very sensitive to changes in the values of its parameters (Ponce & Hawkins, 1996; Mishra *et al*., 2006). In addition, Reistetter and Russell (2011) found that the *NC* varies over time at the same site and recommended better discretization of land uses, avoiding average *NC* values for large areas in order to more accurately use *NC*.

The method has had diverse uses and been subject to frequent improvements and some occasional criticisms in Latin American countries, where it has ended up as only a user-spectator of what the SCS did 70 years ago (Ponce, 1996). Chagas *et al.* (2008) reviewed antecedent moisture conditions; Paz-Pellat (2009) reviewed the implications of the hypothesis of curve number methods, concluding that the method has no hydrological bases (a questionable statement that should be analyzed in more detail); Campos-Aranda (2011) has used it to identify the *NC*, along with the unit hydrograph theory in seven basins in the Upper Grijalva River; and Ares, Varni, Chagas and Entraigas (2012) identified the *NC* of a 116 km^2 basin in Argentina.

According to Hjelmfelt (1991), the method has been the subject of different studies, with the objective of finding a theoretical basis for it so as to facilitate its use in regions and climates with conditions that have not been previously evaluated and to support its application. *NC* values are experimentally obtained from rainfall and runoff measurements over a wide range of geographic soils and land management conditions, but in Mexico only some of the basins contain instrumentation.

The curve number method is widely used in Mexico because of its simplicity and the lack of instrumentation in basins. Nevertheless, the land use conditions are different than those in the United States, where the method's tables were developed. The southern Mexican border is particularly different since it is located in a humid tropical zone and contains land with uses that do not exist in the *NC* tables. Therefore, the objective of this work was to identify the curve number for land uses in the monitored micro-basins located in the Coatan River Basin in the state of Chiapas, Mexico.

Materials and Methods

The Coatan River Basin

The area of the Coatan River Basin is 426 km^2, up to the Malpaso gauging station. Forty percent of the basin is in Guatemala and 60% in Mexico. The basin belongs to Hydrological Region 23, Chiapas Coast. The elevations here range from 0 masl at the Pacific Ocean to 4 058 masl. The precipitation ranges from 2 300 to 3 900 mm, on average (Conagua, 2006). The Coatan River runs through the city of Tapchula, Chiapas.

Study Micro-basins

Micro-basins were selected in the Coatan River Basin that had an uninterrupted registry since 2011 of rainfall-runoff information. The instrumentation at this site resulted from monitoring conducted by Conagua on

the Chiapas coast (2011). Table 1 shows the coordinates and some of the characteristics of the micro-basins found on the Mexican side of the lower, middle and upper Coatan River Basin.

Measurement of Precipitaiton and Runoff

Precipitaiton was measured using a Hellman rain gauge imported from Germany. Accumulated rainfall for each event included in the study was obtained from the rain gauge graphs.

To measure runoff, an H-gauge water stage recorder (Stevens brand) was used, which also has a clock system and, therefore, the rainfall events registered with the pluviograph were related to the corresponding water stage recorder. The water stage recorder, along with a gauging weir, were located at the outlet of the study basin. The pluviographs were located near the micro-basins studied. They could not be placed inside the small basins since the vegetation there would interfere with the measurements. They were placed within 300 meters of the micro-basins.

Conversion of Water Stage Recorders into Hydrographs

El cero del limnograma correspondió al nivel The zero of the water stage recorder corresponded to the base flow level for all cases. They were interpreted with the gauge calibration table. Discharges were obtained for different intervals and the area under the curve of the hydrographs was obtained, which corresponds to total runoff volume. The runoff was calculated by dividing total volume by the area of the micro-basin.

Obtainment of the Curve Number using the SCS Method

The method established by the SCS uses a table of *NC* values generated experimentally in basins in the United States. It contains primarily four selection criteria (USDA-SCS, 1972): hydrological soil group, land use, land practice in the case of agricultural regions and hydrological conditions (the hydrological condition is only defined for forests, jungles and grassland. The *NC* selected was corrected for antecedent moisture and slope.

After analyzing the runoff potential of over 4 000 soils, SCS scientists (McCuen, 2005; NRCS, 2013) classified the hydrological soil groups into four categories, identified by the letters A, B, C and D according to infiltration capacity. The hydrological conditions or vegetation cover density (forest, jungle or grassland) refers to the density of the cover and encompasses three categories: (a) poor, less than 50% of the surface is protected by vegetation cover; (b) normal, 50- 75% is protected, and (c) good, dense cover, with over 75% of the soil protected by vegetation.

Antecedent Moisture Condition

Antecedent moisture conditions have a significant effect on the runoff volume and

Table 1. Physical and geometric characteristics of microbasins.

Microbasin	Latitude (° ′ ″)	Longitude (° ′ ″)	Área (m^2)	Elevation (masl)	Channel length (m)	Slope of channel (%)	Texture	Land use/cover
Vega de los Gatos	15° 01′ 44″	92° 13′ 55″	23 494	471	314	29.6	Loam	Low and medium jungle
Chanjalé	15° 12′ 35″	92° 11′ 45″	44 838	1 473	343	63.2	Loam	Coffee with low and medium jungle
Progreso	15° 45′ 05´´	92° 11′ 46″	27 609	944.5	365	24.9	Sandy loam	Coffee, bananas, fruit trees

rate. Recognizing it as an important factor, three antecedent moisture "conditions" (AMC) were developed by the SCS: a) condition 1 refers to dry soils but not to the point of wilting, presenting satisfactory conditions for crops, accumulated precipitation under 34 mm during the five previous days; b) condition 2 refers to average conditions, accumulated precipitation between 34 and 54 mm during the five previous days; c) condition 3 refers to intense daytime rainfall and low temperatures during the previous five days, saturated soils, accumulated precipitation over 54 mm during the five previous days.

Runoff Curve Number Corrected for Slope

The curve number tables proposed by the SCS were developed in basins with slopes of up to 5%. Therefore, years later an equation to correct for slopes was proposed (Neitsch *et al.*, 2011):

$$NC_{2s} = \frac{\left(NC_3 - NC_2\right)}{3}\left[1 - 2\exp\left(-13.86\,slp\right)\right] + NC_2 \quad (1)$$

where NC_{2s} = curve number corrected for slope; NC_3 = curve number for antecedent moisture condition 3; NC_2 = curve number as shown in the SCS tables; *slp* = average split basin slope.

Calculation of the Curve Number

Equation (6) was used to calculate the *NC* for real data, resulting in the combination of equation (2) proposed by Hawkins (1979) and the proposal by SCS (equation (3)) to obtain the maximum retention potential:

$$S = 5\left(P + 2Q - \sqrt{4Q^2 + 5PQ}\right) \quad (2)$$

$$S = \frac{25\,400}{NC} - 254 \quad (3)$$

where S is the maximum retention potential in mm and *NC* is the dimensionless curve number:

$$NC = \frac{25\,400}{5\left(P + 2Q - \sqrt{4Q^2 + 5QP}\right) + 254} \quad (4)$$

where P is the rainfall in mm and Q is the runoff in mm.

Calculation of the Fitting between the Calculated Curve Numbers and those from the Tables

Statistical methods were used to measure the degree of fitting of a hydrological model (Yusop, Chan, & Katimon, 2007). In addition to the root means square error (RMSE) and the relative error (RE), the Nash-Sutcliffe efficiency criteria were used (1970), which compares the observed and simulated hydrographs (Yusop *et al.*, 2007). This was calculated with:

$$E = 1 - \frac{\sum_{t=1}^{T}\left(Q_o^t - Q_m^t\right)^2}{\sum_{t=1}^{T}\left(Q_o^t - \overline{Q}_o\right)^2} \quad (5)$$

where $Q_o{}^t$ is the observed value, $Q_m{}^t$ is the value calculated by the model and $\overline{Q}_o$ is the mean of the observed values. Equation (5) can lead to comparing the *NC* from the tables and the "measured" *NC*, as in:

$$E = 1 - \frac{\sum_{i=1}^{n}\left(NC_{\text{meas}}^i - NC_{\text{tables}}^i\right)^2}{\sum_{t=1}^{n}\left(NC_{\text{meas}}^i - \overline{NC}_{\text{meas}}\right)^2} \quad (6)$$

where NC_{meas} is the measured curve number, dimensionless, and NC_{tables} is the curve number obtained from the tables, dimensionless.

The Nash efficiency can range from -∞ to 1. An efficiency of 1 corresponds to a perfect combination of measured data and observed

data. An efficiency of 0 indicates that the predictions of the model are as accurate as the measurement of the observed data. And an efficiency less than 0 results when the observed data is a better predictor than the model, that is, when the residual variance is greater than the variance of the data. In general, the closer the value of the efficiency is to 1 the better the model's prediction.

Results and Discussion

For each micro-basin, the *NC* was obtained from SCS tables with their respective corrections for antecedent moisture and slope. The observed *NC* were obtained, calculated with rainfall and runoff data measured for each event in each micro-basin. In the case of Vega de los Gatos, the *NC* was calculated for 36 events, in Progreso for 13 and in Chanjale for 13. The rainfall events are the maximum registered and varied from 25 to 150 mm.

Tables 2, 3 and 4 show the results obtained from the calculated curve numbers and those from the tables. The comparison of the statistics between the values from the tables and the calculated values for the Vega de los Gatos micro-basin are: RMSE equal to 16.02, RE of 6.15 and Nash coefficient of -73.62. The latter indicates that the means of the values from the SCS tables are different than those for the values calculated with measurements, which was statistically proven.

The results indicate that the *NC* calculated according to the SCS tables are very different than those obtained with measured variables. What may first be said is that the *NC* does not work, that it is a method with no hydrological basis, it does not explain the physical nature of the rainfall-runoff phenomenon; and other criticisms. Nevertheless, the method was originally designed for conditions different than those found in Chiapas. The tables are not made for land uses that are predominant in this region. To use the tables, a land use similar to the dominant one is taken. In the case of the study basin, the land is jungle, while in the United states, where this method was developed, this land use does not exist. If there is a desire to use this methodology accepting its supposition, curve numbers for the land use of interest must be generated based on measurements for the greatest accuracy and thereby avoiding subjectivity by using curve numbers from SCS tables for land uses that they do not included.

In addition to the results shown in Table 3 for the Progreso site, the comparison statistics between the SCS table and calculated values are: RMSE of 15.7, RE of 21.9 and a Nash efficiency coefficient of -69.9. As can be seen, the efficiency coefficient shows that there is no similitude between the table and the values obtained using measurements.

At the Chanjale site (Table 4), the comparison statistics between the table and the values calculated are: RMSE of 11.3, RE of 2.43 and Nash efficiency coefficient of -6.9. It is worth noting that the Nash coefficient was less than 0 at the Progreso and Chanjale sites, which indicates that the mean of the observed values was different than the mean of the values from the tables, which was the case for the Vega de los Gatos site as well. This will later be statistical proven, although the errors and the efficiency coefficient are more conservative at Chanjale and there is a discrepancy with the theory by Nash and Sutclife (1970).

The *NC* values obtained from the tables with the land use parameters mentioned, corrected for antecedent moisture conditions and slope, were compared with those calculated based on equation (4), a solution using the quadratic equation of the SCS equation to obtain the *NC* values with rainfall and runoff measurements.

Se realizó un análisis estadístico de la información para verificar si existe diferencia significativa entre los valores de tablas y los calculados con datos medidos, por lo que se aplicó una estadística de prueba que permite determinar la diferencia de medias entre dos poblaciones.

A statistical analysis was performed of the information to verify whether a significant difference exists between the values from the

Table 2. Curve numbers calculations and from tables for the Vega de los Gatos Microbasin.

Event	Date	Runoff (mm)	Precipitation (mm)	Calculated *NC*	*CN* from SCS[1] tables
1	20/04/11	4.0	65.1	58.5	79.56
2	16/05/11	6.9	57.1	67.5	79.56
3	24/05/11	5.9	89.3	51.2	79.56
4	07/06/11	18.7	97.2	61.2	79.56
5	25/06/11	3.6	25.8	83.2	79.56
6	26/06/11	27.6	145.8	51.0	79.56
7	02/07/11	2.3	46.3	65.0	79.56
8	04/07/11	7.2	91	52.3	79.56
9	10/07/11	14.9	77.2	66.6	79.56
10	14/07/11	4.4	52.6	65.9	79.56
11	15/07/11	2.8	31	77.1	79.56
12	18/07/11	24.0	122.1	56.0	79.56
13	19/07/11	13.7	71.3	68.3	79.56
14	24/07/11	3.8	41.3	71.9	79.56
15	29/07/11	2.5	38.9	70.5	79.56
16	31/07/11	7.0	86.9	53.6	79.56
17	07/08/11	3.3	33.1	76.6	79.56
18	08/08/11	6.0	29.8	84.2	79.56
19	14/08/11	2.4	23.1	82.7	79.56
20	16/08/11	7.9	58.9	68.0	79.56
21	17/08/11	2.8	24.4	82.5	79.56
22	18/08/11	11.2	57.3	73.0	79.56
23	19/08/11	8.3	42.3	78.5	79.56
24	26/08/11	3.8	94.9	46.1	79.56
25	27/08/11	3.1	15.6	91.0	79.56
26	27/08/11	10.0	51.7	74.8	79.56
27	30/08/11	13.1	73.3	66.6	79.56
28	01/09/11	2.4	25.8	80.5	79.56
29	04/09/11	3.4	25.1	83.3	79.56
30	05/09/11	17.7	128.4	49.6	79.56
31	12/09/11	4.0	60	61.1	68.43
32	13/09/11	3.6	57.6	61.4	79.56
33	14/09/11	4.5	34.4	78.2	79.56
34	18/09/11	7.9	46.6	75.3	79.56
35	19/09/11	24.8	129.6	54.1	79.56
36	29/09/11	2.7	28.4	79.1	79.56
Average				**68.5**	**79.20**
Variance				**130.0**	**3.99**
CV				**0.2**	**0.03**

[1]Note: corrected for antecedent moisture and slope.

Table 3. Curve numbers calculations and from tables for Progreso Microbasin.

Event	Date	Runoff (mm)	Precipitation (mm)	Calculated *NC*	*CN* from SCS tables
1	23/04/11	2.6	43.8	67.5	69
2	08/06/11	4.7	110.1	42.9	80
3	06/07/11	1.0	58.1	54.2	75
4	10/07/11	2.8	70.0	53.7	80
5	27/08/11	2.3	59.7	57.3	80
6	30/08/11	1.0	55.3	55.6	80
7	31/08/11	1.2	57.4	55.3	80
8	04/09/11	1.2	55.8	56.1	80
9	06/09/11	1.0	46.3	60.5	80
10	14/09/11	1.4	52.8	58.5	80
11	19/09/11	13.4	186.7	34.0	80
12	21/09/11	1.5	55.3	57.5	80
13	27/09/11	1.2	55.2	56.5	80
Average				**54.6**	**79**
Variance				**76.0**	**12**
CV				**0.16**	**0.04**

Table 4. Curve numbers calculations and from tables for Chanjale Microbasin.

Event	Date	Runoff (mm)	Precipitation (mm)	Calculated *NC*	*CN* from SCS[1] tables
1	21/07/11	0.693	45.4	59.8	69
2	29/09/11	0.378	27.2	71.0	80
3	30/09/11	0.713	36.0	66.1	80
4	23/08/11	0.310	43.1	58.8	69
5	06/07/11	0.033	12.4	82.2	80
6	26/08/11	0.011	28.2	65.3	80
7	07/08/11	0.058	29.3	65.7	75
8	10/09/11	0.042	44.8	54.8	80
9	25/08/11	0.002	9.3	84.9	80
10	23/07/11	0.024	12.7	81.5	80
11	24/07/11	0.028	20.7	72.7	80
12	03/08/11	0.002	5.3	91.0	80
13	14/08/11	0.009	15.6	77.5	80
Average				**71.7**	**78**
Variance				**140**	**20**
CV				**0.16**	**0.06**

tables and those calculated with measured data. Therefore, a test statistic was applied to determine the difference in means between the two populations. Based on the normality assumption, a homogeneity test of sampling variances was performed. The technique used

for the latter was that described by Montgomery (2004). With the means test corresponding to the three sites, a significant difference in means was found, with a significance level of 0.05.

Conclusions

The curve number 69 was identified for the land use at the Vega de los Gatos micro-basin, corresponding to a low-medium jungle; 55 for the Progreso micro-basin, corresponding to coffee, bananas and fruits; and 72 for the Chanjale micro-basin, corresponding to a combination of coffee and low-medium jungle. These values can be used in future hydrological studies.

The statistical comparison between the means of the values from the SCS tables and those calculated showed a significant difference for all three micro-basins, with a level of significance of 0.05. This indicates that, for hydrological studies pertaining to the three study sites, the use of calculated *NC* is more accurate than the tables.

The SCS curve numbers are limited to land uses exclusive to the United States and, therefore, it is subjective and difficult to determine a use of the tables that can really be adapted to the conditions in Mexico. For the various land use possibilities, the SCS tables are not sufficiently discretized to provide more accurate values.

Considering the means resulting from the study herein, the *NC* tables overestimate the *NC* identified by the measurements. This indicates that there is theoretically less runoff in the basin. Nevertheless, the values found represent less infiltration due to different factors, such as the slope in the study area.

SCS curve numbers cannot be applied with certainty if the tables do not contain the specific type of land use; not because it is wrong but rather because each type of vegetation, in combination with other characteristics, modifies runoff.

The SCS method was developed in conditions different than those prevalent on the Chiapas coast. The suppositions of the method are not valid in this or any other region. It should be understood that the method can provide some idea of the rainfall-runoff relationship, but it was not created for all of the hydrological conditions found in Mexico. Even so, it is helpful for determining effective precipitation when only precipitation is measured. To use the method accurately and obtain the best approximation of rainfall-runoff, the *NC* need to be generated for the land uses and hydrological conditions in Mexico.

Acknowledgements

We wish to thank the National Water Commission (Comisión Nacional del Agua) and in particular the Gerencia de Distritos de Temporal Tecnificado de Oficinas Centrales

Received: 30/11/12
Accepted: 17/12/13

References

Ares, M. G., Varni, M., Chagas, C., & Entraigas, I. (agosto-septiembre, 2012). Calibración del número *N* de la curva de escurrimiento en una cuenca agropecuaria de 116 km^2 de la provincia de Buenos Aires, Argentina. *Agrociencia, 46*(6), 535-541.

Campos-Aranda, D. F. (septiembre, 2011). Identificación del número N mediante el método del HUT, en siete cuencas del alto río Grijalva, México. *Ingeniería, Investigación y Tecnología*, *12*(3), 269-276.

Chagas, C. I., Santanatoglia, O. J., Castiglioni, M. G., Massobrio, M. J., Bujan, A., & Irurtia, C. (enero-julio, 2008). Número de curva de escurrimiento para una microcuenca de Pampa ondulada bajo labranza convencional y siembra directa. *Ciencia del Suelo*, *26*(1), 63-69.

Conagua (2006). *Evaluación de los efectos del cambio de uso de suelo en la erosión hídrica y las relaciones precipitación-escurrimiento en las cuencas de los Ríos Huixtla, Huehuetán y Coatán del Estado de Chiapas* (250 pp.). México, DF: Conagua.

Conagua (2011). *Monitoreo de procesos hidrológicos erosivos en las cuencas de los ríos Huixtla, Huehuetán y Coatán, en la costa de Chiapas.*(300 pp.). Convenio de colaboración con la Universidad Autónoma Chapingo No. SGIH-GDTT-UACH-11/09/rf/cc. México, DF: Conagua.

Ferrer, M., Rodríguez, J., & Estrela, T. (1995). Generación automática del número de curva con sistemas de información geográfica. *Ingeniería del Agua*, *2*(4), 43-58.

Hawkins, R. H. (December, 1979). Runoff Curve Numbers from Partial Area Watersheds. *Journal Irrigation and Drainage*, *ASCE*, *105*(4), 375-389.

Hjelmfelt, A. T. (June, 1991). Investigation of Curve Number Procedure. *Journal of Hydraulic Engineering*, *ASCE*, *117*(6), 725-737.

McCuen, R. H. (2005). *Hydrologic Analysis and Design* (888 pp.). Upper Saddle River, USA: Prentice-Hall.

Mishra, S. K., Sahu, R. K., Eldho, T. I., & Jain, M. K. (2006). An Improved Ia-S Relation Incorporating Antecedent Moisture in SCS-CN Methodology. *Water Resources Management*, *20*(5), 643-660.

Mishra, S. K., & Singh, V. P. (July, 1999). Another Look at SCS-CN Method. *Journal of Hydrologic Engineering*, *ASCE*, *4*(3), 257-264.

Montgomery, D. C. (2004). *Diseño y análisis de experimentos* (686 pp.). Segunda edición. México, DF: Limusa-Wiley.

Nash, J. E., & Sutcliffe, J. V. (1970). River Flow Forecasting through Conceptual Models. Part I – A Discussion of Principles. *Journal of Hydrology*, *10*, 282-290.

NRCS (2013). *National Engineering Handbook, Part 4-Hydrology*. USA: Natural Resources Conservation Service. Consultado el 12 de noviembre de 2013. Recuperado de http://www.hydrocad.net/neh/630contents.htm.

Neitsch, S. L., Arnold, J. G., Kiniry, J. R., & Williams, J. R. (2011). *Soil and Water Assessment Tool, Theoretical Documentation* (618 pp.). Temple, USA: Blackland Research and Extension Service-USDA (Editorial).

Paz-Pellat, F. (julio-agosto, 2009). Mitos y falacias del método hidrológico del número de curva del SCS/NRCS. *Agrociencia*, *43*(5), 521-528.

Ponce, M. (1996). *Miguel Ponce Conversation with Victor Mockus on July 12*. Consultado el 27 de noviembre de 2013. Recuperado de file:///C:/HIDROLOGIA_LIC/Miguel%20Ponce%20conversation%20with%20Victor%20Mockus%20_%20NRCS.htm.

Ponce, V. M., & Hawkins, R. H. (January, 1996). Runoff Curve Number: Has it Reached Maturity? *Journal of Hydrologic Engineering*, *1*(1), 11-19.

Rawls, W. J., Onstad, C. A., & Richardson, H. H. (1980). Residue and Tillage Effects on SCS Runoff Curve Numbers. *Transactions American Society of Agricultural and Biological Engineers*, *23*(2), 357-361.

Reistetter, J. A., & Russell, M. (2011). High-Resolution Land Cover Dataset, Composite Curve Numbers, and Storm Water Retention in the Tampa Bay, FL Region. *Applied Geography*, *31*(2), 740-747.

USACE (2010). *Hydrologic Modeling System HEC-HMS. Version 3.5 User´s Manual* (318 pp.) Davis, USA:: Hydrologic Engineers Center, U.S. Army Corps of Engineers (USACE).

USDA-SCS (1972). *SCS Natural Engineering Handbook, section 4, Hydrology. Estimation of Direct Runoff from Storm Rainfall* (pp. 1-24). Washington, DC: U.S. Department of Agriculture-Natural Resources Conservation Service.

Yusop, Z., Chan, C. H., & Katimon, A. (2007). Runoff Characteristics and Application of HEC-HMS for Modeling Stormflow Hydrograph in an Oil Palm Catchment. *Water Science and Technology*, *56*(8), 41-48.

Institutional Address of the Authors

Dr. Homero Alonso Sánchez
Dra. Laura Alicia Ibáñez Castillo
Dr. Ramón Arteaga Ramírez
Dr. Mario Alberto Vázquez Peña

Universidad Autónoma Chapingo
Carretera México-Texcoco kilómetro 38.5
56230 Texcoco, Estado de México, México
Teléfono: +52 (595) 9521 649
Fax: +52 (595) 9521 650

alonso_m77@hotmail.com
libacas@gmail.com
rarteagar@taurus.chapingo.mx
mvazquezp@correo.chapingo.mx

Click here to write the autor

Hydropneumatic tanks to pump industrial water, Vidrio Flotado plant, Colombia.

Photo provided by Alfonso Herrán Sandoval.

Technical Note

Calculation of Capacity of Hydropneumatic Tanks

• Alfonso Herrán-Sandoval* •
Ingetec, S.A., Colombia
*Corresponding Author

Abstract

Herrán-Sandoval, A. (July-August, 2014). Calculation of Capacity of Hydropneumatic Tanks. *Water Technology and Sciences* (in Spanish), *5*(4), 157-165.

Water pumping systems usually require the calculation and sizing of hydropneumatic tanks that operate along with the process pumps which are used in hydraulic systems for several purposes. In this technical note the author presents a general calculation method which makes it possible to size a given tank according to the flows through the pump and the system, without exceeding a maximum number of motor starts per unit time. The proposed method makes it possible to calculate smaller tanks than those calculated by well-established conventional methods, decreasing the size of the corresponding pump according to the increase in its operating time. The article presents the equations proposed and respective graphs illustrating the goodness of the method, as well as an example of the calculation of the size of a pair of hydropneumatic tanks using this method, which are installed and operating in a large float glass factory located in the outskirts of the city of Bogota, Colombia. Finally, the results from this calculation and the final sizes of the tanks are compared with results obtained using traditional methods and conclusions are presented regarding the applicability of the method.

Keywords: Capacity, hydropneumatic tanks, volume.

Resumen

Herrán-Sandoval, A. (julio-agosto, 2014). Tanques hidroneumáticos. Cálculo de la capacidad. Tecnología y Ciencias del Agua, *5(4), 157-165.*

En sistemas de bombeo de agua usualmente se necesita calcular y dimensionar tanques hidroneumáticos que operen junto con bombas de proceso en sistemas hidráulicos para usos varios. En esta nota técnica, el autor presenta un método de cálculo general, el cual permite dimensionar un tanque dado, en función de los caudales de la bomba y del sistema, sin exceder el máximo número de arranques del motor por unidad de tiempo. El método propuesto permite dimensionar tanques más pequeños que los calculados por los métodos clásicos establecidos y disminuir también el tamaño de la bomba asociada, en razón al aumento del tiempo de operación de ésta. En el texto se presentan las ecuaciones propuestas, las figuras respectivas que ilustran la bondad del método y un ejemplo de cálculo de un par de tanques hidroneumáticos así dimensionados, los cuales se encuentran instalados y en servicio en una importante fábrica de vidrio flotado localizada en las afueras de la ciudad de Bogotá, Colombia. Finalmente, el resultado de este cálculo y las dimensiones finales de los tanques se comparan con las obtenidas por los métodos tradicionales y se concluye sobre su aplicabilidad.

Palabras clave: *tanques hidroneumáticos, capacidad, volumen.*

Introduction

The books and literature on fluid mechanics, as well as pumping installation manuals (see references: Fairbanks Morse Pump Corporation, 1998; Karassik, Messina, Cooper, & Heald, 2001), describe calculation and sizing methods for hydropneumatic tanks based on the Boyle-Mariott law for air compression and expansion at a constant temperature. The premise is that the flow volume supplied by the pump is twice that required by the system, which implies that the pump would function half of the operating time, thereby determining the size of the tank.

The objective of the method proposed in this technical note is to offer the designer of the hydraulic system the ability to determine the size of the tank according to the relation between the flow volumes of the pump and the system. If this relation is less than 2.0 (it should always be above 1.25), the size of the tank and the pump can be reduced, compensating the

system with a longer pump operating time. The method enables evaluating tanks of various sizes and pumps with different capacities in order to obtain the best relationship between investment cost and operating energy cost.

The method is based on two key equations. In the first, the continuous functioning time of the pump during the operating interval is established based on the relation between the flow volumes of the pump and the system, and considering the maximum number of starts per unit of time permitted by the electric drive motor. The second calculates the useful volume of water to be stored in the tank during one cycle according to the relation between flow volumes and total operating time. Then, based on maximum and minimum pressure established previously, and using the Boyle-Mariott model, the air volume required and the total volume of the tank are determined.

Permanent Flow Volume of the System and Pump Flow Volume

According to the requirements of the process, the user must determine the permanent flow volume of water, *Qs*, to be supplied to the system at the minimum pressure required. The minimum *Qs* will be equal to the continuous consumption of the system plus discontinuous or sporadic consumption, affected by the simultaneity factors of each installation.

In all cases, the nominal *Qb* supplied by the pump or pumps should be larger than *Qs*, such that a portion of *Qb* feeds the system and the remaining portion simultaneously feeds the hydropneumatic tank. In the case in which *Qb* is equal to *Qs*, the hydropneumatic tank would not be needed, since all of the water sent by the pump to the system would be continuously consumed by it.

In order to justify the need for a hydropneumatic tank for a determined installation, *Qb* would be at least of the order of 1.25 times the *Qs* at the minimum pressure required by the system. A good practice is for *Qb* to be equal to or larger than 1.5 times the flow volume of the *Qs* system.

The larger *Qb* is in comparison to *Qs*, the less the operating time of the pump over a time interval determined by the number of motor starts/h, and the larger the size of the hydropneumatic tank. When *Qb* is equal to 2*Qs*, the pump will operate half of the interval time and the other half of the time the flow volume will be supplied to the system by the hydropneumatic tank.

If the pump is centrifugal, a variation in the flow volume in function of pressure should be taken into account. In that case, for calculation purposes, the *Qb* value will be the average of the maximum and minimum flow volumes of the pump (*Q*max + *Q*min)/2, according to the range of pressures in which the pump is operating and the indications of the characteristic curve. If a positive displacement pump is used, *Qb* will be a fixed value, since with this type of pump the flow volume does not vary according to pressure.

Number of Starts of the Electric Motor

The maximum number of starts of the electric motor per unit of time depends on the size of the installation and the power required by the pumps. For calculation purposes, the values indicated in Table 1 will be used.

Table 1. Number of electric motor starts (Source: KSB, 1968).

Size of installation. Electric motor power	Maximum number of starts/hr
Small	15 to 30
Medium	8 to 12
Large	6 to 8

Calculation of the Time Interval and the Operating Time of the Pump

The operating time interval of the pump motor and hydropneumatic tank, jointly, will be *ti* (*h*) = 1/ no. starts/h and during time *ti* the pump will turn on once and operate for a time *tb*, such that *tb* < *ti*. During *tb*, the pump will supply both the *Qs* and the flow volume needed to complete the useful volume (*UV*) of the hydropneumatic tank, which will be discharged into the system once the pump stops and for a time equal to (*ti*-*tb*). *Qb* x *tb* = *Qs* x *ti*, therefore *tb* = *ti* x *Qs*/*Qb*, and with the flow volume relation *Qb*/*Qs* = *f*, we get:

$$tb = ti/f \qquad (1)$$

Figure 1 shows the variation in the operating time of the pump during the interval in function of the flow volume relation *f* = *Qb*/*Qs* and for different numbers of starts/h of the motor.

Pressure and Operating Volumes

The minimum and maximum operating pressures in the hydropneumatic tank were determined previously according to the characteristics of the system, and correspond to the pump's start-up and shut-off pressures, respectively.

The relation between the *P*min and *P*max pressures of the pump will depend on the specific velocity, such that both pressures will always be in the operating range of the characteristic curve, with acceptable efficiencies. If the pump speed is variable, the range of pressures will be larger. In general, for industrial installations, the difference between the minimum and maximum pressure does not exceed 2.5 bar (250 kPa) .

Figure 2 shows the partial volumes into which the hydropneumatic tank is divided for one complete cycle of total interval time *ti*, as described next.

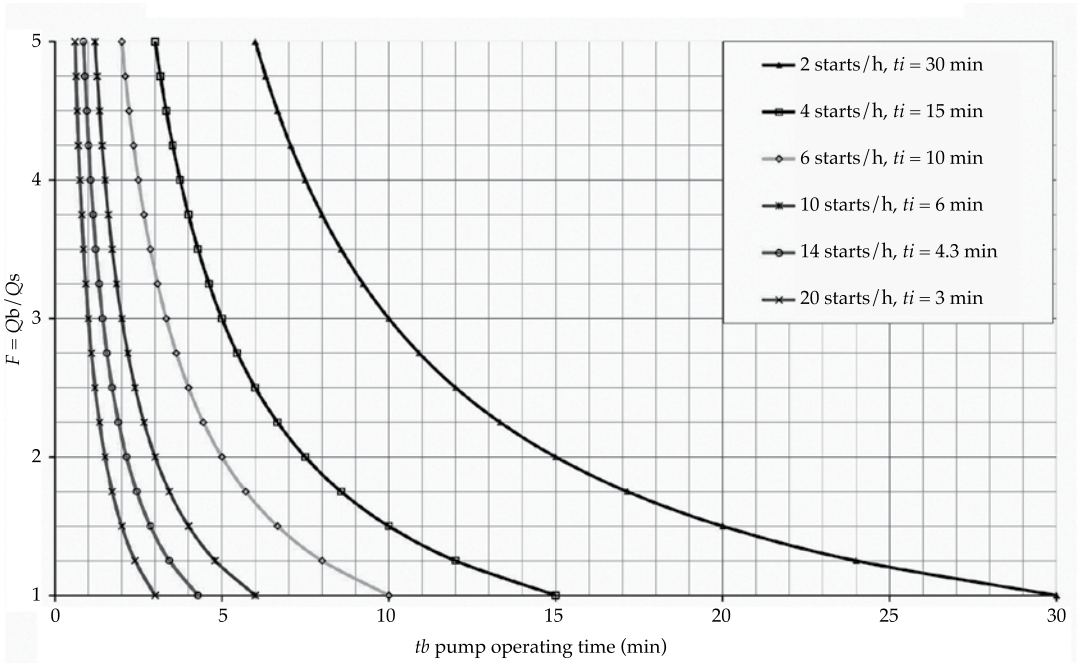

Figure 1. Operating time of the pump*tb* – *VS* - Flow volume relation *f* = *Qb*/*Qs*.

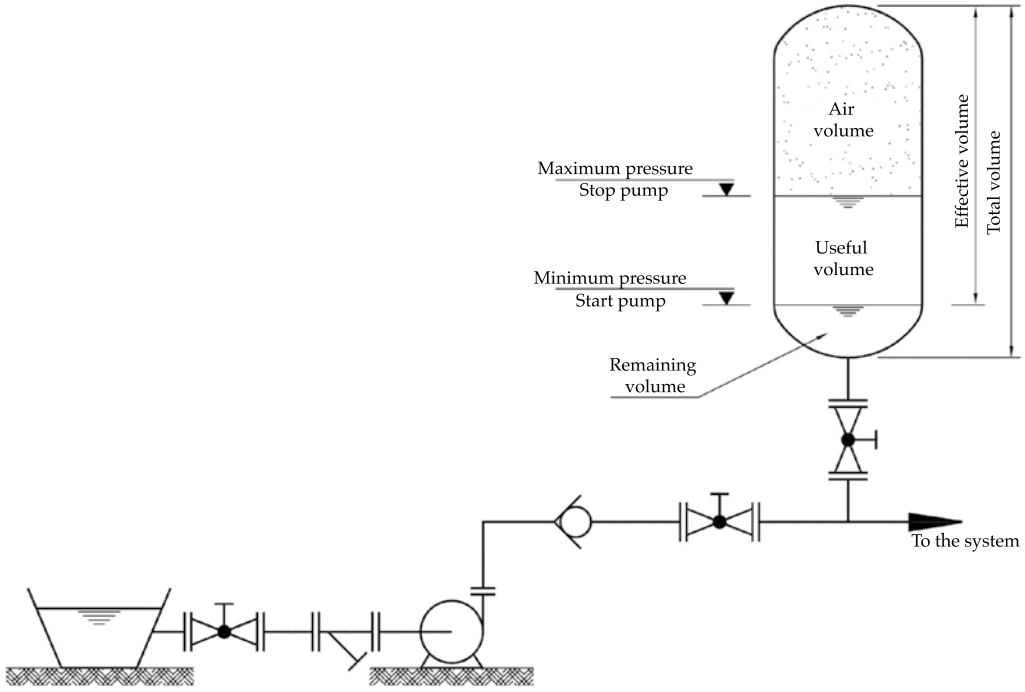

Figure 2. Single file diagram: hydropneumatic pump-tank.

Air Volume (AV) Under Pressure

The air volume under pressure is what determines the useful volume of the water and discharges it into the system after pumping stops.

The water is discharged as a result of the expansion of the air volume from *P*max to *P*min over time (*ti* - *tb*). In tanks without membranes, the air will dissolve slowly in the water and this volume will need to be recharged periodically.

Useful Volume (UV)

This is the volume stored in the tank during one cycle and will be fed to the system when the pump stops, that is during time (*ti* - *tb*).

Effective Volume (EV)

This is the variable volume during one cycle, that is, the sum of the AV at maximum pressure and the UV. At the end of the interval, the effective volume EV will be occupied only by the air at minimum pressure.

Remaining Volume (RV)

This is the safety volume that remains at the bottom of the tank and in the case of tanks without membranes, prevents the air from escaping into the system. RV should be > = 25% EV.

Total Volume (TV)

The total volume of the hydropneumatic tank will be the sum of EF + RV.

Calculation of the volume necessary to the well tank

Once the pump stops, the useful volume, UV, stored in the hydropneumatic tank will continue supplying the *Qs* flow volume during the remaining time (*ti* - *tb*) and :

$$UV = Qs\ ti - Qs\ tb \text{ de where } UV = Qs\ (ti - tb)$$

and according to equation (1) we have UV = *Qs* (*ti* – *ti*/*f*), from which:

$$UV = Qs\ ti\ (1 - 1/f) \quad (2)$$

and since *ti* is known and the flow volume relation $f = Qb/Qs$, the UV can be calculated. From Figure 3, UV/Qs can also be calculated in function of the operating time of the p ump and for different numbers of motor start-ups/h.

Calculation of Effective Volume

Considering the compression and decompression of the air to be isothermal and according to the Boyle-Mariott Law, it can be inferred that:

$AV\ (\ P\text{max} + P\text{bar}) = EF\ (P\text{min} + P\text{bar})$ and considering that $AV = (EV - UV)$ we have:

$$EF\ /\ UV = (P\text{max} + P\text{bar})/(P\text{max} - P\text{min}) \quad (3)$$

Figure 4 shows the variation in *EF*/*UV* in function of (*P*mad + *P*bar) and depending on the difference between the maximum and minimum pressures.

Calculation Example

A glass manufacturing plant has an industrial water supply system with design criteria and consumptions as follows:

- Continuous flow volume: 12.1 m^3/h – discontinuous flow volume = 20.37 m^3/h
- *Qs* defined = *Q* continuous x 1.15 + ½ x *Q*
- discontinuous = 24.1 m^3/h
- Installation site = Bogota, DC, at 2 650 masl.
- Barometric pressure = 0.72 bar (72 kPa).
- Pressures: *P*max = 5.0 bar (500 kPa), *P*min = 4.0 bar (400 kPa).

Pump Selected

- *Qb* = 36.15 m^3/h equivalent to 1.5 *Qs*. Average efficiency of the pump = 70%.
- Braking power kW = 9.81 x 36.15 m^3/h x 51.0 mcda/(1 000 x 0.7) = 25.83 kW = 34.62 Hp.

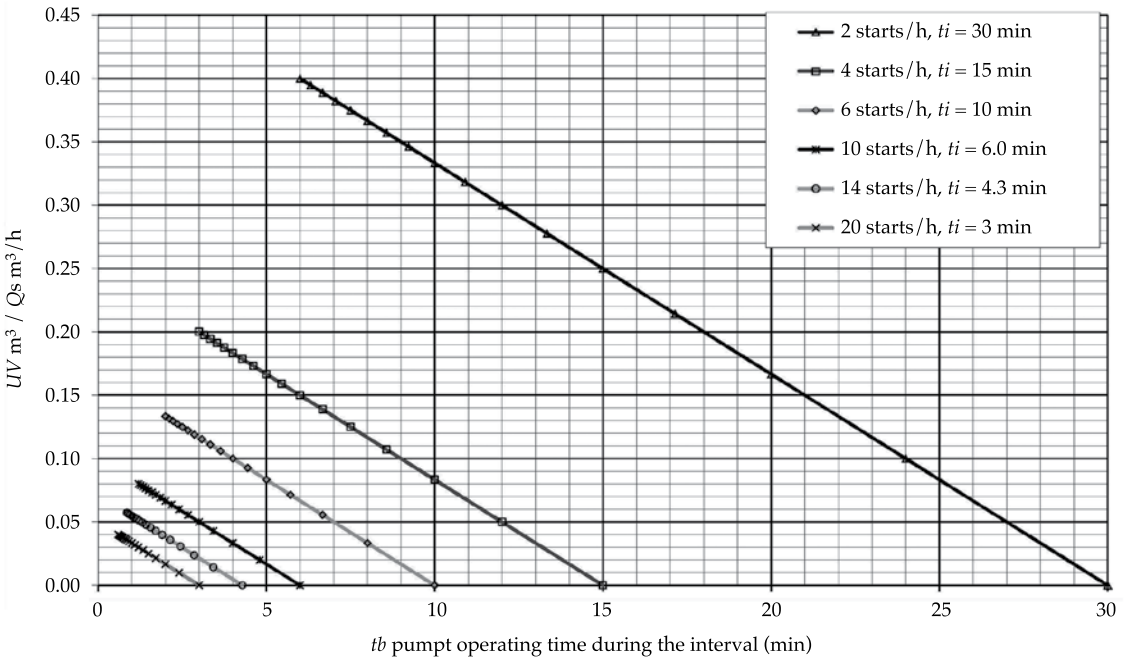

Figure 3. Useful volume of hydropneumatic tank.

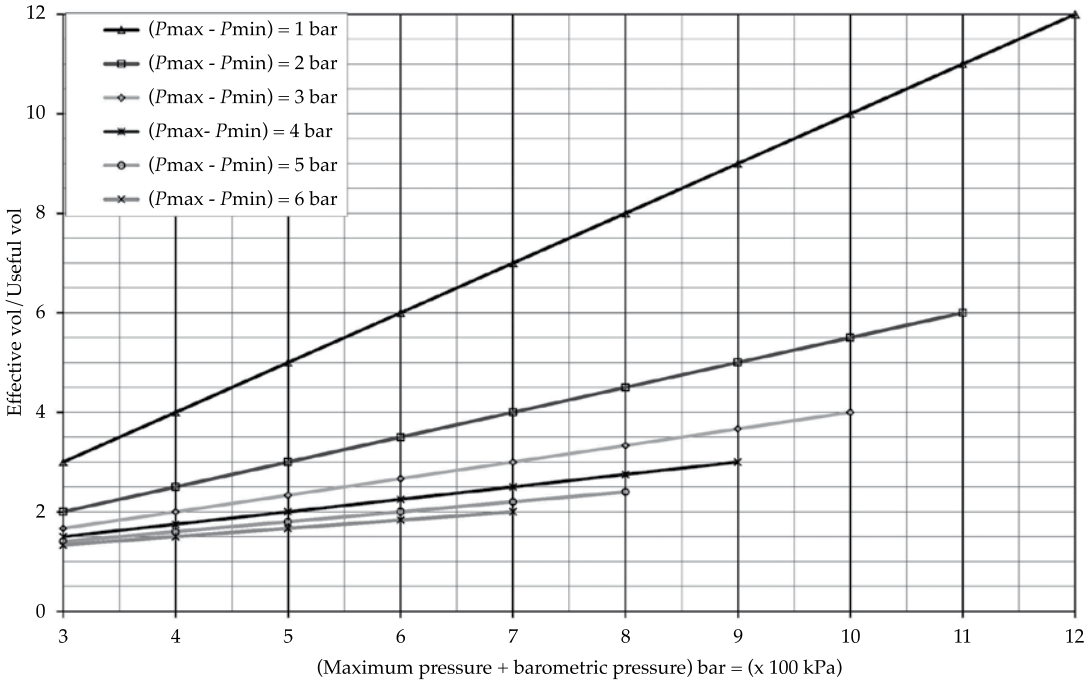

Figure 4. Effective volume of the hydropneumatic tank.

- Nominal power of the electric pump selected = 40 Hp.
- Potencia nominal del motor eléctrico seleccionado = 40 Hp.

Interval and Operating Time of the Pump

- Maximum number of starts/h = 10 (see Table 1 for mean power).
- Interval time *ti* = 1/no. of starts/h = 0.1 h = 6.0 min.
- Relation of flow volumes *f* = *Qb*/*Qs* = 36.15/24.1 = 1.5.
- *tb* = *ti*/*f* = 6.0 min/1.5 = 4.0 min (see equation (1) and/or Figure 1).

Calculation of Volumes

- Useful volume: UV = *Qs ti* (1 - 1/*f*) = 24.1 x 0.1 x (1 - 1/1.5) = 0.8 m^3 (see equation (2) and/or Figure 3).
- Effective volume: EV/UV = (*P*max + *P*bar)/(*P*max – *P*min) = (5.0 + 0.72)/(5.0 - 4.0) = 5.72, from which: *EF* = 5.72 x 0.8 = 4.58 m^3.
- Air volume under pressure: *AV* = *EV* – *UV* = 4.58 - 0.8 = 3.78 m^3.
- Remaining volume: RV = 0.25 x *EV* = 0.25 x 4.58 = 1.15 m^3.
- Total volume: Total V of the tank = EV + RV = 4.58 + 1.15 = 5.73 m^3.

Table 2 and Figure 5 present a sensitivity analysis of the size of the tank in function of *Qb*/*Qs*.

Considering the total calculated capacity, 5.73 m^3 (1 513.7 gallons), it was decided to install two tanks in parallel, each one with a total normalized capacity of 2.99 m^3 (792.0 gallons, tanks with normalized size, designed and manufactured according to ASME code (American Society of Mechanical Engineers).

Table 2: Example analysis of sensitivity of pump size.

$f = Qb/Qs$	$tb = ti / f$	$tb = 0.1/f$ in h	tb in min	UV in m³	EV in m³	AV in m³	RV in m³	Total V in m³
5.00	$ti/5.0$	0.020	1.20	1.93	11.03	9.10	2.76	13.79
4.00	$ti/4.0$	0.025	1.50	1.81	10.34	8.53	2.58	12.92
3.00	$ti/3.0$	0.033	2.00	1.61	9.19	7.58	2.30	11.49
2.00	$ti/2.0$	0.050	3.00	1.21	6.89	5.69	1.72	8.62
1.50	***ti*/1.5**	**0.067**	**4.00**	**0.80**	**4.60**	**3.79**	**1.15**	**5.73**
1.25	$ti/1.25$	0.080	4.80	0.48	2.76	2.28	0.69	3.45
1.00	$ti/1.0$	0.100	6.00	0.00	0.00	0.00	0.00	0.00

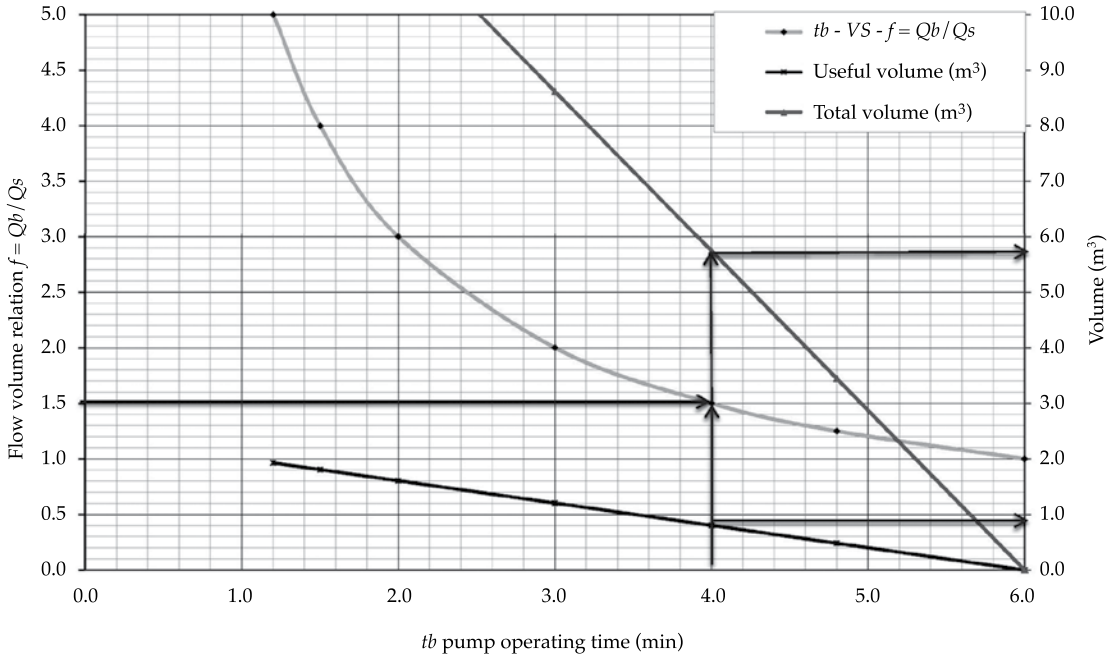

Figure 5. Example: sensitivity of the tank size.

Calculation of the Required Tank Capacity according to the Traditional Method and the Current State-of-Art

According to the KSB Centrifugal Pump Lexicon and the Pump Handbook (KSB, 1975), the total volume of the tank will be:

$$V = K \times 0.312 \times Qm/Z \times (P'a + Pb)/(P'a - P'e)$$

where:

V = volume in m³.

Qm = mean capacity of the pump m³/h = $(Q'e + Q'a)/2$ (noted as Qb in the previous pages).

Z = number of starts 1/h.

$Q'e$ = pump flow volume at minimum pressure m³/h.

$Q'a$ = pump flow volume at maximum pressure m³/h.

$P'a$ = maximum bar pressure.

$P'e$ = minimum bar pressure.

Pb = barometric bar pressure.

K = correction factor = 1.0 if $Q'a/Q'e < 0.5$, when applicable.

Since the mean flow volume of the pump $Qb/Qs = 2.0$, we have $Qb = Qm = 2.0 \times 24.1 = 48.2$ ^{3}/h and $V = 1.0 \times 0.312 \times 48.2 / 10 \times (5.0 + 0.72)/(5.0 - 4.0) = 8.6$ m^3.

Therefore, the total volume of the tank, of 8.6 m^3, calculated by the traditional method, corresponds to values indicated in Table 2 (8.62 m^3) and in Figure 5 for $Qb/Qs = 2.0$, as expected.

The value of 8.6 m^3 is 50% more than the value of 5.73 m^3, calculated using the proposed method, considering $Qb/Qs = 1.5$. The capacity (36.15 m^3/h) of the pump installed in the system is lower than the 48.2 m^3/h suggested by the traditional method.

Conclusions

The result of the calculation of the size of the hydropneumatic tank based on the relation Qb/Qs ranges from 1.25 to 2.0, without exceeding the maximum number of motor starts. This makes it possible to evaluate the benefit of decreasing the tank and pump sizes and thereby decreasing the initial investment cost in exchange for an increase in pump operating time during the cycle, and the corresponding increase in operating costs (energy). For Qb/Qs relations over 2.0, the tank and pump sizes increase notably, as well as the respective cost.

It can also be concluded that determining the capacity required of a given hydropneumatic tank based on the variation in Qb/Qs for a maximum start number represents a general calculation method, and the current state-of-art in which the fixed relation $Qb/Qs = 2.0$ is established is a particular case based on the method proposed in this technical note.

Received: 29/05/13
Accepted: 16/11/13

References

Fairbanks Morse Pump Corporation (1988). *Hydraulic Handbook*. Twelfth Edition. Kansas City: Fairbanks Morse Pump Corporation.

Karassik, I. J., Messina, J. P., Cooper, P. & Heald, C. C. (2001). *Pump Handbook*. Third Edition. New York: McGrow Hill.

KSB (1975). *Centrifugal Pump Lexicon*. Frankenthal, Germany: Klein, Schanzlin & Becker Aktiengesellschaft (KSB).

Figure 6. The author alongside the two 792 gallon tanks (2.99 m^3) cited in the example.

KSB (1968). *KSB Pump Handbook. New Edition.* Frankenthal, Germany: Klein, Schanzlin & Becker Aktiengesellschaft (KSB).

Institutional address of the author

Ing. Alfonso Herrán-Sandoval

Universidad Nacional de Colombia.
Ingeniero Asociado de Ingetec, S.A.
Carrera 6° # 30 A-30
Bogotá, D.C., Colombia
Teléfono: +57 (1) 3238 050, extensión 336
aherran@ingetec.com.co
aherrans@yahoo.com

Click here to write the autor

Measuring water quality, Verde River, Oaxaca, Mexico.

Photo: José Javier Sánchez Chávez.

Technical Note

Extension of Annual Runoff Volume Records Based on Regional Information and Ridge Regression

• Daniel Francisco Campos-Aranda •
Profesor jubilado de la Universidad Autónoma de San Luis Potosí, México
*Corresponding Author

Abstract

Campos-Aranda, D. F. (July-August, 2014). Extension of Annual Runoff Volume Records Based on Regional Information and Ridge Regression. *Water Technology and Sciences* (in Spanish), *5*(4), 167-179.

The planning, design and management of water infrastructure are typically based on available historical records of annual floods, runoff and rainfall. The more years covered by these records the more accurate the hydrological estimates. Therefore, it is always necessary to expand short records (*Y*), for example, through *multiple linear regression* (MLR), which uses available *regional* information. Establishing a MLR has several difficulties, perhaps the most important regarding the transport of hydrological information is the presence of correlation between the auxiliary or predictor variables (X_i), which gives rise to a problem of multicollinearity. In this work, the quantitative evaluation of multicollinearity is presented in detail through variance inflation factors and eigenvalues for the $\mathbf{X}' \cdot \mathbf{X}$ matrix. In addition, the biased or Ridge MLR is described extensively as a strategy to minimize the effects of multicollinearity, seeking its biasing parameter based on the Ridge trace. A numerical application is presented in detail, which expands the annual runoff volume records in the Santa Isabel gauging station in the upper Grijalva River using four broad records nearby. Lastly, several conclusions are formulated which highlight the advantages of using the Ridge MLR.

Keywords: Multicollinearity, variance inflation factors, eigenvalues, eigenvectors, upper Grijalva River.

Resumen

Campos-Aranda, D. F. (julio-agosto, 2014). Ampliación de registros de volumen escurrido anual con base en información regional y regresión de tipo Ridge. Tecnología y Ciencias del Agua, *5(4), 167-179.*

En general, la planeación, diseño y manejo de las obras de infraestructura hidráulica se realiza con base en los registros históricos disponibles de crecientes, escurrimientos y lluvias anuales. Conforme tales registros abarcan más años, sus estimaciones hidrológicas tienen una mayor exactitud. Por lo anterior, siempre es necesario ampliar los registros cortos (Y), por ejemplo a través de la regresión lineal múltiple (RLM), la cual utiliza la información regional disponible. El establecimiento de una RLM tiene varias dificultades, quizá la más importante en el transporte de información hidrológica sea la presencia de correlación entre los registros auxiliares o variables predictivas (X_i), lo cual da origen a un problema de multicolinealidad. En este trabajo se expone con detalle el diagnóstico cuantitativo de tal problema por medio de los factores de inflación de la varianza y de los eigenvalores de la matriz $\mathbf{X}' \cdot \mathbf{X}$*. También se describe ampliamente la RLM de tipo Ridge o sesgada como estrategia para minimizar los efectos de la multicolinealidad, buscando su parámetro de sesgo con base en la traza Ridge. Se detalla una aplicación numérica para ampliar el registro de volúmenes escurridos anuales en la estación hidrométrica Santa Isabel de la cuenca del Alto Río Grijalva, utilizando cuatro registros amplios cercanos. Por último se formulan las conclusiones, las cuales destacan las ventajas del uso de la RLM de tipo Ridge.*

Palabras clave: *multicolinealidad, factores de inflación de la varianza, eigenvalores, eigenvectores, alto río Grijalva.*

Introduction

In general, hydraulic works are planned, designed and operated based on the available historical records of hydrological data, primarily in relation to annual floods, runoff and rainfall. When only having small registries, the reliability of statistical calculations is low and, therefore, additional information and techniques to expand the available series are sought (Salas *et al.*, 2008). For the specific case of annual runoff, the most common source of additional data is large registries from nearby hydrometric stations, and multiple linear regression (MLR)

is the statistical technique most commonly used for what is called the *regional transport of hydrological information*.

With this approach, the small registry (Y) must have a period of information in common with the large series (X_i, *regressors*) and be dependent on or correlated with them to some degree. Once the equation is obtained and validated, the calculations that expand the small registry can be obtained based on the observed values of the regressors. This statistical technique is complex in only three aspects (Ryan, 1998): (1) selection of how many and which expanded and independent registries to use, (2) interpretation of the results, particularly the regression coefficients (β_i), and (3) determination of when a fitting method (as opposed to least squares of the residuals) should be used.

Since the small registry must be correlated with the auxiliary or nearby registries, is it logical to expect that they will also show a certain degree of dependency among themselves, since in addition to being close they are correlated with the dependent variables. The correlation between regressors implies that some portion of the statistical information contained in each one also is present in some of the other $i-1$ independent variables (Haan, 1977). This situation creates a multicollinearity problem due to the similarity or correlation between the registries involved. This problem must be diagnosed and resolved, for example, with the use of Ridge regression (Montgomery *et al.*, 1998; 2002).

The present work has three primary objectives: (1) describe the statistical theory related to MLR and its fitting with the least squares of the residuals ; (2) explain the concepts and quantitative diagnostics of multicollinearity and (3) demonstrate and apply the Ridge or biased regression as an efficient method to counteract the linear dependence between regressors. This work performs a numerical application with five hydrometric stations in the upper Grijalva River Basin in order to expand small registry of annual runoff volume from the Santa Isabel station. The results are compared with those obtained previously using the exhaustive selection of predictive variables.

Summary of the Operating Theory

Multiple Linear Regression (MLR) and its fit

A linear relationship can often be established between the dependent variable (Y) and various (p) independents, X_1, X_2,..., X_p, which is a generalization or natural expansion of the simple linear regression, expressed as (Ryan, 1998):

$$Y=\beta_0+\beta_1X_1+\beta_2X_2+\beta_3X_3\cdots+\beta_pX_p+\varepsilon \qquad (1)$$

As a result, the principles that govern the linear regression apply to the MLR. For example, both Y and X_i have normal distributions and the errors, ε, are independent and have mean-zero normal distributions and the same variance (σ^2) for each X_i. In general, the regression coefficients (β_i) are calculated by the fitting of the least squares of the residuals. This matricial solution for the MLR, in the general case of p independent variables or *regressors*, and n observations or Y, X_1, X_2,..., X_p data is (Ryan, 1998):

$$\mathbf{Y}=\mathbf{X}\cdot\boldsymbol{\beta}+\boldsymbol{\varepsilon} \qquad (2)$$

where:

$$\boldsymbol{Y}=\begin{bmatrix} Y_1 \\ Y_2 \\ \vdots \\ Y_n \end{bmatrix}, \quad \boldsymbol{X}=\begin{bmatrix} 1 & X_{11} & X_{21} & \cdots & X_{p1} \\ 1 & X_{12} & X_{22} & \cdots & X_{p2} \\ \vdots & \vdots & & \vdots & \vdots \\ 1 & X_{1n} & X_{2n} & \cdots & X_{pn} \end{bmatrix},$$

$$\boldsymbol{\beta}=\begin{bmatrix} \beta_0 \\ \beta_1 \\ \beta_2 \\ \vdots \\ \beta_p \end{bmatrix}, \quad \boldsymbol{\varepsilon}=\begin{bmatrix} \varepsilon \\ \varepsilon_2 \\ \vdots \\ \varepsilon_n \end{bmatrix}$$

This solution implies that the summation of 1 to *n* squared residuals must be minimized, that is:

$$\sum_{i=1}^{n}\varepsilon_i^2 = \sum_{i=1}^{n}\left(Y_i - \hat{Y}_i\right)^2$$

$$= \sum_{i=1}^{n}\left(Y_i - \beta_0 - \beta_1 X_{1i} - \beta_2 X_{2i} - \cdots - \beta_p X_{p\,i}\right)^2 = 0 \quad (3)$$

Then, differentiating the right side of the previous equation with respect to β_0, β_1, β_2,..., β_p produces the *normal* equations, a function of the unknown parameters. In matricial notation, these equations are:

$$\left(\mathbf{X}'\cdot\mathbf{X}\right)\cdot\hat{\beta} = \mathbf{X}'\cdot\mathbf{Y} \quad (4)$$

whose solution is:

$$\hat{\beta} = \left(\mathbf{X}'\cdot\mathbf{X}\right)^{-1}\cdot\left(\mathbf{X}'\cdot\mathbf{Y}\right) \quad (5)$$

In which **X′** is the transposed matrix of **X** and $(\mathbf{X}'\cdot\mathbf{X})^{-1}$ indicates the inverse of **X′ · X.**

Multiple Determination Coefficient

This is designated by R^2 and is probably the statistic most used to measure the suitability of a regression model. It indicates how much of the variance in Y is explained by the model. Therefore, its expression is (Hirsch *et al.*, 1993):

$$R^2 = \frac{SC_Y - SC_{Res}}{SC_Y} = 1 - \frac{\sum_{i}^{n}\left(Y_i - \hat{Y}_i\right)^2}{\sum_{1}^{n}\left(Y_i - \overline{Y}\right)^2} \quad (6)$$

in which $\hat{Y}_i$ is the calculation of variable Y_i using the regression equation. Therefore, SC_{Res} is the sum of the squares of the residuals and SC_Y is the total variance of the dependent variable, whose arithmetic mean is $\overline{Y}$.

Unit Length Scaling of the Data

Subtracting the arithmetic mean from each independent variable, or regressor, is known as the *center* of the data and its key advantage is that the matrices **X** with ***n*** rows now have *p* columns, given that the MLR equation is:

$$Y - \overline{Y} = \beta_1\left(X_1 - \overline{X_1}\right) + \beta_2\left(X_2 - \overline{X_2}\right)$$

$$+ \cdots + \beta_p\left(X_p - \overline{X_p}\right) \quad (7)$$

which rearranged to obtain equation (1) implies that:

$$\beta_0 = \overline{Y} - \beta_1\overline{X_1} - \beta_2\overline{X_2} - \cdots - \beta_p\overline{X_p} \quad (8)$$

Whose of the unit length scaling, in addition to the center, implies the division by the square root of the variance (Montgomery *et al.*, 2002), therefore:

$$E_{j\,i} = \frac{X_{j\,i} - \overline{X_j}}{S_j^{1/2}} \text{ con } i = 1,2,3,\ldots,n,\ j = 1,2,3,\ldots,p \quad (9)$$

$$Y_i = \frac{Y_i - \overline{Y}}{S_Y^{1/2}} \text{ con } i = 1,2,3,\ldots,n \quad (10)$$

Where:

$$S_j = \sum_{i=1}^{n}\left(X_{j\,i} - \overline{X_j}\right)^2 \quad (11)$$

$$S_Y = \sum_{i=1}^{n}\left(Y_i - \overline{Y}\right)^2 \quad (12)$$

In relation to equation (4), because of the unit length scaling of the **E′ · E** matrix becomes a simple correlation matrix among the regressors X_j. In addition, the **E′ · Y** is now a simple correlation matrix between each regressor X_j and the dependent variable Y. This scaling and the normal produce *standardized regression coefficients* where the comparison of regressors defines the importance of each one.

Another scaling that is often required is associated with the numerical stability of the

inverse matrix **E′ · E**, since it is common to obtain with **A · A**–1 = **I.** When transforming matrix **A** into the identity matrix **I** and performing the same operations with **I**, this becomes the matrix $\mathbf{A}^{-1}$ which was sought. When matrix **A** has very large elements, its inverse will present very small elements and then the rounding errors become important. In these cases, it is useful to divide (*scale*) all the data by a fixed amount or reducer quotient (RQ) before applying equation (5), and then multiply the results from equation (1) by the RQ.

Multicollinearity: Definition and Solutions

As was already indicated, in the case of an expansion of the hydrological registry based on the available *regional* information, the set of data will always show a certain degree of multicollinearity, unless the columns in matrix **X** are orthogonal; that is, if **X′ · X** were a diagonal matrix, which will only occur in an experimental design (Montgomery *et al.*, 1998; 2002). Where $\mathbf{X}_j$ is the *nth* column in matrix **X**, the *multicollinearity* is formally defined as the linear dependence among those columns, that is, a set of constants $t_1, t_2,..., t_p$, not all zero, such that:

$$\sum_{j=1}^{p} t_j \cdot \mathbf{X}_j = 0 \qquad (13)$$

If the above equation is exactly valid for a subset of the columns in **X,** the range of the matrix **X′ · X** will be less than p and then $(\mathbf{X}' \cdot \mathbf{X})^{-1}$ will not exist. When equation (13) is valid, multicollinearity will exist only approximately, that is, matrix **X′ · X** will present certain degree of deterioration. In general, when the least squares of the residuals method is applied to data presenting multicollinearity, the calculation of the regression coefficients will not be reliable, since the absolute value will be overestimated and unstable.

There are three basic techniques to address multicollinearity (Ryan, 1998; Montgomery *et al.*, 1998):

1. Obtain more data, which may not be possible and the new data would likely reflect the behavior of the previous ones.
2. Specify the model again, redefining the regressors. For example, if X_1, X_2 and X_3 are linearly dependent, a function of those of the type $X = (X_1 + X_2)/X_3$ can be adopted, or $X = X_1 \cdot X_2 \cdot X_3$, which preserves the contents of the information in the original regressors while reducing the deterioration of the data resulting from multicollinearity. Another very effective re-specification method is to eliminate one or more variables or regressors, which definitively reduces multicollinearity but may notably damage the predictive capacity of the model.
3. Obtain biased estimates such as the Ridge regression.

Quantitative Diagnostics of Multicollinearity based on $(E' \cdot E)^{-1}$

The simplest way to identify multicollinearity is by inspecting the **E′ · E** matrix, in which the elements that are outside the main diagonal correspond to simple correlation coefficients between regressor pairs. Then, if absolute values over 0.80 exist, there is a dependency between the pair. This method only detects multicollinearity but does not quantify it. Rather, when the variance inflation factors (VIF) are greater than 10 the regression coefficients obtained with equation (5) are not reliable because of collinearity. The VIF expression is (Montgomery *et al.*, 1998; 2002):

$$\mathrm{VIF}_j = C_{jj} = \frac{1}{\left(1 - R_j^2\right)} \qquad (14)$$

where R_j^2 is the determination coefficient resulting from the MLR between the regressor X_j as the dependent variable and the rest, p – 1, as regressors. VIF_j corresponds to the main diagonal in the inverse matrix **E′ · E**.

Quantitative Diagnostics of Multicollinearity based on Eigenvalues

The eigenvalues of the matrix $\mathbf{E}' \cdot \mathbf{E}$ are designated by $\lambda_1, \lambda_2, \lambda_3, \ldots, \lambda_p$. These are also known as own values and correspond to the roots of the characteristic equation INSERTAR ECUACIÓN of matrix **A**. They are obtained using numerical methods, for example, the powers method (Carnahan *et al.*, 1969). If one or more nearly linear dependencies exist in the data, one or more of the eigenvalues will be small. The *condition number* κ of matrix $\mathbf{E}' \cdot \mathbf{E}$ is defined as (Montgomery *et al.*, 1998; 2002):

$$\kappa = \frac{\lambda_{máx}}{\lambda_{mín}} \qquad (15)$$

and represents the range of variation in the eigenvalues of matrix $\mathbf{E}' \cdot \mathbf{E}$. In general, when κ is less than 100, there are virtually no multicollinearity problems. When it increases from 100 to 1 000 there is a moderate to strong multicollinearity problem and when over 1 000 there will certainly be serious problems associated with it. The *condition indices* κ_j of matrix $\mathbf{E}' \cdot \mathbf{E}$ are:

$$\kappa_j = \frac{\lambda_{máx}}{\lambda_j} \quad \text{with} \quad j = 1,2,3,\ldots, p \qquad (16)$$

The values of κ_j define the number and magnitude of the linear dependencies existing among the data. In addition, with the eigenvectors associated with each eigenvalues, the linear dependency that exists among the regressors can be established, as shown in the numerical application.

Ridge Regression

El método de mínimos cuadrados de los resi- The method of least squares of the residuals ensures that the variance in calculation $\hat{\beta}$ (equation (5)) is minimum, but the multicollinearity generates a very large variance and, therefore, the calculations are unstable. Assuming that a biased estimator of $\hat{\beta}^*$ can be obtained that has a much smaller variance, then a small amount of bias in $\hat{\beta}^*$ can be accepted, in which case the quadratic mean error of $\hat{\beta}^*$ is less than the variance of the unbiased $\hat{\beta}$ estimator. The lower variance of the biased estimator implies that $\hat{\beta}^*$ is a more stable estimator of β than unbiased $\hat{\beta}$.

Various procedures have been developed to obtain biased estimators of regression coefficients β. One of those is the *Ridge regression*, or crest, proposed in the early 1970s by Hoerl and Kennard (1970). It is named for the similarity between its mathematical operations and those of the Ridge analysis used to describe the second order response behavior of surfaces. The Ridge estimator $\hat{\beta}_R$ is obtained by solving a slightly modified version of the normal equations, expressed as equations (4) and (5). This is (Montgomery *et al.*, 1998; 2002):

$$\left(\mathbf{E}' \cdot \mathbf{E} + k \cdot \mathbf{I}\right) \cdot \hat{\beta}_R = \mathbf{E}' \cdot \mathbf{Y} \qquad (17)$$

therefore:

$$\hat{\beta}_R = \left(\mathbf{E}' \cdot \mathbf{E} + k \cdot \mathbf{I}\right)^{-1} \cdot \left(\mathbf{E}' \cdot \mathbf{Y}\right) \qquad (18)$$

In the above expressions, the constant $k \geq 0$, called the *bias parameter*, is selected during the process of applying the Ridge regression. In reality, the Ridge estimator is a linear transformation of the estimator of the least squares of the residuals, whose bias increases as k increases, while at the same time the variance decreases. With the Ridge regression, a stable estimate of the coefficients is obtained in exchange of it not being best fitted to the data and, therefore, there is no conclusive mathematical demonstration of regression equations that function better than the least squares of the residuals to predict future observations.

Hoerl and Kennard (1970) suggest that a suitable value of k can be calculated by inspecting the *Ridge trace*. This is a graph of the

magnitudes of $\hat{\beta}_R$ plotted on the ordinates versus the respective values of k on the abscissas. The values of k usually fall within the interval of 0 to 1. If the multicollinearity is serious, the $\hat{\beta}_R$ coefficients will vary a large amount, but they stabilize within a certain value of k, whereas the $\hat{\beta}_R$ are already stable. Thus a regression equation with a lower mean square error than that of the least squares can be obtained.

Numerical Application

Data from the Upper Grijalva River

Figure 1 shows the location of five basins corresponding to hydrometric stations Santa Isabel, La Escalera, El Boquerón II, Las Flores II and Santa María, in Hydrological Region 30 (Grijalva and Usumacinta Rivers). Their general data is shown in Table 1. Overall, this numerical application expands the small Santa Isabel registry using the Ridge regression based on the other four large registries. This calculation was already performed (Campos, 2012) with the method to select predictive variables.

In the BANDAS system (IMTA, 2002), Campos (2012) compiled the available data for annual runoff volume (Mm^3) from the stations cited and calculated the monthly missing values for incomplete years to determine the magnitude of the annual missing values during the period in common (1956-1973). Campos also established 1974 to 1994 as the expansion period. These data are presented in Table 2. Lastly, this author proved that the data did not have deterministic components and verified its origin from a normal distribution using the Shapiro and Wilk test (Shapiro, 1998).

Diagnostics of Multicollinearity

The matrices $\mathbf{E'} \cdot \mathbf{E}$, $\mathbf{E'} \cdot \mathbf{Y}$ and $(\mathbf{E'} \cdot \mathbf{E})^{-1}$ obtained for the data in Table 1, processed logically with unit scaling and subroutines for the multiplication and inversion of matrices developed *ex professo* are:

$$\mathbf{E'} \cdot \mathbf{E} = \begin{array}{c} \begin{matrix} X_1 & X_2 & X_3 & X_4 \end{matrix} \\ \begin{bmatrix} 1.000000 & 0.706983 & 0.522109 & 0.409604 \\ 0.706983 & 1.000000 & 0.867273 & 0.759131 \\ 0.522109 & 0.867273 & 1.000000 & 0.911521 \\ 0.409604 & 0.759131 & 0.911521 & 1.000000 \end{bmatrix} \end{array} \begin{matrix} X_1 \\ X_2 \\ X_3 \\ X_4 \end{matrix}$$

$$\mathbf{E'} \cdot \mathbf{Y} = \begin{bmatrix} 0.742823 \\ 0.651777 \\ 0.576905 \\ 0.365996 \end{bmatrix} \begin{matrix} X_1 \\ X_2 \\ X_3 \\ X_4 \end{matrix}$$

$$(\mathbf{E'} \cdot \mathbf{E})^{-1} = \begin{bmatrix} 2.175362 & -2.174041 & 0.340291 & 0.449162 \\ -2.174041 & 6.304874 & -4.623234 & 0.318447 \\ 0.340291 & -4.623233 & 10.405540 & -6.114622 \\ 0.449162 & 0.318447 & -6.114621 & 6.147887 \end{bmatrix}$$

The inspection of the $\mathbf{E'} \cdot \mathbf{E}$ matrix shows that only two important correlations exist: the larger ($r_{xy} = 0.9115$), between X_3 and X_4, and the smaller ($r_{xy} = 0.8673$), between $X2$ and X_3. Therefore, a multicollinearity problem is detected in the data, but it may be acceptable or moderate. In relation to the vector $\mathbf{E'} \cdot \mathbf{Y}$, none of the correlations are significant and they decrease as the distance of the hydrometric stations from the Santa Isabel station increases (see Figure 1).

The quantitative diagnostics of the multicollinearity is shown in Table 3. The first row of results corresponds to the values of the variance inflation factors (VIF_j) and are the elements of the main diagonal of the inverse matrix of $\mathbf{E'} \cdot \mathbf{E}$. Since the largest magnitude of the VIF_j rarely exceeds 10, an acceptable multicollinearity is found. In addition, since none of the condition indices (κ_j) exceed 100, then the problems associated with multicollinearity will not be serious, which affirms the previous conclusion.

Based on the elements of the fourth eigenvector, which corresponds to the smallest eigenvalues, the following equation (13) is established, relative to the multicollinearity present:

$$-0.0629 \cdot X_1 + 0.3877 \cdot X_2 - 0.7862 \cdot X_3 + 0.4771 \cdot X_4 = 0 \qquad (19)$$

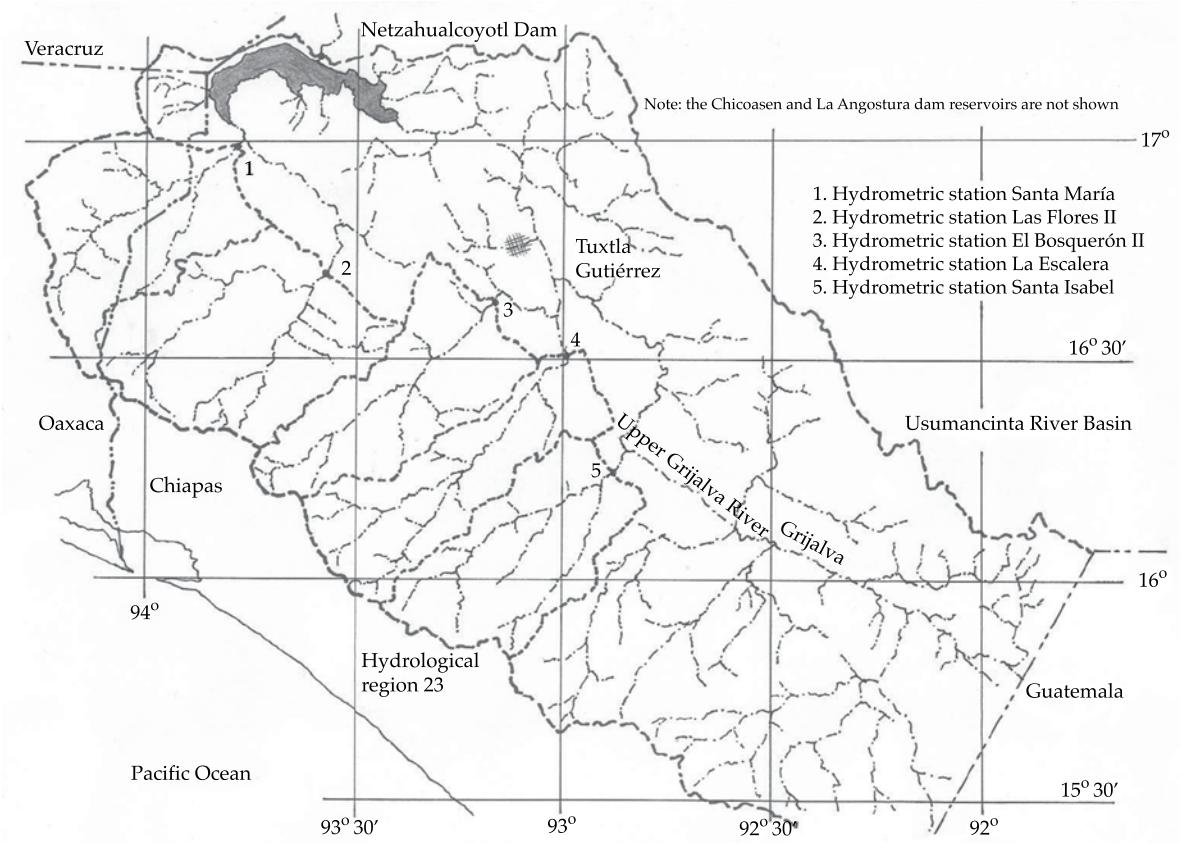

Figure 1. Geographic location of the five hydrometric stations processed, Upper Grijalva River.

Table 1. Overall characteristics of the hydrometric stations used in the Upper Grijalva River basin.

Name	Code*	Gauged river	Lat N	Long WG	Basin Area (km²)	Registry (missing years)
Santa Isabel	30053	El Dorado	16° 16′	92° 53′	1 873	1956-1973 (0)
La Escalera	30041	Santo Domingo	16° 32′	92° 57′	1 808	1954-2002 (4)
El Boquerón II	30020	Suchiapa	16° 40′	93° 09′	1 870	1949-2002 (6)
Las Flores II	30072	Zoyatenco	16° 42′	93° 33′	2 551	1962-2002 (5)
Santa María	30071	Encajonado	16° 57′	93° 46′	1 958	1962-2001(13)

* According to *BANDAS* system.

considering that the coefficient of X_1 is close to zero, we get:

$$0.3877 \cdot X_2 + 0.4771 \cdot X_4 \cong 0.7862 \cdot X_3 \qquad (20)$$

$$X_3 \cong 0.4931 \cdot X_2 + 0.6068 \cdot X_4 \qquad (21)$$

The above equation establishes the approximate relation of X_3 with X_2 and X_4.

Calculation and Analysis of the Ridge Trace

The application of equation (18) based on a computer program developed *ex professo*, which uses the *k* values indicated in Table 4, resulted in

Table 2. Annual runoff volumes (Mm3) and their statistical parameters at the hydrometric stations inidcated in the Upper Grijalva River Basin.

No	Year	Santa Isabel (Y)	La Escalera (X_1)	El Boquerón II (X_2)	Las Flores II (X_3)	Santa María (X_4)
1	1956	1 113.119	524.303	700.426	617.200	1 348.100
2	1957	846.957	343.245	327.830	195.700	829.200
3	1958	1 134.394	759.834	576.979	477.500	1 176.100
4	1959	748.138	538.022	456.217	340.900	1 008.000
5	1960	1 259.572	831.507	544.870	441.200	1 131.400
6	1961	876.884	555.208	340.309	209.800	846.500
7	1962	1 345.812	700.956	594.985	528.749	780.873
8	1963	1 151.548	793.521	519.857	509.515	1 062.852
9	1964	1 103.385	809.059	572.255	428.682	1 040.491
10	1965	1 227.758	619.464	424.201	311.510	926.283
11	1966	671.762	612.066	543.392	400.731	1 234.455
12	1967	629.364	302.969	337.493	319.296	820.282
13	1968	863.049	443.917	327.265	245.051	886.820
14	1969	1 071.681	872.190	702.579	654.717	1 475.765
15	1970	1 182.934	636.918	674.119	971.609	2 071.694
16	1971	1 131.230	737.992	707.531	499.456	1 156.651
17	1972	627.775	313.800	287.889	244.434	823.366
18	1973	1 183.812	701.963	800.585	800.408	1 714.570
1	1974	–	270.474	431.411	447.160	1 185.743
2	1975	–	285.090	429.059	258.044	1 006.232
3	1976	–	219.347	280.568	127.823	852.063
4	1977	–	272.813	253.843	95.508	710.200
5	1978	–	563.517	609.759	288.524	1 018.654
6	1979	–	286.202	371.625	318.484	1 124.668
7	1980	–	590.997	552.401	1 312.039	2 438.163
8	1981	–	844.403	729.838	659.665	1 516.715
9	1982	–	662.449	442.376	190.252	954.137
10	1983	–	436.859	545.409	395.663	874.889
11	1984	–	600.143	572.296	522.289	1 250.051
12	1985	–	434.315	392.148	190.942	736.901
13	1986	–	409.003	424.557	234.945	794.653
14	1987	–	298.749	334.747	143.007	764.274
15	1988	–	618.826	671.978	731.723	1 318.376
16	1989	–	601.612	738.056	662.633	988.181
17	1990	–	393.349	437.495	253.685	791.806
18	1991	–	177.277	257.679	137.659	751.560
19	1992	–	612.984	432.906	162.104	843.562
20	1993	–	414.408	504.291	375.818	1 096.850
21	1994	–	153.414	230.450	73.578	657.381
Maximum		1 345.812	872.190	800.585	1 312.09	2 438.163
Minimum		627.775	153.414	230.450	73.578	657.381
$\overline{X}$		1 009.399	519.055	489.274	404.564	1 077.14
S		229.553	202.140	154.990	257.809	369.465
Cv		0.227	0.389	0.317	0.637	0.343
Cs		–0.509	–0.040	0.179	1.447	1.953
Ck		2.377	2.141	2.240	6.014	7.703
r_1		–0.196	0.216	–0.103	0.229	0.175

Table 3. Results of the diagnostics of the multicollinearity of the data from the Upper Grijalva River.

Indicators	Regressors			
	X_1	X_2	X_3	X_4
VIF_j	2.17536	6.30487	10.40554	6.14789
λ_j	3.11744	0.67478	0.14690	0.06089
$\kappa_j = \lambda_{max}/\lambda_j$	1.000	4.620	21.222	51.198
Regressors	**Eigenvectors**			
X_1	0.4096	0.8201	0.3946	–0.0629
X_2	0.5377	0.1170	–0.7395	0.3877
X_3	0.5380	–0.2964	–0.0679	–0.7862
X_4	0.5036	–0.4753	0.5411	0.4771

the Ridge regression coefficients concentrated there. Their corresponding determination coefficients (R^2) are also shown in this table. The calculation of R^2 was performed by centering of data and using an RQ = 500. The Ridge trace (Figure 2) was constructed based on the results from Table 4.

The study of the Ridge trace shows that only the regression coefficient of the X_1 variable —that is, for the hydrometric station La Escalera— is stable. Those for Las Flores II (X_3) and Santa María (X_4) vary greatly and in a similar manner. Lastly, the coefficient for El Boquerón II (X_2) varies less, but its sign also changes. In order to establish the lowest value of the bias parameter (k), the coefficients in the Ridge trace are accepted to be stable at 0.25, and more properly at 0.35.

Ridge Calculations and its Contrast

Table 5 shows the 18 calculations of the dependent variables ($\hat{Y}_i$), that is, the historical record from the Santa Isabel hydrometric station for the period 1956 to 1973, as well as the corresponding residuals. These were performed using Ridge regressions with k = 0.250 and 0.350. The respective regression coefficients are shown in Table 6 and were obtained with centered data and based on a RQ of 500.

Table 6 shows the comparison between the residuals from the two best regression models obtained with the selection of predictive variables (Campos, 2012) and the Ridge regressions adopted. The Ridge regression results in slightly larger values than the negative residuals and few are less than the positive residuals. The sum of the squared residuals is larger since it is not the best fit to the data, but the algebraic sum of errors is smaller.

Ridge Calculations Adopted

Lastly, Table 7 presents the 21 annual runoff volumes calculated for the Satna Isabel hydrometric station for the period 1974 to 1994 using the adopted Ridge regressions, as well as their respective statistical parameters.

Figure 3 compares the second series of annual runoff volumes calculated with the Ridge regression with the values adopted based on the selection of predictive variables (Campos, 2012). It can be seen that the behavior is the same for both series, but the one from the Ridge regression is larger and has smaller maximum values, resulting in a mean value of 862.3 Mm3 and a variation coefficient of 0.223. These data are more similar to the historical data for Santa Isabel (mean of 1 009.4 Mm3 and variation coefficient of 0.227) than those obtained with the selection of regressors (831.1 Mm3 and 0.293, respectively).

Conclusions

The Ridge regression is a direct procedure that can be easily implemented with the solution of the least squares of the residuals (equations (5)

Table 4. Ridge coefficient regressions ($\hat{\beta}_R$) obtained for the values of the bias parameter indicated.

$\hat{\beta}_R$	**Values of the bias parameter (*k*)**							
	0.000	**0.005**	**0.010**	**0.020**	**0.030**	**0.040**	**0.050**	**0.075**
β_1	0.5596	0.5533	0.5476	0.5378	0.5294	0.5219	0.5152	0.5003
β_2	-0.0562	-0.0266	-0.0018	0.0376	0.0671	0.0898	0.1077	0.1386
β_3	1.0045	0.9334	0.8724	0.7731	0.6958	0.6340	0.5835	0.4903
β_4	-0.7363	-0.6878	-0.6457	-0.5760	-0.5204	-0.4749	-0.4369	-0.3638
R^2	0.6892	0.6891	0.6890	0.6885	0.6878	0.6870	0.6861	0.6834
$\hat{\beta}_R$	**Values of the bias parametero (*k*)**							
	0.100	**0.120**	**0.150**	**0.180**	**0.200**	**0.250**	**0.300**	**0.350**
β_1	0.4873	0.4778	0.4646	0.4523	0.4446	0.4267	0.4105	0.3963
β_2	0.1576	0.1678	0.1781	0.1845	0.1874	0.1915	0.1930	0.1929
β_3	0.4267	0.3887	0.3457	0.3138	0.2968	0.2641	0.2409	0.2236
β_4	-0.3110	-0.2781	-0.2388	-0.2079	-0.1907	-0.1560	-0.1294	-0.1084
R^2	0.6805	0.6782	0.6746	0.6711	0.6689	0.6633	0.6580	0.6530

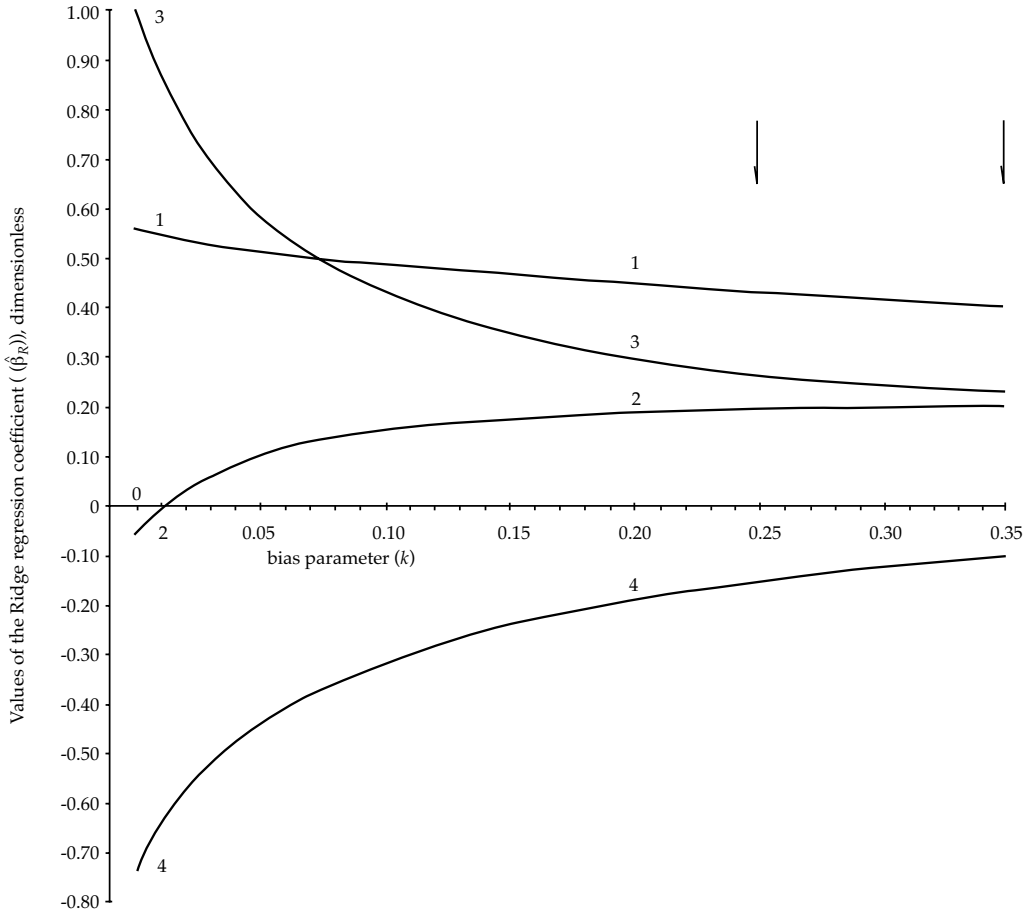

Figure 2. Ridge trace for the data from the Upper Grijalva River.

Table 5. Calculations (Mm^3) of the dependent variable ($\hat{Y}_1$) obtained with the Ridge regressions and their corresponding residuals.

Year	$k = 0.250$	Residual	$k = 0.350$	Residual
1956	1 025.148	87.971	1 027.709	85.410
1957	730.486	116.471	740.300	106.657
1958	1 108.431	25.963	1 106.384	28.010
1959	913.045	-164.907	917.222	-169.084
1960	1 136.477	123.095	1 132.984	126.588
1961	866.418	10.466	871.102	5.782
1962	1 214.719	131.093	1194.033	151.779
1963	1 167.052	-15.504	1 155.790	-4.242
1964	1 146.003	-42.618	1 140.809	-37.424
1965	961.314	266.444	961.738	266.020
1966	949.722	-277.960	958.822	-287.060
1967	783.116	-153.752	784.173	-154.809
1968	805.278	57.771	811.278	51.771
1969	1 225.672	-153.990	1 222.444	-150.763
1970	1 099.002	83.932	1 101.088	81.846
1971	1 140.574	-9.344	1 139.339	-8.109
1972	734.440	-106.665	740.087	-112.312
1973	1 162.270	21.542	1 163.875	19.937
Maximum	1 225.672	266.444	1 222.444	266.020
Minimum	730.486	-277.960	730.300	-287.060

Table 6. Indicators of the residuals obtained with the best least squares models and the Ridge regression.

Model analyzed	Regression coefficients					Residual values			
	β_0	β_1	β_2	β_3	β_4	Minimum	Maximum	$\sum_{i=1}^{18} e_i$	$\sum_{i=1}^{18} e_i^2$
$Y = f(X_1, X_3, X_4)$	648.9886	0.6939	–	1.0636	-0.4884	-225.249	269.998	0.298	278 905.4
$Y = f(X_1, X_2, X_3, X_4)$	657.9566	0.7188	-0.0818	1.1091	-0.4903	-220.896	267.891	0.347	278 457.1
Ridge with $k = 0.250$	1.128022	0.61220	0.20869	0.58922	-0.27422	-277.960	266.444	0.006	301 594.6
Ridge with $k = 0.350$	1.111032	0.58847	0.23013	0.51196	-0.23256	-287.060	266.020	-0.003	310 879.8

and 18)); and the interpretation and use of the Ridge trace present no difficulties.

In relation to the problems related to fitting caused by multicollinearity, there is consensus in recommending that it is better to use some of the statistical information from all the regressors, as is done with the Ridge regression, rather than using all the information from some regressors and none from others, as in the method to select predictive variables.

With respect to the numerical application described, a problem previously addressed by eliminating variables, the results of the Ridge regression are quite similar (see Figure 3), but closer to the historical statistical parameters for the Santa Isabel station (Table 2).

Finally, in terms of problems with the six or seven widely available registries, as is common

Table 7. Calculated annual runoff volumes (Mm3) for the Santa Isabel station using the Ridge regression.

Year	$k = 0.250$	$k = 0.350$	Year	$k = 0.250$	$k = 0.350$
1974	757.946	767.132	1988	1 152.709	1 142.331
1975	704.198	720.120	1989	1 205.796	1 188.828
1976	598.509	616.445	1990	828.465	833.405
1977	645.525	658.206	1991	601.333	614.829
1978	926.913	938.268	1992	893.815	902.676
1979	696.028	710.956	1993	843.611	852.755
1980	1 145.583	1 135.113	1994	596.110	583.616
1981	1 206.035	1 205.375	Mzx	1 206.035	1 205.375
1982	912.337	922.659	Min	569.110	583.616
1983	938.495	937.210	$\overline{X}$	856.160	862.282
1984	1 015.802	1 017.064	S	200.618	192.259
1985	822.168	827.724	Cv	0.234	0.223
1986	823.526	829.383	Cs	0.420	0.396
1987	691.446	703.830	Ck	2.580	2.566

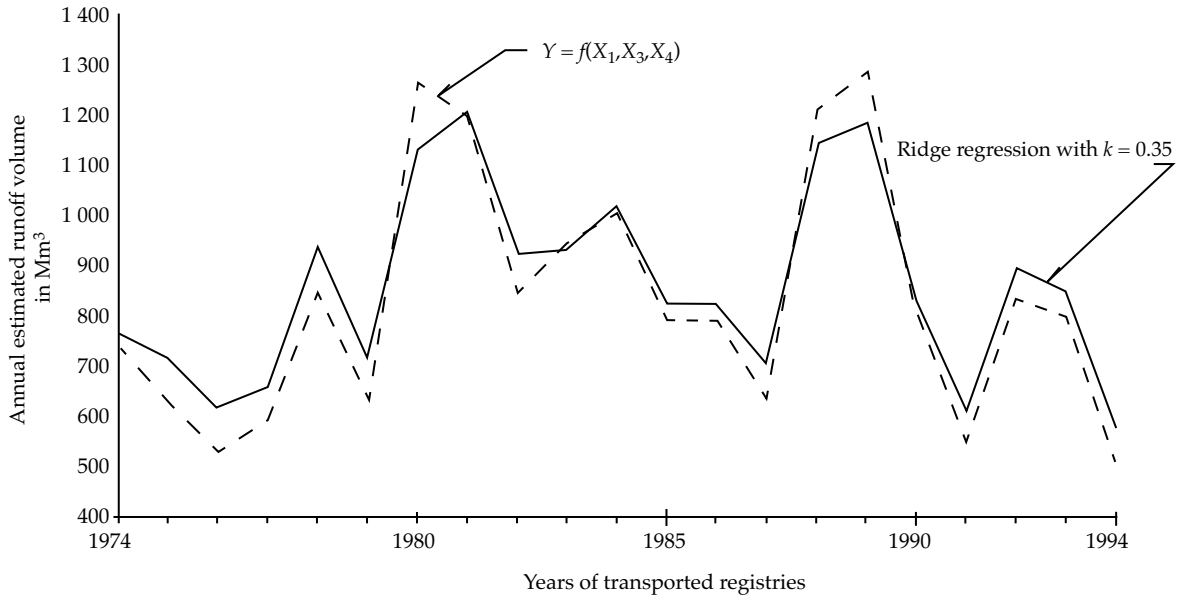

Figure 3. Comparison of calculations for the Santa Isabel hydrometric station, Upper Grijalva River.

when transporting annual rainfall registries, the Ridge regression is a better option than inspecting 64 or 128 possible models obtained by the least squares of the residuals, as shown by the scheme to eliminate predictive variables.

Received: 26/12/12
Accepted: 09/01/14

References

Campos-Aranda, D. F. (2012). *Ampliación de registros de volumen escurrido anual a través de Regresión Lineal Múltiple, con selección de variables predictivas*. XXII Congreso Nacional de Hidráulica. Tema: Aprovechamiento Integral de Cuencas, Ponencia 29, del 7 al 9 de noviembre, Acapulco, Guerrero.

Carnahan, B., Luther, H. A., & Wilkes, J. O. (1969). Matrices and Related Topics. Chapter 4. In *Applied Numerical Methods* (pp. 210-268). New York: John Wiley & Sons.

Haan, C. T. (1977). Multivariate Analysis. Chapter 12. In *Statistical Methods in Hydrology* (pp. 236-262). Ames, USA: The Iowa State University Press.

Hirsch, R. M., Helsel, D. R., Cohn, T. A., & Gilroy, E. J. (1993). Statistical Analysis of Hydrologic Data. Chapter 17. In D. R. Maidment (Ed.), *Handbook of Hydrology* (pp. 17.1-17.55). New York: McGraw-Hill, Inc.

Hoerl, A. E., & Kennard, R. W. (1970). Ridge Regression: Biased Estimation for Nonorthogonal Problems. *Technometrics*, *12*, 55-67.

IMTA (2002). *Banco Nacional de Datos de Aguas Superficiales (BANDAS)*. 8 CD's. Jiutepec, México: Secretaría de Medio Ambiente y Recursos Naturales, Comisión Nacional del Agua, Instituto Mexicano de Tecnología del Agua.

Montgomery, D. C., Peck, E. A., & Simpson, J. R. (1998). Multicollinearity and Biased Estimation in Regression. Chapter 16. In H. M. Wadsworth (Ed.), *Handbook of Statistical Methods for Engineers and Scientists* (pp. 291-342). Second edition. New York: McGraw-Hill, Inc.

Montgomery, D. C., Peck, E. A., & Vining, G. G. (2002). Multicolinealidad. Capítulo 10. En *Introducción al análisis de regresión lineal* (pp. 291-342). México, DF: Compañía Editorial Continental.

Ryan, T. P. (1998). Linear Regression. Chapter 14. In H. M. Wadsworth (Ed.), *Handbook of Statistical Methods for Engineers and Scientists* (pp. 14.1–14.43). New York: McGraw-Hill, Inc.

Salas, J. D., Raynal, J. A., Tarawneh, Z. S., Lee, T. S., Frevert, D., & Fulp, T. (2008). Extending Short Record of Hydrologic Data. Chapter 20. In V. P. Singh (Ed.), *Hydrology and Hydraulics* (pp. 717-760). Highlands Ranch, USA: Water Resources Publications.

Shapiro, S. S. (1998). Selection, Fitting and Testing Statistical Models. Chapter 6. In H. M. Wadsworth (Ed.), *Handbook of Statistical Methods for Engineers and Scientists* (pp. 6.1-6.35). Second edition. New York: McGraw-Hill, Inc.

Corresponding author

Dr. Daniel Francisco Campos Aranda

Profesor jubilado de la Universidad Autónoma de San Luis Potosí
Genaro Codina 240, Colonia Jardines del Estadio
78280 San Luis Potosí, San Luis Potosí, México
Teléfono: +52 (444) 8151 431
campos_aranda@hotmail.com

Click here to write the autor

Old dam, Guanajuato, Mexico.

Photo: Raúl Flores Berrones.

Nota técnica

El uso del método de los elementos distintos como una herramienta para la detección de problemas de estabilidad en las excavaciones del vertedero profundas

• Eduardo Botero-Jaramillo* • Miguel P. Romo • Bogart Méndez •
Universidad Nacional Autónoma de México
*Autor de correspondencia

• Humberto Marengo •
Comisión Federal de Electricidad

Resumen

Botero-Jaramillo, E., Romo, M. P., Méndez, B., & Marengo, H. (julio-agosto, 2014). El uso del método de los elementos distintos como una herramienta para la detección de problemas de estabilidad en las excavaciones del vertedero profundas. *Tecnología y Ciencias del Agua*, *5*(4), 181-191.

Este trabajo describe un estudio para determinar la estabilidad de las excavaciones en roca para el canal del vertedor de La Yesca utilizando análisis numéricos. Los resultados llevaron a la implementación de cambios importantes en la concepción original del vertedor (reorientación, geometría del canal y longitud), con el fin de garantizar la estabilidad de los taludes de roca en condiciones estática y sísmica. Se detalla el modelado numérico 3D de un talud de 280 m (correspondiente al proyecto original) construido en un macizo rocoso que tiene estructuras geológicas complejas. El modelado se llevó a cabo para evaluar la estabilidad estática y dinámica del talud proyectado en roca. El sitio de construcción presenta características geológicas complejas, como fallas y diques, así como varias formaciones geológicas resultantes de diferentes calidades de la roca y condiciones de fracturamiento. Los datos del campo disponibles hicieron posible la incorporación de la mayoría de las características geológicas y topográficas más importantes. La excavación del vertedor se simuló utilizando cuatro etapas. El efecto del daño inducido por las voladuras y la relajación de esfuerzos en la masa de roca también se tuvo en cuenta. Posterior a la simulación del proceso de excavación, se implementó el sismo de diseño de la presa La Yesca. Los análisis dinámicos simularon el comportamiento en tres dimensiones del vertedor, lo cual permitió la identificación de posibles bloques inestables, determinando de este modo si era posible estabilizarlos o modificar el diseño del vertedor original.

Palabras clave: método de los elementos diferentes, análisis sísmico, estabilidad de taludes, problemas de vertedores.

Abstract

Botero-Jaramillo, E., Romo, M. P., Méndez, B., & Marengo, H. (July-August, 2014). Use of the Distinct Element Method as a Tool to Detect Stability Problems in Deep Spillway Excavations. Water Technology and Sciences *(in Spanish), 5(4), 181-191.*

This paper describes a study to determine the stability of rock excavations in the La Yesca spillway channel using numerical analysis. The results of the analysis led to implementing important changes in the original conception of the spillway (reorientation, channel geometry and length) in order to ensure rock slope stability under static and seismic conditions. This paper describes the 3D numerical modeling of a 280 m high slope (corresponding to the original project) cut in a rock mass having complex geological formations. The modeling was carried out to evaluate both the static and dynamic stability of the projected rock slope. The construction site presented complex geological features such as faults and dikes as well as several geological formations resulting from varying qualities and fracture conditions. Available field data made it possible to incorporate the most important geological and topographical features. The spillway excavation was simulated using four stages. The effect of blast-induced damage and stress relaxation on the rock mass was also taken into account. After the simulation of the excavation process was completed, the seismic motion design for the La Yesca dam was input. These dynamic analysis simulated the three-dimensional behavior of the spillway which enabled identifying possible block instabilities, thereby determining whether to stabilize them or modify the original spillway layout.

Keywords: *Distinct element method, seismic analysis, slope stability, spillway problems.*

Introducción

La Yesca es un importante proyecto hidroeléctrico (750 MW) localizado en el noroeste de México, sobre el Río Santiago, en el límite entre los estados de Jalisco y Nayarit. La construcción del canal del vertedero implica una construcción muy alta de 280 m de altura (vea la figura 1) en una masa de roca altamente fracturada y geológicamente compleja, lo cual fue de gran preocupación. El diseño original del vertedero consistió en un canal individual de 500 m de largo y 96 m de ancho en su base. Las principales características topográficas y geológicas del sitio se capturaron en un modelo de elemento discreto tridimensional que toma en cuenta características tales como la presencia de fracturas de roca, fallas, uniones y contactos geológicos. Las discontinuidades geológicas representativas se modelaron explícitamente y la fracturación masiva en la roca se tomó en cuenta representando estos materiales como una masa de roca, de acuerdo con el criterio de Hoek-Brown (1997). El pobre comportamiento hidráulico del vertedero debido a su obstrucción parcial resultado de caídas de las rocas del talud impone un gran riesgo a la seguridad de la presa. En consecuencia, dada la gran importancia que los vertederos tienen en el comportamiento seguro de presas, se juzgó de mayor importancia efectuar un análisis numérico detallado para evaluar la seguridad del talud de las construcciones de roca elevadas. Este artículo presenta el análisis efectuado para el diseño original del vertedero de la presa de La Yesca y las decisiones que se tomaron para disminuir los riesgos asociados con la excavación.

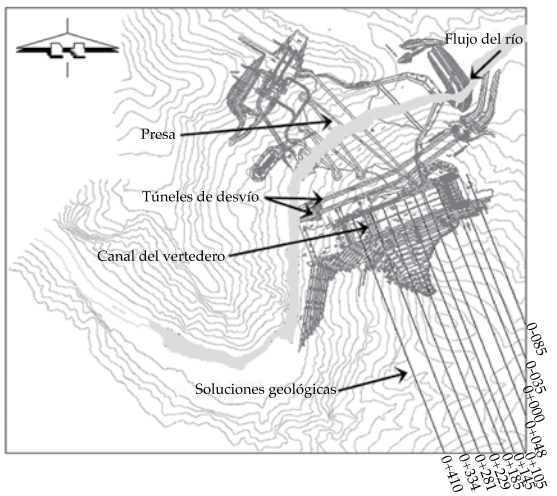

Figura 1. Proyecto original del canal del vertedero.

El modelo numérico se valoró primero evaluando la estabilidad de la masa de roca antes de su excavación y comparando después con las condiciones estables observadas de la masa de roca con el paso el tiempo. Después se simuló la construcción de rocas en cuatro etapas de excavación consecutivas. Se calcularon los estados de esfuerzos, campos de desplazamiento y distribución espacial de factores de seguridad para cada paso. Por último, se llevó a cabo el análisis de estabilidad dinámica considerando tanto el terremoto base de operación (TDO) y el terremoto confiable máximo (TCM), los cuales son los dos movimientos sintéticos propuestos por la International Commission of Large Dams (ICOLD,2010), representativos del ambiente sísmico del sitio (en este caso del mecanismo generador de terremotos de la subducción mexicana) con 200 y 10 000 años de periodo de retorno, respectivamente. Sobre las bases de los resultados de análisis, se evaluaron los riesgos asociados a la disposición original del vertedero y se tomaron decisiones.

Exploración del sitio

La caracterización de materiales geológicos del sitio se llevo acabo con base en una amplia exploración geológica y geofísica (CFE, 2006.). Estas son predominantemente volcánicas, pero también se encontraron algunos depósitos de aluviales y astrágalo. Las rocas ígneas estaban muy fracturadas y se presentaron algunas cunetas. Las principales unidades litológicas incluyeron dacitas, riolitas, andesitas, brechas y toba volcánica. Se presentaron varias fallas en la región, siendo la falla del Vertedor la

más importante. La figura 2 muestra las fracturas, fallas y la distribución espacial de los geomateriales en la sección principal del vertedero. La marca de la excavación del talud se incluye como referencia, donde la línea escalonada (línea azul) describe el perímetro de la excavación inicial y la línea continua (línea roja) ilustra la inclinación promedio del talud modelo. Los números en círculos se refieren a materiales específicos, los cuales se presentan en la tabla 1. Dada la longitud del vertedero, se entiende que no todos los materiales existentes son visibles en la sección que se muestra en esta figura.

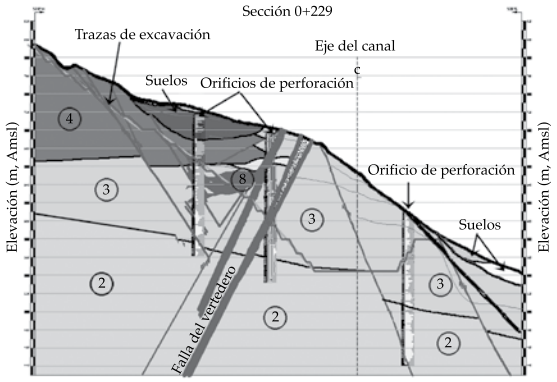

Figura 2. Estructura geológica en la sección principal del vertedero.

Propiedades de los materiales

Propiedades de la masa de roca

Las pruebas triaxiales se efectuaron en roca intacta. Los resultados se usaron junto con los valores estimados del índice de resistencia geológica (IRG), obtenido de las observaciones de campo, para determinar las propiedades de resistencia y deformabilidad de los geomateriales utilizando el criterio de fallas de Hoek y Brown para masas de roca unidas (Hoek & Brown, 1997; Hoek, Carranza-Torres, & Corkum, 2002). El módulo de elasticidad E_m se estimó para dos condiciones de roca de construcción: daño cero, $D = 1$ y $D = 0.7$, el cual se relaciona con un daño moderado, inducido por un proceso de excavación adecuado y controlado (Brady & Brown, 2004). La velocidad de la onda de compresión de los materiales constitutivos, V_p, se midió a partir de exploraciones geofísicas (vea la tabla 1). El criterio de falla de Hoek y Brown se usó para todos los materiales y se relacionó con el criterio de falla de Coulomb para estimar un ángulo de fricción equivalente, ϕ', y una consistencia cohesiva, c', de acuerdo con las ecuaciones (1) a (3):

$$\sin\phi = \frac{k-1}{k+1} \qquad (1)$$

Tabla 1. Propiedades de materiales.

Material	ρ (kg/m³)	ν	m_b
1. Dacita $V_p = 3.8$ km/s	2 500	0.35	6.25
2. Dacita $V_p = 3.2$ km/s	2 500	0.35	6.71
3. Dacita $V_p = 2.7$ km/s	2 500	0.35	4.69
4. Brecha fracturada $V_p = 2.5$ km/s	2 500	0.35	3.34
5. Dacita no comprimida	2 500	0.35	2.37
6. Brecha no comprimida	2 500	0.35	1.78
7. Dacita-riolita $V_p = 1.7$ km/s	2 500	0.35	1.64
8. Cuneta (andesita)	1 680	0.35	0.80
9. Falla del vertedor	2 500	0.35	0.93
10. Toba volcánica vítrea	2 500	0.35	1.19

$$c' = \frac{\sigma_{cm}}{2\sqrt{k}} \quad (2)$$

$$\sigma_{cm} = \sigma_{ci} s^a \quad (3)$$

Donde k es la pendiente de la línea que relaciona los esfuerzos principales mayor y menor σ'_1 y σ'_3; σ_{cm} y σ_{ci} son las resistencias compresivas uniaxiales de la masa rocosa y de la roca intacta, respectivamente; s y a son constantes que dependen de las características de masa de la roca. La variación de ϕ' y c' se obtuvo como una función de σ'_3 a través de un proceso de ajuste (Hoek & Brown, 1997):

$$\sin\phi = \frac{6\,a\,m_b\left(s + m_b\,\sigma'_{3n}\right)^{a-1}}{2(1+a)(2+a) + 6\,a\,m_b\left(s + m_b\,\sigma'_{3n}\right)^{a-1}} \quad (4)$$

$$c' = \sigma_{ci}\cdot\frac{\left[(1+2\,a)\,s + (1-a)\,m_b\,\sigma'_{3n}\right]\left(s + m_b\,\sigma'_{3n}\right)^{a-1}}{(1+a)(2+a)\sqrt{1+\left[6\,a\,m_b\left(s + m_b\,\sigma'_{3n}\right)^{a-1}\right]/\left[(1+a)(2+a)\right]}} \quad (5)$$

Donde m_b es el valor de la constante m (vea la tabla1) para la masa rocosa y $\sigma'_3 = \sigma'_{3máx}/\sigma_{ci}$ es el límite superior del esfuerzo de confinamiento sobre el cual la relación entre los criterios de Hoek y Brown y Mohr-Coulomb son considerados. Su valor se determinó de la teoría de elasticidad donde la razón de esfuerzos σ'_3/σ'_1 para la condición k_0 está dada por:

$$\frac{\sigma'_3}{\sigma'_1} = k_0 = \frac{\nu}{1-\nu} \quad (6)$$

El esfuerzo σ'_1 in situ se determinó del campo de esfuerzos geoestáticos. En consecuencia, $\sigma'_{3máx}$ se calculó utilizando la ecuación (6) y las razones de Poisson, ν, dadas en la tabla 1. Los valores de c' y ϕ' (obtenidos respectivamente de las ecuaciones 4 y 5), así como de otros parámetros de resistencia, calculados para cada material en el intervalo $0 < \sigma'_3 < \sigma'_{3máx}$, se presentan en la tabla 2.

Propiedades de contacto de bloques de rocas

El método numérico utilizado para el análisis tiene una formulación de contacto blando, el cual usa la normal, k_n, y corte, k_s, rigidez y un criterio de plasticidad para simular el comportamiento de la unión. Se usó el modelo de unión de Mohr-Coulomb dada su simplicidad y su aplicabilidad probada para los problemas de fricción compleja. La resistencia a la fricción τ' (como función de σ'_n) entre bloques de rocas se consideró como

Tabla 2. Parámetros de resistencia del material rocoso.

Material	c' (MPa)	ϕ'	σ_{cm} (MPa)
1. Dacita $V_p = 3.8$ km/s	2.84	49	8.60
2. Dacita $V_p = 3.2$ km/s	4.36	49	14.13
3. Dacita $V_p = 2.7$ km/s	2.41	47	5.42
4. Brecha fracturada $V_p = 2.5$ km/s	1.68	44	3.33
5. Dacita no comprimida	1.01	41	1.13
6. Brecha no comprimida	0.91	39	0.64
7. Dacita-riolita $V_p = 1.7$ km/s	0.34	34	0.39
8. Cuneta (andesita)	0.03	25	0.14
9. Falla del vertedor	0.15	26	0.22
10. Toba volcánica vítrea	0.28	33	0.28

$\tau' = 0.85\,\sigma'_n$ para $\sigma'_n < 200$ MPa y $\tau' = 0.50 + 0.60\,\sigma'_n$ para $\sigma'_n > 200$ MPa (Byerlee, 1978). Vale la pena mencionar que el valor de esfuerzo principal máximo calculado en el modelo numérico fue mucho menor que 200 MPa, el cual de acuerdo con Byerlee (1978) produciría un coeficiente de fricción de 0.85 (ϕ' aproximadamente igual a 40°). Dadas las muchas incertidumbres implicadas en el problema de fricción roca-roca, se juzgó conveniente suponer un valor máximo conservador de 36°. El valor mínimo se supuso de 25°, el cual corresponde al valor mínimo obtenido a través del criterio de Hoek-Brown (vea la tabla 2). La tabla 3 muestra los valores reales utilizados para cada contacto material. Es importante subrayar el hecho de que cuando estuvieron en contacto dos materiales diferentes se consideró el ángulo de fricción más bajo.

La magnitud de k_n se calculó a través de k_s, suponiendo una relación elástica entre ellos (Kulhawy, 1975):

$$k_s = \frac{k_n}{2(1+\nu)}; \quad k_n = 2\,k_s\left(1+\upsilon\right) \qquad (7)$$

Donde ν es la razón de Poisson del material de unión y k_s es la rigidez de corte incluida en la tabla 3.

Modelo numérico

El modelo numérico se diseño apropiadamente de manera que sus condiciones de frontera no afectaran los resultados del proceso de excavación (figura 3). El modelo consistió de 225 955 elementos sólidos tetraédricos de deformación constante, y 88 655 nodos. El modelo se construyó a partir de 11 secciones geológicas espaciadas aproximadamente cada 50 m a lo largo del canal del vertedero (vea la figura 1). Desde la elevación de 544 a 624 anmm (arriba del nivel medio del mar), el talud izquierdo de la excavación se modeló con una inclinación de 0.88:1 (H:V); de 624 a 700 anmm la inclinación del talud fue 1.40:1; y de 700 anmm hasta la parte superior del talud, de 1.33:1. El talud derecho del canal del vertedero tuvo una inclinación constante a lo largo de su altura (elevación de 544 a 580 anmm) de 0.54:1.

El modelo numérico se basó en una diferencia finita del procedimiento de solución del tiempo en marcha que permite simular explícitamente los contactos y discontinuidades entre bloques. La interacción entre bloques se toma en cuenta a través de relaciones de desplazamientos de esfuerzos para cada contacto. Los esfuerzos internos en cada bloque se calculan a través del método de diferencias finitas. Las más importantes discontinuidades

Tabla 3. Propiedades de contacto.

Material	ϕ'	τ' (MPa)	U_c (m)	k_n (MPa/m)	k_s (MPa/m)
1. Dacita $V_p = 3.8$ km/s	36	1.73	0.004	1 168	433
2. Dacita $V_p = 3.2$ km/s	36	1.62	0.004	1 093	405
3. Dacita $V_p = 2.7$ km/s	36	1.80	0.005	972	360
4. Brecha fracturada $V_p = 2.5$ km/s	30	1.94	0.006	872	323
5. Dacita no comprimida	30	2.07	0.006	934	346
6. Brecha no comprimida	30	2.13	0.007	820	304
7. Dacita-riolita $V_p = 1.7$ km/s	30	2.22	0.007	854	316
8. Cuneta (andesita)	25	2.33	0.015	420	155
9. Falla del vertedor	25	2.31	0.015	416	154
10. Toba volcánica vítrea	27	2.28	0.015	410	152

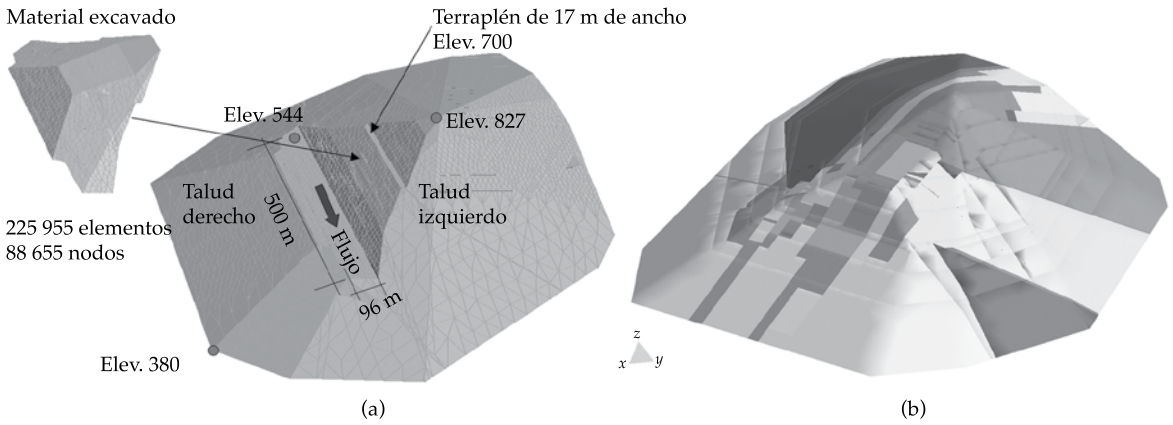

Figura 3. Geometría 3D del modelo numérico.

y fallas geológicas se incluyeron en el modelo, mientras que las fracturas menores de rocas interactuando a lo largo de las principales discontinuidades se tomaron en cuenta considerando las rocas fracturadas como masas rocosas (Hoek & Brown, 1997).

Condiciones iniciales del sitio

Los resultados de los cálculos estáticos y sísmicos [condiciones sísmicas OBE (operating basis earthquake) y MCE (maximum credible earthquake)] de las condiciones iniciales del sitio no mostraron indicación de alguna inestabilidad, lo cual concuerda con la estabilidad histórica de la masa de roca.

Simulación del proceso de excavación

El proceso de excavación desde una elevación de 827 hasta 544 anmm se simuló en cuatro etapas. Los desplazamientos y factores de seguridad se calcularon para cada etapa con el fin de evaluar cualquier deslizamiento potencial del talud durante el proceso de excavación. Los resultados indican que después de que se finalizó la excavación, el campo de desplazamiento se debió principalmente a la expansión de las rocas causada por la relajación de esfuerzos, como se muestra en las figura 4(a) a 4(d). El análisis señala que el proceso de excavación con mayor probabilidad no inducirá caídas de rocas masivas. Sin embargo, en las figuras de la 5(a) a la 5(d) se ve que el factor de seguridad en algunas áreas del talud indica que es más probable que ocurran inestabilidades durante el proceso de construcción. En consecuencia, se consideró que cantidades importantes de desechos podrían caer por la colina, poniendo en peligro la construcción estable de los taludes del vertedero.

Efecto del proceso de excavación en la masa de roca y sus implicaciones en el factor de seguridad

Debido al proceso de excavación la masa rocosa sufre cierto daño causando reducciones de esfuerzos principalmente cerca de la superficie del talud. En consecuencia, se consideró un factor de daño de 0.7, lo cual corresponde a un proceso de excavación de buena calidad (Brady & Brown, 2004). La figura 5d muestra el factor de la distribución de seguridad en la sección máxima del talud para esta condición dañada. Es notable que una zona de bajo factor de seguridad se desarrolle en la parte superior del talud. Estos resultados sugieren que es probable que se desarrollen inestabilidades potenciales de rocas durante el proceso de

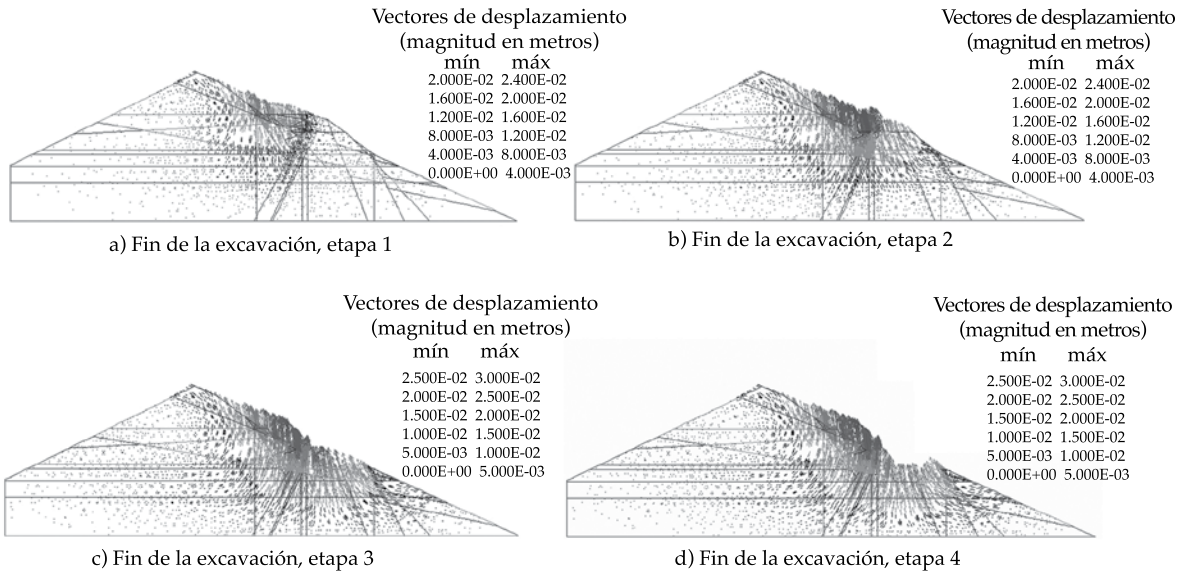

a) Fin de la excavación, etapa 1

b) Fin de la excavación, etapa 2

c) Fin de la excavación, etapa 3

d) Fin de la excavación, etapa 4

Figura 4. Campo de desplazamiento resultante debido al proceso de excavación.

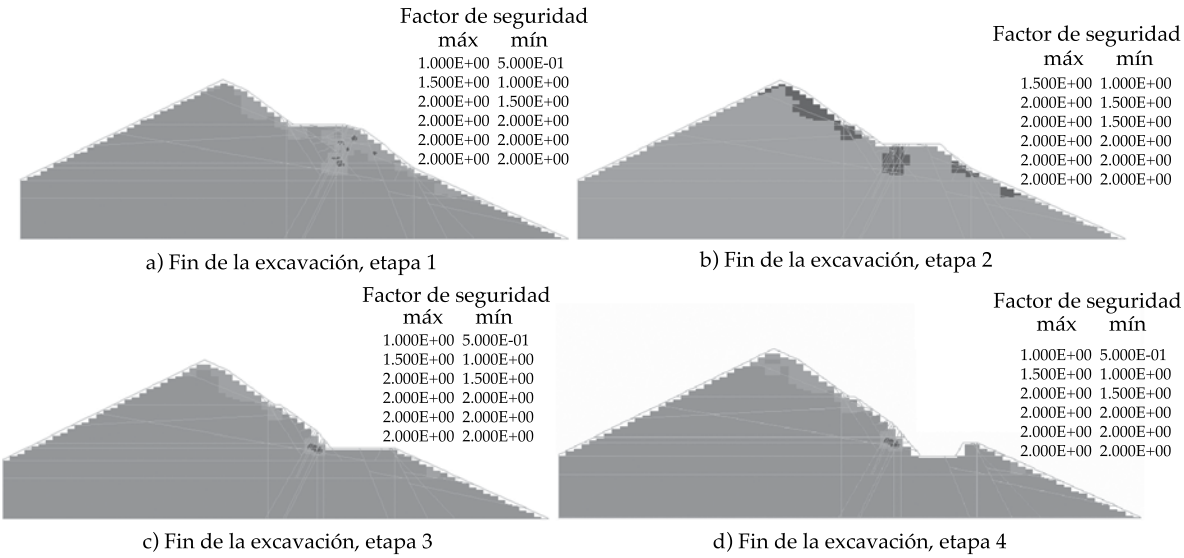

a) Fin de la excavación, etapa 1

b) Fin de la excavación, etapa 2

c) Fin de la excavación, etapa 3

d) Fin de la excavación, etapa 4

Figura 5. Evolución del factor de seguridad debido al proceso de excavación.

construcción, lo que indica que la excavación debe monitorearse de manera apropiada para detectar cualquier signo de movimientos de roca y proceder a estabilizar el área según se requiera.

Análisis sísmico

A pesar de que el efecto de que las cargas transitorias pueden afectar notablemente el comportamiento de las masas rocosas, la física

del fenómeno apenas se comprende (Jing, 2003). Desde ahora, los modelos lineales elásticos de rocas se aceptan ampliamente para analizar las respuestas sísmicas de las masas rocosas. La respuesta dinámica del talud se calculó tanto para el OBE como para el MCE de acuerdo con los criterios de diseño utilizados para la presa de La Yesca (ICOLD, 2010). Se desarrollaron terremotos sintéticos para obtener las series de tiempo del OBE y el MCE. Los movimientos de entrada calculados fueron representativos del mecanismo de generación de terremotos de la subducción mexicana (placa de Cocos).

La respuesta sísmica del talud al final de la excavación para el OBE se muestra en la figura 6, donde se ve que se desarrollaron desplazamientos hasta de 40 cm en la parte superior del talud. Esto indica que pueden ocurrir inestabilidades sobre esa área, lo cual en caso de desechos de rocas que se deslizan hacia el canal del vertedor, podrían llevar a su obstrucción o a un mal funcionamiento del mismo, poniendo en peligro a la propia presa. Además, los resultados muestran que puede desarrollarse un bloque potencialmente inestable del punto superior del talud.

El MCE es un evento sísmico altamente grave. Los desplazamientos resultantes del talud por la acción de este terremoto aumentan drásticamente con respecto al OBE. En la parte superior del talud los desplazamientos indican la falla en esta zona de la construcción en la roca (figura 7). Los desplazamientos en la parte superior del talud también aumentan fuertemente. Las magnitudes de desplazamiento en la parte superior del talud alcanzan casi 40 cm, lo que indica posibles desprendimientos de bloques bajo la acción del máximo terremoto creíble. Esto podría llevar a un mayor deslizamiento del talud hacia el canal del vertedero.

Acciones correctivas

Los resultados del análisis muestran las inestabilidades potenciales de los taludes del vertedero y por consiguiente afectan su operación correcta. Por ello se decidió modificar tanto su disposición inicial como su diseño geométrico. Para este fin la Comisión Federal de Electricidad (propietaria del proyecto) implementó importantes cambios que se observan cuando se comparan la figura 8 (diseño original) con las figuras 9 y 10 (diseño final). La principal modificación en la disposición del vertedero fue el cambio de la orientación (con respecto a la original) en 28° hacia el sureste, lo cual redujo la altura máxima del talud en 15 m. Esto tuvo un efecto benéfico en la disminución de los volúmenes de excavación y en la reducción de los peligros de la caída de bloques de roca en el canal del vertedero que podrían probablemente afectar su operación adecuada o incluso obstruirlo, poniendo en alto

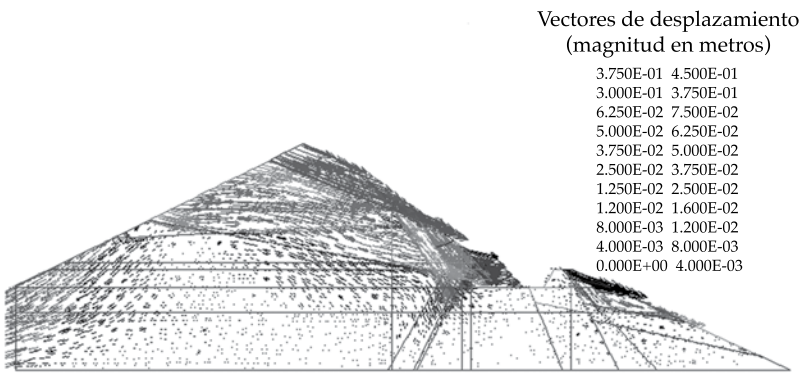

Figura 6. Desplazamientos resultantes al final de la excavación.

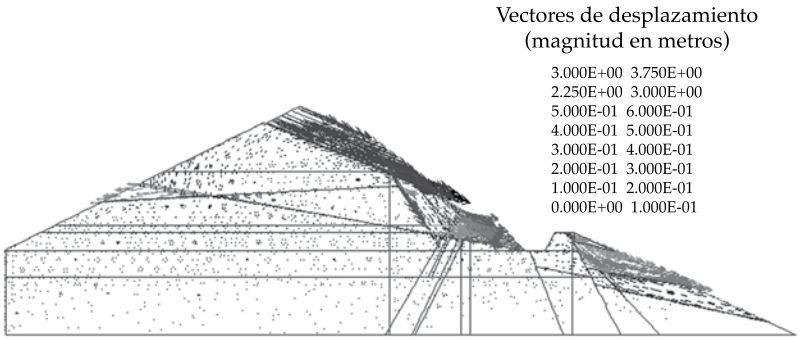

Figura 7. Desplazamientos del talud resultantes por la acción del MCE.

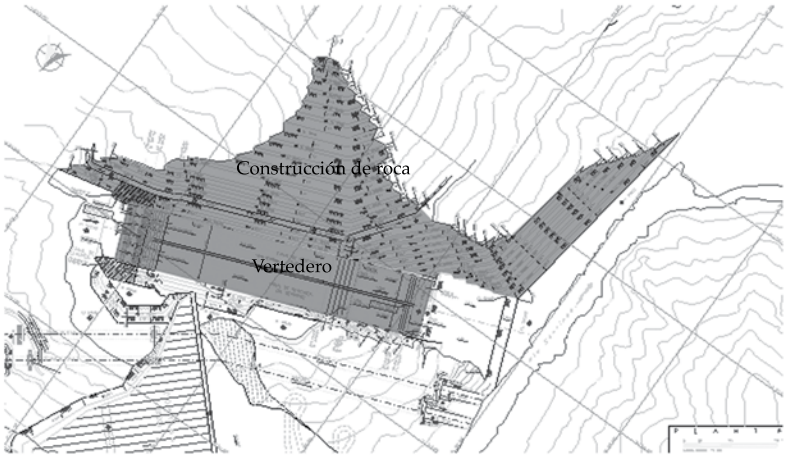

Figura 8. Concepción original del vertedero.

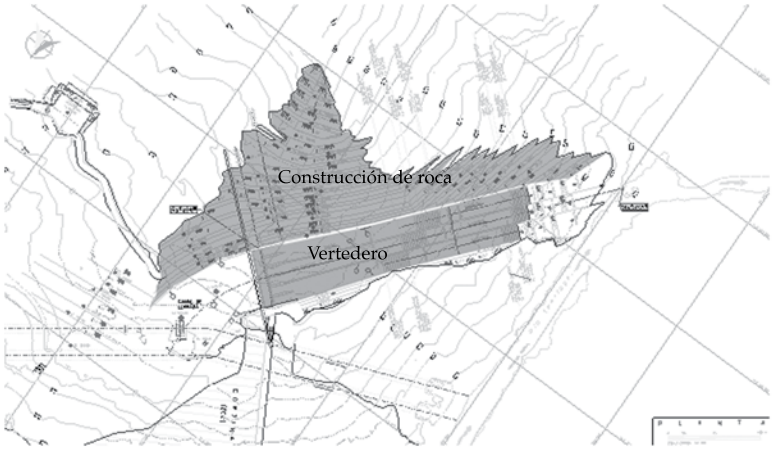

Figura 9. Diseño final del vertedero.

Figura 10. Conformación final del vertedero (modificado www.cfe.gob.mx).

riesgo la seguridad de la presa. En cuanto a la modificación del vertedero original consistente en dividir la sección de un canal en la sección de tres canales, lo cual además incrementó la estabilidad total de los taludes del vertedero, se disminuyó la excavación del volumen de material. La fotografía 10 describe una vista de la configuración final del vertedero de la presa de La Yesca.

Conclusiones

- Del análisis efectuado, puede concluirse que el modelado numérico es una herramienta importante en la evaluación de los proyectos geotécnicos. Los resultados de dichos análisis permiten prevenir posibles problemas que pueden surgir mediante la ejecución del proyecto. Además el modelado numérico es una herramienta útil para seleccionar las zonas donde debe realizarse un monitoreo detallado.
- Sin embargo, los modelos numéricos, como bien se sabe, deben alimentarse con propiedades realistas de los materiales obtenidas de pruebas del laboratorio y/o campo para obtener resultados significativos. Cuando las propiedades de los materiales no se conocen de manera apropiada, deben efectuarse estudios paramétricos para evaluar la influencia de diversos parámetros. Vale la pena mencionar que el vertedero, junto con su nuevo trazo y los cambios de geometría mencionados, se ejecutó sin ningún problema mayor. También debe señalarse que el análisis numérico permitió la determinación de problemas "ocultos", los cuales no pueden detectarse con otros procedimientos. En consecuencia, los métodos numéricos son herramientas poderosas que proporcionan pistas para tomar decisiones de diseño informadas y mejorar consecuentemente la seguridad estructural y ayudar a reducir los niveles de riesgo.
- Los cambios implementados fueron muy importantes y la visualización de los problemas potenciales solo fue posible con el estudio numérico 3D.

Enviado: 16/04/13
Aceptado: 11/04/13

Referencias

Brady, B. H. G., & Brown, E. T. (2004). *Rock Mechanics for Underground Mining* (3rd edition). Boston: Kluwer Academic Publishers.

Byerlee, J. (1978). Friction of Rocks. *Pageoph*, *16*, 615-26.

CFE (2006). *Geological Survey Report for the Spillway Channel, La Yesca Hydroelectrical Project*. México, DF: CFE.

Hoek, E., & Brown, E. T. (1997). Practical Estimates of Rock Mass Strength. *International Journal of Rock Mechanics & Mining Sciences*, *34*(8), 1165-86.

Hoek, E., Carranza-Torres, C., & Corkum, B. (2002). Hoek-Brown Failure Criterion – 2002 Edition. Mining and Tunnelling Innovation and Opportunity. In R. Hammah, W. Bawden, J. Curran, & M. Telesnicki (Eds.), *Proc. 5th North Am. Rock Mech. Symp. & 17th Tunn. Assn. Can. Conf.* (pp. 267-273), University of Toronto.

ICOLD (2010). Concrete Face Rockfill Dams: Concepts for Design and Construction. *Bulletin*, *141*, 108.

Jing, L. (2003). A Review of Techniques, Advances and Outstanding Issues in Numerical Modelling for Rock Mechanics and Rock Engineering. *International Journal of Rock Mechanics & Mining Sciences*, *40*(3), 283-353.

Kulhawy, F. H. (1975). Stress Deformation Properties of Rock and Rock Discontinuities. *Journal of Engineering Geology*, *9*(4), 327-50.

Dirección institucional de los autores

Dr. Eduardo Botero Jaramillo
Dr. Miguel P. Romo
Dr. Bogart Méndez

Instituto de Ingeniería
Universidad Nacional Autónoma de México
Ed. 4-217 Ciudad Universitaria, Delegación Coyoacán
04510 México, D.F., México
Teléfono: +52 (55) 56233 600, ext. 8462, 3648
eboj@pumas.iingen.unam.mx
mromo@pumas.iingen.unam.mx
bmendezu@iingen.unam.mx

Dr. Humberto Marengo

Comisión Federal de Electricidad
Río Mississippi 71, Colonia Cuauhtémoc
Tecoyotitla 262-3
06500 México, D.F., México
Teléfono: +52 (55) 5229 4400
Fax: +52 (55) 5207 0287
humberto.marengo@cfe.gob.mx

Click here to write the autor

View of the Cutzamala Aqueduct at the Lerma River, State of Mexico, Mexico.

Photo: Jorge Izurieta.

Discussion

Technical notes and technical articles are open to discussion according to the following guidelines:

- The discussion will be written in the third person.
- The writer of the discussion shall use the term "commentator" when referring to oneself and the term "author" when referring to the one responsible for the technical note or article.
- The discussion shall be sent within 12 months of the last day of the quarter in which the a technical article or note was published.
- The length of the discussion may be extended by written request from the commentator.
- The discussion is to be presented according to the Guide for Collaborators published in this journal (omitting data referring to the length and abstract). In addition, the bibliographical citation of the technical notes or articles to which the discussion refers shall be included.
- The maximum length of the discussion is 4 journal pages (approximately 10 cuartillas, including figures and tables).
- The figures and tables presented by the commentator shall be progressively marked with Roman numbers and when citing those generated by the author the original numeration should be respected.
- The editors will suppress data that does not pertain to the subject of the discussion.
- The discussion will be rejected if it contains topics addressed by other sources, promotes personal interests, is carelessly prepared, raises controversy involving already established facts, is purely speculative or falls outside the purpose of the journal.
- The discussion will be published along with commentaries from the author or authors to which it refers.
- The discussion will be directed by the editor in chief.

Vasco de Quiroga Fountain, Patcuaro, Michoacan, Mexico.

Photo: Fernando Flores Prior.

Guide for Collaborators

The journal ***Tecnología and Ciencias del Agua*** invites specialists to collaborate with original, unpublished technical articles or notes **related to water, resulting from investigations and provide original contributions**, based on the disciplines of hydrology, hydraulics, water management, water and energy, water quality, and physical, biological and chemical sciences as well as political and social sciences, among other disciplines, according to the guidelines stated below.

PREPARATION OF THE ARTICLE

FORMAT

Font: Palatino throughout the entire document (body of text, tables and figures).

Font Size: Use 8, 9, 10 and 20 points, according to the following table:

8 points (Palatino)	9 points (Palatino)
• Tables. • Figures. • Acknowledgements.	• Name of authors. • Institution of authors. • Abstract. • *Abstract* and *keywords*. • Institutional address of the authors.
10 points (Palatino)	**20 points capital letters (Palatino)**
• Body of the text. • Title of the work in Spanish.	• Title of the work in English.

Line Spacing: double-spaced.

Page Numbers: all pages shall be numbered.

Length
Technical article: **30 pages** (numbered), including figures and tables.
Technical note: **10 pages** (numbered), including figures and tables.

CONTENS

Title
The article shall present significant contributions to scientific and technological knowledge pertaining to the specialty. It shall be based on finished works or those that have completed a development cycle. It shall show results from a series of experiences over 1 year or more of investigations and be supported by an adequate bibliographical review. **The basic structure of the text shall contain an introduction, the development and the conclusions**. The classic layout is preferable: abstract, introduction, methodology, results, discussion, conclusion and references.

Title
The title, **written in Spanish and English**, shall be informative and not exceed 12 words.

Abstract
The abstract, **written in Spanish and English**, shall be concise and provide a broad overview of the investigation (objective, method, results and conclusions) without exceeding 250 words.

Key Words
Eight words or key phrases (maximum) shall be provided **in Spanish and English** that facilitate the identification of the information.

Footnotes
Not admitted. The information is to be incorporated into the text.

Acknowledgements
To be included after the text and before the references.

Tables
- One page for each table.
- A list of all the tables cited shall be presented after the references.

Figures
- One page for each figure.
- All the names of the figures shall be included after the tables.
- They should be high-resolution (300 dpi).

Note: When the article is approved by the publication, the author shall send each figure in JPG format with high-resolution (300 dpi).

References
- The entire bibliography must be referenced in the main body of the text.
- In the case of addressing scientific and technological topics that are common domain, works that denote the knowledge of the authors about the state-of-art shall be cited.
- Avoid self-citations to the extent possible
- APA format shall be used as a basis.

Some examples of references in APA format are:

Complete Books

Last name, A. A. (Year). Title of work. city published: Publisher.
Last name, A. A. (Year). Title of work. Consulted at http://www.xxxxx
Last name, A. A. (Year). Title of work. doi:xxxxx
Last name, A. A. (Ed.). (year).City published: Publisher.

Book Chapters

Last Name, A. A., & Last Name, B. B. (Year).. Title of chapter or entry. In A. Last Name, B. Last Name & C. Last Name (Eds.), Title of book (pp. xxx-xxx). Place: Publisher.
Last Name, A. A., & Last Name, B. B. (Year).. Title of chapter or entry. In A. Last Name, B. Last Name & C. Last Name (Eds.), Title of book (pp. xxx-xxx). Consulted at http://www.xxxxxxx

Newspaper Article or Note Consulted Online

Last Name, A. A., & Last Name, B. B. (Year). Title of article. Title of publication, issue (number), pp. Consulted at http://www.xxxxxxx

That is: Last Name, A. A., & Last Name, B. B. (Year). Title of article. Title of publication, 1(2), 5-17, pp. Consulted at http://www.xxxxxxx

Printed Newspaper Article or Note

Last Name, A. A., & Last Name, B. B. (Year). Article Title. Title of publication, 8(1), 73-82.

Newspaper Article Publication with DOI

Last Name, A. A., & Last Name, B. B. (Year). Article Title. Title of publication, 8(1), 73-82, doi:xxxxxx

Conferences or Symposiums

Collaborator, A. A., Collaborator, B. B., Collaborator, C. C., & Collaborator, D. D. (Month, year). Title of collaboration. In E. E. President (Presidency), Title of symposium. Symposium held at the conference by Name of Organization, Place.

Language

Spanish or English

Separation of numbers and use of decimal points

In *Tecnología and Ciencias del Agua*, the separation between thousands is denoted with a blank space. A decimal point is used to separate whole numbers from fractions. In this regard, refer to Diccionario panhispánico de dudas, edited by the Real Academia Espyearla and the Asociación de Academias de la Lengua Espyearla, in 2005, with respect to numeric expressions: "**the Anglo-Saxon use of the period is accepted, normal in some Hispano-American countries…: $\pi = 3.1416$.".**

Delivery of Article

Send the article in *Word* with the name of the authors and institutional address to **revista.tyca@gmail.com**, with copy to Elizabeth Peña Montiel, elipena@tlaloc.imta.mx.

General Information

The review process will begin once the material is received, during which time the manuscript could be rejected. If the text is suitable for review, having fulfilled the Editorial Policy and the Editorial Committee having determined so, it will proceed to the review stage.

Depending on the review process, the text may be accepted without changes, with minor changes, with extensive changes or rejected.

Once a work is published, the main author has the right to two journals and ten offprints free of charge.

In there are any questions, please write to Helena Rivas López, hrivas@tlaloc.imta.mx or Elizabeth Peña Montiel, elipena@tlaloc.imta.mx

Citations within the body of the text

Type of citation	First appearance in text	Subsequent appearances	Format in parenthesis, first citation in text	Format in parenthesis, subsequent citing in text
Work by one author	Last name (Year)	Last name (Year)	(Last name, year)	(Last name, year)
Work by two authors	Last name and Last name (Year)	Last name and Last name (Year)	(Last name & Last name, Year)	(Last name & Last name, Year)
Work by three authors	Last name, Last name and Last name (Year)	Last name *et al*. (Year)	(Last name, Last name, & Last name, year)	(Last name of first author *et al*., year)
Work by four authors	Last name, Last name, Last name and Last name (Year)	Last name *et al*. (Year)	(Last name, Last name, Last name, & Last name, year)	(Last name of first author *et al*., year)
Work by five authors	Last name, Last name, Last name, Last name and Last name (Year)	Last name *et al*. (Year)	(Last name, Last name, Last name, Last name, & Last name, year)	(Last name of first author *et al*., 2008)
Work by six or more authors	Last name of first author *et al*. (Year)	Last name of first author *et al*. (Year)	(Last name of first author *et al*., Year)	(Last name of first author *et al*., year)
Groups (easily identified with abbreviations) such as authors	Complete name of institution (Acronym, year)	Acronym (Year)	(Complete name of institution [acronym], year)	(Institution, year)
Groups (without abbreviations) such as authors	Complete name of institution (year)	Complete name of institution (year)	(Complete name of institution, year)	

Editorial Policy

Mission

Disseminate scientific and technical knowledge and advances related to water through the publication of previously unpublished articles and technical notes that provide original contributions.

Our Principles

- Impartiality
- Objectivity
- Honesty

Our Values

- Knowledge
- Experience
- Thematic expertise

Contents

Interdisciplinary, composed of previously unpublished articles and technical notes related to water, that result from research and provide original scientific and technological contributions or innovations, developed based on the fields of knowledge of diverse disciplines.

Topics Covered

Interdisciplinary, related to water, with priority topics in the following knowledge areas:

- Water and energy
- Water quality
- Physical, biological and chemical sciences
- Hydro-agricultural sciences
- Political and social sciences
- Scientific and technological development and innovation
- Water management
- Hydrology
- Hydraulics

Type of Contributions

Technical article: scientific document that addresses and communicates, for the first time, results from a successful investigation or innovation, whose contributions provide and increase current knowledge about the topic of water.

Technical note: text that addresses advances in the field of hydraulic engineering and professional practices in the field of water, while not necessarily making an original contribution in every case it must be a previously unpublished work.

Some of the articles submitted to the review process can result in being published as notes and vice versa. This will occur through a proposal and process of mutual agreement between the authors and the editor responsible for the topic. The article and the note have nearly the same structure (abstract, introduction, methodology, results, discussion, conclusion, references).

Review Process

The journal is governed by a rigorous review process which establishes that each article be analyzed separately by three reviewers who recommend its acceptance, acceptance with minor changes, acceptance with extensive changes, rejection or acceptance as a technical note with the required changes.

At least one of three reviewers will be sought from a foreign institution.

The reviewers may not belong to the same institution as the authors proposing the article for publication.

When the decisions are opposing or inconsistent, the involvement of other reviewers or the members of the Editorial Committee may be requested.

On occasion, the approval of an article will be decided by two reviewers in addition to the opinion of the editor of the corresponding topic or, the editor in chief.

A rejected article will not be accepted for a new review process.

The review process will be performed in such a way that neither the authors nor the reviewers know the names of the other party.

The review process is performed by high-level specialists and experts who are national and internationally renowned in their professional fields and have the ability to reliably evaluate, in a timely manner, the quality as well as the originality of contributions, in addition to the degree of scientific and technological innovation in the topic under which it is submitted for possible publication.

This participation is considered a professional contribution and will be performed as a courtesy.

The reviews have a "Guide for the Reviewer" provided by the journal's Editorial Department.

Final Ruling

The ruling resulting from the review process is not subject to appeal.

Authors

Works are published from authors of any nationality who present their contributions in Spanish; nevertheless, we all accept works in Spanish or English.

Responsibility of the Authors

Submitting a proposal for the publication of an article commits the author not to simultaneously submit it for consideration by other publications. In the event an article has been submitted to another media for eventual publication, the author agrees to do so with the knowledge of the Editorial Department, which will suspend the review process and inform the Editorial Committee of the decision by the authors.

Collaborators whose articles have been accepted will formally cede the copyright to ***Tecnología y Ciencias del Agua***.

The authors are responsible for the contents of the articles.

The author is responsible for the quality of the Spanish used. If the writing is deficient the work will be rejected. ***Water Technology and Sciences*** will only be responsible for the editorial management.

The author commits to making the changes indicated by the editor of the topic in the time frame establish by the editor. In the event these indications are not met, the article will be removed from the review process and be classified as rejected.

The author shall be attentive to resolving the questions and proposals presented by the editors and the editorial coordinator.

Each author shall approve the final printed proofs of their texts.

It is suggested that authors consult the "Guide for Collaborators."

Readers

Academics, investigators, specialists and professionals interested in the analysis, investigation and search for knowledge and solutions to problems related to water.

Reception of Articles

The reception of articles and notes is ongoing.

Time period

Bimonthly, appearing in the second month of the period.

Subscription and Distribution

The journal is distributed through paid and courtesy subscriptions.

Open Access

Water Technology and Sciences, previously ***Hydraulic Engineering in Mexico***, provides a digital version of all the material published since 1985.

Special editions and issues

Water Technology and Sciences will publish special numbers independently or in collaboration with other journals, professional associations or editorial houses with renowned prestige and related to water resources.

In addition, it will publish articles by invitation, acknowledging the professional advances of prominent investigators.

In both cases, the quality of the technical continents and scientific contributions will be reviewed.

Water Technology and Sciences is registered in the following national and international indices and abstracts:

• Thomson Reuters Science Citation Index® (ISI) • Expanded Thomson Reuters Research Alert® (ISI) • Índice de revistas mexicanas de investigación científica y tecnológica del Consejo Nacional de Ciencia y Tecnología (Conacyt) (2013-2018) • Sistema de Información Científica Redalyc (Red de Revistas Científicas de América Latina y El Caribe, España y Portugal), Universidad Autónoma del Estado de México • EBSCO (Fuente Académica Premier NISC; Geosystems, como Marine, Oceanographic and Freshwater Resources) • ProQuest (Cambridge Scientific Abstracts) • Elsevier (Fluid Abstracts: Process Engineering; Fluid Abstracts: Civil Engineering) • CAB Abstracts, CAB International • Latindex (Sistema Regional de Información en Línea para Revistas Científicas de América Latina, el Caribe, España y Portugal), Universidad Nacional Autónoma de México • Periódica (Índice de Revistas Latinoamericanas en Ciencias), Universidad Nacional Autónoma de México • Catálogo Hela (Hemeroteca Latinoamericana), Universidad Nacional Autónoma de México • Actualidad Iberoamericana, CIT-III, Instituto Iberoamericano de Información en Ciencia y Tecnología.

Other Sources

The journal can also be found archived in Google scholar.